



Institut de recherche
en mathématique et physique

Quantum and Thermal Effects on Inflation and Neutrino Dynamics in the Early Universe

Doctoral dissertation presented by

GILLES BULDGEN

in fulfilment of the requirement for the degree of Doctor of Sciences.

Thesis Committee

Prof. M. DREWES (<i>Advisor</i>)	UCLouvain
Prof. F. MALTONI (<i>Co-Advisor</i>)	UCLouvain
Prof. V. LEMAÎTRE (<i>President</i>)	UCLouvain
Prof. G. BRUNO	UCLouvain
Prof. B. GARBRECHT	TUMunich
Prof. M. RAMSEY-MUSOLF	TDLI Shanghai/UMass

2020

Acknowledgements

Even though a PhD thesis is a single-authored manuscript, it goes without saying that the research presented here was not just conducted by myself in the past three years. Here, I would like to express my gratitude to those who supported me and helped me all along this journey.

First and foremost, I would like to deeply thank my supervisor Marco for his thoughtful guidance and for giving me the opportunity to enjoy all aspects of my PhD, from the science to the experience of travelling in Europe and overseas in multiple occasions. I would also like to express my profound appreciation to Michael Ramsey-Musolf and Yvonne Wong for having welcomed me with open arms to their institutes for extended research stays. Thank you both for the great opportunities, for the science, and for always being of good advice.

Then, I also wish to thank my closest collaborators Jack Bennett, Jin U Kang and Ui Ri Mun. Jack, I really appreciated working with you, many thanks for your friendship and for the amazing road trips. Jin U and Ui Ri, I want to thank you both for our fruitful collaboration, writing this thesis would not have been possible without you. I hope we meet again.

I would also like to extend my gratitude to many of my co-workers at IRMP. Particularly, Robin, Bram, cheers to the whisky tasting afternoons and the coffee breaks. Also Dražen, thanks for your friendship, your wisdom and for sharing my interests. I too am very grateful to the great administrative staff of CP3. Carinne, Stéphanie, thank you so much for your work and for making my life so much easier these past three years. Special thanks also go to my friends and colleagues from the USA: Julie, Maya, Ryan, Sasha, John and Jordy, thank you for making me feel at home in Amherst.

Then, I would like to express my appreciation to my thesis committee and jury for taking the time to read and assess the scientific quality of this manuscript.

Pour finir, j'aimerais remercier ma famille et mes amis proches de m'avoir soutenu dans mon projet de thèse durant ces trois dernières années. Merci Maman, JC, Florence et François, pour votre présence, soutien et stabilité. Merci aux colloqs Gilles, Egor, Romain, Quentin et Peter pour les moments inoubliables au SR6. Et enfin, merci à Marian et Angélique pour leur présence et soutien indispensables durant la période de confinement covid-19 et de rédaction de ma thèse.

Contents

1	Common background	17
1.1	Elements of (non)equilibrium field theory	17
1.2	The 2 Particle Irreducible (2PI) effective action formalism . . .	41
I	Quantum and thermal effects on nonequilibrium scalar field dynamics in the early Universe	49
2	Markovian dynamics for scalars in slowly-evolving backgrounds	53
2.1	The Markovian equation: a derivation	54
2.2	Interpretation of the leading friction term	56
3	2PI formalism for interacting \mathbb{Z}_2-symmetric scalars	59
3.1	The 2PI equations of motion	60
3.2	The 2PI dynamics at three-loop order	61
4	A slowly-rolling, homogeneous and isotropic scalar	67
4.1	The Markovian equation	69
4.2	The homogeneous and isotropic 2PI equations of motion	74
4.3	Adiabatic solutions of the Kadanoff-Baym equations	75

4.4	The leading order equation of motion for the condensate φ . . .	80
4.5	The NLO equation of motion	92
5	On the feasibility of warm inflation	97
5.1	Observational evidence for non-standard cosmology and possible explanations	97
5.2	Slow-roll parameters	104
5.3	The viability of warm inflation: state of the art	106
5.4	Flat-space slow-roll parameters	107
5.5	Slowly rolling with \mathbb{Z}_2 -symmetric scalars	109
	Conclusion and Outlook	115
II	Towards a precision computation of N_{eff} in the standard model of particle physics and cosmology	117
6	N_{eff} and cosmological thermodynamics	121
6.1	Kinematics in FLRW spacetimes	121
6.2	Dynamics in FLRW spacetimes	123
6.3	Thermodynamics in FLRW spacetimes	124
6.4	N_{eff} from FLRW thermodynamics	129
6.5	Estimate of the neutrino decoupling temperature T_d	134
6.6	Measuring N_{eff} in the Standard Model: a quick overview	142
7	Corrections to $N_{\text{eff}} = 3$	151
7.1	BSM corrections: a theoretical and experimental overview . . .	152
7.2	The neutrino-never-coupled (NNC) approximation	156
7.3	Finite-temperature corrections to the QED equation of state .	158
7.4	Results within the instantaneous decoupling approximation (I)	167
7.5	Theoretical uncertainties from errors on measurements	168

Conclusion and Outlook	173
Appendices	175
A The 2PI effective action at 1-loop order	177
A.1 Leading order 1PI effective action	178
A.2 Next-to-leading order 1PI effective action	179
A.3 The one-loop 2PI effective action.	181
B Adiabatic propagators	183
B.1 Wentzel-Kramers-Brillouin solutions: derivation	183
B.2 The Boltzmann equation from QFT	190
B.3 The iterative solution of the Boltzmann equation	190
B.4 Gradient expansion of the distribution function	192
C Renormalising the 2PI equations of motion	195
C.1 Counterterms in the 2PI effective action	195
C.2 Renormalising at one-loop	197
C.3 Computations of the loops diagrams in the KBE	199
C.4 Renormalising the Kadanoff-Baym equations	203
C.5 Renormalised Markovian equation of motion	205
D Evaluating the crab diagram	209
E The neutrino-QED interaction rate	215
E.1 Connection of the damping rate to the Boltzmann collision term	215
E.2 Leading-order calculation of the damping rate	221

Introduction

The Universe we live in is undoubtedly expanding [1]. Particles, planets, galaxies, or structures in general are moving away from each other, and the greater the distance between them, the speedier the distancing velocity. They move apart because their support, our spacetime itself, is inflating, and it appears to have done so ever since the very first instants of its existence. Now turning the arrow of time, the Universe expansion becomes nothing but its contraction, and it collapses into itself. Therefore, at very early times, there are no more planets, or galaxies, just a very hot and dense primordial plasma made of elementary constituents of our Universe. The energy densities and conditions to which particles are exposed at those early times are tremendously more intense than any human-designed experiment will ever achieve. Therefore, the primordial Universe constitutes a perfect laboratory for physicists to try and test their high-energy fundamental theories of nature, simply by looking at nature itself. Describing the origin and evolution of our Universe, from its smallest elementary constituents that composed the primordial plasma to the large scale structures that make up the world around us today, is the field of physics known as cosmology.

After years and years of combined efforts, generations of relentless mathematicians and physicists have eventually come up with two mathematically very complicated, yet fantastically well-working theories of nature, namely the Standard Model (SM) of particle physics, and the Einstein gravity theory of General Relativity (GR), both of which are heavily used in cosmology. On one hand, the SM describes the quantum world of all elementary particles¹ and their interactions in the framework of relativistic quantum mechanics, also known as quantum field theories (QFT).

¹Particles which do not have subconstituents.

On the other, GR encodes gravity and the expansion of the Universe by a curved spacetime in which those particles move, interact and evolve. Those two theories combined with standard thermodynamics provide a rock solid framework to describe our Universe, from 10^{-43} seconds after its creation to the cosmos we observe today. Fortunately, this is not the end of this beautiful story. There are still many puzzles to be solved!

Indeed, claiming that the SM together with GR strictly suffice to go from 10^{-43} seconds after the creation of the Universe, all the way to today is an overstatement. They need to be supplemented by (a) a theory of cosmic inflation, (b) a dark matter candidate, and (c) a dark energy content, and all three must be consistent with observations. Let us briefly describe them.

In a nutshell, cosmic inflation (a) is a period of quasiexponentially accelerated expansion of the primeval Universe. We shall very shortly explain in detail why it ought to exist. Dark matter (b) is an optically invisible, gravitational source which we know must be present to e.g. explain certain galaxy rotations [2, 3]. Dark energy (c), also known as cosmological constant Λ , is a form of energy of negative pressure that is insensitive to the Universe expansion [4]. As it grows bigger and bigger, the dark energy density remains constant while other standard forms of energy get diluted away.

The current total energy budget of our Universe is constituted of 5% of ordinary matter, 27% of dark matter and 68% of dark energy. While those three features (a)-(c) of our Universe are crucial for our theoretical modelling of the cosmos, there is yet no consensus as to what is responsible for the origins of these peculiarities. Nevertheless, their existence is well-established in the scientific community and altogether, they compose the so-called standard big-bang models of cosmology, or Λ CDM cosmologies which thus far, pass with flying colors most observational tests they are confronted with.

With the ever-growing experimental precision, not only is there hope that we will eventually be able to distinguish different modellings of inflation, dark matter or energy, but also most certainly will we be able to pinpoint more accurately where exactly the standard model needs to be modified or completed. That of course is a valid statement only provided that theoretical predictions within the standard model match the current and forthcoming experimental resolutions. Unconventional models of inflation and precision cosmology precisely are the motivations for my PhD thesis, which is thus divided in two independent and equally important parts.

Part I. The first of these is motivated by the so-called warm inflation models [5–7], of potentially recognisable experimental signatures which, if chosen by nature, would radically change our perspectives on the formation of the seeds for galaxy formation. Let us briefly describe them. Cosmic inflation [8], be it standard or warm, is a period of quasiexponentially accelerated expansion of the Universe which, although initially invented to solve the problem of the absence of magnetic monopoles in theories of grand unification, is nowadays summoned to solve three “problems” of the standard model, namely

- **The homogeneity and isotropy problem.** Our cosmos is observed homogeneous and isotropic (up to very small perturbations), see Fig. 5.1. While this sounds appealing and reasonable, there is *a priori* no justification for it from a theoretical point of view, apart from the so-called “cosmological principle” which simply stipulates it to be so. As good physicists, we do not like postulates, we want logical explanations.
- **The flatness problem.** On cosmological scales, the spacetime curvature of the observable Universe appears to be flat, but again, we have no idea why, GR *a priori* allows for other geometries, too.
- **The horizon problem.** Due to Einstein’s theory of special and general relativity, our spacetime has a causal structure governed by the speed of light. Information cannot be passed from one source to the other instantaneously, and the transmission velocity is limited by the speed of light, hence creating so-called causal horizons, as depicted in Fig. 2. The horizon problem is that structures which should be causally disconnected according to the standard expansion of the Universe seem to have quite strongly communicated in the far past.

By drastically expanding the size of our Universe by at least 26 orders of magnitude, starting 10^{-36} seconds after the big-bang singularity, cosmic inflation solves all these three problems for almost any type of initial conditions. First, it nearly instantaneously dilutes away any particle content, hence bringing the Universe in an isotropic and homogeneous state. Second, it effectively flattens any curvature by making the observable Universe just a tiny portion of its total size, which globally may or may not be curved. And third, by enhancing the expansion rate, cosmic inflation enlarges the past horizons, causally reconnecting structures that would otherwise be disconnected. The observational constraints on cosmic inflation primarily affect its duration, it must be long enough so as to actually solve the aforementioned three problems. While this

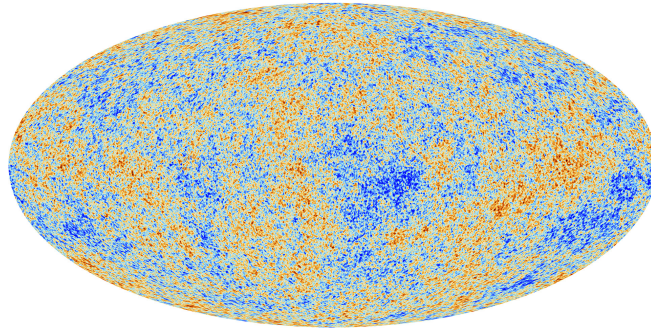


Figure 1: Full-sky measurement of the temperature of our Universe, which up to small deviations, is homogeneous and isotropic $T = 2.726 \pm 10^{-5}$ K [9].

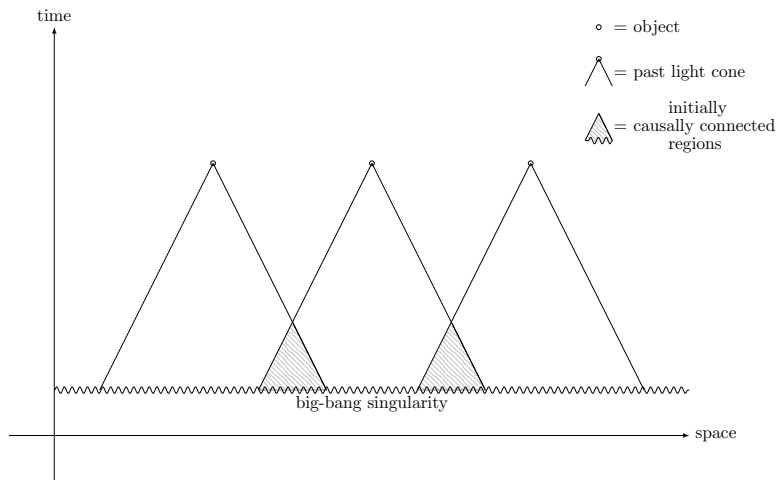


Figure 2: Two-dimensional causal structure of our Universe.

makes its modelling rather flexible, cosmic inflation is most commonly realised in the framework of relativistic QFT, by adding one or several scalar particles to the Standard Model of particle physics, the so-called inflaton(s). The standard inflationary paradigm [8, 10–12] unfolds as summarised in Fig. 3.

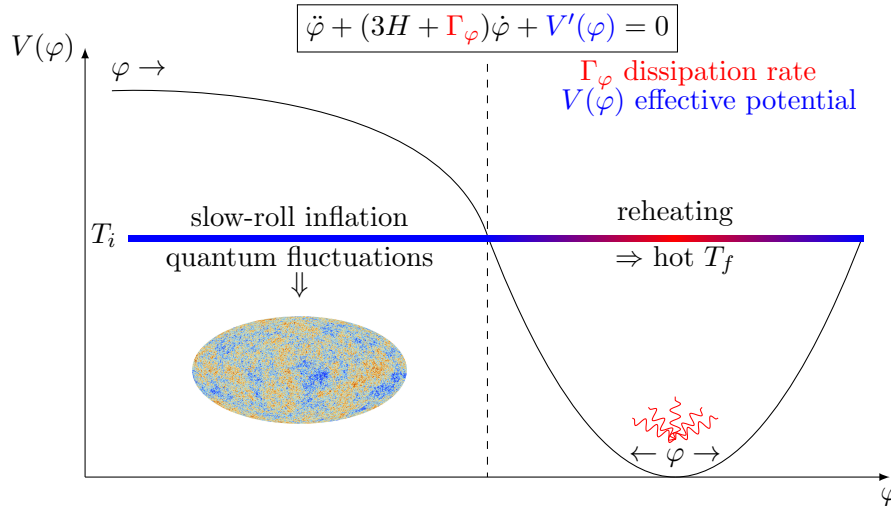


Figure 3: Effective potential driving standard inflation.

It takes place in two distinguished phases. It starts 10^{-36} seconds after the big-bang with a slowly-rolling field φ which potential energy $V(\varphi)$ dominates that of the Universe and consequently triggers inflation, cooling down the Universe down to a near-absolute-zero freezing temperature. The tiny quantum fluctuations of this field, once inflated on large scales, give rise to the tiny temperature fluctuations observed in the sky today. As the inflaton rolls down, its potential energy decreases more and more and eventually inflation stops. Then, the inflaton undergoes a phase of reheating during which most of its energy budget is transferred to SM particles via particle decays. The Universe transits from an ultracold quasiempty state to a hot soup of ultrarelativistic particles about 10^{-32} seconds after the big-bang singularity. This has to be the starting point of the thermal history of the Universe as we currently understand it. During both regimes, the fields follows the dynamical, differential equation of motion

$$\ddot{\varphi} + (3H + \Gamma_{\varphi})\dot{\varphi} + V'(\varphi) = 0 \quad (1)$$

where dots are time derivatives, H is the Universe expansion rate, also known as Hubble rate, Γ_{φ} is the damping rate, and $V'(\varphi)$ is the effective force determined from the slope of the potential. Depending on what phase of standard inflation is under consideration, inflation or reheating, then the dynamics is respectively potential- or dissipation-dominated and it is the careful, first principles analysis of these two that determine the feasibility of inflation models.

Though this standard picture for inflation is well-established and commonly accepted in the literature, in the late 1990s, there was proposed an alternative scenario to the standard paradigm, the so-called warm inflation scenario [5], which we summarise in Fig.4.

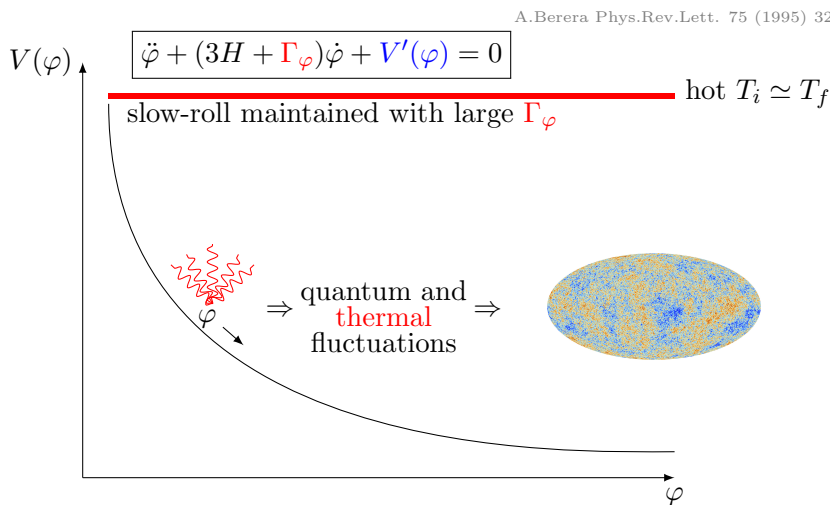


Figure 4: Effective potential driving warm inflation.

Instead of occurring in two distinguished, somewhat discontinuous phases, warm inflation smoothly transits from the inflationary regime to a hot radiation-dominated era. The long duration of inflation is guaranteed by a strong-dissipation-enforced slow-roll motion of the field, maintained through an enormous particle production which balances out with the cosmic inflation, and also keeps the temperature quasiconstant. In this scenario, the fluctuations that give rise to the observed temperature fluctuations are not only quantum, but also thermal, hence radically changing our conception of the origins of the seeds for galaxy formation.

While warm inflation is an attractive alternative to the standard archetype, its viability at the background level is disputed, see e.g. [5–7, 13, 14] for encouraging pieces of research that indicate its feasibility, in particular the most recent [15], vs. e.g. the more critical and pessimistic [16, 17]. Whatever the beliefs, all agree that formulating the model from first principles of nonequilibrium QFT is a complicated and rather poorly understood exercise which warrants investigation. It requires to address fundamental questions about the far-from-

equilibrium dynamics of scalar fields in the very early Universe and the first part of my thesis is precisely devoted to that.

Part II. The second part of this PhD thesis focuses on a precision computation of the effective number of cosmological neutrinos N_{eff} , a well-measured and beyond-standard-model-physics-sensitive cosmological observable. At temperatures of around $T \sim 10 \text{ MeV} \sim 10^{11} \text{ K}$, the Universe is primarily made of (anti)electrons e^\pm , photons γ and neutrinos, respectively kept at equilibrium by their electromagnetic and weak interactions. Roughly speaking, N_{eff} is then computed from precisely evaluating the late-time ratio of the photon to neutrino energy densities. Under the most simplifying assumptions, we find $N_{\text{eff}} = 3$, which is the number of neutrinos in the standard model, hence its name. A more refined computation of N_{eff} ought to be obtained from quantum thermofield dynamics. While this second part is less fundamental and conceptual than the first, it is more technical and required finer analytic and numerical techniques to achieve the unprecedented level of precision we were aiming at.

Outline of this thesis

In chapter 1, we review the framework of (non)equilibrium relativistic quantum field theory, which is used in both parts of the thesis.

Part I. In chapter 2, we derive from first principles of nonequilibrium QFT a model-independent inflation-like equation of motion (1) for a slowly-rolling scalar field φ . In the next two chapters 3 and 4, we particularise the discussion to a two-field scalar model wherein we perform a careful study and derive the main characteristics of the effective potential and damping rate associated with the method presented in the previous chapter 2. Then in chapter 5, we comment on the feasibility of warm inflation in that model. Eventually, we conclude and comment on future perspectives to part I.

Part II. In chapter 6, we briefly review ingredients of thermodynamics in expanding spacetimes and properly define N_{eff} in the framework of cosmological thermodynamics, and list where deviations from $N_{\text{eff}} = 3$ potentially come from. In chapter 7, we provide a standard model theoretical prediction for N_{eff} of unprecedented accuracy, a would-be state-of-the-art value for N_{eff} for future generations of experiments. Eventually, we conclude and comment on future perspectives to part II.

This PhD thesis is based on the following publications:

- G. Buldgen, M. Drewes, J. U. Kang and U. R. Mun, *General Markovian Equation for Scalar Fields in a Slowly Evolving Background*, 1912.02772,
- J. J. Bennett, G. Buldgen, M. Drewes, Y. Y. Wong, *Towards a precision calculation of the effective number of neutrinos N_{eff} in the Standard Model : The QED equation of state*, 1911.04504, JCAP 03 (2020) 003,
- G. Buldgen, M. Drewes, J. U. Kang and U. R. Mun, *Dissipation in a Coleman-Weinberg potential* (in preparation),
- J. J. Bennett, G. Buldgen, P. F. de Salas, M. Drewes, S. Gariazzo, S. Pastor and Y. Y. Wong, *Towards a precision calculation of N_{eff} in the Standard Model: Neutrino decoupling in the presence of flavour oscillations and finite-temperature QED* (in preparation).

Part I is the final outcome of my work with my closest collaborators Marco Drewes, Jin U Kang and Ui Ri Mun. Part II is a piece of work done in close collaboration with Marco Drewes, Jack Bennett and Yvonne Wong.

I also acknowledge the support of the National Fund for Scientific Research (F.R.S.- FNRS Belgium) through a FRiA grant for my PhD thesis.

Chapter 1

Common background

In this chapter, we dive into technicalities and present a detailed literature review of the theoretical frameworks employed throughout this thesis. We articulate the description of the background knowledge in two parts:

- (Non)equilibrium quantum field theory.
- 2 Particle Irreducible (2PI) effective action formalism.

We shall particularise the discussion to real scalar field degrees of freedom and provide a complete description of that case study, heavily relying on Refs. [18–22], wherein generalisations to other spins can be found, too. Throughout this thesis we shall use a unit system where the vacuum speed of light c , the reduced Planck constant \hbar and the Boltzmann constant k_B are unity $c = \hbar = k_B = 1$. Our Minkowski metric is $\eta = \text{diag}(+1, -1, -1, -1)$.

1.1 Elements of (non)equilibrium field theory

In this section we briefly describe how (non)equilibrium systems of interacting quantum fields can be studied using diagrammatic techniques by means of the so-called *Schwinger-Keldysh* [23, 24] or *Closed Time-Path* (CTP) formalism.

1.1.1 The system

The time evolution of the system under consideration is driven by the full, time-dependent Hamiltonian $H(t)$ which we decompose as

$$H(t) = H_0(t) + H_{\text{int}}(t), \quad (1.1)$$

where H_0 is the free Hamiltonian and H_{int} encodes the nontrivial time dependence and interactions between the fields. Unless specified otherwise, operators will be considered in the full Heisenberg picture, where their time evolution is dictated by the full Hamiltonian $H(t)$. In nonequilibrium situations, only the initial density matrix, which we denote $\varrho(t_i)$, is known and one is interested in computing the statistically weighted quantum expectation values

$$\langle O \rangle = \frac{\text{tr}[\varrho(t_i)O]}{\text{tr}[\varrho(t_i)]}, \quad (1.2)$$

also known as *ensemble averages*. The trace operator tr performs an average over the entire Hilbert space of the theory. If one has the decomposition

$$\varrho(t_i) = \sum_n \varrho_n |n\rangle\langle n|, \quad (1.3)$$

ensemble averages then evaluate to

$$\langle O \rangle = \frac{1}{Z} \sum_n \varrho_n \langle n|O|n \rangle, \quad (1.4)$$

where $Z = \sum_n \varrho_n$ is a normalisation factor and ϱ_n is the statistical weight of the quantum state $|n\rangle$.

Equilibrium systems. At thermal equilibrium, when a temperature $\beta = T^{-1}$ can be defined at all times, we have the grand canonical density matrix

$$\varrho = e^{-\beta(H-\mu N)}, \quad (1.5)$$

with μ the chemical potential and N the particle number operator. For the sake of this work, the systems under consideration will always be of vanishing chemical potential $\mu = 0$, hence studied in the so-called canonical formalism of statistical mechanics¹. The canonical density matrix reads

$$\varrho = \varrho^{(\text{eq})} = e^{-\beta H}. \quad (1.6)$$

¹Though notationally heavier, generalisations to the grand canonical ensemble in the presence of non vanishing chemical potentials are straightforward, see e.g. Ref. [21].

Together with the Hamiltonian eigenbasis $H|n\rangle = E_n|n\rangle$, this yields the usual Boltzmann weight $\varrho_n = e^{-\beta E_n}$ and equilibrium partition function

$$Z(\beta) = \text{Tr}[e^{-\beta H}] = \sum_n e^{-\beta E_n}, \quad (1.7)$$

which indicate that a system tends to relax to the microstate which minimises its energy functional. The lower the energy, the more statistically likely the state. An important point to be made here is the following. At thermal equilibrium, on top of ensemble averages of microphysical quantities, we can also determine thermodynamic quantities (and their associated quantum corrections) such as the pressure P , energy ρ and entropy s densities which characterise thermally averaged, bulk properties of the entire system. They are computed from the quantum partition function using the standard thermodynamic relations for infinite volume

$$P(T) = \frac{T}{V} \ln Z, \quad (1.8)$$

$$\rho(T) = \frac{T^2}{V} \frac{\partial \ln Z}{\partial T} = -P + T \frac{\partial P}{\partial T}, \quad (1.9)$$

$$s(T) = \frac{\rho + P}{T}. \quad (1.10)$$

The energy density $\rho(T)$ is not to be confused with the density matrix $\varrho(t)$.

1.1.2 Why do we need the Closed Time-Path ?

Ensemble averages are fundamentally different objects than the S-matrix elements one is usually interested in in zero temperature field theory or vacuum field theory. Therefore, they must unsurprisingly be studied using different tools. In this section, we argue why standard QFT techniques cannot straightforwardly be applied to compute nonequilibrium ensemble averages.

Zero-temperature field theory methods to compute vacuum quantum expectation values entirely rely on the so-called *Gell-Man-Low* (G-ML) theorem [25], which relates correlators on the interacting vacuum $|\Omega\rangle$ to correlators on the free vacuum $|0\rangle$ via the reduction formula

$$\langle \Omega | \mathcal{T} \{ O_1(t_1) \cdots O_n(t_n) \} | \Omega \rangle = \lim_{\epsilon \rightarrow 0^+} \frac{\langle 0 | \mathcal{T} \{ O_{1,I}(t_1) \cdots O_{n,I}(t_n) U_\epsilon(+\infty, -\infty) \} | 0 \rangle}{\langle 0 | U_\epsilon(+\infty, -\infty) | 0 \rangle}, \quad (1.11)$$

where \mathcal{T} is the time ordering operator, O_I are interaction picture operators² and U_ϵ is the time-evolution operator for the Hamiltonian

$$H_\epsilon(t) = H_0(t) + H_{\epsilon,\text{int}}(t) = H_0(t) + e^{-\epsilon|t|} H_{\text{int}}(t). \quad (1.13)$$

It is defined as

$$U(t, t_i) = \mathcal{T} \left\{ \exp \left[-i \int_{t_i}^t dt' H_I(t') \right] \right\}, \quad \text{with } U(t, t_i) = U^\dagger(t_i, t), \quad (1.14)$$

where $H_I(t) = e^{iH_0(t-t_i)} H_{\text{int}}(t) e^{-iH_0(t-t_i)}$ is the interaction Hamiltonian in the interaction picture. Identical expressions can be written with a subscript ϵ .

This whole procedure to evaluate correlators is however not appropriate for generic (non)equilibrium situations for two reasons. On one hand, though it is sometimes omitted in standard references, e.g. in Ref. [26], one has not to forget that the G-ML formula entirely relies on the matching conditions

$$H_0 = \lim_{\epsilon \rightarrow 0^+} H_\epsilon(+\infty), \quad H = \lim_{\epsilon \rightarrow 0^+} H_\epsilon(0), \quad (1.15)$$

which themselves crucially rely on the existence of an adiabatic mapping between H_{int} and $H_{\epsilon,\text{int}}$. In principle, this mapping cannot be achieved for generic nonequilibrium dynamics and in those situations where it is not, one fails to satisfy the GM-L assumptions and the entire zero temperature techniques fail to be reproduced.

On the other hand, ensemble averages of the form of Eq. (1.4) do not only involve vacuum correlators, rather they also require the computation of quantum expectation values on any state that spans the complete Hilbert space of the theory. There is no G-ML-like formula for these states whatsoever because another crucial assumption that leads to the GM-L formula is the nondegeneracy of the Hamiltonian spectrum. There is no obvious reasons to assume that the energy spectrum of a generic nonequilibrium system is nondegenerate.

Finally, we would like to comment that even in cases where the adiabatic mapping of Eq. (1.15) can be established, the resulting (non)equilibrium correlators could not be mapped to S-matrix elements via the *Lehmann-Symanzik-Zimmerman* (LSZ) formula. Indeed, the in- and out-states of the S-matrix and LSZ formulae are ill-defined for (non)equilibrium plasma where particles and states are never free and always surrounded by scattering partners.

²Operators in the interaction picture are Heisenberg operators from which the time-evolution of the free Hamiltonian has been extracted. Their time evolution is solely driven by that of H_{int} , and reads

$$O(t) = U(t_i, t) O_I(t) U(t, t_i). \quad (1.12)$$

1.1.3 The Closed Time-Path (CTP) formalism

From the previous discussion, it has become clear that standard techniques cannot be used to calculate (non)equilibrium ensemble averages. In principle, this is a disaster because vacuum field theory can be very conveniently and efficiently studied in the framework of Feynman's diagrammatics and we would of course preferably like to avoid the need for an entirely new formalism.

Based on Ref. [18], we here show that it is possible to construct a diagrammatic language convenient for real-life computations of nonequilibrium correlators, by means of the so-called Closed Time-Path (CTP) formalism.

In order to motivate and understand how it arises naturally, let us show that

$$O(t) = U^\dagger(t, t_i) O_I(t) U(t, t_i) = \mathcal{T}_C \left\{ e^{-i \int_{\mathcal{C}_t} dt' H_I(t')} O_I(t) \right\} \quad (1.16)$$

where \mathcal{T}_C is the time-ordering along the time-path \mathcal{C}_t depicted on Fig. 1.1.

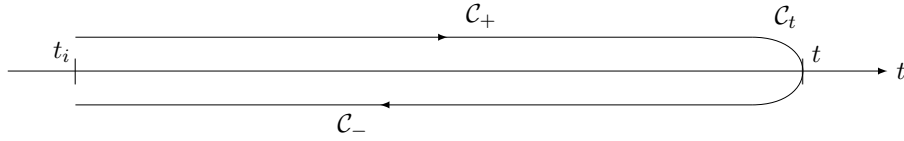


Figure 1.1: Finite-time Closed Time-Path (CTP).

Let us first expand the exponential, we find

$$\begin{aligned} & \mathcal{T}_C \left\{ e^{-i \int_{\mathcal{C}_t} d\tau H_I(\tau)} O_I(t) \right\} \\ &= \sum_{n=0}^{\infty} \frac{(-i)^n}{n!} \int_{\mathcal{C}_t} d\tau_1 \cdots \int_{\mathcal{C}_t} d\tau_n \mathcal{T}_{\mathcal{C}_t} \{ H_I(\tau_1) \cdots H_I(\tau_n) O_I(t) \}. \end{aligned}$$

The products of integrals over $\mathcal{C}_t = \mathcal{C}_+ + \mathcal{C}_-$ give rise to 2^n terms. Since the integration variables are dummy ones, we can rename them at our convenience to recast those 2^n terms into $\frac{n!}{m!(n-m)!}$ identical terms. Then, making use of

the time orientation along \mathcal{C}_t , we find

$$\begin{aligned} & \mathcal{T}_{\mathcal{C}} \left\{ e^{-i \int_{\mathcal{C}_t} d\tau H_I(\tau)} O_I(t) \right\} \\ &= \sum_{n=0}^{\infty} \frac{(-i)^n}{n!} \sum_{m=0}^n \frac{n!}{m!(n-m)!} \\ & \quad \times \int_{\mathcal{C}_-} d\tau_{m+1} \cdots \int_{\mathcal{C}_-} d\tau_n \mathcal{T}_{\mathcal{C}_-} \{ H_I(\tau_{m+1}) \cdots H_I(\tau_n) \} O_I(t) \\ & \quad \times \int_{\mathcal{C}_+} d\tau_1 \cdots \int_{\mathcal{C}_+} d\tau_m \mathcal{T}_{\mathcal{C}_+} \{ H_I(\tau_1) \cdots H_I(\tau_m) \}. \end{aligned}$$

Now by hand introducing a Kronecker's delta which allows us to re-express the sums, and then evaluating the sum over n explicitly, we find

$$\begin{aligned} & \mathcal{T}_{\mathcal{C}} \left\{ e^{-i \int_{\mathcal{C}_t} d\tau H_I(\tau)} O_I(t) \right\} \\ &= \sum_{n=0}^{\infty} \sum_{k=0}^{\infty} \sum_{m=0}^{\infty} \frac{(-i)^n}{m!k!} \delta_{n,k+m} \\ & \quad \times \int_{\mathcal{C}_-} d\tau_1 \cdots \int_{\mathcal{C}_-} d\tau_k \mathcal{T}_{\mathcal{C}_-} \{ H_I(\tau_1) \cdots H_I(\tau_k) \} O_I(t) \\ & \quad \times \int_{\mathcal{C}_+} d\tau_1 \cdots \int_{\mathcal{C}_+} d\tau_m \mathcal{T}_{\mathcal{C}_+} \{ H_I(\tau_1) \cdots H_I(\tau_m) \} \\ &= \sum_{k=0}^{\infty} \sum_{m=0}^{\infty} \frac{(-i)^k (-i)^m}{m!k!} \int_{\mathcal{C}_-} d\tau_1 \cdots \int_{\mathcal{C}_-} d\tau_k \mathcal{T}_{\mathcal{C}_-} \{ H_I(\tau_1) \cdots H_I(\tau_k) \} O_I(t) \\ & \quad \times \int_{\mathcal{C}_+} d\tau_1 \cdots \int_{\mathcal{C}_+} d\tau_m \mathcal{T}_{\mathcal{C}_+} \{ H_I(\tau_1) \cdots H_I(\tau_m) \}. \end{aligned}$$

Therefore, we find

$$\mathcal{T}_{\mathcal{C}} \left\{ e^{-i \int_{\mathcal{C}_t} d\tau H_I(\tau)} O_I(t) \right\} = \mathcal{T}_{\mathcal{C}_-} \left\{ e^{-i \int_{\mathcal{C}_-} d\tau H_I(\tau)} \right\} O_I(t) \mathcal{T}_{\mathcal{C}_+} \left\{ e^{-i \int_{\mathcal{C}_+} d\tau H_I(\tau)} \right\}. \quad (1.17)$$

On one hand, since the forward region of the CTP is just the usual time orientation $\mathcal{T}_{\mathcal{C}_+} = \mathcal{T}$, we can immediately see that

$$\mathcal{T}_{\mathcal{C}_+} \left\{ e^{-i \int_{\mathcal{C}_+} d\tau H_I(\tau)} \right\} = T \left\{ e^{-i \int_{t_i}^t d\tau H_I(\tau)} \right\} = \hat{U}(t, t_i).$$

On the other hand, using $H_I^\dagger = H_I$ and that the time orientation of \mathcal{C}_- is just about running backwards, we evaluate

$$\begin{aligned}
& \mathcal{T}_{\mathcal{C}_-} \left\{ e^{-i \int_{\mathcal{C}_-} d\tau H_I(\tau)} \right\} \\
&= \sum_{n=0}^{\infty} \frac{(-i)^n}{n!} \int_t^{t_i} d\tau_1 \cdots d\tau_n \mathcal{T}_{\mathcal{C}_-} \{ H_I(\tau_1) \cdots H_I(\tau_n) \} \\
&= \sum_{n=0}^{\infty} \frac{(-i)^n}{n!} \int_t^{t_i} d\tau_1 \cdots d\tau_n (\mathcal{T} \{ H_I(\tau_1) \cdots H_I(\tau_n) \})^\dagger \\
&= \left(\sum_{n=0}^{\infty} \frac{(-1)^n (-i)^n}{n!} \int_t^{t_i} d\tau_1 \cdots d\tau_n \mathcal{T} \{ H_I(\tau_1) \cdots H_I(\tau_n) \} \right)^\dagger \\
&= \left(\sum_{n=0}^{\infty} \frac{(-i)^n}{n!} \int_{t_i}^t d\tau_1 \cdots d\tau_n \mathcal{T} \{ H_I(\tau_1) \cdots H_I(\tau_n) \} \right)^\dagger = U^\dagger(t, t_i).
\end{aligned}$$

At the end of the day, we find

$$\mathcal{T}_{\mathcal{C}} \left\{ e^{-i \int_{\mathcal{C}_i} d\tau H_I(\tau)} O_I(t) \right\} = U^\dagger(t, t_i) O_I(t) U(t, t_i) = O(t). \quad (1.18)$$

This result is crucial. We showed that any operator in the full Heisenberg picture can formally be described by CTP-ordered products of operators. This motivates the natural democratisation of standard time arguments to CTP-generalised ones. Taking this step forward, one embarks on the Schwinger-Keldysh or CTP formulation of nonequilibrium QFT.

1.1.4 CTP-ordered n -point functions

Let us apply this method to contour-ordered two-point functions $\Delta(x, y)$ to show it expresses it in terms of Feynman diagrams in a similar fashion to the zero temperature case. $\Delta(x, y)$ is defined as the connected part of the contour-ordered 2-point functions, namely

$$\Delta(x, y) = \langle \mathcal{T}_{\mathcal{C}} \{ \phi(x) \phi(y) \} \rangle - \varphi(x) \varphi(y), \quad (1.19)$$

where $\varphi(x) = \langle \phi(x) \rangle$. Though not necessary strictly speaking, for simplicity, we shall assume $\varphi(x) = 0$ and find for the contour-ordered two-point function

$$\begin{aligned}
\Delta(x, y) &= Z^{-1} \text{tr} \left[\varrho(t_i) \mathcal{T}_{\mathcal{C}} \left\{ e^{-i \int_{\mathcal{C}_x} d\tau H_I(\tau)} \phi_I(x) \right\} \mathcal{T}_{\mathcal{C}} \left\{ e^{-i \int_{\mathcal{C}_y} d\tau H_I(\tau)} \phi_I(y) \right\} \right] \\
&= Z^{-1} \text{tr} \left[\varrho(t_i) \mathcal{T}_{\mathcal{C}} \left\{ e^{-i \int_{\mathcal{C}_x + \mathcal{C}_y} d\tau H_I(\tau)} \phi_I(x) \phi_I(y) \right\} \right],
\end{aligned}$$

where the subscript x (resp. y) denotes that the contour \mathcal{C}_x (resp. \mathcal{C}_y) stretches from t_i to x^0 (resp. y^0) and back to t_i , as shown on Fig. 1.2. Here we also

have used that under contour ordering, operators commute and exponentials of operators can be assembled as one usually would with exponentials of numbers.

Now realising that the contributions from the dashed regions of the closed contours \mathcal{C}_x and \mathcal{C}_y depicted on Fig. 1.2 cancel because in those regions the field operators do not intervene and need not be ordered, we obtain

$$\Delta(x, y) = Z^{-1} \text{tr} \left[\varrho(t_i) \mathcal{T}_C \left\{ e^{-i \int_{\mathcal{C}_{t_{\max}}} d\tau H_I(\tau)} \phi_I(x) \phi_I(y) \right\} \right], \quad (1.20)$$

where $t_{\max} = \max(x^0, y^0)$.

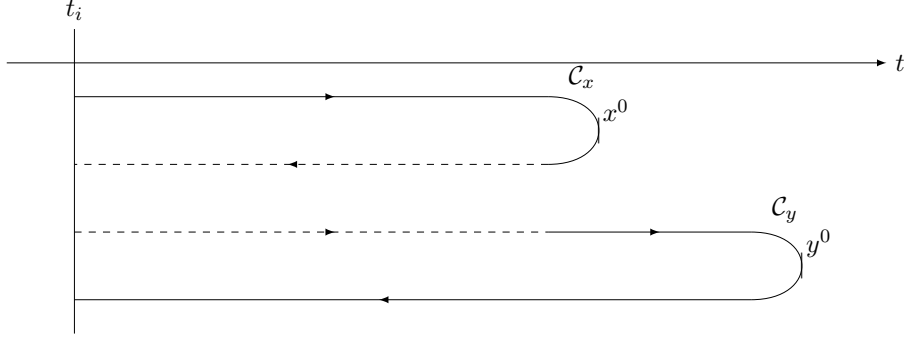


Figure 1.2: Overlapped closed contours for nonlocal two-point functions.

Playing the same game with the insertions of the field operators, one can equivalently extend $\mathcal{C}_{t_{\max}}$ all the way to $+\infty$, leading to the usual CTP, denoted \mathcal{C}_i , which extends from t_i to $+\infty$ and back. The latter is depicted on Fig. 1.3. For the nonequilibrium two-point function, we obtain

$$\Delta(x, y) = Z^{-1} \text{tr} \left[\varrho(t_i) \mathcal{T}_C \left\{ e^{-i \int_{\mathcal{C}_i} d\tau H_I(\tau)} \phi_I(x) \phi_I(y) \right\} \right]. \quad (1.21)$$

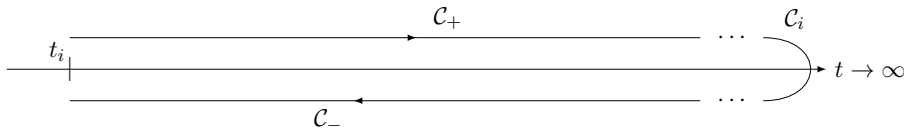


Figure 1.3: Infinite-time Closed Time-Path (CTP)

Realising that this procedure could have equivalently been dealt with, with infinitely many field operator insertions, we find the n -point correlators as

$$\langle \mathcal{T}_C \{ \phi_1(x_1) \cdots \phi_n(x_n) \} \rangle_{\text{conn.}} = \frac{\text{tr} \left[\varrho(t_i) \mathcal{T}_C \left\{ e^{-i \int_{C_i} d\tau H_I(\tau)} \phi_{1,I}(x_1) \cdots \phi_{n,I}(x_n) \right\} \right]}{\text{tr}[\varrho(t_i)]}. \quad (1.22)$$

This can be further simplified in the equilibrium case where

$$\varrho(t_i) = \varrho^{(\text{eq})} = e^{-\beta H} = e^{-\beta H_0} \mathcal{T}_\downarrow \left\{ e^{-i \int_{t_i}^{t_i - i\beta} d\tau H_I(\tau)} \right\} \quad (1.23)$$

where the integration is made along the imaginary axis, from t_i to $t_i - i\beta$ following a downward-oriented (denoted by \downarrow) path. Combining this together with Eq. (1.21), we can eventually recast everything in terms of one single contour-ordered integral along a specific time-path \mathcal{C}_β depicted in Fig. 1.4.

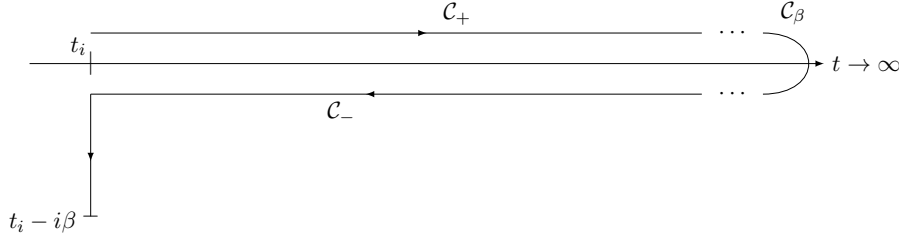


Figure 1.4: Finite temperature CTP.

The resulting equilibrium propagator reads

$$\Delta^{(\text{eq})}(x, y) = Z^{(\text{eq})-1} \text{tr} \left[e^{-\beta H_0} \mathcal{T}_{\mathcal{C}_\beta} \left\{ e^{-i \int_{\mathcal{C}_\beta} d\tau H_I(\tau)} \phi_I(x) \phi_I(y) \right\} \right]. \quad (1.24)$$

Again using that while subject to contour-ordering, operators commute, together with the relation $\mathcal{T}_C \left\{ e^{-i \int_{C_i} d\tau H_I(\tau)} \right\} = \mathbb{I}$, we have that the denominator of Eq. (1.24) rewrites

$$\begin{aligned} Z^{(\text{eq})} &= \text{tr} \left[e^{-\beta H_0} \mathcal{T}_\downarrow \left\{ e^{-i \int_{t_i}^{t_i - i\beta} d\tau H_I(\tau)} \right\} \right] \\ &= \text{tr} \left[e^{-\beta H_0} \mathcal{T}_{\mathcal{C}_\beta} \left\{ e^{-i \int_{\mathcal{C}_\beta} d\tau H_I(\tau)} \right\} \right], \end{aligned} \quad (1.25)$$

simply because $\mathcal{C}_\beta = \mathcal{C}_i + [t_i, t_i - i\beta]$. Eq. (1.24) therefore reads

$$\Delta^{(\text{eq})}(x, y) = \frac{\text{tr} \left[e^{-\beta H_0} \mathcal{T}_{\mathcal{C}_\beta} \left\{ e^{-i \int_{\mathcal{C}_\beta} d\tau H_I(\tau)} \phi_I(x) \phi_I(y) \right\} \right]}{\text{tr} \left[e^{-\beta H_0} \mathcal{T}_{\mathcal{C}_\beta} \left\{ e^{-i \int_{\mathcal{C}_\beta} d\tau H_I(\tau)} \right\} \right]}. \quad (1.26)$$

When put under this form, the connection to zero-temperature QFT [26] is clearer. Wick's theorem together with the combinatorial arguments apply, the disconnected diagrams from the numerator precisely cancel with the sum of vacuum diagrams of the denominator. Then, one is left with a suitable perturbative expansion of connected Feynman diagrams, except it is for contour-ordered propagators, such that a matrix structure underlies the diagrammatical construction. Adopting the path integral formalism, we shall explicitly show this both for the equilibrium and nonequilibrium propagators. Before moving on to that, let us quickly comment and define how yet another contour, the Schwinger-Keldysh one, can be employed for certain nonequilibrium systems.

1.1.5 The Schwinger-Keldysh contour

In situations where the microscopic time scale τ_{int} of the particle interactions is shorter than the macroscopic time scale which characterises the time evolution of bulk properties of the system, we can let $t_i \rightarrow -\infty$. This corresponds to $\tau_{\text{int}} \rightarrow 0$ versus the macroscopic evolution time scale. In such situations, one is left with the so-called *Schwinger-Keldysh* contour depicted on Fig. 1.5, both in the equilibrium and nonequilibrium cases.

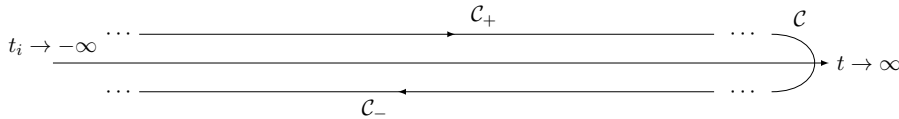


Figure 1.5: Schwinger-Keldysh CTP

Looking at Eqs. (1.24) and (1.36), it is less obvious that one ends up with the Schwinger-Keldysh CTP starting from the equilibrium contour \mathcal{C}_β of Fig. 1.4, because that means we somehow got rid of the $[t_i, t_i - i\beta]$ part of the contour. Let us explain why this is effectively what happens when we let t_i approach $-\infty$. Physically, this is because any propagator with a time argument in the imaginary time stretch gets damped very quickly, on the microscopic time scales of scattering events τ_{int} . Mathematically, it can be shown [20] that any two-point function with a time argument belonging in the imaginary stretch $[-\infty, -\infty - i\beta]$ is vanishing. Equivalently the integration of the $[-\infty, -\infty - i\beta]$ band at the level of the generating functional (to be defined next) can be performed, and it leaves us with an inconsequential normalisation factor [21]. We shall prove both later for the leading order thermal propagators.

On the Schwinger-Keldysh contour, two-point functions, e.g. the contour-ordered propagators $\Delta(x, y)$, are split in four components

$$\Delta(x, y) = \begin{cases} \Delta^{++}(x, y) = \Delta^F(x, y), & \text{if } x^0, y^0 \in \mathcal{C}_+ \\ \Delta^{+-}(x, y) = \Delta^<(x, y), & \text{if } x^0 \in \mathcal{C}_+, y^0 \in \mathcal{C}_- \\ \Delta^{-+}(x, y) = \Delta^>(x, y), & \text{if } x^0 \in \mathcal{C}_-, y^0 \in \mathcal{C}_+ \\ \Delta^{--}(x, y) = \Delta^{\bar{F}}(x, y), & \text{if } x^0, y^0 \in \mathcal{C}_- \end{cases}$$

where F and \bar{F} respectively stand for Feynman- and anti-Feynman-ordered propagators, $>$ and $<$ stand for the usual greater and lesser Wightman propagators. For those, the time ordering is automatically set since their time arguments belong to different branches of the contour. The same decomposition can be achieved for all functions on the CTP. The more time arguments x_1^0, \dots, x_n^0 , the more Schwinger-Keldysh labels or polarities \pm, \dots, \pm .

1.1.6 The CTP generating functional

From the previous discussion, a natural CTP-generalised generating functional for both the in- and out-of-equilibrium 1- and 2-point functions is

$$Z[J, R] = \text{tr} \left[\varrho(t_i) \mathcal{T}_C \left\{ e^{i \left[\int_x J(x) \phi(x) + \frac{1}{2} \int_{x,y} R(x,y) \phi(x) \phi(y) \right]} \right\} \right], \quad (1.27)$$

where $\int_x = \int_{\mathcal{C}_i} \int d^3\mathbf{x}$. $J(x)$ and $R(x, y)$ respectively are the local and nonlocal sources, both of which will be needed later on to define the 2 Particle Irreducible effective action 1.2. Taking functional derivatives of $Z[J, R]$ with respect to J (resp. R), evaluating it for vanishing sources and normalising the result to $Z(0, 0)$, one obviously obtains the n -point functions of the theory.

Expanding the trace operator and using the *initial time* completeness relation³, let us re-express the generating functional by means of a path integral

$$\begin{aligned} Z[J, R] &= \int d\phi_1 \langle \phi_1 | \varrho(t_i) \mathcal{T}_C \left\{ e^{i \left[\int_x J(x) \phi(x) + \frac{1}{2} \int_{x,y} R(x,y) \phi(x) \phi(y) \right]} \right\} | \phi_1 \rangle \\ &= \int d\phi_1 d\phi_2 \langle \phi_1 | \varrho(t_i) | \phi_2 \rangle \langle \phi_2 | \mathcal{T}_C \left\{ e^{i \left[\int_x J(x) \phi(x) + \frac{1}{2} \int_{x,y} R(x,y) \phi(x) \phi(y) \right]} \right\} | \phi_1 \rangle \\ &= \int d\phi_1 d\phi_2 \langle \phi_1 | \varrho(t_i) | \phi_2 \rangle \longrightarrow \text{initial conditions} \\ &\times \underbrace{\int_{\phi(t_i^+) = \phi_1}^{\phi(t_i^-) = \phi_2} \mathcal{D}\phi e^{i [S_{C_i}[\phi] + \int_x J(x) \phi(x) + \frac{1}{2} \int_{x,y} R(x,y) \phi(x) \phi(y)]]}_{\longrightarrow \text{quantum dynamics}}, \end{aligned} \quad (1.28)$$

³We expand on the initial time configuration space $\phi(t_i, \mathbf{x}) | \phi_1; t_i \rangle = \phi(t_i, \mathbf{x}) | \phi_1 \rangle = \phi_{1\mathbf{x}} | \phi_1 \rangle$. Same for $|\phi_2\rangle$. In the Schrödinger picture, the states are then evolved according to time evolution operator as $\langle \phi; t_i | e^{-iH\Delta t} = \langle \phi; t_i + \Delta t |$.

where $S_{\mathcal{C}_i}[\phi] = \int_{\mathcal{C}_i} \int d^3\mathbf{x} \mathcal{L}$ is the action functional of the field theory under consideration, where the time integration is performed over \mathcal{C}_i . Rigorously speaking, one should quickly comment that we have an abuse of notation was made in Eq. (1.28). First, we did not distinguish the field operator of Eq. (1.27) from its functional counterpart of Eq. (1.28). Second, we used a condensed way of referring to the infinitely many field theoretical degrees of freedom $\phi_{\mathbf{x}}(t) = \phi(t, \mathbf{x}) = \phi(x)$, $\forall \mathbf{x} \in \mathbb{R}^3$, carefully distinguishing between a standard ($d\phi$) and a functional ($\mathcal{D}\phi$) integration measure⁴

$$\int d\phi = \int \prod_{\mathbf{x} \in \mathbb{R}^3} d\phi_{\mathbf{x}}, \quad \langle \phi | = \bigotimes_{\mathbf{x} \in \mathbb{R}^3} \langle \phi_{\mathbf{x}} |, \quad (1.29)$$

$$\int_{\phi(t_i^+) = \phi_1}^{\phi(t_i^-) = \phi_2} \mathcal{D}\phi = \int_{\phi(t_i^+, \mathbf{x}) = \phi_{1\mathbf{x}}, \forall \mathbf{x} \in \mathbb{R}^3}^{\phi(t_i^-, \mathbf{x}) = \phi_{2\mathbf{x}}, \forall \mathbf{x} \in \mathbb{R}^3} \prod_{\mathbf{x} \in \mathbb{R}^3} \mathcal{D}\phi(t, \mathbf{x}). \quad (1.30)$$

The generating functional of Eq. (1.28) can equivalently be used for both equilibrium and out-of-equilibrium situations. Under this form, it displays the two main features of nonequilibrium quantum field theory, expressed as an initial value problem: the dependence on initial conditions is captured by the initial-time correlators $\langle \phi_1 | \varrho(t_i) | \phi_2 \rangle$ and the quantum dynamics is to be identified with the subsequent path integral in Eq.(1.28).

Gaussian initial conditions. The case of nonequilibrium Gaussian initial conditions where all n -point functions can be determined from the 1- and 2-point correlators allows for further simplifications of the generating functional. First, note that $\langle \phi_1 | \varrho(t_i) | \phi_2 \rangle$ in Eq. (1.28) can be brought through the path integral $\int_{\phi(t_i^+) = \phi_1}^{\phi(t_i^-) = \phi_2} \mathcal{D}\phi$. That said, it is shown [19] that for arbitrary Gaussian initial conditions we have for $\mathcal{F}[\phi]$ some arbitrary functional of ϕ

$$\int_{\phi(t_i^+) = \phi_1}^{\phi(t_i^-) = \phi_2} \mathcal{D}\phi \langle \phi_1 | \varrho(t_i) | \phi_2 \rangle \mathcal{F}[\phi] = \mathcal{N} \int_{\phi(t_i^+) = \phi_1}^{\phi(t_i^-) = \phi_2} \mathcal{D}\phi e^{if[\phi]} \mathcal{F}[\phi], \quad (1.31)$$

where \mathcal{N} is an irrelevant normalisation factor, $f[\phi] = \alpha_0 + \int_x \alpha_1(x)\phi(x) + \frac{1}{2} \int_{xy} \alpha_2(x, y)\phi(x)\phi(y)$ depends on the explicit Gaussian form of $\varrho(t_i)$ and ϕ is precisely that of the path integral. Indeed, the Gaussian initial density matrix $\varrho(t_i)$ is expressed through a Gaussian function of the field operators evaluated

⁴Here the infinite factor that arises from the discretisation of the time interval under consideration was also absorbed into the definition of the path integral measure [22, 27]. That physically irrelevant prefactor always cancels out to give a finite results for all quantities of interest in this work.

at t_i . Therefore, due to the path integral boundary conditions, those initial-time operators equivalently evaluate to ϕ once they act on the initial-time states $|\phi_1\rangle$ or $|\phi_2\rangle$. One last subtlety is hidden in the functions $\alpha_i(x)$, $i = 1, 2$, which in $f[\phi]$ appear to be generic functions for arbitrary time arguments. However, those technically only evaluate to nonzero values when $x^0 = t_i$ since they are parameters that characterise the initial density matrix $\varrho(t_i)$. In mathematical words the last two statements regarding ϕ and the functions α_i can be understood by explicitly expanding our condensed notation

$$\begin{aligned} \int_x \alpha_1(x)\phi(x) &= \int d^3\mathbf{x} [\alpha_1^+(\mathbf{x})\phi(t_i^+, \mathbf{x}) + \alpha_1^-(\mathbf{x})\phi(t_i^-, \mathbf{x})] \\ &= \int d^3\mathbf{x} [\alpha^+(\mathbf{x})\phi_{1\mathbf{x}} + \alpha^-(\mathbf{x})\phi_{2\mathbf{x}}] \end{aligned}$$

and similarly for $\alpha_2(x, y)$ except the structure is slightly more complicated since there are two CTP integrations to deal with.

Bringing these expressions into a form where we unnecessarily integrate them over the whole CTP however helps us rewrite the generating functional in a more familiar shape. Indeed, by making the replacements $J \rightarrow J - \alpha_1$ and $R \rightarrow R - \alpha_2$ and neglecting the multiplicative constant $\mathcal{N}e^{i\alpha_0}$, we get the Gaussian generating functional

$$\begin{aligned} Z[J, R] &= \int d\phi_1 d\phi_2 \\ &\int_{\phi(t_i^+) = \phi_1}^{\phi(t_i^-) = \phi_2} \mathcal{D}\phi \exp i \left[S_{C_i}[\phi] + \int_x J(x)\phi(x) + \frac{1}{2} \int_{xy} R(x, y)\phi(x)\phi(y) \right] \end{aligned} \quad (1.32)$$

which is independent of $\varrho(t_i)$. Since we integrate over all configurations $|\phi_i\rangle$, $i = 1, 2$, we can equivalently rewrite this as

$$Z[J, R] = \int \mathcal{D}\phi \exp i \left[S_{C_i}[\phi] + \int_x J(x)\phi(x) + \frac{1}{2} \int_{xy} R(x, y)\phi(x)\phi(y) \right] \quad (1.33)$$

where we implicitly integrate over all possible paths of arbitrary boundary conditions at t_i^\pm , the end and beginning of the CTP. It is important to note here that while this trick of replacing $J \rightarrow J - \alpha_1$ and $R \rightarrow R - \alpha_2$ conveniently expresses the generating functional in the standard form (1.33), it also very subtly gets rid of our initial conditions. Therefore, it should not be forgotten that the generating functional (1.33) can only be used for nonequilibrium problems with (arbitrary) Gaussian initial conditions, which always ought to be

supplemented “by hand” to any dynamical equations for the n -point correlators, as e.g. derived from an n PI effective action [19]. Had we not absorbed the boundary terms in the sources, they would just appear as surface terms in the action of the generating functional, and then consequently in the equations of motion for the n -point functions. The same goes for non-Gaussian initial conditions [28].

The equilibrium generating functional. At equilibrium, the density matrix reads $\varrho(t_i) = \varrho^{(\text{eq})} = e^{-\beta H}$ and Eq. (1.27) can be rewritten as

$$Z^{(\text{eq})}[J, R] = \int d\phi \langle \phi; t_i | e^{-\beta H} \mathcal{T}_C \left\{ e^{i \left[\int_x J(x) \phi(x) + \frac{1}{2} \int_{xy} R(x, y) \phi(x) \phi(y) \right]} \right\} | \phi; t_i \rangle \quad (1.34)$$

which, recalling that H is the generator of time translations, yields

$$Z^{(\text{eq})}[J, R] = \int d\phi \langle \phi; t_i - i\beta | \mathcal{T}_C \left\{ e^{i \left[\int_x J(x) \phi(x) + \frac{1}{2} \int_{xy} R(x, y) \phi(x) \phi(y) \right]} \right\} | \phi; t_i \rangle. \quad (1.35)$$

Again turning this into a functional integral, we find that one has to integrate over paths which not only have to be analytically continued to the complex plane, but also have to be $-i\beta$ -cyclic. Therefore, we naturally are led to consider configurations which time evolutions take place on the time-path \mathcal{C}_β of Fig. 1.4. In mathematical words, making the same abuse of notation, one obtains

$$Z^{(\text{eq})}[J, R] = \int_{\text{cyclic}}^{} \mathcal{D}\phi(t) e^{i \left[S_{\mathcal{C}_\beta}[\phi] + \int_x J(x) \phi(x) + \frac{1}{2} \int_{xy} R(x, y) \phi(x) \phi(y) \right]}, \quad (1.36)$$

where \int_x is now performed over \mathcal{C}_β and the path integration is performed over all $-i\beta$ -cyclic fields. As we shall come back to later on, this cyclicity is what is responsible for all finite temperature effects in field theory. As an example, let us study the leading-order equilibrium partition function $Z(\beta)$.

1.1.7 Leading-order equilibrium thermodynamics

For vanishing sources $J = R = 0$, the generating functional (1.36) also gives the perturbative expansion for the field theoretical partition function $Z(\beta)$ of Eq. (1.7). In perturbative real scalar quantum field theories, we have

$$S[\phi] = \frac{1}{2} \int_x \phi(x) (\square_x + m^2) \phi(x) + \lambda \mathcal{F}[\phi] \quad (1.37)$$

where $\square = \partial_\mu \partial^\mu = \partial_t^2 - \nabla^2$ and λ is a small expansion parameter and $\mathcal{F}[\phi]$ an arbitrary functional of ϕ that has the dimensions of an action. Therefore, at leading order in λ , the thermodynamic partition function reads

$$Z^{(0)}(\beta) = \int_{\text{cyclic}}^{-i\beta} \mathcal{D}\phi(t) e^{-\frac{i}{2} [\int_x \phi(x) (\square_x + m^2) \phi(x)]}, \quad (1.38)$$

where the superscript (0) refers to the zeroth order expansion in λ . Due to their $-i\beta$ cyclicity, without loss of generality, the field configurations can be decomposed in Fourier series

$$\phi(x) = \sqrt{\frac{-i\beta}{V}} \sum_{n=-\infty}^{+\infty} e^{-i\omega_n x^0} \sum_{\mathbf{p}} e^{i\mathbf{p}\cdot\mathbf{x}} \phi(\mathbf{p}), \quad (1.39)$$

with V the thermodynamic volume and $\omega_n = \frac{2\pi n}{-i\beta}$. The function $\phi(x)$ is now solely determined by its amplitudes $\phi_n(\mathbf{p})$ and using the real scalar property $\phi_{-n}(-\mathbf{p}) = (\phi_n(\mathbf{p}))^*$, the partition function rewrites

$$Z^{(0)}(\beta) = \mathcal{N} \int_{-\infty}^{+\infty} \prod_m d|\phi_m(\mathbf{p})| \exp \left[-\frac{\beta^2}{2} \sum_n \sum_{\mathbf{p}} (-\omega_n^2 + \omega_{\mathbf{p}}^2) |\phi_n(\mathbf{p})|^2 \right],$$

where \mathcal{N} is an irrelevant constant for thermodynamic considerations and $\omega_{\mathbf{p}}^2 = m^2 + \mathbf{p}^2$ is the leading-order dispersion relation. Performing the independent Gaussian integrals over each individual $|\phi_n(\mathbf{p})|$, and neglecting yet another irrelevant constant, we find

$$\ln Z^{(0)}(\beta) = -\frac{1}{2} \sum_n \sum_{\mathbf{p}} \ln (\beta^2 (-\omega_n^2 + \omega_{\mathbf{p}}^2)) = -\frac{1}{2} \sum_n \sum_{\mathbf{p}} \ln [(2\pi n)^2 + \beta^2 \omega_{\mathbf{p}}^2]. \quad (1.40)$$

The frequency sum over n can be evaluated using the following two relations

$$\begin{aligned} \ln [(2\pi n)^2 + \beta^2 \omega_{\mathbf{p}}^2] &= \int_1^{\beta^2 \omega_{\mathbf{p}}^2} \frac{d\rho^2}{\rho^2 + (2\pi n)^2} + \ln [1 + (2\pi n)^2], \\ \sum_n (n^2 + (\rho/2\pi)^2)^{-1} &= \frac{2\pi^2}{\rho} (1 + 2f_B(\rho)). \end{aligned}$$

where

$$f_B(\omega_{\mathbf{p}}) = (e^{\beta\omega_{\mathbf{p}}} - 1)^{-1}, \quad (1.41)$$

is the so-called Bose-Einstein phase space distribution function. It satisfies

$$1 + f_B(q^0) + f_B(-q^0) = 0, \quad \coth\left(\frac{\beta q^0}{2}\right) = 1 + 2f_B(q^0), \quad (1.42)$$

often used throughout this thesis. Neglecting a V - and β -independent term and letting $\sum_{\mathbf{p}} \rightarrow V \int \frac{d^3 \mathbf{p}}{(2\pi)^3}$, we find

$$\ln Z^{(0)}(\beta) = V \int \frac{d^3 \mathbf{p}}{(2\pi)^3} \left(-\frac{\beta \omega_{\mathbf{p}}}{2} - \ln [1 - e^{-\beta \omega_{\mathbf{p}}}] \right). \quad (1.43)$$

The first term is the so-called zero-point energy that arises for quantum mechanical harmonic oscillators too and it ought to be subtracted if the vacuum is to be a zero-energy state. The remaining associated leading-order pressure (1.8) and energy density (1.9) are

$$P^{(0)} = -T \int \frac{d^3 \mathbf{p}}{(2\pi)^3} \ln [1 - e^{-\beta \omega_{\mathbf{p}}}] = \int \frac{d^3 \mathbf{p}}{(2\pi)^3} \frac{\mathbf{p}^2}{3\omega_{\mathbf{p}}} f_B(\omega_{\mathbf{p}}), \quad (1.44)$$

$$\rho^{(0)} = \int \frac{d^3 \mathbf{p}}{(2\pi)^3} \omega_{\mathbf{p}} f_B(\omega_{\mathbf{p}}). \quad (1.45)$$

These $P^{(0)}$ and $\rho^{(0)}$ are nothing but the usual pressure and energy densities for an ideal gas of noninteracting bosons. At high temperatures with respect to the particles bare mass, i.e. when $T \gg m$, and the particles are effectively ultrarelativistic and

$$P^{(0)} \xrightarrow{T \gg m} P_r = \frac{\pi^2}{90} T^4, \quad \rho^{(0)} \xrightarrow{T \gg m} \rho_r = \frac{\pi^2}{30} T^4 = 3P_r. \quad (1.46)$$

These are the pressure and energy densities for an ideal gas of bosonic radiation or ultrarelativistic bosons, which equation of state reads $\rho_r = 3P_r$.

Higher order corrections to those ideal gas quantities involve quantum field theoretical perturbative computations expressed in terms of Feynman diagrams and products of contour-ordered correlation functions. In the next section, using functional techniques, we describe how (non)equilibrium perturbation theory can be consistently formulated in these terms.

1.1.8 Perturbation theory

In this section we shall describe how equilibrium perturbation theory can be consistently formulated by means of standard diagrammatic expressions generalised to contour-ordered integrals. The nonequilibrium case is dealt with identically and is even simpler because there is no $-i\beta$ -cyclicity involved. Nonequilibrium real-life computations are nevertheless harder, because they do not enjoy that extra property.

Let us distinguish the free and interacting parts of the action in terms of their corresponding Lagrangians $S_{C_\beta}[\phi] = \int_x \mathcal{L}$ and articulate the discussion using

$$\mathcal{L} = \mathcal{L}_0 + \mathcal{L}_{\text{int}}, \quad (1.47)$$

with $\mathcal{L}_0 = -\frac{1}{2}\phi(\square + m^2)\phi$, $\square = \partial_\mu\partial^\mu = \partial_t^2 - \nabla^2$ and \mathcal{L}_{int} describes the interactions that the field ϕ is subject to. In perturbative quantum field theories, the latter always is accompanied by a tiny coupling constant and one performs a power expansion in \mathcal{L}_{int} at the level of the generating functional (1.36). For the time being, we can disregard the nonlocal source $R(x, y)$ as it plays no role in what follows, and write (1.36) as

$$Z^{(\text{eq})}[J] = \int_{\text{cyclic}}^{-i\beta} \mathcal{D}\phi(t) \sum_{n=0}^{\infty} \frac{i^n}{n!} \left[\int_x \mathcal{L}_{\text{int}} \right]^n e^{i \int_x (\mathcal{L}_0 + J(x)\phi(x))}. \quad (1.48)$$

If $\mathcal{L}_{\text{int}} = -\frac{\lambda}{\ell!}\phi^\ell$, we can even replace it by $-\frac{\lambda}{\ell!} \frac{\delta^\ell}{(i\delta J(x))^\ell}$ and organise perturbation theory in terms of Feynman diagrams, as we shall detail now.

Let us define $iG_0(x, y) = iG_0(x-y)$ the $-i\beta$ -cyclic (in time) free theory Green's function defined on the contour \mathcal{C}_β as

$$iG_0^{-1}(x, y) = \frac{\delta^2 \mathcal{S}_{\mathcal{C}_\beta, 0}[\phi]}{\delta\phi(x)\delta\phi(y)} \Leftrightarrow (\square_x + m^2)iG_0(x, y) = \delta_{\mathcal{C}_\beta}(x - y), \quad (1.49)$$

and perform the following functional change of variables

$$\phi'(x) = \phi(x) - i \int_y G_0(x, y)J(y). \quad (1.50)$$

At the level of functional integrals, the latter is nothing but a mere shift which Jacobian leaves the path integral measure unchanged. Note however that, had we not by hand enforced $G_0(x, y)$ to be $-i\beta$ -cyclic, the field redefinition would not have been consistent with the path integration of Eq. (1.91). Dropping the primes, we find

$$Z^{(\text{eq})}[J] = \int_{\text{cyclic}}^{-i\beta} \mathcal{D}\phi(t) e^{iS_0} \sum_{n=0}^{\infty} \frac{i^n}{n!} \left[-\frac{\lambda}{\ell!} \int_x \frac{\delta^\ell}{(i\delta J(x))^\ell} \right]^n e^{-\frac{1}{2} \int_{x,y} J(x)G_0(x,y)J(y)} \quad (1.51)$$

and this formula proves the claims made below Eq. (1.24). Starting from here, it is clear that a suitable perturbative expansion can be performed, and that the usual combinatorial arguments apply identically to the vacuum case. Whenever one computes an n -point correlator, disconnected diagrams from the numerator conspire with the vacuum diagrams from the denominator and cancel. Only connected diagrams survive the perturbative expansion.

From Eq. (1.51), one can infer the usual Schwinger-Dyson equation [26]

$$\Delta^{-1}(x, y) = G_0^{-1}(x, y) - \Pi(x, y), \quad (1.52)$$

with $\Pi(x, y)$ the *1 Particle Irreducible* (1PI) selfenergy. The Schwinger-Dyson equation (1.52) is usually interpreted as a geometric series which we depicted on Fig. 1.6. It is equivalently written as

$$\int_z G_0^{-1}(x, z)\Delta(z, y) - \int_z \Pi(x, z)\Delta(z, y) = \delta_C(x - y). \quad (1.53)$$



Figure 1.6: Geometric series of the Schwinger-Dyson equation (1.52). Thick (resp. thin) solid lines represent fully dressed (resp. free) propagators.

So far, all these equations look very similar, if not identical, to those encountered in vacuum QFT textbooks [26] and as a matter of fact, there are only two differences with zero temperature field theory. The first one is a pure finite temperature effect, hidden in the $-i\beta$ -cyclic field configurations in the path integral, which led to the $-i\beta$ -cyclicity of the propagator. The second one is that all spacetime integrals in e.g. Eq. (1.53) are defined on a closed time-contour, thus generating a matrix structure for the propagators which in the Schwinger-Keldysh limit 1.1.5 is of the form

$$\int_z \Pi(x, z)\Delta(z, y) \sim \sum_{b=\pm} b \int_{-\infty}^{+\infty} dz^0 \int d^3\mathbf{z} \Pi^{ab}(x, z)\Delta^{bc}(z, y) \quad (1.54)$$

where $a, b, c = \pm$ are the so-called Schwinger-Keldysh polarities. In the next section, we discuss the two-point functions on the CTP relevant for this work, as well as their associated properties.

1.1.9 Contour-ordered two-point functions

Let us start by recalling the definition of the contour-ordered propagator $\Delta(x, y)$ for a scalar field $\phi(x)$ on an arbitrary time contour \mathcal{C}

$$\Delta(x, y) = \langle \mathcal{T}_{\mathcal{C}} \phi(x)\phi(y) \rangle - \varphi(x)\varphi(y). \quad (1.55)$$

Here $\mathcal{T}_{\mathcal{C}}$ is the time-ordering operator along the time-path \mathcal{C} and

$$\varphi(x) = \langle \phi(x) \rangle, \quad (1.56)$$

is the field one-point function, also known as the field condensate or background field. From the definition of the *Wightman* two-point functions

$$\Delta^{\gt}(x, y) = \langle \phi(x)\phi(y) \rangle - \varphi(x)\varphi(y) = \Delta^{-+}(x, y), \quad (1.57)$$

$$\Delta^<(x, y) = \langle \phi(y)\phi(x) \rangle - \varphi(x)\varphi(y) = \Delta^{+-}(x, y), \quad (1.58)$$

follows the relation

$$\Delta(x, y) = \theta_{\mathcal{C}}(x^0 - y^0)\Delta^>(x, y) + \theta_{\mathcal{C}}(y^0 - x^0)\Delta^<(x, y), \quad (1.59)$$

with $\theta_{\mathcal{C}}(t)$ is the Heaviside step function on the contour \mathcal{C} . One can further define the so-called *statistical* and *spectral* two-point functions, respectively denoted by $\Delta^+(x, y)$ and $\Delta^-(x, y)$, as

$$\Delta^+(x, y) = \frac{1}{2}\langle \{\phi(x), \phi(y)\} \rangle - \varphi(x)\varphi(y) = \frac{1}{2}(\Delta^>(x, y) + \Delta^<(x, y)), \quad (1.60)$$

$$\Delta^-(x, y) = i\langle [\phi(x), \phi(y)] \rangle = i(\Delta^>(x, y) - \Delta^<(x, y)), \quad (1.61)$$

where $[\cdot, \cdot]$ and $\{\cdot, \cdot\}$ are the commutator and anti-commutator operators. In coordinate space, $\Delta^+(x, y)$ and $\Delta^-(x, y)$ are real-valued functions which are respectively symmetric and anti-symmetric under $x \leftrightarrow y$ permutations. From this statement, together with equal time canonical commutation relations

$$\begin{aligned} [\phi(x), \phi(y)]|_{x^0=y^0} &= [\dot{\phi}(x), \dot{\phi}(y)]|_{x^0=y^0} = 0, \\ [\phi(x), \dot{\phi}(y)]|_{x^0=y^0} &= i\delta(\mathbf{x} - \mathbf{y}), \end{aligned}$$

$\Delta^-(x, y)$ satisfies the following relations

$$\Delta^-(x, y)|_{x^0=y^0} = 0, \quad (1.62)$$

$$\partial_{x^0}\Delta^-(x, y)|_{x^0=y^0} = -\partial_{y^0}\Delta^-(x, y)|_{x^0=y^0} = \delta(\mathbf{x} - \mathbf{y}), \quad (1.63)$$

$$\partial_{x^0}\partial_{y^0}\Delta^-(x, y)|_{x^0=y^0} = 0. \quad (1.64)$$

In particular for $x^0 = y^0 = t_i$, we obtain that canonical quantisation readily enforces a set of initial conditions on the spectral two-point functions. It also is interesting to note that the latter, i.e. Δ^- , is related to the usual *Källén-Lehmann spectral density* [26] $\wp(x, y)$

$$\wp(x, y) = \langle [\phi(x), \phi(y)] \rangle = \Delta^>(x, y) - \Delta^<(x, y), \quad (1.65)$$

via the relation $\Delta^- = i\wp$. Note here that the spectral density $\wp(x, y)$ is not to be confused with the density matrix $\varrho(t)$ or the energy density $\rho(T)$. In terms of its real statistical and spectral components, the propagator (1.55) reads

$$\Delta(x, y) = \Delta^+(x, y) - \frac{i}{2}\text{sign}_{\mathcal{C}}(x^0 - y^0)\Delta^-(x, y), \quad (1.66)$$

with $\text{sign}_{\mathcal{C}}(t)$ the contour-ordered sign function. On the real axis $[t_i, +\infty]$, one can also define the *retarded* and *advanced* propagators

$$\Delta^R(x, y) = \theta(x^0 - y^0)\Delta^-(x, y) = \Delta^{++}(x, y) - \Delta^{+-}(x, y), \quad (1.67)$$

$$\Delta^A(x, y) = -\theta(y^0 - x^0)\Delta^-(x, y) = \Delta^{++}(x, y) - \Delta^{-+}(x, y). \quad (1.68)$$

The selfenergy $\Pi(x, y)$ has a similar decomposition as that of the contour-ordered propagator $\Delta(x, y)$, except for its local component which has to be separately dealt with. It is given by

$$\Pi(x, y) = -i\Pi^{\text{loc}}(x)\delta_{\mathcal{C}}(x-y) + \theta_{\mathcal{C}}(x^0 - y^0)\Pi^>(x, y) + \theta_{\mathcal{C}}(y^0 - x^0)\Pi^<(x, y). \quad (1.69)$$

From that definition, one can similarly define the *statistical* and *spectral* self-energies as

$$\Pi^+(x, y) = \frac{1}{2}(\Pi^>(x, y) + \Pi^<(x, y)) \quad (1.70)$$

$$\Pi^-(x, y) = i(\Pi^>(x, y) - \Pi^<(x, y)) \quad (1.71)$$

such that

$$\Pi(x, y) = -i\Pi^{\text{loc}}(x)\delta_{\mathcal{C}}(x-y) + \Pi^+(x, y) - \frac{i}{2}\text{sign}_{\mathcal{C}}(x^0 - y^0)\Pi^-(x, y), \quad (1.72)$$

together with the *retarded* and *advanced* selfenergies, which read

$$\Pi^R(x, y) = \theta(x^0 - y^0)\Pi^-(x, y) = \Pi^{++}(x, y) - \Pi^{+-}(x, y) \quad (1.73)$$

$$\Pi^A(x, y) = -\theta(y^0 - x^0)\Pi^-(x, y) = \Pi^{++}(x, y) - \Pi^{-+}(x, y). \quad (1.74)$$

They satisfy the same properties as those of the analogous propagators.

Spacetime translation invariant systems. In spacetime translation invariant systems, e.g. systems at thermal equilibrium, two-point correlators are only functions of the difference of their spacetime arguments, and

$$\Delta(x, y) = \Delta(z) \quad (1.75)$$

where $z = x - y$, and one can Fourier transform with respect to z . For any function $F(z)$, we define its Fourier transformations as

$$F(z) = \int \frac{d^4q}{(2\pi)^4} F(q)e^{-iq \cdot z}, \quad F(q) = \int d^4z F(z)e^{iq \cdot z} \quad (1.76)$$

where we made the usual abuse of notation and did not distinguish between the function itself and its Fourier transform, though they are technically different.

From their properties in position space, the Fourier space two-point functions have useful properties, too. Relevant for this work are the following

$$\Delta^\pm(\pm q) = \pm \Delta^\pm(q) \quad (1.77)$$

$$\Delta^\pm(q)^* = \pm \Delta^\pm(q) \quad (1.78)$$

$$2i\text{Im}\Delta^R(q) = \Delta^-(q) \quad (1.79)$$

$$\text{Im}\Delta^R(-q) = -\text{Im}\Delta^R(q) \quad (1.80)$$

$$\text{Re}\Delta^R(q^0, \mathbf{q}) = \mathcal{P} \int_{-\infty}^{\infty} \frac{d\omega}{\pi} \frac{\text{Im}\Delta^R(\omega, \mathbf{q})}{\omega - q^0} \quad (1.81)$$

$$\text{Re}\Delta^R(-q) = \text{Re}\Delta^R(q) \quad (1.82)$$

$$\int_{-\infty}^{+\infty} \frac{dq^0}{2\pi} q^0 \wp(q^0, \mathbf{q}) = 1, \quad (1.83)$$

where \mathcal{P} is the Cauchy principal value. These relations are to be satisfied at all orders in perturbation theory and therefore hold for the corresponding selfenergies, too.

Thermal equilibrium Let us now particularise the discussion to $\varrho = \varrho^{(\text{eq})} = e^{-\beta H}$, i.e. to systems at thermal equilibrium, and study the associated two-point functions. Again, recalling that H is the infinitesimal generator of time translations, we will interpret $e^{-\beta H}$ as a time translation operator in the imaginary direction and derive useful properties satisfied by two-point functions, the most famous one being the Kubo-Martin-Schwinger (KMS) relation.

For this purpose, let us e.g. compute the ensemble average of two operators $O_1(x)$ and $O_2(y)$. At equilibrium,

$$\langle O_1(x^0, \mathbf{x}) O_2(y^0, \mathbf{y}) \rangle = \text{tr} [e^{-\beta H} O_1(x^0, \mathbf{x}) O_2(y^0, \mathbf{y})]. \quad (1.84)$$

Now inserting $\mathbb{I} = e^{\beta H} e^{-\beta H}$ between $O_1(x)$ and $O_2(y)$ and using the cyclicity of the trace operator, it is immediate to show that

$$\langle O_1(x^0, \mathbf{x}) O_2(y^0, \mathbf{y}) \rangle = \langle O_2(y^0, \mathbf{y}) O_1(x^0 + i\beta, \mathbf{x}) \rangle, \quad (1.85)$$

or equivalently

$$\langle O_1(x^0 - i\beta, \mathbf{x}) O_2(y^0, \mathbf{y}) \rangle = \langle O_2(y^0, \mathbf{y}) O_1(x^0, \mathbf{x}) \rangle. \quad (1.86)$$

Had we done the same exercise for an n -point correlator, we would have obtained that thermal n -point correlators effectively only depend on $n - 1$ times.

In particular for $O_1 = \phi = O_2$, this leads to the KMS relation

$$\Delta_{(\text{eq})}^>(z^0, \mathbf{z}) = \Delta_{(\text{eq})}^<(z^0 + i\beta, \mathbf{z}). \quad (1.87)$$

At the level of their Fourier transforms with respect to z^0 , this translates into

$$\Delta_{(\text{eq})}^<(q^0, \mathbf{z}) = e^{-\beta q^0} \Delta_{(\text{eq})}^>(q^0, \mathbf{z}), \quad \Delta_{(\text{eq})}^<(q) = e^{-\beta q^0} \Delta_{(\text{eq})}^>(q). \quad (1.88)$$

The latter can be re-expressed in terms of the spectral density (1.65) as

$$\Delta_{(\text{eq})}^>(q) = (1 + f_B(q^0)) \wp_{(\text{eq})}(q), \quad \Delta_{(\text{eq})}^<(q) = f_B(q^0) \wp_{(\text{eq})}(q), \quad (1.89)$$

where the Bose-Einstein distribution function (1.41) is a built-in feature of thermal field theory for bosons. In terms of the statistical and spectral two-point functions, we find

$$\Delta_{(\text{eq})}^+(q) = -i \left(\frac{1}{2} + f_B(q_0) \right) \Delta_{(\text{eq})}^-(q) = \left(\frac{1}{2} + f_B(q_0) \right) \wp_{(\text{eq})}(q), \quad (1.90)$$

again naturally displaying the bosonic nature of scalar fields.

Contour-ordered free propagator for scalars. The so-called free generating functional $Z_0^{(\text{eq})}[J, R]$ is nothing but the zeroth order generating functional obtained from truncating the power series of Eq. (1.51) after the zeroth order term which square bracket then evaluates to 1. It is given by

$$Z_0^{(\text{eq})}[J] = \int_{\text{cyclic}}^{-i\beta} \mathcal{D}\phi(t) e^{iS_0[\phi]} e^{-\frac{1}{2} \int_{x,y} J(x) G_0(x-y) J(y)}. \quad (1.91)$$

and the associated free propagator reads

$$\Delta_0^{(\text{eq})}(x, y) = \frac{1}{Z_0^{(\text{eq})}[0]} \left. \frac{\delta^2 Z_f^{(\text{eq})}[J]}{i\delta J(x) i\delta J(y)} \right|_{J=0} = G_0(x, y). \quad (1.92)$$

The latter is nothing but the free $-i\beta$ -cyclic Green's function on \mathcal{C}_β which is independent of the specific interactions that ϕ undergoes. It is the same for any real scalar field theory. Taking its Fourier transform with respect to $\mathbf{z} = \mathbf{x} - \mathbf{y}$ the solution of Eq. (1.49), subject to $-i\beta$ -cyclicity in time, as well as time ordering along \mathcal{C}_β , is given by

$$\begin{aligned} \Delta_0^{(\text{eq})}(z^0; \mathbf{q}) = G_0(z^0, \mathbf{q}) = & \frac{f_B(\omega_{\mathbf{q}})}{2\omega_{\mathbf{q}}} \left[\theta_{\mathcal{C}_\beta}(z^0) \left(e^{\beta\omega_{\mathbf{q}}} e^{-i\omega_{\mathbf{q}}z^0} + e^{i\omega_{\mathbf{q}}z^0} \right) \right. \\ & \left. + \theta_{\mathcal{C}_\beta}(-z^0) \left(e^{\beta\omega_{\mathbf{q}}} e^{i\omega_{\mathbf{q}}z^0} + e^{-i\omega_{\mathbf{q}}z^0} \right) \right], \end{aligned} \quad (1.93)$$

where $\omega_{\mathbf{q}} = \sqrt{m^2 + \mathbf{q}^2}$. Here, a few comments are in order. First, in the limit where $T \rightarrow 0$, or $\beta \rightarrow +\infty$, it reproduces the standard zero temperature propagator on \mathcal{C}_+ . Second, it satisfies the KMS relation (1.84). Third, it is an

even function of z^0 , as in the vacuum case. Fourth, we can explicitly show the statement made about the Schwinger-Keldysh contour and the irrelevance of the imaginary time stretch. For this purpose, let us write $z^0 = t - t_i$ and let us assume that $t = t' + i\tau$ has an imaginary component. Then, let us send t_i to $-\infty$. We find $\lim_{t_i \rightarrow \infty} G_0(t' + i\tau - t_i, \mathbf{q}) = 0$. As a result, when it is justified to let t_i approach $-\infty$, we infer that both at the level of the propagator and the generating functional, the only relevant part of the contour \mathcal{C}_β of Fig. 1.4 is that of Fig. 1.5, i.e. \mathcal{C} the Schwinger-Keldysh contour. Eventually, when put under this form, it is a rather straightforward exercise to identify the different Schwinger-Keldysh polarities by investigating the Heaviside functions. Taking their z^0 -Fourier transforms, we find

$$\Delta_{0,(\text{eq})}^{++}(q) = \Delta_{0,(\text{eq})}^F(q) = \frac{i}{q^2 - m^2 + i\epsilon} + 2\pi f_B(|q^0|)\delta(q^2 - m^2), \quad (1.94)$$

$$\Delta_{0,(\text{eq})}^{+-}(q) = \Delta_{0,(\text{eq})}^<(q) = 2\pi f_B(q^0)\text{sign}(q^0)\delta(q^2 - m^2), \quad (1.95)$$

$$\Delta_{0,(\text{eq})}^{-+}(q) = \Delta_{0,(\text{eq})}^>(q) = 2\pi(1 + f_B(q^0))\text{sign}(q^0)\delta(q^2 - m^2), \quad (1.96)$$

$$\Delta_{0,(\text{eq})}^{--}(q) = \Delta_{0,(\text{eq})}^{\bar{F}}(q) = \frac{-i}{q^2 - m^2 - i\epsilon} + 2\pi f_B(|q^0|)\delta(q^2 - m^2), \quad (1.97)$$

and, thanks to the KMS relation (1.88), we thus identify the equilibrium Källén–Lehmann free spectral density $\varphi_0^{(\text{eq})}(q) = 2\pi\text{sign}(q^0)\delta(q^2 - m^2)$, which satisfies the sum rule Eq. (1.83).

1.1.10 Finite temperature Dirac fermions in a nutshell

Thus far, almost identical conclusions can be drawn for Dirac fermions [18, 21], too, except for a few minor subtleties, which we shall briefly comment on.

The classical action for a Dirac fermion is

$$A[\psi, \bar{\psi}] = \int_x \bar{\psi}(i\cancel{\partial} - m)\psi + A_{\text{int}}[\psi, \bar{\psi}], \quad (1.98)$$

where $\bar{\psi} = (\gamma^0\psi)^\dagger$, $\cancel{\partial} = \gamma^\mu\partial_\mu$ and γ^μ are the gamma matrices which satisfy the Dirac algebra $\{\gamma^\mu, \gamma^\nu\} = 2\eta^{\mu\nu}\mathbb{1}_{4\times 4}$. The contour-ordered propagator reads

$$S(x, y) = \langle \mathcal{T}_{\mathcal{C}}\{\psi(x)\bar{\psi}(y)\} \rangle \quad (1.99)$$

$$= \theta_{\mathcal{C}}(x^0 - y^0)S^>(x, y) + \theta_{\mathcal{C}}(y^0 - x^0)S^<(x, y), \quad (1.100)$$

with $S^>(x, y) = \langle \psi(x)\bar{\psi}(y) \rangle$ and $S^<(x, y) = -\langle \bar{\psi}(x)\psi(y) \rangle$ and the other propagators can be defined analogously to the scalar case. Only the fermion sum

rule is different, it reads

$$\frac{1}{4} \int_{-\infty}^{+\infty} \frac{dq^0}{2\pi} \text{Tr}[\gamma^0 \wp^\psi(q^0, \mathbf{q})] = 1 \quad (1.101)$$

where the factor 1/4 arises from spin averaging.

Also, the fermionic equilibrium KMS relation (1.88) picks up an extra minus sign from commuting Grassman variables in Eq. (1.84). Therefore, we have

$$S_{(\text{eq})}^>(z^0, \mathbf{z}) = -S_{(\text{eq})}^<(z^0 + i\beta, \mathbf{z}), \quad S_{(\text{eq})}^<(q) = -e^{-\beta q^0} S_{(\text{eq})}^>(q), \quad (1.102)$$

which can again be expressed in terms of the fermionic equilibrium spectral density as

$$S_{(\text{eq})}^>(q) = (1 - f_D(q^0)) \wp_{(\text{eq})}^\psi(q), \quad S_{(\text{eq})}^<(q) = -f_D(q^0) \wp_{(\text{eq})}^\psi(q), \quad (1.103)$$

where

$$f_D(q^0) = (e^{\beta q^0} + 1)^{-1} \quad (1.104)$$

and the Fermi-Dirac distribution function is a built-in feature of thermal field theory for fermions.

Then, the whole procedure with the equilibrium path integral for scalars described in the previous section can be reproduced for Dirac fermions, too, to obtain the Schwinger-Dyson equation for fermionic propagators

$$S^{-1}(x, y) = K_0^{-1}(x, y) - \Sigma(x, y), \quad (1.105)$$

with $K_0(x, y)$ the contour-ordered, $-i\beta$ -anti-cyclic Dirac Green's function

$$iK_0^{-1}(x, y) = \frac{\delta^2 A_0[\psi, \bar{\psi}]}{\delta\psi(x)\delta\bar{\psi}(y)} = (i\not{\partial} - m)\delta_{\mathcal{C}}(x - y), \quad (1.106)$$

and $\Sigma(x, y)$ the fermionic 1PI selfenergy. Setting $\Sigma(x, y) = 0$ to obtain the free spin-averaged propagators, we have

$$S_{0,(\text{eq})}^{++}(q) = S_{f,(\text{eq})}^F(q) = (\not{q} + m) \left[\frac{i}{q^2 - m^2 + i\epsilon} - 2\pi f_D(|q^0|)\delta(q^2 - m^2) \right], \quad (1.107)$$

$$S_{0,(\text{eq})}^{+-}(q) = S_{f,(\text{eq})}^<(q) = -2\pi f_D(q^0)\text{sign}(q^0)(\not{q} + m)\delta(q^2 - m^2), \quad (1.108)$$

$$S_{0,(\text{eq})}^{-+}(q) = S_{f,(\text{eq})}^>(q) = 2\pi(1 - f_D(q^0))\text{sign}(q^0)(\not{q} + m)\delta(q^2 - m^2), \quad (1.109)$$

$$S_{0,(\text{eq})}^{--}(q) = S_{f,(\text{eq})}^{\bar{F}}(q) = (\not{q} + m) \left[\frac{-i}{q^2 - m^2 - i\epsilon} - 2\pi f_D(|q^0|)\delta(q^2 - m^2) \right], \quad (1.110)$$

and the free spectral density $\wp_{0,(eq)}^\psi(q) = 2\pi \text{sign}(q^0)(q + m)\delta(q^2 - m^2)$ which satisfies the sum rule (1.101).

The leading order partition function can be determined too by using similar tricks to those presented in the scalar discussion. For vanishing chemical potentials, we find

$$\ln Z_\psi^{(0)}(\beta) = 2V \int \frac{d^3\mathbf{p}}{(2\pi)^3} (\beta\omega_{\mathbf{p}} + 2 \ln [1 + e^{-\beta\omega_{\mathbf{p}}}]). \quad (1.111)$$

Here, there are two prefactors 2 which have a physical explanation. While the overall prefactor 2 which multiplies the volume V comes from the two relativistic spin degrees of freedom for spin 1/2 fields, the one that multiplies the logarithm owes its presence to the contribution of both the particles and anti-particles. The associated pressure and energy densities read

$$P_\psi^{(0)} = 4T \int \frac{d^3\mathbf{p}}{(2\pi)^3} \ln [1 + e^{-\beta\omega_{\mathbf{p}}}] = 4 \int \frac{d^3\mathbf{p}}{(2\pi)^3} \frac{\mathbf{p}^2}{3\omega_{\mathbf{p}}} f_D(\omega_{\mathbf{p}}), \quad (1.112)$$

$$\rho_\psi^{(0)} = 4 \int \frac{d^3\mathbf{p}}{(2\pi)^3} \omega_{\mathbf{p}} f_D(\omega_{\mathbf{p}}). \quad (1.113)$$

Those are nothing but the usual pressure and energy densities for an ideal gas of noninteracting fermions. At high temperatures with respect to the particles bare mass $T \gg m$, the particles are effectively massless and

$$P_\psi^{(0)} \xrightarrow{T \gg m} P_{r,\psi} = 4 \frac{7}{8} \frac{\pi^2}{90} T^4, \quad \rho_\psi^{(0)} \xrightarrow{T \gg m} \rho_{r,\psi} = 4 \frac{7}{8} \frac{\pi^2}{30} T^4 = 3P_{r,\psi}. \quad (1.114)$$

They are the pressure and energy densities for an ideal gas of fermionic radiation or ultrarelativistic fermions, which equation of state reads $\rho_{r,\psi} = 3P_{r,\psi}$.

These last expressions close the discussion on (non)equilibrium field theory that is relevant for this thesis, and we now move to the description of the 2 Particle Irreducible effective action formalism which we motivate first.

1.2 The 2 Particle Irreducible (2PI) effective action formalism

Eqs. (1.52)(1.105) are of primordial importance in this work. They describe how the free propagator gets resummed with insertions of 1PI bubbles. It is well known in (non)equilibrium field theory that resummation effects can be of great importance. They give rise to significant effects that naive perturbation theory does not account for, through contributions to physical quantities that

are proportional to noninteger powers of the coupling constant, see e.g. [21, 22]. They too give rise to qualitatively new (collective) excitations in the quasiparticle spectrum of quantum field theories, see e.g. [22] for holes in abelian gauge theories and [29] for luons in scalar ones.

In this section, heavily relying on Ref. [19], we describe the so-called 2 Particle Irreducible (2PI) formalism that systematically and selfconsistently implements resummation effects onto the one- and two-point functions of a field theory, including couplings to external backgrounds.

1.2.1 2PI effective action

For simplicity, let us consider a theory constituted of several real scalar fields $\{\Phi_a\}$, where a labels the fields degrees of freedom. The quantum dynamics of the system is described by the generating functional

$$Z[J, R] = \int \mathcal{D}\Phi \exp \left[i \left(S[\Phi] + \int_x J_a(x) \Phi_a(x) + \frac{1}{2} \int_{xy} R_{ab}(x, y) \Phi_a(x) \Phi_b(y) \right) \right], \quad (1.115)$$

which, as long as initial conditions are Gaussian (cf. (1.33) and the discussion around), is appropriate for both equilibrium and nonequilibrium systems. $\int_x = \int_{\mathcal{C}} \int d^3\mathbf{x}$, where \mathcal{C} is the time-path chosen to suit the problem of interest. It need not necessarily be the Schwinger-Keldysh contour, and we insist that a and b are labels for field degrees of freedom, not Schwinger-Keldysh polarities. Repeated indices are summed over. We collectively refer to the set $\{\Phi_a\}$ by using the condensed notation Φ . $S[\Phi]$ designates the classical field theory action functional. We assume that it can be put in the shape of $S[\Phi] = \int_x \left(\frac{1}{2} \partial_\mu \Phi_a \partial^\mu \Phi_a - \frac{1}{2} m_a^2 \Phi_a^2 + \mathcal{L}_{\text{int}}[\Phi] \right)$ with canonical kinetic terms, where $\mathcal{L}_{\text{int}}[\Phi]$ contains all interaction terms between the fields. As long as perturbation theory holds, they need not be specified.

The generating functional for connected correlators $W[J, R]$ is defined as

$$iW[J, R] = \ln Z[J, R], \quad (1.116)$$

and the one- and contour-ordered connected two-point functions in the presence of sources are found as

$$\frac{\delta W[J, R]}{\delta J_a(x)} = \varphi_a(x), \quad \frac{\delta W[J, R]}{\delta R_{ab}(x, y)} = \frac{1}{2} (\varphi_a(x) \varphi_b(y) + \Delta_{ab}(x, y)). \quad (1.117)$$

Eqs. (1.117) are to be interpreted as relations among the four arbitrary functions φ , Δ , J and R which mix them together two by two, i.e. the knowledge

of two of them formally suffices to determine the two others. From now on, we shall make the following abuse of notation and refer to φ (resp. Δ) as both the arbitrary function resulting from a Legendre transform with respect to J (resp. R) and the full contour-ordered one-point (resp. two-point) function.

The 1 Particle Irreducible (1PI) effective action $\Gamma[\varphi, R]$ is then defined as the Legendre transform of $W[J, R]$ with respect to J

$$\Gamma[\varphi, R] = W[J, R] - \int_x \varphi_a(x) J_a(x) \quad (1.118)$$

where we have identified $\frac{\delta W[J, R]}{\delta J_a(x)} = \varphi_a(x)$. On the right hand side of this equation, J is to be dealt with as a functional of φ and R , and $J = J[\varphi, R]$ as a result of the Legendre transformation. We shall always omit those implicit dependences resulting from Legendre transformations, in order to avoid notational clutter.

$\Gamma[\varphi, 0] = \Gamma[\varphi]$ is the usual 1PI effective action, i.e. the generating functional for 1PI diagrams, and $\Gamma[\varphi, R]$ can formally be viewed as that of the modified classical theory

$$S[\Phi, R] = S[\Phi] + \frac{1}{2} \int_{xy} R_{ab}(x, y) \Phi_a(x) \Phi_b(y). \quad (1.119)$$

Performing a second Legendre transform of $W[J, R]$ with respect to R ,⁵ we arrive at the 2PI effective action,⁶ defined as

$$\Gamma[\varphi, \Delta] = W[J, R] - \int_x \varphi_a(x) J_a(x) - \frac{1}{2} \int_{xy} \varphi_a(x) \varphi_b(y) R_{ab}(x, y) - \frac{1}{2} \text{Tr}[\Delta R]. \quad (1.120)$$

It is equivalent to the R -Legendre transform of the 1PI effective action $\Gamma[\varphi, R]$

$$\begin{aligned} \Gamma[\varphi, \Delta] &= \Gamma[\varphi, R] - \int_{xy} \frac{\delta \Gamma[\varphi, R]}{\delta R_{ab}(x, y)} R_{ab}(x, y) \\ &= \Gamma[\varphi, R] - \frac{1}{2} \int_{xy} \varphi_a(x) \varphi_b(y) R_{ab}(x, y) - \frac{1}{2} \text{Tr}[\Delta R], \end{aligned} \quad (1.121)$$

since $\frac{\delta \Gamma[\varphi, R]}{\delta R_{ab}(x, y)} = \frac{\delta W[J, R]}{\delta R_{ab}(x, y)}$. Carefully accounting for the implicit functional dependences, it is also a straightforward exercise to show that functional derivatives of the 2PI effective action evaluated for vanishing external sources generate quantum kinetic equations of motion for φ and Δ , the relevant one- and

⁵Here the trace operator has to be distinguished from that of Eq. (1.4). The one under consideration now does not perform a quantum average over the Hilbert space, rather it sums over all field degrees of freedom a, b and integrates all spacetime arguments.

⁶The different effective actions (1PI vs. 2PI) are notationally distinguished by their arguments.

two-point functions of the quantum theory, via

$$\left. \frac{\delta\Gamma[\varphi, \Delta]}{\delta\varphi_a(x)} \right|_{J=R=0} = 0, \quad \left. \frac{\delta\Gamma[\varphi, \Delta]}{\delta\Delta_{ab}(x, y)} \right|_{J=R=0} = 0, \quad (1.122)$$

hence justifying the abuse of notation described below Eq. (1.117). A careful reader might note here that for nonequilibrium problems with Gaussian initial conditions, the sources J and R actually implicitly contain information on the initial condition, cf. (1.33) and the discussions around it. Therefore, it may seem odd to just set them to zero. As far as we know, there are two schools of thought regarding this issue. The one adopted here, which follows [19], sets the sources to zero anyway, and then “by hand” supplements the n -point function equations of motion (1.121) with Gaussian initial conditions, as constraints on the side. However, as emphasised below (1.33), this is not compulsory. The initial conditions need not be absorbed in the sources, in which case they also need not be supplemented by hand and are dealt with as boundary terms in the generating functional itself. Following this approach which is e.g. taken in [28], the initial conditions then manifestly appear in the right hand sides of (1.121). This too allows for non-Gaussian initial conditions to be dealt with in a similar manner.

$\Gamma[\varphi, \Delta]$ is usually split into a tree-level contribution $S[\varphi]$, a one-loop correction $\Gamma_1[\varphi, \Delta]$ and all higher-loop corrections are gathered in an object $\Gamma_2[\varphi, \Delta]$, where the subscript 2 refers to all diagrams of two or more loops. It rewrites

$$\Gamma[\varphi, \Delta] = S[\varphi] + \Gamma_1[\varphi, \Delta] + \Gamma_2[\varphi, \Delta] = S[\varphi] + \Gamma_{\text{loop}}[\varphi, \Delta] \quad (1.123)$$

and only Γ_{loop} is a functional of Δ . Though referred to as the classical action, $S[\varphi]$ really is the classical action functional evaluated at the statistical and quantum ensemble averages $\langle\Phi_a\rangle$. Performing a functional Gaussian integral as detailed in appendix A, the one-loop term can be expressed as

$$\Gamma_1[\varphi, \Delta] = \frac{i}{2} \text{Tr} \ln (\Delta^{-1}) + \frac{i}{2} \text{Tr} (G_0^{-1}[\varphi] \Delta), \quad (1.124)$$

where $G_{0,ab}^{-1}[\varphi]$ are the inverse tree-level operators

$$\begin{aligned} iG_{0,ab}^{-1}[\varphi](x, y) &= \left. \frac{\delta^2 S[\Phi]}{\delta\Phi_a(x) \delta\Phi_b(y)} \right|_{\langle\Phi\rangle} \\ &= \left(-(\square + m_a^2) \delta_{ab} + \left. \frac{\delta^2 \mathcal{L}_{\text{int}}[\Phi(x)]}{\delta\Phi_a(x) \delta\Phi_b(x)} \right|_{\langle\Phi\rangle} \right) \delta_C(x - y), \end{aligned} \quad (1.125)$$

defined in analogy to Eq. (1.49), where $\langle_{\mathbb{F}}$ evaluates all fields at their quantum and statistical expectation values φ . $G_{0,ab}^{-1}[\varphi]$ is to be handled as explicit φ -dependent inputs to $\Gamma_2[\varphi, \Delta]$. At equilibrium, this one-loop contribution is what gives rise to the finite-temperature Coleman-Weinberg potential [30].

Taking the functional derivative of Eq. (1.123) and implicitly setting the sources to zero, the equation of motion for φ reads

$$\frac{\delta\Gamma[\varphi, \Delta]}{\delta\varphi_a(x)} = -(\square + m_a)\varphi_a(x) + \frac{\delta\mathcal{L}_{\text{int}}[\varphi(x)]}{\delta\varphi_a(x)} + \frac{\delta\Gamma_{\text{loop}}[\varphi, \Delta]}{\delta\varphi_a(x)} = 0. \quad (1.126)$$

Analogously, the equations of motion for the full (resummed) connected two-point functions $\Delta_{ab}(x, y)$ are derived from

$$\frac{\delta\Gamma[\varphi, \Delta]}{\delta\Delta_{ab}(x, y)} = 0 \quad (1.127)$$

From Eq. (1.123), Eq. (1.127) yields

$$\Delta_{ab}^{-1}(x, y) = G_{0,ab}^{-1}[\varphi](x, y) - \Pi_{ab}[\varphi, \Delta](x, y), \quad (1.128)$$

where, in comparison with Eq. (1.52), we defined

$$\Pi_{ab}[\varphi, \Delta](x, y) = 2i \frac{\delta\Gamma_2[\varphi, \Delta]}{\delta\Delta_{ab}(x, y)}. \quad (1.129)$$

More closely looking at Eq. (1.128) together with Eq. (1.52), we conclude that only 1PI diagrams contribute to $\Pi_{ab}[\varphi, \Delta](x, y)$ since it has to be the 1PI contour-ordered selfenergy. This in turn implies that only 2PI diagrams contribute to $\Gamma_2[\varphi, \Delta]$,⁷ hence its name and definition

$$\Gamma_2 = (-i) \times (\text{sum of all 2PI diagrams/symmetry factors}). \quad (1.130)$$

Convolving Eq. (1.128) with $\Delta_{bc}(z, y)$, one obtains

$$\sum_b \int_z G_{0,ab}^{-1}[\varphi](x, z) \Delta_{bc}(z, y) - \sum_b \int_z \Pi_{ab}[\varphi, \Delta](x, z) \Delta_{bc}(z, y) = \delta_{ac} \delta_{\mathcal{C}}(x - y). \quad (1.131)$$

Here, $\delta_{\mathcal{C}}(x - y)$ is the four-dimensional delta function with time arguments on the contour \mathcal{C} . Eqs. (1.128) (1.131) are nothing but generalisations of Eqs. (1.52)(1.53) in the presence of condensates φ_a which contribute to the tree-level Green's functions, too. The leading-order propagator is no longer the free one, but readily resums couplings to the backgrounds.

⁷Diagrammatically, taking a derivative with respect to Δ cuts open a line of a diagram.

On the formal independence of Δ and φ in $\Gamma[\varphi, \Delta]$. At the level of the 2PI effective action, one- and two-point correlators are independent degrees of freedom. They stem from Legendre transforms with respect to independent variables. It is important to note that this statement is only valid before solving the 2PI equations of motion.

As an example, take a system solely made of one scalar field, described by the effective action $\Gamma[\varphi, \Delta]$, functional of only two independent variables φ and Δ , which respectively obey Eqs. (1.126) and (1.131). In practice, one adopts a perturbative approach to solve these equations, and expands Γ_{loop} and Π in terms of Feynman graphs. Mathematically speaking, these are nothing but convolved integrals involving Δ and φ , i.e. integrals of products of Δ and φ .

Then, Eqs. (1.126) and (1.131) form a set of coupled integro-differential quantum kinetic equations of motion for Δ and φ . At any given order in perturbation theory, we can write the solution of Eq. (1.131) as a formal function of φ which we denote $\Delta[\varphi]$. Plugging $\Delta[\varphi]$ back into (1.126) yields an effective action $\Gamma[\varphi, \Delta[\varphi]]$ for φ at the desired order in perturbation theory⁸. Since $\Delta[\varphi]$ solves its 2PI equation of motion, the dynamical equation derived from $\Gamma[\varphi, \Delta[\varphi]]$ is equivalent to that derived from $\Gamma[\varphi, \Delta]$, namely

$$\frac{\delta\Gamma[\varphi, \Delta[\varphi]]}{\delta\varphi(z)} = \frac{\partial\Gamma[\varphi, \Delta[\varphi]]}{\partial\varphi(z)} + \underbrace{\int_{x,y} \frac{\partial\Gamma[\varphi, \Delta]}{\partial\Delta_{ab}(x,y)} \Big|_{\Delta[\varphi]}}_{=0} \frac{\delta\Delta_{ab}[\varphi](x,y)}{\delta\varphi(z)}. \quad (1.132)$$

Had we solved for φ first, an analogous conclusion would have been drawn.

2PI formalism for fermions. For a Dirac fermion (1.98), the 2PI formalism is almost identical to that for a scalar. We briefly comment on the very few differences which all arise from the distinguished fermionic and bosonic path integral measures $\int \mathcal{D}\phi \rightarrow \int \mathcal{D}\psi \mathcal{D}\bar{\psi}$, and actions $S[\Phi] \rightarrow A[\psi, \bar{\psi}]$. Performing the fermionic functional integrals *à la* appendix A, we again get a functional determinant, except it is for the free Dirac operator this time. Turning it into a trace and playing the same game as in appendix A, we obtain the one-loop effective action in absence of fermionic condensates

$$\Gamma_1[S] = -i\text{Tr} \ln [S^{-1}] - i\text{Tr} [SK_0^{-1}], \quad (1.133)$$

where the fermionic inverse tree-level propagator K_0^{-1} is precisely (1.106). The difference between scalars and fermions is $\frac{i}{2} \rightarrow -i$ in front of the two traces.

⁸In opposition to $\Gamma[\varphi, \Delta]$, $\Gamma[\varphi, \Delta[\varphi]]$ can no longer be used as an effective action for Δ .

At arbitrary loop order, the 2PI effective action thus reads

$$\Gamma[S] = -i\text{Tr} \ln [S^{-1}] - i\text{Tr} [SK_0^{-1}] + \Gamma_2[S], \quad (1.134)$$

where $\Gamma_2[S]$ is made of 2PI diagrams of two or more loops. The equation of motion for S is derived in the same way as in the previous scalar case, only the definition of the selfenergy gets changed, precisely because of that change in the prefactor of the one-loop effective action. We have

$$S^{-1}(x, y) = K_f^{-1}(x, y) - \Sigma[S](x, y) \quad (1.135)$$

where we defined the fermionic selfenergy $\Sigma[S](x, y) = -i \frac{\delta \Gamma_2[S]}{\delta S(x, y)}$.

1.2.2 The Kadanoff-Baym equations

On the CTP of Fig. 1.3, the evolution equations for the two-point functions, i.e. the Schwinger-Dyson equation (1.131), can conveniently be rewritten in terms of their statistical and spectral components, cf. Eqs. (1.61)(1.60) and (1.71)(1.70). Plugging these in Eq. (1.131) and using the identity

$$\begin{aligned} \int_C dy^0 \text{sign}_C(x^0 - y^0) &= \int_{t_i}^{x^0} dy^0 + \int_{x^0}^{t_f} dy^0 (-1) + \int_{t_f}^{t_i} dy^0 (-1) \\ &= 2 \int_{t_i}^{x^0} dy^0 \end{aligned} \quad (1.136)$$

we obtain the so-called Kadanoff-Baym equations (KBEs) for Δ^+ and Δ^-

$$\left(\square_x \delta_{ac} + M_{ac}^{\text{tree}}(x)^2 + \Pi_{ac}^{\text{loc}}(x) \right) \Delta_{cb}^-(x, y) = - \int_{y_0}^{x_0} dz \Pi_{ac}^-(x, z) \Delta_{cb}^-(z, y), \quad (1.137)$$

$$\begin{aligned} \left(\square_x \delta_{ac} + M_{ac}^{\text{tree}}(x)^2 + \Pi_{ac}^{\text{loc}}(x) \right) \Delta_{cb}^+(x, y) &= - \int_{t_i}^{x_0} dz \Pi_{ac}^-(x, z) \Delta_{cb}^+(z, y) \\ &\quad + \int_{t_i}^{y_0} dz \Pi_{ac}^+(x, z) \Delta_{cb}^-(z, y). \end{aligned} \quad (1.138)$$

Here, we used the abbreviated notation $\int_{t_1}^{t_2} dz = \int_{t_1}^{t_2} dz^0 \int_{-\infty}^{\infty} d^3\mathbf{z}$ and $M_{ac}^{\text{tree}}(x)$ stands for the tree-level mass defined by

$$M_{ac}^{\text{tree}}(x)^2 = m_a^2 \delta_{ac} - \left. \frac{\delta^2 \mathcal{L}_{\text{int}}[\Phi(x)]}{\delta \Phi_a(x) \delta \Phi_c(x)} \right|_{\langle \Phi \rangle}. \quad (1.139)$$

These equations can quite rarely be solved analytically as the memory integrals of the right hand sides involve very complicated convoluted loop integrals, which are both highly nonlinear and nonlocal in the functions of interest. Nevertheless, significant efforts have been deployed in the last two decades, successfully leading to an improvement of our understanding of both their analytic [28, 31–34] and numerical solutions [19, 28, 32, 34]. Under a certain approximation scheme known as the Wentzel-Kramers-Brillouin (WKB) approximations which is based on a separation of microscopic and macroscopic time scales, we shall explicitly solve the Kadanoff-Baym equations later in this work.

Part I

Quantum and thermal effects on nonequilibrium scalar field dynamics in the early Universe

Introduction

Many features of the Universe we observe around us today are the outcome of nonequilibrium phenomena that have taken place in the early stages of its thermal history. Of particular relevance for this section are those phenomena that involve scalar fields. While the prominent initial motivation for this work is warm inflation, understanding and describing the properties of scalar fields in a thermal and nonequilibrium environment has a wider range of applicability than just inflationary cosmology. Indeed, scalar fields are involved in many other areas of science, this e.g. includes the Landau theory of phase transitions [35], the Ising model [36,37], the Landau-Ginzburg theory of superconductivity [38] or the Brout-Englert-Higgs mechanism [39–41]. In cosmology, on top of scalar-driven cosmic inflation models mentioned in the introduction, they too may solve the strong CP-problem [42], explain Dark Matter [43–46] or Dark Energy [47–50]. They too can trigger phase transitions, e.g. relevant for electroweak physics and baryogenesis [51–54].

In this part of the thesis, we study the nonequilibrium dynamics of scalars from first principles of statistical mechanics and quantum field theory. In particular, we shall focus on systems which bulk properties are adiabatically evolving, wherein well-defined quasiparticles arise in the spectrum of the theory. We shall also derive the master equation that drives the adiabatic evolution of the field condensate, would-be inflaton, which will be of the form $\ddot{\varphi} + \Gamma_{\varphi}\dot{\varphi} + V'(\varphi) = 0$, where the transport coefficients Γ_{φ} and $V'(\varphi)$ are respectively the damping rate and φ -derivative of the effective potential $V(\varphi)$. Those will be computed exactly in a specific \mathbb{Z}_2 -symmetric scalar model from first principles of nonequilibrium field theory using the 2PI formalism. The viability of warm inflation in that model will be discussed too. On top of inflationary cosmology, the results presented in this part of the thesis can be potentially applied to any quantum system which nonequilibrium dynamics is effectively described by (pseudo)scalars.

Chapter 2

Markovian dynamics for scalars in slowly-evolving backgrounds

The evolution equations, or equations of motion, that dictate the nonequilibrium dynamics of the n -point functions of interacting quantum fields are usually highly nonlocal and nonlinear in those very n -point functions, as can e.g. be seen from the 2PI dynamics equations for the one- and two-point functions, respectively Eq.(1.126) and Eqs.(1.137)(1.138). There, the nonlocalities come from the loop contributions to the 2PI effective action, as many 2PI diagrams have vertices which are separated in spacetime.

Local, also known as Markovian, differential equations have very satisfactory properties, e.g. they possess well-defined coefficients describing well-understood physics. Typically, one articulates the discussion in terms of quantities multiplying certain powers or derivatives of the function which dynamics is under consideration. As emphasised in the introduction, relevant for this work is the equation $\ddot{\varphi} + \Gamma_{\varphi}\dot{\varphi} + V'(\varphi) = 0$, where Γ_{φ} is identified with the friction rate and $V'(\varphi)$ with the effective force.

In this chapter, we will show how the equations of motion for the condensates of scalar fields can be Markovianised in this form under certain circumstances, namely when the only time-varying quantities that break time-translation invariance are slowly-evolving backgrounds to which the fields are coupled. For a more refined discussion on the localisation procedure in the presence of slowly-varying functions, we invite the interested reader to e.g. consult [55].

The general set-up under consideration here is that of Section 1.2, restricting ourselves to spatially homogeneous and isotropic systems. While this simplifying assumption is taken, our analysis can be extended to spatial gradients as well, but it becomes notationally heavier. Then, again for simplicity, we shall assume that only one of the degrees of freedom among $\{\Phi_a\}$, say ϕ , acquires a nonvanishing expectation value which we denote φ . The latter will serve as a prototype of macroscopic quantity which time-evolution is characterised by much larger time scales than those of quantum events, such as collisions or scatterings of particles. Therefore, we shall assume that the expansion

$$\varphi(t')^n = \varphi(t)^n + n(t' - t)\dot{\varphi}(t)\varphi(t)^{n-1} + \mathcal{O}[\dot{\varphi}^2], \quad (2.1)$$

is justified under loop integrals, which will help us localise them. Physically, this assumes that the background is quasiconstant during quantum interactions. Mathematically, this is justified because in the 2PI equations of motions, non-local contributions come under the form of convolutions of φ with quantum n -point correlators. Those are power-law suppressed for large time separations with respect to the typical microphysical time scale τ_{int} and hence effectively act as “window functions” of finite supports. The precise definition of τ_{int} and associated power-law suppressions are model dependent, see e.g. [56].

Based on these considerations, we provide a general method to derive an effective quantum kinetic equation of the form¹

$$\ddot{\varphi} + \sum \Gamma_{\varphi}^{(n)} \dot{\varphi}^n + V'(\varphi) = 0 \quad (2.2)$$

where $\Gamma_{\varphi}^{(n)}$ and $V(\varphi)$ respectively are the damping rates and effective potential that govern the dynamics of φ .

2.1 The Markovian equation: a derivation

Let us show how one can derive a Markovian equation of motion for φ from $\Gamma[\varphi, \Delta[\varphi]]$, i.e. using the 2PI effective action (1.123) and (1.126), where one has plugged in the solution of the 2PI equation of motion (1.131) for the propagators, which we formally denote $\Delta[\varphi]$. We first perform a Taylor expansion of

¹Note that this equation describes the dynamics of the statistically weighted quantum average $\varphi = \text{Tr}[\rho(t_i)\phi]$. The latter averages out noise terms of the fluctuation-dissipation theorem which we would have obtained if we had derived the Langevin equation of motion for $\phi(x)$ instead [56, 57].

$\partial\Gamma[\varphi, \Delta[\varphi]]/\partial\varphi$ about $\bar{\varphi}$ in functional space with $\varphi = \bar{\varphi} + \delta\bar{\varphi}$ and find

$$\begin{aligned} \left. \frac{\partial\Gamma_{\text{loop}}[\varphi, \Delta[\varphi]]}{\partial\varphi(x)} \right|_{\bar{\varphi}+\delta\bar{\varphi}} &= \left. \frac{\partial\Gamma_{\text{loop}}[\varphi, \Delta[\varphi]]}{\partial\varphi(x)} \right|_{\bar{\varphi}} + \\ &\sum_{n=1}^{\infty} \frac{1}{n!} \prod_{i=1}^n \int_{\mathcal{C}} dx_i^0 \int d^3\mathbf{x}_i \delta\bar{\varphi}(x_i) \left[\frac{\delta^n}{\delta\varphi(x_1)\cdots\delta\varphi(x_n)} \left(\frac{\partial\Gamma_{\text{loop}}[\varphi, \Delta[\varphi]]}{\partial\varphi(x)} \right) \right] \Bigg|_{\bar{\varphi}} \end{aligned} \quad (2.3)$$

where the implicit dependence on φ of $\Delta[\varphi]$ is not affected by the partial functional derivatives $\partial/\partial\varphi$, as those only act on the explicit dependence of Γ_{loop} . The expansion (2.3), is widely utilised in the literature, especially around $\bar{\varphi} = 0$, known as the small field expansion, but it is actually valid for any $\bar{\varphi}$ if one is interested in sufficiently small variations around it. It diagrammatically corresponds to expanding the φ -dependent vertices and lines around the reference value $\bar{\varphi}$ in functional space. Of course, this approach has the following shortcomings: it breaks down in situations where one needs to track large field excursions over sizeable time intervals.

In our case, the range of validity of this approximation can be enhanced by the “window function argument” which suppresses the nonlocal loop integrals in Γ_{loop} for time separations larger than τ_{int} , provided that we judiciously choose $\bar{\varphi}$. For this purpose, we take it to be a constant function which value is the self-consistent solution of the equation of motion evaluated at the reference time $t = x^0$ set by that of the equation of motion, $\bar{\varphi} = \varphi(t)$. In doing so, we can Markovianise the *a priori* nonlocal contribution (2.3) by using (2.1) inside the loop integrals, which effectively makes the equation (2.3) local in time. And indeed, this does not restrict the field elongations as this expansion can locally be applied at each instant $t = x^0$. Using $\delta\bar{\varphi}(x_i) = \dot{\varphi}(t)(x_i^0 - t)$, we obtain for the single-condensate isotropic version of equation (1.126)

$$\ddot{\varphi} + \sum_{n=1}^{+\infty} \Gamma_{\varphi}^{(n)} \dot{\varphi}^n + V'(\varphi) = 0 \quad (2.4)$$

with

$$V'(\varphi) = -\frac{\partial\mathcal{L}_{\text{int}}[\varphi(t)]}{\partial\varphi(t)} - \left. \frac{\partial\Gamma_{\text{loop}}[\varphi, \Delta[\varphi]]}{\partial\varphi(x)} \right|_{\bar{\varphi}=\varphi(t)} \quad (2.5)$$

and

$$\Gamma_{\varphi}^{(n)} = -\frac{1}{n!} \prod_{i=1}^n \int_{\mathcal{C}} dx_i^0 (x_i^0 - t) \int d^3\mathbf{x}_i \left[\frac{\delta^n}{\delta\varphi(x_1)\cdots\delta\varphi(x_n)} \left(\frac{\partial\Gamma_{\text{loop}}[\varphi, \Delta[\varphi]]}{\partial\varphi(x)} \right) \right] \Bigg|_{\bar{\varphi}}. \quad (2.6)$$

A few comments are in order. Note that this expansion allows to implement powers of $\dot{\varphi}$ to all orders, but neglect higher order derivatives. Terms proportional to $\ddot{\varphi}$ will essentially correct the kinetic terms which already are present in the classical theory, and hence perturbative loop corrections to it are neglected, though they could in principle be included *à la* [58]. In contradistinction, the dissipation rates $\Gamma_\varphi^{(n)}$, which only arise from loop corrections, are qualitatively new with respect to what is present in the classical dynamics. Higher order derivatives usually give rise to ugly and unstable behaviours in Markovian, loop-truncated equations of motion. Nevertheless, if the fundamental theory is well-behaved and the derivative expansion is properly performed, this spurious dynamics can be kept under control [59].

2.2 Interpretation of the leading friction term

Neglecting terms proportional to $\dot{\varphi}^n$ for $n \geq 2$, which in this work is justified as φ is slowly rolling, Eq. (2.4) for φ precisely gives the Markovian equation²

$$\ddot{\varphi} + \Gamma_\varphi \dot{\varphi} + V'(\varphi) = 0 \quad (2.7)$$

where $\Gamma_\varphi = \Gamma_\varphi^{(1)}$ is the leading friction term. Let us try to interpret it in terms of microphysical processes in a model-independent fashion. In certain cases, e.g. when ϕ resides in a near-equilibrium thermal bath, the effective potential and friction rate, respectively (2.5) and (2.6) can be expressed in terms of real and imaginary parts of retarded self-energies, evaluated at integer multiples of excitations oscillation frequencies, cf. e.g. Refs. [32, 61–63] for detailed derivations. As long as the optical theorem applies, which it does at thermal equilibrium, imaginary parts of selfenergies can be related to Cutkosky cut Feynman diagrams [64–69], hence Γ_φ can be interpreted in terms of microphysical scatterings or particle productions [61, 64, 70, 71]. A striking consequence of cutting rules is that local diagrams do not have imaginary parts as they cannot be cut through, and therefore, local diagrams do not generate dissipation and friction solely arises from the non-local term $\Gamma_2[\varphi, \Delta[\varphi]]$. As a matter of fact, this is no longer true for the nonequilibrium problem at hand.

Indeed, let us evaluate Γ_φ from (2.6) and split it as

$$\Gamma_\varphi = \Gamma_\varphi^{[1]} + \Gamma_\varphi^{[2]} \quad , \quad \Gamma_\varphi^{[i]} = \int_{\mathcal{C}} \int d^3 \mathbf{x}_1 dx_1^0 (x_1^0 - t) \Pi_\varphi^{[i]}(x_1, x) \quad (2.8)$$

²Note that this equation is strictly identical to the equation of motion derived in linear response theory where an expansion in small deviations around $\bar{\varphi} = 0$ is performed, and truncated at leading order in $\delta\varphi$ [57, 60]. This should not be confused with the approach taken here, which relies on a derivative expansion in $\dot{\varphi}$ and not in the smallness of the field elongation, which is arbitrarily large in our case.

with

$$\Pi_\varphi^{[1]}(x_1, x) = - \left. \frac{\partial^2 \Gamma_{\text{loop}}[\varphi, \Delta[\varphi]]}{\partial \varphi(x_1) \partial \varphi(x)} \right|_{\bar{\varphi}}, \quad (2.9)$$

$$\Pi_\varphi^{[2]}(x_1, x) = - \sum_{a,b} \int_y \int_z \left(\left. \frac{\partial^2 \Gamma_{\text{loop}}[\varphi, \Delta]}{\partial \Delta_{ab}(y, z) \partial \varphi(x)} \right|_{\Delta[\varphi]} \frac{\delta \Delta_{ab}[\varphi](y, z)}{\delta \varphi(x_1)} \right) \Big|_{\bar{\varphi}}. \quad (2.10)$$

The damping rate Γ_φ receives two contributions, respectively $\Pi_\varphi^{[1]}$, which comes from the explicit φ -dependence of Γ_{loop} and $\Pi_\varphi^{[2]}$. In terms of the perturbative loop expansion, the former arises from the φ -dependent vertices that appear in the action when splitting $\phi = \varphi + \eta$ and the latter comes from the φ -dependence of the resummed propagators $\Delta[\varphi]$.

Let us now argue that local diagrams can indeed contribute to dissipation in nonequilibrium field theory. First, note that the functions $\Pi_\varphi^{[i]}(x_1, x)$ are convolved with $(x_1^0 - t)$ in order to define Γ_φ , and hence any that contains $\delta(x_1^0 - t)$ in $\Pi_\varphi^{[i]}(x_1, x)$ will eventually yield a vanishing contribution to the dissipation rate. Therefore, it is tempting to believe that ‘‘local diagrams’’, e.g. the one-loop diagrams of Γ_1 , will not contribute to the friction rate, just as in the equilibrium case. However, while this is true for $\Pi_\varphi^{[1]}$, it is not for $\Pi_\varphi^{[2]}$.

The contribution to $\Pi_\varphi^{[1]}(x_1, x)$ from the one-loop effective action Γ_1 reads

$$\begin{aligned} \Pi_\varphi^{[1]}(x_1, x) &\supset - \left. \frac{\partial^2 \Gamma_1[\varphi, \Delta[\varphi]]}{\partial \varphi(x_1) \partial \varphi(x)} \right|_{\bar{\varphi}} \\ &= - \frac{i}{2} \sum_{a,b} \int_z \int_{z'} \left(\left. \frac{\partial^2 G_{0,ab}^{-1}[\varphi](z, z')}{\partial \varphi(x_1) \partial \varphi(x)} \Delta_{ab}[\varphi](z, z') \right) \right) \Big|_{\bar{\varphi}}, \quad (2.11) \end{aligned}$$

where partial derivatives solely act on $G_{0,ab}^{-1}[\varphi]$ as explained below Eq. (1.125). Using the definition of $G_{0,ab}^{-1}[\varphi](z, z')$ (1.125), we find

$$\begin{aligned} \frac{\partial^2 i G_{0,ab}^{-1}[\varphi](z, z')}{\partial \varphi(x_1) \partial \varphi(x)} &= \frac{1}{2} \frac{\partial^2}{\partial \varphi(x_1) \partial \varphi(x)} \left(\left. \frac{\partial^2 S[\Phi]}{\partial \Phi_a(z) \partial \Phi_b(z')} \right) \Big|_{\langle \Phi \rangle} \right) \\ &\propto \delta_C(z - z') \delta_C(z - x_1) \delta_C(z - x). \quad (2.12) \end{aligned}$$

Putting the last two equations together, the local Γ_1 contribution to $\Pi_\varphi^{[1]}(x_1, x)$ is multiplied by $\delta_C(x_1^0 - t)$ which, once convolved with the factor $(x_1^0 - t)$ of $\Gamma_\varphi^{[1]}$, vanishes. Following this line of thought, we conclude that Γ_{loop} can be replaced by Γ_2 in $\Pi_\varphi^{[1]}$ and only 2PI diagrams which have two separate background-dependent vertices can contribute to the damping rate $\Gamma_\varphi^{[1]}$.

Nevertheless, the one-loop effective action Γ_1 does contribute to Γ_φ through $\Pi_\varphi^{[2]}(x_1, x)$. First note that $\Pi_\varphi^{[2]}(x_1, x)$ in (2.10) is made of two distinguished factors, one that involves derivatives of the effective action, and the other of the propagators. Let us first focus on the Γ_1 contribution to the first factor. Using Eqs.(1.124) and (1.125), we find for the first factor in (2.10)

$$\frac{\partial^2 \Gamma_1[\varphi, \Delta]}{\partial \Delta_{ab}(y, z) \partial \varphi(x)} \Big|_{\Delta[\varphi]} = \frac{1}{2} \frac{\partial}{\partial \varphi(x)} \left(\frac{\partial^2 S[\Phi]}{\partial \Phi_a(y) \partial \Phi_b(z)} \Big|_{\langle \Phi \rangle} \right) \propto \delta_C(y-z) \delta_C(y-x). \quad (2.13)$$

Now using the relation $\delta A = -A \delta(A^{-1}) A$, which holds for any invertible matrix/operator A , we can express the second factor as

$$\begin{aligned} \frac{\delta \Delta_{ab}[\varphi](y, z)}{\delta \varphi(x_1)} &= - \left(\Delta \frac{\delta \Delta^{-1}}{\delta \varphi(x_1)} \Delta \right)_{ab} [\varphi](y, z), \quad (\text{in the matrix product sense}) \\ &= - \sum_{a'b'} \int_{y'} \int_{z'} \Delta_{aa'}[\varphi](y, y') \frac{\delta \left(G_{0,a'b'}^{-1}[\varphi](y', z') - \Pi_{a'b'}[\varphi](y', z') \right)}{\delta \varphi(x_1)} \Delta_{b'b}[\varphi](z', z). \end{aligned} \quad (2.14)$$

Multiplying the functional derivatives $G_0^{-1}[\varphi]$ and of $\Pi[\varphi]$ with Eq. (2.13) above, we see that both can *a priori* lead to nonvanishing contributions to the damping rate, and they both arise from “local” one-loop diagrams. This seems to indicate that time-dependent backgrounds and their backreactions violate the optical theorem and dissipation rates are no longer to be read off from Cutkosky cut Feynman diagrams. In an attempt to save that interpretation, we could nevertheless argue that local diagrams are effectively nonlocal once resummation effects are properly taken into account, as we did in the above equation by inserting the Schwinger-Dyson equation for the propagator.

Therefore, the one- and higher-loop contributions to the effective action, namely Γ_1 and Γ_2 behave very differently when it comes to the way they enter computations of dissipation coefficient. While Γ_2 leads to friction terms regardless what thermodynamic state the system is in, e.g. thermal equilibrium, the damping from local diagrams is a peculiar feature which arises from nonequilibrium dynamics and the backreaction of time-dependent background on quasiparticles properties. Those comments close our remarks on the microphysical interpretation of the dissipation term derived herewith and for the remainder of this part, we shall particularise our results and 2PI investigations to a generic Z_2 -symmetric renormalisable field theory.

Chapter 3

2PI formalism for interacting \mathbb{Z}_2 -symmetric scalars

We here study the 2PI effective action and its resulting equations of motion for a renormalisable \mathbb{Z}_2 -symmetric field theory made of two real scalar fields, namely $\phi(x)$ and $\chi(x)$. The defining Lagrangian density reads

$$\mathcal{L} = \frac{1}{2}\partial_\mu\phi\partial^\mu\phi - \frac{m_\phi^2}{2}\phi^2 - \frac{\lambda_\phi}{4!}\phi^4 + \frac{1}{2}\partial_\mu\chi\partial^\mu\chi - \frac{m_\chi^2}{2}\chi^2 - \frac{\lambda_\chi}{4!}\chi^4 - \frac{h}{4}\phi^2\chi^2 \quad (3.1)$$

and in order to apply the techniques developed in the previous chapter, we first have to study the 2PI ingredients of such a scalar system, which is what this chapter is dedicated to. For this purpose, we assume that only $\phi(x)$ acquires a thermal expectation value $\varphi(x) = \langle\phi(x)\rangle$ and that $\chi(x)$ does not. Therefore $\varphi(x)$ constitutes the only time-varying background field of our system, just as in the previous chapter. We formulate the theory on the CTP of Fig. 1.3 of initial time t_i , suitable for nonequilibrium perturbation theory, assuming that a power expansion in all three dimensionless couplings λ_ϕ , h and λ_χ is justified.

Using Eq. (1.125) we find the tree-level propagator for the ϕ field of this theory

$$iG_{0,a}^{-1}[\varphi](x, y) = -(\square_x + M_a^{\text{tree}}(x)^2)\delta_C(x - y), \quad (3.2)$$

where δ_C is the four-dimensional delta function on the closed contour, and $M_a^{\text{tree}}(x) = \sqrt{m_a^2 + \frac{g_a}{2}\varphi(x)^2}$ is the tree-level time-dependent mass with g_a the coupling constant that couples a to ϕ in the Lagrangian (3.1), i.e. $g_\phi = \lambda_\phi$ and $g_\chi = h$. With that expression at our disposal, we can now move on and derive the 2PI equations of motion for a \mathbb{Z}_2 -symmetric theory of interacting scalars.

3.1 The 2PI equations of motion

On one hand, using Eqs. (1.126)(1.123)(1.124) together with Eq. (3.2) we find that the equation of motion for the condensate for the problem at hand reads

$$\left(\square_x + m_\phi^2 + \frac{\lambda_\phi}{6} \varphi(x)^2 + \frac{\lambda_\phi}{2} \Delta_\phi(x, x) + \frac{h}{2} \Delta_\chi(x, x) \right) \varphi(x) = \frac{\delta \Gamma_2[\varphi, \Delta]}{\delta \varphi(x)}. \quad (3.3)$$

On the other hand, the Kadanoff-Baym equations (1.137)(1.138) for the propagators of \mathbb{Z}_2 -symmetric scalar theories with only one condensate read

$$\left(\square_x + M_a^{\text{tree}}(x)^2 + \Pi_a^{\text{loc}}(x) \right) \Delta_a^-(x, y) = - \int_{y_0}^{x_0} dz \Pi_a^-(x, z) \Delta_a^-(z, y), \quad (3.4)$$

$$\begin{aligned} \left(\square_x + M_a^{\text{tree}}(x)^2 + \Pi_a^{\text{loc}}(x) \right) \Delta_a^+(x, y) = & - \int_{t_i}^{x_0} dz \Pi_a^-(x, z) \Delta_a^+(z, y) \\ & + \int_{t_i}^{y_0} dz \Pi_a^+(x, z) \Delta_a^-(z, y), \end{aligned} \quad (3.5)$$

as there is no mixing between the full propagators (resp. selfenergies) external legs: $\Delta_{ab} = \Delta_a \delta_{ab}$ (resp. $\Pi_{ab} = \Pi_a \delta_{ab}$) and the Kadanoff-Baym are diagonal in the space of field labels. This statement is nontrivial, so let us carefully explain it. Splitting the only condensating field ϕ into its ensemble average plus quantum fluctuations around it, themselves parametrised by a quantum field η , namely $\phi = \varphi + \eta$, the part of the interaction action which is relevant for the construction of 2PI diagrams is given by

$$iS_{\text{int}} \supset \int_x \left[\frac{(-i\lambda_\phi)}{4!} \eta^4 + \frac{(-i\lambda_\phi \varphi)}{3!} \eta^3 + \frac{(-i\lambda_\chi)}{4!} \chi^4 + \frac{(-ih\varphi)}{2} \eta \chi^2 + \frac{(-ih)}{4} \eta^2 \chi^2 \right]. \quad (3.6)$$

Let us now prove that these interactions forbid mixing between propagators. Such a mixing would have to be the result of some non vanishing $\Pi_{\phi\chi}$, so let us assume it exists and one has a 1PI selfenergy, which external legs are a ϕ and a χ particle. Now closely looking at Eq. (3.6), we infer that whatever interactions constitute this $\Pi_{\phi\chi}$, it must have an even number, say $2N$, of χ lines attached to each of its vertices. Therefore the number of internal χ lines within $\Pi_{\phi\chi}$ is given by $(2N-1)/2$ which is noninteger and cannot be, hence $\Pi_{\phi\chi}$ cannot exist. Note that if χ had a nonvanishing condensate $\langle \chi \rangle \neq 0$, the \mathbb{Z}_2 -symmetry in the χ interactions would be broken and that statement would not hold anymore. Diagonal KBEs describe \mathbb{Z}_2 -symmetric scalar theories if and only if solely one field acquires a nonvanishing expectation value.

3.2 The 2PI dynamics at three-loop order

According to Eqs. (1.130) and (3.6), the 2PI diagrams at 3-loop order (which is also at most of second order in the coupling constant expansion for all relevant couplings λ_ϕ , h and λ_χ) are depicted in Fig. 3.1 and the associated effective action reads

$$\begin{aligned}
\Gamma_2[\varphi, \Delta] = & -\frac{i}{2^2} \left[\frac{(-i\lambda_\phi)}{2} \int_x \Delta_\phi(x, x)^2 + \frac{(-i\lambda_\chi)}{2} \int_x \Delta_\chi(x, x)^2 \right. \\
& \left. + (-ih) \int_x \Delta_\phi(x, x) \Delta_\chi(x, x) \right] \\
& - \frac{i}{2 \cdot 3!} \int_{x,y} (-i\lambda_\phi \varphi(x)) (-i\lambda_\phi \varphi(y)) \Delta_\phi(x, y)^3 \\
& - \frac{i}{2 \cdot 2} \int_{x,y} (-ih\varphi(x)) (-ih\varphi(y)) \Delta_\phi(x, y) \Delta_\chi(x, y)^2 \\
& - \frac{i}{4!2} \left[(-i\lambda_\phi)^2 \int_{x,y} \Delta_\phi(x, y)^4 + (-i\lambda_\chi)^2 \int_{x,y} \Delta_\chi(x, y)^4 \right] \\
& - \frac{i}{2^3} \int_{x,y} (-ih)^2 \Delta_\phi(x, y)^2 \Delta_\chi(x, y)^2. \tag{3.7}
\end{aligned}$$

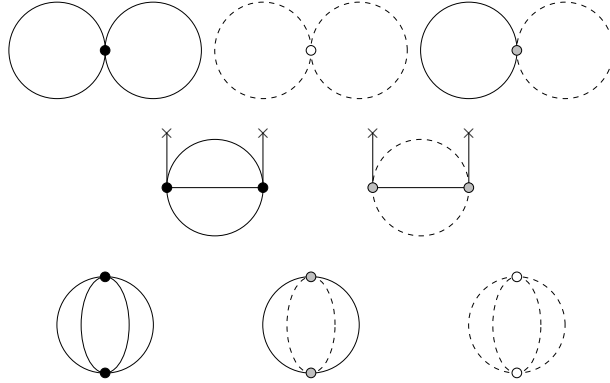


Figure 3.1: The three-loop $\Gamma_2[\varphi, \Delta]$. Solid (resp. dashed) lines correspond to ϕ (resp. χ) quanta. Solid (resp. light gray, empty) dots correspond to λ_ϕ (resp. h , λ_χ) couplings. Crosses correspond to couplings to the background condensate φ .

3.2.1 Equation of motion for φ

At second order in the loop and coupling constant perturbation theory, we have

$$\frac{\delta\Gamma_2[\varphi, \Delta]}{\delta\varphi(x)} = i \int_y \left[\frac{\lambda_\phi^2}{3!} \Delta_\phi(x, y)^3 + \frac{h}{2} \Delta_\chi^2(x, y) \Delta_\phi(x, y) \right] \varphi(y), \quad (3.8)$$

which should be substituted into the right hand side (3.3). Doing so and using the spectral and statistical decompositions of the propagators (1.66), we find

$$\begin{aligned} & \left(\square_x + m_\phi^2 + \frac{\lambda_\phi}{6} \varphi(x)^2 + \frac{\lambda_\phi}{2} \Delta_\phi^+(x, x) + \frac{h}{2} \Delta_\chi^+(x, x) \right) \varphi(x) \\ & + \int_{t_i}^{x^0} dy^0 \int d^3\mathbf{y} \Pi_\phi^{-\text{sun}}(x, y) \varphi(y) = 0, \end{aligned} \quad (3.9)$$

where

$$\begin{aligned} \Pi_\phi^{-\text{sun}}(x, y) = & \frac{1}{4} \left[\frac{\lambda_\phi^2}{3!} \Delta_\phi^-(x, y)^3 + \frac{h^2}{2} \Delta_\chi^-(x, y)^2 \Delta_\phi^-(x, y) \right] \\ & - \frac{\lambda_\phi^2}{2} \Delta_\phi^+(x, y)^2 \Delta_\phi^-(x, y) \\ & - \frac{h^2}{2} \left(2\Delta_\chi^-(x, y) \Delta_\chi^+(x, y) \Delta_\phi^+(x, y) + \Delta_\chi^+(x, y)^2 \Delta_\phi^-(x, y) \right). \end{aligned} \quad (3.10)$$

The superscript sun is used because those nonlocal contributions arise from the nonlocal two-loop sunset diagrams in the middle line of Fig. 3.1. Note that this selfenergy should *a priori* not be confused with those derived from (1.129) which contribute to the Kadanoff-Baym equations and shall be dealt with next. However, in this particular case, $\Pi_\phi^{-\text{sun}}(x, y)$ is precisely the one that will contribute to the 2PI equation for the propagator.

3.2.2 Selfenergies for the Kadanoff-Baym equations

Taking the functional derivative of (3.7) following Eq. (1.129), which diagrammatically amounts to cutting open a line of the close 2PI diagrams of Fig. 3.1,

we find the following selfenergies

$$\begin{aligned}\Pi_\phi[\varphi, \Delta](x, y) = & -\frac{i}{2} \left(\lambda_\phi \Delta_\phi^+(x, x) + h \Delta_\chi^+(x, x) \right) \delta_C(x - y) \\ & - \frac{1}{2} \lambda_\phi^2 \varphi(x) \varphi(y) \Delta_\phi(x, y)^2 - \frac{h^2}{2} \varphi(x) \varphi(y) \Delta_\chi(x, y)^2 \\ & - \frac{\lambda_\phi^2}{3!} \Delta_\phi(x, y)^3 - \frac{h^2}{2} \Delta_\phi(x, y) \Delta_\chi(x, y)^2,\end{aligned}\quad (3.11)$$

and

$$\begin{aligned}\Pi_\chi[\varphi, \Delta](x, y) = & -\frac{i}{2} \left(\lambda_\chi \Delta_\chi^+(x, x) + h \Delta_\phi^+(x, x) \right) \delta_C(x - y) \\ & - h^2 \varphi(x) \varphi(y) \Delta_\phi(x, y) \Delta_\chi(x, y) \\ & - \frac{\lambda_\chi^2}{3!} \Delta_\chi(x, y)^3 - \frac{h^2}{2} \Delta_\phi(x, y)^2 \Delta_\chi(x, y),\end{aligned}\quad (3.12)$$

which have to be decomposed in their statistical and spectral components for the sake of the Kadanoff-Baym equations. Plugging in the decomposition (1.66) and using its selfenergy counterpart, the relevant $\Pi_a^{\text{loc}}(x, x)$, $\Pi_a^+(x, y)$ and $\Pi_a^-(x, y)$ are identified as

$$\Pi_\phi^{\text{loc}}(x) = \frac{\lambda_\phi}{2} \Delta_\phi^+(x, x) + \frac{h}{2} \Delta_\chi^+(x, x), \quad (3.13)$$

$$\Pi_\chi^{\text{loc}}(x) = \frac{\lambda_\chi}{2} \Delta_\chi^+(x, x) + \frac{h}{2} \Delta_\phi^+(x, x), \quad (3.14)$$

$$\Pi_\phi^+(x, y) = \Pi_\phi^{+\text{crab}}(x, y) + \Pi_\phi^{+\text{sun}}(x, y), \quad (3.15)$$

$$\Pi_\chi^+(x, y) = \Pi_\chi^{+\text{crab}}(x, y) + \Pi_\chi^{+\text{sun}}(x, y), \quad (3.16)$$

$$\Pi_\phi^-(x, y) = \Pi_\phi^{-\text{crab}}(x, y) + \Pi_\phi^{-\text{sun}}(x, y), \quad (3.17)$$

$$\Pi_\chi^-(x, y) = \Pi_\chi^{-\text{crab}}(x, y) + \Pi_\chi^{-\text{sun}}(x, y), \quad (3.18)$$

with $\Pi^{\pm\text{crab}}(x, y)$ and $\Pi^{\pm\text{sun}}(x, y)$ being the crab and setting-sun contributions (cf. Fig. 3.2) respectively, given by

$$\begin{aligned}\Pi_\phi^{+\text{crab}}(x, y) = & -\frac{1}{2} \varphi(x) \varphi(y) \left[\lambda_\phi^2 \left(\Delta_\phi^+(x, y)^2 - \frac{1}{4} \Delta_\phi^-(x, y)^2 \right) \right. \\ & \left. + h^2 \left(\Delta_\chi^+(x, y)^2 - \frac{1}{4} \Delta_\chi^-(x, y)^2 \right) \right],\end{aligned}\quad (3.19)$$

$$\begin{aligned}\Pi_\phi^{+\text{sun}}(x, y) = & -\lambda_\phi^2 \left(\frac{1}{3!} \Delta_\phi^+(x, y)^3 - \frac{1}{8} \Delta_\phi^+(x, y) \Delta_\phi^-(x, y)^2 \right) \\ & - h^2 \left(\frac{1}{2} \Delta_\phi^+(x, y) \Delta_\chi^+(x, y)^2 - \frac{1}{8} \Delta_\phi^+(x, y) \Delta_\chi^-(x, y)^2 \right. \\ & \left. - \frac{1}{4} \Delta_\chi^+(x, y) \Delta_\chi^-(x, y) \Delta_\phi^-(x, y) \right),\end{aligned}\quad (3.20)$$

$$\Pi_{\chi}^{+\text{crab}}(x, y) = -\varphi(x)\varphi(y) h^2 \left(\Delta_{\phi}^{+}(x, y)\Delta_{\chi}^{+}(x, y) - \frac{1}{4}\Delta_{\phi}^{-}(x, y)\Delta_{\chi}^{-}(x, y) \right), \quad (3.21)$$

$$\begin{aligned} \Pi_{\chi}^{+\text{sun}}(x, y) &= -\lambda_{\chi}^2 \left(\frac{1}{3!}\Delta_{\chi}^{+}(x, y)^3 - \frac{1}{8}\Delta_{\chi}^{+}(x, y)\Delta_{\chi}^{-}(x, y)^2 \right) \\ &- h^2 \left(\frac{1}{2}\Delta_{\chi}^{+}(x, y)\Delta_{\phi}^{+}(x, y)^2 - \frac{1}{8}\Delta_{\chi}^{+}(x, y)\Delta_{\phi}^{-}(x, y)^2 \right. \\ &\quad \left. - \frac{1}{4}\Delta_{\phi}^{+}(x, y)\Delta_{\phi}^{-}(x, y)\Delta_{\chi}^{-}(x, y) \right), \end{aligned} \quad (3.22)$$

$$\Pi_{\phi}^{-\text{crab}}(x, y) = -\varphi(x)\varphi(y) \left(\lambda_{\phi}^2\Delta_{\phi}^{+}(x, y)\Delta_{\phi}^{-}(x, y) + h^2\Delta_{\chi}^{+}(x, y)\Delta_{\chi}^{-}(x, y) \right), \quad (3.23)$$

$$\begin{aligned} \Pi_{\phi}^{-\text{sun}}(x, y) &= -\lambda_{\phi}^2 \left(\frac{1}{2}\Delta_{\phi}^{+}(x, y)^2\Delta_{\phi}^{-}(x, y) - \frac{1}{4!}\Delta_{\phi}^{-}(x, y)^3 \right) \\ &- h^2 \left(\Delta_{\phi}^{+}(x, y)\Delta_{\chi}^{+}(x, y)\Delta_{\chi}^{-}(x, y) + \frac{1}{2}\Delta_{\phi}^{-}(x, y)\Delta_{\chi}^{+}(x, y)^2 \right. \\ &\quad \left. - \frac{1}{8}\Delta_{\phi}^{-}(x, y)\Delta_{\chi}^{-}(x, y)^2 \right), \end{aligned} \quad (3.24)$$

$$\Pi_{\chi}^{-\text{crab}}(x, y) = -\varphi(x)\varphi(y) h^2 \left(\Delta_{\phi}^{+}(x, y)\Delta_{\chi}^{-}(x, y) + \Delta_{\phi}^{-}(x, y)\Delta_{\chi}^{+}(x, y) \right), \quad (3.25)$$

$$\begin{aligned} \Pi_{\chi}^{-\text{sun}}(x, y) &= -\lambda_{\chi}^2 \left(\frac{1}{2}\Delta_{\chi}^{+}(x, y)^2\Delta_{\chi}^{-}(x, y) - \frac{1}{4!}\Delta_{\chi}^{-}(x, y)^3 \right) \\ &- h^2 \left(\Delta_{\chi}^{+}(x, y)\Delta_{\phi}^{+}(x, y)\Delta_{\phi}^{-}(x, y) + \frac{1}{2}\Delta_{\chi}^{-}(x, y)\Delta_{\phi}^{+}(x, y)^2 \right. \\ &\quad \left. - \frac{1}{8}\Delta_{\chi}^{-}(x, y)\Delta_{\phi}^{-}(x, y)^2 \right). \end{aligned} \quad (3.26)$$

Their names and superscripts defined in Eqs. (3.13)-(3.18) find their origins in their diagrammatic representations which we explicitly illustrated for χ in Fig. 3.2. We note in passing that we indeed checked that the propagator self-energy (3.24), $\Pi_{\phi}^{-\text{sun}}(x, y)$, is precisely the one that appears in the condensate equation of motion, too.

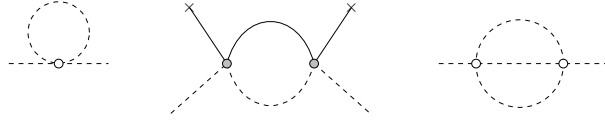


Figure 3.2: Reading from left to right, those diagrams respectively represent the local, crab and sunset selfenergy contributions to Π_χ of Eq. (3.12).

The Kadanoff-Baym equations (3.4)(3.5) with those selfenergies plugged in, together with the background field evolution equation (3.3) form the order $\mathcal{O}(\lambda^2)$ closed set of integro-differential 2PI equations that govern the dynamics of the one- and two-point functions of \mathbb{Z}_2 -symmetric scalars. For the remainder of this part of this thesis, we shall study selfconsistent solutions of these equations, carefully paying attention to the dynamics of the condensate and its quantum and thermal effective potential and damping rate. On one-hand by carefully following the method outlined in chapter 2 and on the other by providing approximate analytic solutions of the nonequilibrium Kadanoff-Baym equations, using the so-called Wentzel-Kramers-Brillouin (WKB) approximation scheme. Both approaches rely on a separation of microscopic vs. macroscopic time scales and we will show that the resulting condensate dynamics is identical.

Chapter 4

A slowly-rolling, homogeneous and isotropic scalar

In this chapter, which heavily relies on the two previous ones and the assumptions made therein, we shall particularise the study of last chapter's interacting \mathbb{Z}_2 -symmetric scalar theory

$$\mathcal{L} = \frac{1}{2} \partial_\mu \phi \partial^\mu \phi - \frac{m_\phi^2}{2} \phi^2 - \frac{\lambda_\phi}{4!} \phi^4 + \frac{1}{2} \partial_\mu \chi \partial^\mu \chi - \frac{m_\chi^2}{2} \chi^2 - \frac{h}{4} \phi^2 \chi^2 - \frac{\lambda_\chi}{4!} \chi^4, \quad (4.1)$$

to the case where there is a clear separation of microscopic vs. macroscopic time scale in an homogeneous and isotropic environment. Microscopic time scales dictate the dynamics of particle interactions and macroscopic that of the time evolution of bulk properties of the system, such as $\varphi = \langle \phi \rangle$, assumed to be the only time-dependent quantity of the system that breaks time translation invariance. In particular, and of greatest importance for this chapter, we shall assume that the frequencies ω that describe the mode decomposition of all fields evolve adiabatically $\dot{\omega}/\omega^2 \ll 1$. This allows for many quantum and dissipative aspects of the dynamics to be understood in terms of well-defined quasiparticles that propagate freely between spacetime-confined interactions.

For this purpose, we assume that the χ degrees of freedom constitute a thermal reservoir of temperature T , maintained at equilibrium through their interactions which take place on time scales τ_{int} that are much shorter than those that describe the dynamics of $\varphi(t)$: $\tau_{\text{int}} \dot{\varphi}/\varphi \ll 1$. This can e.g. be realised if χ has large gauge couplings to many other field degrees of freedom. In this

situation, it is justified to formulate our theory on the Schwinger-Keldysh contour of nonequilibrium field theory, as explained in section 1.1.5, wherein the classical action reads $S[\phi, \chi] = \int_x \mathcal{L}$ and $\int_x = \int_C dx^0 \int d^3\mathbf{x}$ implicitly integrates over the Schwinger-Keldysh contour.

Furthermore, these considerations allow for the techniques developed in chapter 2 to be applied and the equation of motion for φ to be Markovianised as in the previous chapter, i.e. $\ddot{\varphi} + \sum_{n=1}^{+\infty} \Gamma_\varphi^{(n)} \varphi^n + V'(\varphi) = 0$, where the transport coefficients $\Gamma_\varphi^{(n)}$ and $V'(\varphi)$ can be perturbatively organised and computed in terms of Feynman diagrams. We shall do so using two methods. On one hand, we shall apply the method of chapter 2 to the letter and derive the associated $\Gamma_\varphi^{(n)}$ and $V'(\varphi)$ from the truncated effective action studied in chapter 3. On the other, we shall repeat a similar analysis based on adiabatic solutions of the homogeneous and isotropic Kadanoff-Baym equations and plugging them back in the evolution equation for the background φ . Both procedures shall lead to identical transport coefficients expressed in terms of Feynman diagrams and convolutions of correlations functions. As formal expressions, those do not require further approximations, however evaluating the loop integrals analytically does and those calculations are greatly simplified when we can use close-to-equilibrium propagators. The use of near-equilibrium propagators applies to the following set of initial conditions:

- The fluctuations of all fields have close-to-equilibrium initial conditions. In particular, even though φ is initially offset from its equilibrium ground state, the quantum fluctuations η in $\phi = \varphi + \eta$ are at thermal equilibrium.
- The fluctuations η are far from their equilibrium states, and our analysis only applies to systems with the coupling hierarchy $\lambda_\phi \ll \hbar$ such that the contributions from the nonequilibrium excitations ($\sim \lambda_\phi$) can be disregarded from those of the thermal bath ($\sim \hbar$).
- The fluctuations η are far from thermal equilibrium and there is no hierarchy in the couplings, but a very large number of the fields that compose the bath couple directly to ϕ , hence effectively making \hbar very large¹ [17].

¹Note that this does not invalidate perturbation theory. It is perturbative results which for many degrees of freedom add up and effectively can be described by a large \hbar .

4.1 The Markovian equation

We first investigate our method of chapter 2 to Markovianise the 2PI equation of motion (3.9). In particular, we shall evaluate the leading-order damping rate explicitly, using Eqs. (2.8)(2.9)(2.10) derived in the previous chapter.

For the sake of simplicity, let us assume that $\lambda_\chi, \lambda_\phi \ll \hbar$ for the time being and discard those interactions in (3.7) that arise from the ϕ -selfinteractions. Lifting that assumption is straightforward and identically dealt with, only prefactors slightly differ because diagrams from selfinteractions have different symmetry properties. As far as φ is concerned, this amounts to focusing on a two-scalar theory which solely interacts via $\mathcal{L}_{\text{int}} = -\hbar\phi^2\chi^2/4$.

We first evaluate $\Pi_\varphi^{[1]}$ from (2.9). As shown after Eq. (2.12), Γ_φ does not receive a contribution from Γ_1 through $\Pi_\varphi^{[1]}$ because of the convolution with $(x_1^0 - t)$ in Eq. (2.8). We therefore focus on $\Gamma_2[\varphi, \Delta]$ and looking at Fig. 3.1, it is clear that only the setting-sun diagram with two couplings to the external background φ can contribute because the partial functional derivative in (2.9) only acts on the explicit factors φ at the vertices, not on the implicit φ -dependence of the propagators. Calculating it explicitly, we obtain

$$-\left. \frac{\partial^2 \Gamma_2[\varphi, \Delta[\varphi]]}{\partial \varphi(x_1) \partial \varphi(x)} \right|_{\bar{\varphi}} = -\frac{i\hbar^2}{2} \Delta_\chi^2[\bar{\varphi}](x, x_1) \Delta_\phi[\bar{\varphi}](x, x_1), \quad (4.2)$$

which still has to be convolved with $(x_1^0 - t)$ to obtain the final contribution to Γ_φ . The loop integrals are to be evaluated with full propagators, but with $\varphi = \bar{\varphi}$, i.e., in a (locally) static background. This diagram has been studied before in the literature, see e.g. Ref. [62], and the resulting contribution reads

$$\begin{aligned} \Gamma_\varphi^{[1]} &\simeq \frac{\hbar^2 T^2}{(4\pi)^3 M_\eta} \log\left(\frac{M_\eta}{M_\chi}\right), \text{ for } T \gg M_\eta \gg M_\chi, \\ \Gamma_\varphi^{[1]} &\simeq \frac{\hbar^2 T^2}{(4\pi)^3 M_\chi} \log\left(\frac{M_\chi}{M_\eta}\right), \text{ for } T \gg M_\chi \gg M_\eta, \end{aligned} \quad (4.3)$$

where $M_a^2 = m_a^2 + \delta_{a\chi} \frac{\hbar}{2} \bar{\varphi}^2 + \frac{\hbar}{24} T^2$. This term can be interpreted as dissipation from scatterings with χ -quanta in the thermal bath by making connection to thermal field theory [71, 72]. As expected, the friction coefficient grows with T^2 due to the larger number of scattering partners at higher temperature. We shall come back to this damping coefficient and its interpretation in detail shortly in section 4.5.

We now move on to compute the contribution to Γ_φ from $\Pi_\varphi^{[2]}$, which includes contributions from both, Γ_1 and Γ_2 . Starting from (2.10), we first evaluate

the functional derivative of the propagator Δ with respect to φ using the same technique as for Eq. (2.14)

$$\begin{aligned} \frac{\delta\Delta[\varphi]}{\delta\varphi(x_1)} &= -\Delta[\varphi] \frac{\delta\Delta^{-1}[\varphi]}{\delta\varphi(x_1)} \Delta[\varphi] = -\Delta[\varphi] \frac{\delta(G_0^{-1} - \Pi)}{\delta\varphi(x_1)} \Delta[\varphi] \\ &\simeq -\Delta[\varphi] \frac{\delta(G_0^{-1})}{\delta\varphi(x_1)} \Delta[\varphi], \end{aligned} \quad (4.4)$$

where, in the last step, we only kept the leading tree-level contribution, which dominates the one of the self-energy because φ appears with additional powers of h and loop factors in the self-energy ($|\delta(G_0^{-1})/\delta\varphi(x_1)| > |\delta\Pi/\delta\varphi(x_1)|$). Using this result, we calculate at leading order in the coupling constant h

$$\begin{aligned} \int d^3\mathbf{x}_1 \Pi_\varphi^{[2]}(x_1, x) &= - \int d^3\mathbf{x}_1 \left[\sum_{a,b} \int_{y,z} \frac{\partial^2 \Gamma_{\text{loop}}[\varphi, \Delta]}{\partial\varphi(x) \partial\Delta_{ab}(y, z)} \Big|_{\Delta[\varphi]} \frac{\delta\Delta_{ab}(y, z)}{\delta\varphi(x_1)} \right]_{\bar{\varphi}} \\ &\simeq \int d^3\mathbf{x}_1 \int_{y,z} \left[\frac{\partial^2 \Gamma_{\text{loop}}[\varphi, \Delta]}{\partial\varphi(x) \partial\Delta_\chi(y, z)} \Big|_{\Delta[\varphi]} \int_{u,v} \Delta_\chi[\varphi](y, u) \frac{\delta G_{0,\chi}^{-1}[\varphi](u, v)}{\delta\varphi(x_1)} \Delta_\chi[\varphi](v, z) \right]_{\bar{\varphi}} \\ &= ih\bar{\varphi} \int d^3\mathbf{x}_1 \int_{y,z} \left[\frac{\partial^2 \Gamma_{\text{loop}}[\varphi, \Delta]}{\partial\varphi(x) \partial\Delta_\chi(y, z)} \Big|_{\Delta[\varphi]} \Delta_\chi[\varphi](y, x_1) \Delta_\chi[\varphi](x_1, z) \right]_{\bar{\varphi}}. \end{aligned} \quad (4.5)$$

Here we have used the explicit expression (3.2). Now we articulate the discussion in terms of contributions from Γ_1 and Γ_2 to $\Pi_\varphi^{[2]}$, and argue that those of Γ_2 are suppressed compared to that of Γ_1 . Indeed, we evaluate

$$\left[\frac{\partial^2 \Gamma_1[\varphi, \Delta]}{\partial\varphi(x) \partial\Delta_{ab}(y, z)} \Big|_{\Delta[\varphi]} \right]_{\bar{\varphi}} = -\frac{h}{2} \bar{\varphi} \delta_{ab} \delta_{b\chi} \delta_{\mathcal{C}}(y-z) \delta_{\mathcal{C}}(x-y), \quad (4.6)$$

and

$$\begin{aligned} \left[\frac{\partial^2 \Gamma_2[\varphi, \Delta]}{\partial\varphi(x) \partial\Delta_{ab}(y, z)} \Big|_{\Delta[\varphi]} \right]_{\bar{\varphi}} &= \frac{ih^2 \bar{\varphi}}{4} \left[\delta_{\mathcal{C}}(x-y) + \delta_{\mathcal{C}}(x-z) \right] \times \\ &\times \left[2\Delta_\chi(y, z) \Delta_\phi(y, z) \delta_{a\chi} \delta_{ab} + \Delta_\chi^2(y, z) \delta_{a\eta} \delta_{ab} \right]. \end{aligned} \quad (4.7)$$

We conclude from those that the former which originates from Γ_1 dominates significantly, from both the loop and coupling constant expansions. Therefore,

$$\begin{aligned} \int d^3\mathbf{x}_1 \Pi_\varphi^{[2]}(x_1, x) \\ \simeq ih\bar{\varphi} \int d^3\mathbf{x}_1 \left[\int_{y,z} \frac{\partial^2 \Gamma_1[\varphi, \Delta]}{\partial\varphi(x) \partial\Delta_\chi(y, z)} \Big|_{\Delta[\varphi]} \Delta_\chi[\varphi](y, x_1) \Delta_\chi[\varphi](x_1, z) \right]_{\bar{\varphi}}. \end{aligned} \quad (4.8)$$

Since the system under consideration was assumed homogeneous and isotropic we can perform spatial Fourier transforms in the argument differences, and plugging in (4.6), we find

$$\int d^3 \mathbf{x}_1 \Pi_\varphi^{[2]}(x_1, x) = -\frac{ih^2 \bar{\varphi}^2}{2} \int \frac{d^3 \mathbf{p}}{(2\pi)^3} \left[\Delta_\chi[\varphi](t, x_1^0; \mathbf{p})^2 \right]_{\bar{\varphi}}. \quad (4.9)$$

Splitting the propagators in their spectral and statistical parts (1.66), and using the Schwinger-Keldysh contour relation $\int_C dy^0 \text{sign}_C(x^0 - y^0) = 2 \int_{-\infty}^{x^0} dy^0$, we find for (2.10)

$$\begin{aligned} \Gamma_\varphi^{[2]} &= -2 \times \frac{h^2 \bar{\varphi}^2}{2} \int_{-\infty}^t dx_1^0 (x_1^0 - t) \int \frac{d^3 \mathbf{p}}{(2\pi)^3} \left[\Delta_\chi^+[\varphi](t, x_1^0; \mathbf{p}) \Delta_\chi^-[\varphi](t, x_1^0; \mathbf{p}) \right]_{\bar{\varphi}} \\ &= h^2 \bar{\varphi}^2 \int_0^{+\infty} dz z \int \frac{d^3 \mathbf{p}}{(2\pi)^3} \left[\Delta_\chi^+[\varphi](t, t - z; \mathbf{p}) \Delta_\chi^-[\varphi](t, t - z; \mathbf{p}) \right]_{\bar{\varphi}}, \end{aligned} \quad (4.10)$$

where we have defined $z = t - x_1^0$ in the last line. Explicit expressions for the resummed statistical Δ^+ and spectral Δ^- propagators in a static background have e.g. been computed in Ref. [32]. The latter are only a function of z and using a slight abuse of notation, we can further evaluate

$$\begin{aligned} \Gamma_\varphi^{[2]} &= h^2 \bar{\varphi}^2 \int_0^\infty dz z \int \frac{d^3 \mathbf{p}}{(2\pi)^3} \Delta_\chi^+[\bar{\varphi}](z; \mathbf{p}) \Delta_\chi^-[\bar{\varphi}](z; \mathbf{p}) \\ &= \frac{h^2 \bar{\varphi}^2}{2} \int_{-\infty}^\infty dz z \int \frac{d^3 \mathbf{p}}{(2\pi)^3} \Delta_\chi^+[\bar{\varphi}](z; \mathbf{p}) \Delta_\chi^-[\bar{\varphi}](z; \mathbf{p}) \\ &= \frac{h^2 \bar{\varphi}^2}{2} \lim_{\omega \rightarrow 0} \frac{\partial}{i \partial \omega} \int_{-\infty}^\infty dz e^{i\omega z} \int \frac{d^3 \mathbf{p}}{(2\pi)^3} \Delta_\chi^+[\bar{\varphi}](z; \mathbf{p}) \Delta_\chi^-[\bar{\varphi}](z; \mathbf{p}). \end{aligned} \quad (4.11)$$

Now taking the inverse Fourier transform with respect to z ,

$$\begin{aligned} \Gamma_\varphi^{[2]} &= \frac{h^2 \bar{\varphi}^2}{2} \lim_{\omega \rightarrow 0} \frac{\partial}{i \partial \omega} \int_{-\infty}^\infty dz e^{i\omega z} \int \frac{d^3 \mathbf{p}}{(2\pi)^3} \times \\ &\quad \times \int \frac{d\omega'}{2\pi} \int \frac{d\omega''}{2\pi} e^{-i\omega' z} e^{-i\omega'' z} \Delta_\chi^+[\bar{\varphi}](\omega'; \mathbf{p}) \Delta_\chi^-[\bar{\varphi}](\omega''; \mathbf{p}) \\ &= \frac{h^2 \bar{\varphi}^2}{2} \lim_{\omega \rightarrow 0} \frac{\partial}{i \partial \omega} \int \frac{d^3 \mathbf{p}}{(2\pi)^3} \int \frac{d\omega'}{2\pi} \Delta_\chi^+[\bar{\varphi}](\omega'; \mathbf{p}) \Delta_\chi^-[\bar{\varphi}](\omega - \omega'; \mathbf{p}) \\ &= \frac{h^2 \bar{\varphi}^2}{2} \lim_{\omega \rightarrow 0} \frac{\partial}{i \partial \omega} \int \frac{d^4 p}{(2\pi)^4} \Delta_\chi^+[\bar{\varphi}](p_0; \mathbf{p}) \Delta_\chi^-[\bar{\varphi}](\omega - p_0; \mathbf{p}), \end{aligned}$$

and using that the static background propagators fulfill the KMS relation $\Delta^+(p) = -i(\frac{1}{2} + f_B(p_0))\Delta^-(p)$, we eventually find

$$\Gamma_\varphi^{[2]} = -\frac{h^2\bar{\varphi}^2}{4} \int \frac{d^3\mathbf{p}}{(2\pi)^3} \lim_{\omega \rightarrow 0} \frac{\partial}{\partial \omega} I(\mathbf{p}), \quad (4.12)$$

where $I(\mathbf{p}) = \int \frac{dp_0}{2\pi} (f_B(p_0) - f_B(p_0 - \omega)) \Delta_\chi^-[\bar{\varphi}](p_0; \mathbf{p}) \Delta_\chi^-[\bar{\varphi}](\omega - p_0; \mathbf{p})$. To finally evaluate the integral we use the spectral function in a static background computed in [32] from solving the Kadanoff-Baym equation (3.4)

$$\Delta_\chi^-(p) = \lim_{\epsilon \rightarrow 0^+} \frac{-2i\text{Im}\Pi_\chi^R(p) + 2ip_0\epsilon}{(p^2 - (M_\chi^{\text{tree}})^2 - \text{Re}\Pi_\chi^R(p))^2 + (\text{Im}\Pi_\chi^R(p) + p_0\epsilon)^2}. \quad (4.13)$$

Neglecting collective or bound state excitations, the spectral function (4.13) has four poles which we denote by $\pm\hat{\Omega}_\chi$ and $\pm\hat{\Omega}_\chi^*$. Here we have suppressed the dependence of $\hat{\Omega}_\chi$ on the spatial momentum \mathbf{p} for notational simplicity. Under the assumption that the p^0 -integral which constitutes $I(\mathbf{p})$ is dominated by the pole of its integrand, we can evaluate it using Cauchy's residue theorem. Note that technically the function $\Delta^-(p)$ is not analytic in the complex p^0 -plane because it inherits the branch cut that $\Pi^R(p)$ has across the real p_0 -axis, and which defines $\text{Im}\Pi^R(p) = (\Pi^R(p_0 + i\epsilon, \mathbf{p}) - \Pi^R(p_0 - i\epsilon, \mathbf{p})) / (2i)$. This in principle spoils the validity of Cauchy's theorem. However, under the assumption that the integral is dominated by the pole regions, the problem can be simplified by approximating the integrand with a Breit-Wigner p^0 -independent function with peaks of width $\Gamma_\chi = -2\text{Im}\hat{\Omega}_\chi$ at locations $p_0 = \pm\Omega_\chi = \pm\text{Re}\hat{\Omega}_\chi$, as e.g. explained in Refs. [32, 71]. The latter has no branchcuts and is analytic in the complex plane, hence we can apply Cauchy's theorem. Physically, this corresponds to assuming that quantum interactions such as decays or scatterings are dominated by elementary processes involving on-shell quasiparticles. Of course, this approach has its limitations, e.g. when off-shell transports [14, 70, 71] or multiple scatterings [70, 71, 73, 74] matter. Precisely understanding the breakdown of the Breit-Wigner approximation is a very interesting topic which we would like to investigate in the future. In the following calculation it is convenient to introduce

$$\begin{aligned} F(p_0, \omega) &= 4 \left(f_B(p_0) - f_B(p_0 - \omega) \right) \text{Im}\Pi_\chi^R[\bar{\varphi}](p_0) \text{Im}\Pi_\chi^R[\bar{\varphi}](\omega - p_0) \\ &= -4\omega f'_B(p_0) \left(\text{Im}\Pi_\chi^R[\bar{\varphi}](p_0) \right)^2 + \mathcal{O}(\omega^2) \end{aligned} \quad (4.14)$$

and

$$\begin{aligned} G(p_0) &= \lim_{\omega \rightarrow 0} \frac{F(p_0, \omega)}{\omega} = \lim_{\omega \rightarrow 0} \frac{F(-p_0, \omega)}{\omega} = \lim_{\omega \rightarrow 0} \frac{F(p_0 + \omega, \omega)}{\omega} \\ &= -4f'_B(p_0) \left(\text{Im}\Pi_\chi^R[\bar{\varphi}](p_0) \right)^2 = \frac{2 \left(\text{Im}\Pi_\chi^R[\bar{\varphi}](p_0) \right)^2}{T(\cosh(p_0/T) - 1)}. \end{aligned} \quad (4.15)$$

Note that $G(p_0) = G(-p_0)$. We now compute $I(\mathbf{p})$ at linear order in small ω that is needed to evaluate Eq. (4.12), as the latter sets all contributions of order $\mathcal{O}(\omega^2)$ to zero eventually. Using Cauchy's theorem and isolating linear terms in ω as carefully detailed in [75], we arrive at

$$-I(\mathbf{p}) \simeq \frac{G(\hat{\Omega}_\chi^*) \left(i\Omega_\chi \Gamma_\chi + i\hat{\Omega}_\chi^* \Gamma_\chi + 2\hat{\Omega}_\chi^* \Omega_\chi \right)}{16\hat{\Omega}_\chi^{*3} \Omega_\chi^3 \Gamma_\chi^3} \omega + \left(\hat{\Omega}_\chi^* \rightarrow \hat{\Omega}_\chi, i\Gamma_\chi \rightarrow -i\Gamma_\chi \right) \omega. \quad (4.16)$$

Now taking the limit of this result for small ω , and using the Breit-Wigner $\text{Im}\Pi_\chi^{\text{R}}(\hat{\Omega}_\chi) \simeq -\Omega_\chi \Gamma_\chi$ and narrow peak $\hat{\Omega}^* \simeq \Omega$ approximations, we find

$$\lim_{\omega \rightarrow 0} \frac{\partial}{\partial \omega} I(\mathbf{p}) \simeq -\frac{1}{2T\Omega_\chi^2 \Gamma_\chi (\cosh(\Omega_\chi/T) - 1)}, \quad (4.17)$$

Using the above result in Eq. (4.12) we obtain

$$\Gamma_\varphi^{[2]} \simeq \frac{h^2 \varphi^2(t)}{8T} \int \frac{d^3 \mathbf{p}}{(2\pi)^3} \frac{1}{\Omega_\chi^2 \Gamma_\chi (\cosh(\Omega_\chi/T) - 1)}, \quad (4.18)$$

where we have replaced $\bar{\varphi}$ by the value $\varphi(t)$ that fixes it locally. Although derived in a more formal setting, this result is consistent with what had previously been found in Refs. [17, 62] in terms of parametric dependence. Going further with this integral would necessitate the precise knowledge of Ω_χ and Γ_χ and their dependences on \mathbf{p} , which themselves strongly depend on the details of the interactions that χ is subject to. We shall evaluate them later in this chapter. However, we can already understand many properties of the contributions $\Gamma_\varphi^{[1]}$ and $\Gamma_\varphi^{[2]}$ as they are presented in Eqs. (4.3) and (4.18).

As we discussed in the last chapter, $\Gamma_\varphi^{[1]}$ originates from non-local diagrams that are expected to generate dissipation from general considerations in equilibrium thermal field theory. Therefore, the associated contributions can be interpreted in terms of elementary decays and scatterings of quasiparticles in a thermal bath, and specific processes are identified by cutting through the relevant diagrams. Those display properties that are expected from thermal field theory. First, (4.3) grows with the temperature T , and in an equilibrium language, this is awaited because the density of scattering partners grows with T , and so does the occupancy of final states, hence leading to Bose-enhanced transition amplitudes. Then, the rate grows with the square of h , that is h^2 , which could be anticipated because finite temperature cutting rules identify damping rates with squared scattering amplitudes which grow with h at leading order.

The term $\Gamma_\varphi^{[2]}$, on the other hand, is a genuine nonequilibrium effect which finds its origin in the couplings of quasiparticles and fields to the time-dependent

background φ . As we shall explicitly check in more detail later, for large backgrounds $\varphi > T$, the damping rate (4.18) $\Gamma_\varphi^{[2]}$ dominates over that of $\Gamma_\varphi^{[1]}$. This however is not due to the time dependence of the condensate, rather it originates via the effective coupling to φ in the Lagrangian due to the replacement $\phi \rightarrow \eta + \varphi$, cf. (3.6). Then, and in contradistinction to what is commonly expected, $\Gamma_\varphi^{[2]}$ decreases with T . Not only from the explicit factor $1/T$, but also because one also generally gets additional powers of T in the denominator of the integrand, from Ω_χ and Γ_χ , as these quasiparticle energies and thermal widths typically grow with T . As a final comment, note that formally the expression (4.18) diverges in the limit $\Gamma_\chi \rightarrow 0$, but in our approximation scheme, this limit cannot be taken, because we assumed that $\Gamma_\chi > 0$ when using the Breit-Wigner approximation [32, 71] and applying Cauchy's theorem.

In the coming sections, we shall re-derive (4.18) and further study it for specific quasiparticle dispersion relations and thermal widths which arise from generic renormalisable \mathbb{Z}_2 -symmetric interactions. This will allow us to verify our claims in a generic framework. Instead of using the Markovian method, we shall solve the Kadanoff-Baym Eqs. (3.4)(3.5) analytically, assuming a mild adiabatic evolution of the time-dependent quantities and then insert those propagators in the evolution equation for the background field.

4.2 The homogeneous and isotropic 2PI equations of motion

Let us write the 2PI equations of motion for \mathbb{Z}_2 -symmetric scalars in an isotropic and homogeneous environment, on the Schwinger-Keldysh contour. Because of homogeneity and isotropy, any convolution of a two-point function with the background field rewrites

$$\int dt' \int d^3\mathbf{x}' O(x, x') \varphi(x')^n = \int dt' O(t, t'; \mathbf{p} = \mathbf{0}) \varphi(t')^n. \quad (4.19)$$

In particular, the equation of motion (3.3) then rewrites

$$\left(\partial_t^2 + m_\phi^2 + \frac{\lambda_\phi}{6} \varphi(t)^2 + \int \frac{d^3\mathbf{p}}{(2\pi)^3} \left[\frac{\lambda_\phi}{2} \Delta_\phi^+(t, t; \mathbf{p}) + \frac{h}{2} \Delta_\chi^+(t, t; \mathbf{p}) \right] \right) \varphi(t) + \int_{-\infty}^t dt' \Pi_\phi^{-\text{sun}}(t, t'; \mathbf{p} = \mathbf{0}) \varphi(t') = 0. \quad (4.20)$$

where $\Pi_\phi^{-\text{sun}}(t, t'; \mathbf{p} = \mathbf{0})$ is the zero mode of the spatial Fourier transform of $\Pi_\phi^{-\text{sun}}(x, y)$ in Eq. (3.10), which, we recall, is strictly identical to $\Pi_\phi^{-\text{sun}}(x, y)$ of

(3.24). This will come in handy later on in this section. This contribution to the equation of motion is both coupling constant and loop suppressed, hence we shall first focus on this line of the equation, which includes the closed one-loop correction to the equation of motion. In the coupling constant expansion, this constitutes the leading-order (LO) equation of motion for φ and it turns out to be nothing but the one-loop equation of motion too. As we shall demonstrate, this readily generates both dissipative effects as well as quantum and thermal corrections to the tree-level potential, and the friction terms owe their existence to the nonequilibrium properties of the propagators $\Delta_a^+(t, t; \mathbf{p})$. The contribution from $\Pi_\varphi^{-\text{sun}}(t, t'; \mathbf{p} = \mathbf{0})$ will only correct those found at one-loop and constitutes the next-to-leading (NLO) order equation of motion.

The homogeneous and isotropic Kadanoff-Baym equations (3.4)(3.5) rewrite

$$\left(\partial_{t_1}^2 + \omega_a(t_1; \mathbf{p})^2\right) \Delta_a^-(t_1, t_2; \mathbf{p}) = - \int_{t_2}^{t_1} dt' \Pi_a^-(t_1, t'; \mathbf{p}) \Delta_a^-(t', t_2; \mathbf{p}), \quad (4.21)$$

$$\begin{aligned} \left(\partial_{t_1}^2 + \omega_a(t_1; \mathbf{p})^2\right) \Delta_a^+(t_1, t_2; \mathbf{p}) &= - \int_{-\infty}^{t_1} dt' \Pi_a^-(t_1, t'; \mathbf{p}) \Delta_a^+(t', t_2; \mathbf{p}) \\ &\quad + \int_{-\infty}^{t_2} dt' \Pi_a^+(t_1, t'; \mathbf{p}) \Delta_a^-(t', t_2; \mathbf{p}), \end{aligned} \quad (4.22)$$

where we defined the “local” effective time-dependent frequency, function of the homogeneous background and the local selfenergy

$$\omega_a(t; \mathbf{p}) = \sqrt{\omega_a^{\text{tree}}(t; \mathbf{p})^2 + \int \frac{d^3 \mathbf{q}}{(2\pi)^3} \Pi_a^{\text{loc}}(t, t; \mathbf{p})}, \quad (4.23)$$

with

$$\omega_a^{\text{tree}}(t; \mathbf{p}) = \sqrt{M_a^{\text{tree}}(t)^2 + \mathbf{p}^2}, \quad (4.24)$$

the tree-level frequency which readily includes the feedback of the tree-level coupling to the condensate φ , through the effective masses (3.2).

4.3 Adiabatic solutions of the Kadanoff-Baym equations

Formal solutions of Eqs. (4.21)(4.22) for the propagators that were outlined in Ref. [33] is here re-derived in appendix B, using the Wentzel-Kramers-Brillouin

(WKB) approximation scheme. Dropping the subscripts a for notational simplicity, we find

$$\Delta^-(t_1, t_2; \mathbf{p}) = \frac{\sin\left(\int_{t_2}^{t_1} dt' \Omega(t'; \mathbf{p})\right) e^{-\frac{1}{2} \left| \int_{t_2}^{t_1} dt' \Gamma(t'; \mathbf{p}) \right|}}{\sqrt{\Omega(t_1; \mathbf{p}) \Omega(t_2; \mathbf{p})}}, \quad (4.25)$$

$$\Delta^+(t_1, t_2; \mathbf{p}) = \frac{\cos\left(\int_{t_2}^{t_1} dt' \Omega(t'; \mathbf{p})\right) e^{-\frac{1}{2} \left| \int_{t_2}^{t_1} dt' \Gamma(t'; \mathbf{p}) \right|}}{2\sqrt{\Omega(t_1; \mathbf{p}) \Omega(t_2; \mathbf{p})}} \left(1 + 2f(t_B; \mathbf{p})\right), \quad (4.26)$$

where $t_B = \min(t_1, t_2)$ is the time for which a Boltzmann equation can be derived, see appendix B.2. Here the time dependent quasiparticle dispersion relation $\Omega(t; \mathbf{p})$ and width $\Gamma(t; \mathbf{p})$ are defined through the real and imaginary parts of $\hat{\Omega}(t; \mathbf{p}) = \Omega(t; \mathbf{p}) - \frac{i}{2}\Gamma(t; \mathbf{p})$, such that

$$\Omega(t; \mathbf{p}) = \text{Re}\hat{\Omega}(t; \mathbf{p}), \quad \Gamma(t; \mathbf{p}) = -2\text{Im}\hat{\Omega}(t; \mathbf{p}), \quad (4.27)$$

where the quasiparticle pole $\hat{\Omega}$ is the solution of the equation

$$0 = \hat{\Omega}^2(t, \mathbf{p}) - \omega^2(t, \mathbf{p}) - \tilde{\Pi}^-(t, \hat{\Omega}; \mathbf{p}), \quad (4.28)$$

and $\omega(t; \mathbf{p})$ is that of Eq. (4.23). Here we introduced the Laplace transform

$$\tilde{\Pi}^\pm(t, p_0; \mathbf{p}) = \int_0^\infty dz e^{izp_0} \Pi^\pm(t, t-z; \mathbf{p}). \quad (4.29)$$

For weakly coupled field theories, the so-called narrow width condition is observed $\text{Re}\tilde{\Pi}^- \gg \text{Im}\tilde{\Pi}^-$ and we find the transcendental equations

$$\Omega(t; \mathbf{p}) = \sqrt{\omega^2(t; \mathbf{p}) + \text{Re}\tilde{\Pi}^-(t, \hat{\Omega}; \mathbf{p})}, \quad (4.30)$$

$$\Gamma(t; \mathbf{p}) = -\frac{\text{Im}\tilde{\Pi}^-(t, \hat{\Omega}; \mathbf{p})}{\Omega(t; \mathbf{p})}, \quad (4.31)$$

which relate the quasiparticle dispersion relation and width to real and imaginary parts of selfenergies respectively. In particular when time translation invariance is restored, e.g. for thermal equilibrium situations, it is straightforward to show that $\tilde{\Pi}^-(t, p_0; \mathbf{p})$ is precisely the retarded selfenergy $\Pi^R(p^0; \mathbf{p})$ and one recovers the usual equilibrium relations that define the particle decay widths and interaction rates [21], as well as the quasiparticle mass shells, in terms of the retarded selfenergy.

As shown in appendix B.2, the mode-dependent distribution function $f(t; \mathbf{p})$ in Eq. (4.26) follows a Markovian Boltzmann equation,

$$\dot{f}(t; \mathbf{p}) = (1 + f(t; \mathbf{p}))\Gamma^<(t; \mathbf{p}) - f(t; \mathbf{p})\Gamma^>(t; \mathbf{p}) \quad (4.32)$$

where the gain and loss terms $\Gamma^{\gtrless}(t; \mathbf{p})$ are defined through the relations

$$\Gamma = \Gamma^> - \Gamma^<, \quad 2\text{Re}\tilde{\Pi}^+(t, \hat{\Omega}; \mathbf{p}) = -\Omega(t; \mathbf{p})(\Gamma^>(t; \mathbf{p}) + \Gamma^<(t; \mathbf{p})). \quad (4.33)$$

The former of these allows to express the Boltzmann equation (4.32) as

$$\dot{f}(t; \mathbf{p}) = -\Gamma(t; \mathbf{p})(f(t; \mathbf{p}) - \bar{f}(t; \mathbf{p})) \quad (4.34)$$

where \bar{f} is defined by

$$\bar{f} = (\Gamma^>/\Gamma^< - 1)^{-1}. \quad (4.35)$$

Again, those equations are particularly illuminating in the equilibrium case where $\tilde{\Pi}^-(t, p_0; \mathbf{p})$ is the retarded selfenergy $\Pi^R(p^0; \mathbf{p})$, and therefore $\Gamma^{\lessgtr} \propto \Pi^{\lessgtr}$ satisfy the KMS (1.88) or detailed balance relation $\Gamma^>/\Gamma^< = e^{\Omega/T}$, such that $\bar{f} = f_B$ is the Bose-Einstein distribution. Therefore $\Gamma(t; \mathbf{p})$ is the interaction rate that brings the nonequilibrium distribution function f back to its equilibrium value \bar{f} . For readers used to kinetic theory and Boltzmann equations, it may seem odd that the right hand side of (4.34) only depends linearly on f while we started out with \mathbb{Z}_2 -symmetric interactions. However, one has not to forget here that $\Gamma(t; \mathbf{p})$ is the inclusive thermal damping rate for a quasiparticle of given momentum, to which all scattering processes and decays in the plasma contribute, it e.g. includes selfscatterings and is itself a functional of f . When all loop integrals are properly taken into account, the right hand side of (4.34) will eventually be at least quadratic in f , as one would classically expect.

All relations presented here essentially rely on two major assumptions. First, we assumed that quantum selfenergies $\Pi(t, t')$ act as window functions of finite supports which suppress memory integrals for domains which take either of the two arguments away from the other by an amount larger than τ_{int} . Then, the WKB Ansatz (4.25) subtly relies on a peaked Breit-Wigner approximation, which assumes that phase space integrals are primarily dominated by the poles of the spectral function. A more careful discussion of how good approximations they are can e.g. be found in Refs. [14, 56].

Adiabatic distribution function. Again using our adiabaticity assumption, we can further simplify the statistical propagator, which we recall is of uttermost importance to evaluate the one-loop equation of motion for φ .

First let us rewrite the Eq. (4.34) as

$$f(t, \mathbf{p}) = \bar{f}(t, \mathbf{p}) - \frac{\dot{f}(t, \mathbf{p})}{\Gamma(t; \mathbf{p})}. \quad (4.36)$$

Taking an iterative approach to solve this equation, a solution reads

$$f = \bar{f} - \frac{\dot{\bar{f}}}{\Gamma} + \frac{\ddot{\bar{f}}}{\Gamma^2} - \frac{\dot{\Gamma}\dot{\bar{f}}}{\Gamma^3} + \dots \quad (4.37)$$

where \dots includes an infinite series in powers of time derivatives of \bar{f} . In an adiabatically evolving background, those are suppressed and we ignore all terms beyond the second order one to find the approximate solution of (4.34)

$$f(t, \mathbf{p}) \simeq \bar{f}(t, \mathbf{p}) - \frac{\dot{\bar{f}}(t, \mathbf{p})}{\Gamma(t; \mathbf{p})}. \quad (4.38)$$

This truncation always is justified for a sufficiently large temperature and in particular in appendix B.4, we show how large the temperature should be for a field evolving in a harmonic potential. This can be interpreted as

$$f(t, \mathbf{p}) \simeq \bar{f}(t - 1/\Gamma(t; \mathbf{p}); \mathbf{p}), \quad (4.39)$$

where $1/\Gamma$ plays the role of a delay factor between the distribution functions of the bath and the one of the system. A more formal but longer proof of this is presented in appendix B.3. As a final result for this subsection, by plugging Eq. (4.38) into Eq. (4.26), we get the statistical propagator

$$\begin{aligned} \Delta^+(t_1, t_2; \mathbf{p}) &\simeq \frac{\cos\left(\int_{t_2}^{t_1} dt' \Omega(t'; \mathbf{p})\right) e^{-\frac{1}{2} \left| \int_{t_2}^{t_1} dt' \Gamma(t'; \mathbf{p}) \right|}}{2\sqrt{\Omega(t_1; \mathbf{p})\Omega(t_2; \mathbf{p})}} \\ &\times \left(1 + 2\bar{f}(t_B; \mathbf{p}) - \frac{2\dot{\bar{f}}(t_B; \mathbf{p})}{\Gamma(t_B; \mathbf{p})} \right). \end{aligned} \quad (4.40)$$

Local thermal equilibrium in a large reservoir. Assuming a local thermal equilibrium, we locally satisfy the KMS or detailed balance condition $\Gamma^>/\Gamma^< = e^{\Omega/T}$ in Eq. (4.35) that go in loop integrals, so as to have $\bar{f}(t, \mathbf{p}) = f_B(\Omega(t; \mathbf{p}))$ in Eq. (4.40). Therefore, Eq. (4.39) rewrites

$$f(t, \mathbf{p}) \simeq f_B(\Omega(t; \mathbf{p})) - \frac{\dot{f}_B(\Omega(t; \mathbf{p}))}{\Gamma(t; \mathbf{p})}. \quad (4.41)$$

We shall be interested in the regime where $\dot{f}_B(\Omega)/\Gamma$ in Eq. (4.41) is a small perturbation, which describes a local quasiequilibrium situation. This is in particular valid when the time scale $1/\Gamma(t; \mathbf{p})$ on which the distribution is brought to its thermal one is very short. Mathematically, this is stated as

$$\frac{\dot{f}_B(\Omega)}{\Gamma} \lesssim f_B(\Omega), \quad (4.42)$$

which, we note in passing, is the condition used to derive Eq. (4.38). The factor $\dot{f}_B(\Omega)$ is very complicated to deal with in a generic nonequilibrium situation where many quantities have nontrivial time-evolutions. In a local thermal equilibrium situation wherein a time-dependent temperature can be defined, we get for the problem at hand

$$\dot{f}_B(\Omega) = \frac{df_B(\Omega)}{d\Omega} \frac{d\Omega}{d\varphi} \dot{\varphi} + \frac{df_B(\Omega)}{dT} \dot{T}. \quad (4.43)$$

Now further assuming that the plasma of χ -particles acts as a large thermal reservoir of constant temperature, the second term of the previous equation vanishes and one obtains

$$\dot{f}_B(\Omega(t; \mathbf{p})) = \frac{-1}{2T(\cosh(\Omega(t; \mathbf{p})/T) - 1)} \frac{d\Omega(t; \mathbf{p})}{d\varphi(t)} \dot{\varphi}(t). \quad (4.44)$$

The terms proportional to $\dot{\varphi}(t)$ will give rise to dissipation and are therefore of great importance. To compute $\frac{d\Omega}{d\varphi}$, we focus on the tree level contribution and neglect that from the self-energy, which is suppressed by an extra power of the relevant coupling constant, as well as by a loop factor. Using (4.23), we find

$$\frac{d\Omega_a}{d\varphi} \simeq \frac{d\Omega_a}{d\omega_a} \frac{d\omega_a}{d\varphi} \simeq \frac{\omega_a}{\Omega_a} \frac{g_a \varphi / 2}{\omega} = \frac{g_a \varphi}{2\Omega_a}, \quad (4.45)$$

where $g_\phi = \lambda_\phi$ and $g_\chi = h$. Using Eq. (4.45) in (4.44), Eq. (4.38) becomes

$$f_a(t, \mathbf{p}) \simeq f_B(\Omega_a(t; \mathbf{p})) + \frac{g_a \varphi(t) \dot{\varphi}(t)}{4T \Omega_a(t; \mathbf{p}) \Gamma_a(t; \mathbf{p}) \left(\cosh\left(\frac{\Omega_a(t; \mathbf{p})}{T}\right) - 1 \right)}. \quad (4.46)$$

And finally using Eqs. (4.46) and (4.38), Eq. (4.40) reads ($t \rightarrow t_B$)

$$\Delta_a^+(t_1, t_2; \mathbf{p}) \simeq \frac{\cos\left(\int_{t_2}^{t_1} dt' \Omega_a(t'; \mathbf{p})\right) e^{-\frac{1}{2} \left| \int_{t_2}^{t_1} dt' \Gamma_a(t'; \mathbf{p}) \right|}}{2\sqrt{\Omega_a(t_1; \mathbf{p}) \Omega_a(t_2; \mathbf{p})}} \times \left[1 + 2f_B(\Omega_a(t_B; \mathbf{p})) + \frac{g_a \varphi(t_B) \dot{\varphi}(t_B)}{2T \Omega_a(t_B; \mathbf{p}) \Gamma_a(t_B; \mathbf{p}) \left(\cosh\left(\frac{\Omega_a(t_B; \mathbf{p})}{T}\right) - 1 \right)} \right]. \quad (4.47)$$

While the first two terms of this equation correspond to nothing but the quasi-particle approximation to the equilibrium statistical propagator, the third one is a purely out-of-equilibrium feature due to the breaking of time translation invariance from φ . Hence, the latter multiplies $\dot{\varphi}$ and will eventually generate dissipation. We shall carefully study this in the next section.

4.4 The leading order equation of motion for the condensate φ

Plugging our approximated statistical propagator of Eq. (4.47) in the leading order (in the coupling constant) equation of motion for φ (3.9), we find

$$\ddot{\varphi}(t) + \dot{\varphi}(t)\Gamma_{\varphi}^{\text{LO}} + V'(\varphi) = 0. \quad (4.48)$$

with

$$V'(\varphi) = m_{\phi}^2\varphi(t) + \frac{\lambda_{\phi}}{6}\varphi(t)^3 + \sum_{a=\phi,\chi} \frac{g_a\varphi(t)}{2} \int \frac{d^3\mathbf{p}}{(2\pi)^3} \frac{(1 + 2f_B(\Omega_a(t; \mathbf{p})))}{2\Omega_a(t; \mathbf{p})}, \quad (4.49)$$

where $g_{\phi} = \lambda_{\phi}$ and $g_{\chi} = h$, and with

$$\Gamma_{\varphi}^{\text{LO}} = \sum_{a=\phi,\chi} \frac{g_a^2\varphi(t)^2}{8T} \int \frac{d^3\mathbf{p}}{(2\pi)^3} \frac{1}{\Omega_a(t; \mathbf{p})^2 \Gamma_a(t; \mathbf{p}) \left(\cosh\left(\frac{\Omega_a(t; \mathbf{p})}{T}\right) - 1 \right)}. \quad (4.50)$$

This last equation is precisely the result of (4.18) which was obtained from the Markovian method described in chapter 2. Here, we have derived it from the WKB for the propagators, and have particularised it to the two-real-scalar theory (3.6) and have provided the defining equations for the effective dispersion relations (4.30) and widths (4.31). These last two ingredients are the remaining unknowns to be evaluated before having finally derived the master equation for an adiabatically evolving condensate.

4.4.1 The effective frequency and effective potential

The effective frequencies are determined from the Kadanoff-Baym equations (4.21) and (4.22) which yield Eq. (4.30), that is

$$\Omega_a^2(t; \mathbf{p}) = \omega_a^2(t; \mathbf{p}) + \text{Re}\tilde{\Pi}_a^-(t, \hat{\Omega}; \mathbf{p}), \quad (4.51)$$

where $\omega_a^2(t; \mathbf{p})$ is the effective frequency which gets quantum and thermal corrections from the tree-level and local selfenergy insertions, cf. Eq. (4.23). These equations, together with the effective potential (4.49), namely

$$V'(\varphi) = m_{\phi}^2\varphi(t) + \frac{\lambda_{\phi}}{6}\varphi(t)^3 + \sum_{a=\phi,\chi} \frac{g_a\varphi(t)}{2} \int \frac{d^3\mathbf{p}}{(2\pi)^3} \frac{(1 + 2f_B(\Omega_a(t; \mathbf{p})))}{2\Omega_a(t; \mathbf{p})}, \quad (4.52)$$

form a set of divergent transcendental equations that ought to be renormalised selfconsistently, accounting for the presence of time-dependent divergences, because of the time-dependence of *a priori* both the temperature and the background condensate. In Appendix C, we explicitly solve the relevant leading-order one-loop integrals and selfconsistently renormalise the effective frequencies and potential. The time-dependent divergences of the Kadanoff-Baym equations fix all counterterms of the effective potential but both conspire to simultaneously be finite at all times. In Appendix C, we provide expressions for all counterterms and for the finite effective frequencies and potential, imposing renormalisation conditions at arbitrary temperature T_0 , background φ_0 and renormalisation scale² μ , e.g. cf. Eq. (C.32), such that the Lagrangian parameter $m_a = m_a^{\text{phys}}(\varphi_0, T_0)$ is the physical mass of particle excitations of species $a = \phi, \chi$. While this numerically avoids the presence of large logarithms, the expressions are analytically on the longer side of the spectrum and the physical origins of the different terms are less isolated. Therefore, we here only present the effective frequency and potential renormalised at vanishing temperature and background, which, neglecting finite terms from the one-loop crab diagrams, read

$$\begin{aligned} \Omega_a^2(t; \mathbf{p}) &= \mathbf{p}^2 + m_a^2 + \frac{g_a}{2} \varphi^2(t) + T^2 \sum_{b=\phi, \chi} c_{ab} F_b(t) \\ &+ \sum_{b=\phi, \chi} \frac{c_{ab}}{2(4\pi)^2} (M_b^2(t) \ln(M_b(t)^2/\mu^2) - m_b^2 \ln(m_b^2/\mu^2)), \end{aligned} \quad (4.53)$$

$$\begin{aligned} V'(\varphi) &= m_\phi^2 \varphi(t) + \frac{\lambda_\phi}{6} \varphi^3(t) + \varphi(t) T^2 \sum_{a=\phi, \chi} g_a F_a(t) \\ &+ \varphi(t) \sum_{a=\phi, \chi} \frac{g_a}{2(4\pi)^2} (M_a^2(t) \ln(M_a(t)^2/\mu^2) - m_a^2 \ln(m_a^2/\mu^2)), \end{aligned} \quad (4.54)$$

and $m_a = m_a^{\text{phys}}$ is the vacuum physical mass for particle excitations of the field species a . Here we have introduced $g_\phi = \lambda_\phi$, $g_\chi = h$ and c_{ab} a 2×2 matrix of couplings such that $c_{aa} = \lambda_a$ and $c_{ab} = h$, cf. (3.13)(3.14). The time-dependent effective mass $M_a(t)$ takes the generic form

$$M_a^2(t) = m_{a,r}^2 + \frac{g_a}{2} \varphi^2(t) + T^2 \sum_{b=\phi, \chi} c_{ab} F_b^{\text{tree}}(t), \quad (4.55)$$

with the time-dependent function

$$F_b^{\text{tree}}(t) = \frac{1}{(2\pi)^2} \left(\text{Li}_2 \left(e^{-M_b^{\text{tree}}(t)/T} \right) - \frac{M_b^{\text{tree}}(t)}{T} \log \left(1 - e^{-M_b^{\text{tree}}(t)/T} \right) \right)$$

²We keep the renormalisation scale as an arbitrary parameter μ in the equations but whenever needed for plots or numerical analysis, we take $\mu^2 = m_\phi^2/e$ such that $\ln m_\phi^2/\mu^2 = 1$.

(4.56)

and identically without the “tree” superscript. The latter is an estimate of the finite-temperature tadpole, $\frac{1}{T^2} \int \frac{d^3 \mathbf{q}}{(2\pi)^3} \frac{f_B(\omega_b^{\text{tree}}(t; \mathbf{q}))}{\omega_b^{\text{tree}}(t; \mathbf{q})}$ which is commonly encountered in field theory [21], cf. Eq. (C.28). Our analytic approximation exactly interpolates the low temperature $M^{\text{tree}}/T \gg 1$ and high temperature limit $M_b^{\text{tree}}/T \rightarrow 0$ for which the standard result is known in the literature $F|_{M_b^{\text{tree}}/T \rightarrow 0} = 1/24$ [21], with a maximal 15% error in the (narrow) intermediate regime where the field-dependent mass and temperature are comparable. Defining $\Omega_a^2(t; \mathbf{p}) = \mathbf{p}^2 + M_a^{\text{eff}}(t)^2$, we have a definition for a physical, quasi-particle effective mass given by the following expression

$$M_a^{\text{eff}}(t)^2 = m_a^2 + \frac{g_a}{2} \varphi^2(t) + T^2 \sum_{b=\phi, \chi} c_{ab} F_b(t) \quad (4.57)$$

$$+ \sum_{b=\phi, \chi} \frac{c_{ab}}{2(4\pi)^2} (M_b^2(t) \ln(M_b(t)^2/\mu^2) - m_b^2 \ln(m_b^2/\mu^2)),$$

which will be plugged in the loop integrals to evaluate the particle thermal widths (4.31) that feed into the condensate damping rate (4.50).

In Fig. 4.1 we depict the effective force $V'(\varphi)$ as a function of the background φ for various temperatures. We used a logarithmic scale on both axis to carefully display the role of the temperature in the low field regime, and the deviation from the polynomial behaviour in the intermediate regime where the temperature T is comparable to the background φ . In the large field regime, the temperature is negligible and all cases collapse onto one single value, that of the large-field-valued potential. This qualitative behaviour is independent of the choice for the couplings but the plot was made for $\lambda_\phi = 10h = 10\lambda_\chi$, because this case study will be shown to be of greater relevance shortly.

In Fig. 4.2 we depict the effective force $V'(\varphi)$ normalised to its classical counterpart $m_\phi\varphi + \lambda_\phi\varphi^3/6$ as a function of the background φ for various temperatures. Again, the logarithmic scale on both axis clearly shows that thermal corrections matter when $T > \varphi$. In the large field regime, they can however be neglected, and the larger φ , the less important the quantum and thermal corrections, and both the effective and classical forces eventually equate. Again, this qualitative behaviour is independent of the choice for the couplings, and the plot was made for $\lambda_\phi = 10h = 10\lambda_\chi$, because it will be shown of greater relevance shortly.

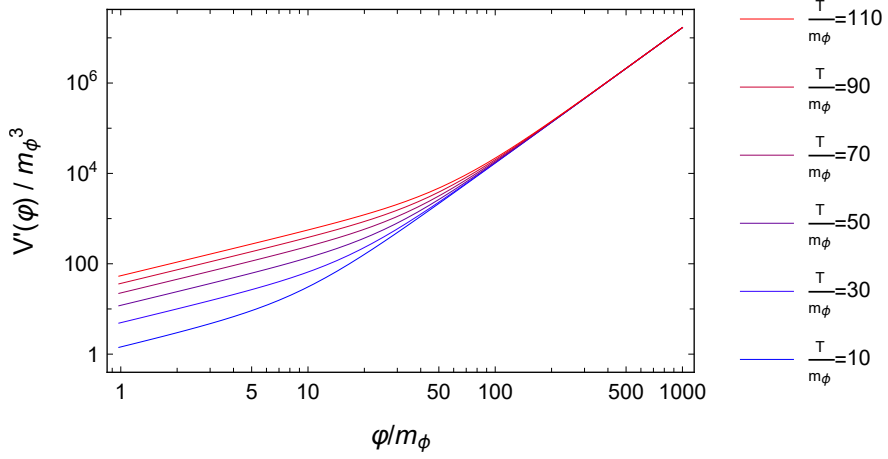


Figure 4.1: The effective force $V'(\varphi)$ of Eq. (4.54) vs. the background field φ , both normalised to the mass m_ϕ , and for various temperatures, with a logarithmic scale on both axis.

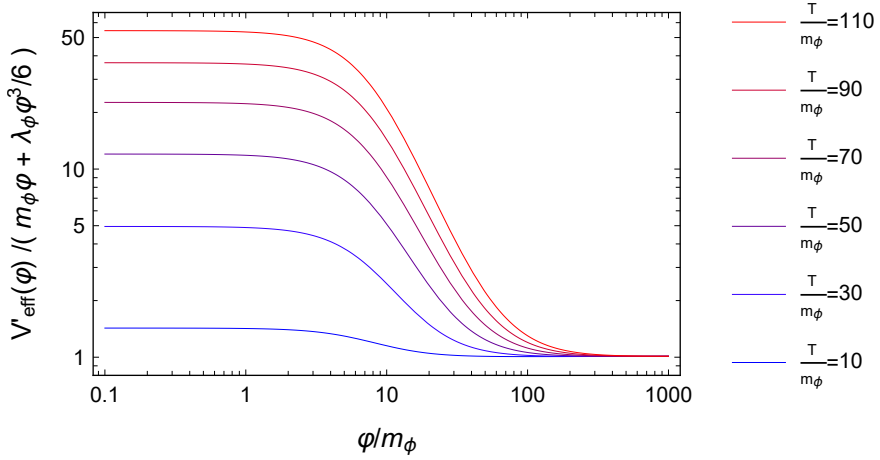


Figure 4.2: The effective force $V'(\varphi)$ of Eq. (4.54) normalised to its classical counterpart $m_\phi\varphi + \lambda_\phi\varphi^3/6$ vs. the background field φ and for various temperatures, with a logarithmic scale on both axis.

4.4.2 The leading order thermal width $\Gamma(t; \mathbf{p})$

Let us determine the leading order thermal width $\Gamma(t; \mathbf{p})$ defined via Eq. (4.31). Again, this *a priori* constitutes a very complicated transcendental equation.

We shall simplify the right hand side of the equation as follows. First, we shall employ zero-width propagators evaluated at the one-loop effective frequency (4.53) which includes both the leading-order condensate backreaction and temperature corrections. Second, and *only within loop integrals*, we shall assume that φ is constant and evaluated at the time t which is set by the time we evaluate $\Gamma(t; \mathbf{p})$ at. We denote this value of φ as $\varphi(t) = \bar{\varphi}$. This is justified because selfenergies act as window functions of finite supports which widths is some positive power of τ_{int} and because all along this chapter, φ was assumed to vary slowly with respect to that time scale. Under these approximations, time translation invariance is restored under loop integrals and our WKB propagators (4.25)(4.26) are only a function of $z = t_1 - t_2$

$$\bar{\Delta}^-(t_1, t_2; \mathbf{p}) \simeq \frac{\sin(\bar{\Omega}(\mathbf{p})z)}{\bar{\Omega}(\mathbf{p})}, \quad \bar{\Delta}^+(t_1, t_2; \mathbf{p}) \simeq \frac{\cos(\bar{\Omega}(\mathbf{p})z)}{2\bar{\Omega}(\mathbf{p})} (1 + 2f_B(\bar{\Omega})). \quad (4.58)$$

We emphasise that the use of these propagators restores time translation invariance, and therefore $\tilde{\Pi}^-(t, \Omega; \mathbf{p}) = \Pi^R(\Omega, \mathbf{p})$ is precisely the four-dimensional Fourier transform of the retarded selfenergy, and therefore $2i\text{Im}\tilde{\Pi}^-(t, \hat{\Omega}; \mathbf{p}) = \Pi^-(p)$ where $\Pi^-(p)$ is the four-dimensional Fourier transform of those spectral selfenergies of Eqs. (3.13)-(3.18), which we shall compute using the aforementioned WKB propagators. Under all these assumptions, we therefore find

$$\Gamma_a(t; \mathbf{p}) \simeq -\frac{\bar{\Pi}_a^-(\bar{\Omega}_a; \mathbf{p})}{2i\bar{\Omega}_a(\mathbf{p})}, \quad (4.59)$$

where Ω_a is defined in Eq. (4.53) and the overbar notation designates that all occurrences of φ are to be evaluated at a constant $\bar{\varphi} = \varphi(t)$ in loop integrals, as explained above. $\bar{\Pi}_a^-$ gets a contribution from the crab and the sunset diagrams separately, see Eqs. (3.13)-(3.18). Therefore we split

$$\Gamma_a(t; \mathbf{p}) = \Gamma_a^{\text{crab}}(t; \mathbf{p}) + \Gamma_a^{\text{sunset}}(t; \mathbf{p}) \quad (4.60)$$

and we now focus on these separate contributions. The cuts through both are depicted in Fig. 4.3. The crab widths are associated with φ -enhanced $\phi \leftrightarrow \chi\chi$ (inverse) decays and the sunset ones with finite-temperature $aa \leftrightarrow bb$ scatterings, with $a, b = \phi, \chi$.



Figure 4.3: Cutkosky cuts through the crab and sunset selfenergies for χ -particles. Similar diagrams can be drawn for the ϕ -case.

The crab widths. We evaluate the crab widths in appendix D and get

$$\Gamma_{\chi}^{\text{crab}}(t; \mathbf{p}) = \theta(\bar{M}_{\phi} - 2\bar{M}_{\chi}) \frac{h^2 T \bar{\varphi}^2}{16\pi |\mathbf{p}| \bar{\Omega}_{\chi}(\mathbf{p})} \log \left(\frac{f_B(\omega_{\chi\phi}^-) f_B(\omega_{\phi\chi}^+)}{f_B(\omega_{\chi\phi}^+) f_B(\omega_{\phi\chi}^-)} \right), \quad (4.61)$$

$$\Gamma_{\phi}^{\text{crab}}(t; \mathbf{p}) = \theta(\bar{M}_{\phi} - 2\bar{M}_{\chi}) \frac{h^2 T \bar{\varphi}^2}{32\pi |\mathbf{p}| \bar{\Omega}_{\phi}(\mathbf{p})} \log \left(\frac{f_B(\omega_{\phi}^-) f_B(-\omega_{\phi}^-)}{f_B(\omega_{\phi}^+) f_B(-\omega_{\phi}^+)} \right), \quad (4.62)$$

with

$$\omega_{\chi\phi}^{\pm} = \frac{(\bar{M}_{\phi}^2 - 2\bar{M}_{\chi}^2) \sqrt{|\mathbf{p}|^2 + \bar{M}_{\chi}^2} \pm |\mathbf{p}| \bar{M}_{\phi} \sqrt{\bar{M}_{\phi}^2 - 4\bar{M}_{\chi}^2}}{2\bar{M}_{\chi}^2}, \quad (4.63)$$

$$\omega_{\phi\chi}^{\pm} = \frac{\bar{M}_{\phi}^2 \sqrt{|\mathbf{p}|^2 + \bar{M}_{\chi}^2} \pm |\mathbf{p}| \bar{M}_{\phi} \sqrt{\bar{M}_{\phi}^2 - 4\bar{M}_{\chi}^2}}{2\bar{M}_{\chi}^2}, \quad (4.64)$$

$$\omega_{\phi}^{\pm} = \frac{\bar{M}_{\phi}^2 \sqrt{|\mathbf{p}|^2 + \bar{M}_{\phi}^2} \pm |\mathbf{p}| \bar{M}_{\phi} \sqrt{\bar{M}_{\phi}^2 - 4\bar{M}_{\chi}^2}}{2\bar{M}_{\phi}^2}. \quad (4.65)$$

Here the overbarred masses are those effective masses from (4.57) where their time-dependence is evaluated at the reference time t for which $\varphi(t) = \bar{\varphi}$, i.e. $\bar{M}_a = M_a^{\text{eff}}(t)$. The Heaviside step function $\theta(\bar{M}_{\phi} - 2\bar{M}_{\chi})$ is nothing but the kinematic threshold for the on-shell decays and annihilations $\phi \leftrightarrow \chi\chi$ from the Cutkosky cuts through the crab diagram, as depicted in Fig. 4.3. Cut lines can be reoriented at finite temperature. In contrast to (4.61) which corresponds to the annihilation rate, the creation rate (4.62) is non-vanishing at zero temperature and reads

$$\lim_{T \rightarrow 0} \Gamma_{\phi}^{\text{crab}} = \theta(\bar{M}_{\eta} - 2\bar{M}_{\chi}) \frac{h^2 \bar{\varphi}^2}{32\pi \bar{\Omega}_{\phi}(\mathbf{p})} \sqrt{1 - \frac{4\bar{M}_{\chi}^2}{\bar{M}_{\phi}^2}}, \quad (4.66)$$

which is the vacuum result for the decay rate of $\phi \rightarrow \chi\chi$, cf. Eq. (D.27).

While the above finite temperature crab widths are known in the context of triscalar interactions with dimensionful couplings, see e.g. [71], they are very much less so when they are obtained from a time-dependent condensate-induced vertex, as it is the case here. In that sense, our results are qualitatively new and as a matter of fact, these contributions to the particle widths have been omitted in the literature in multiple occasions. For instance, see e.g. Ref. [62] where they perform a similar analysis to the one presented here, except it is using the 1PI effective action. More interestingly, and again using the 1PI formalism, the state-of-the-art analytic investigation on the feasibility of two-scalar warm inflation [17] also misses that contribution. Therefore, it goes without saying that it is of great interest to understand the parametric regimes where the crab widths prevail, as those will potentially contain qualitatively different results than [17, 62]. Once identified, we will particularise the discussion to those regimes where the crab widths dominate.

In order to maximise the effects of the crab widths, they better be kinematically allowed to start with, and we want $\theta(\bar{M}_\eta - 2\bar{M}_\chi) = 1$. *A priori*, we have a 5-dimensional space for the Lagrangian parameters, namely $\{m_\phi, m_\chi, \lambda_\phi, \lambda_\chi, h\}$, hence leading to a rich phenomenology as φ and T evolve and feed in the quantum corrected masses (4.57).³

For the problem at hand, we want to find model parameters that maximise the impact of the crab widths over a wide range of temperature and background elongations. As far as $\theta(\bar{M}_\eta - 2\bar{M}_\chi)$ is concerned, numerically scanning through our 5-dimensional parameter space, we see that maintaining $\theta(\bar{M}_\eta - 2\bar{M}_\chi) = 1$ requires

$$m_\phi \gtrsim 2m_\chi, \quad \lambda_\phi \gtrsim 4.1h, \quad h = \lambda_\chi. \quad (4.67)$$

The important point here is that when λ_ϕ falls below $4.1h$, then, at fixed temperature, the kinematic condition $M_\phi > 2M_\chi$ is not always fulfilled and the transition happens between $4h < \lambda_\phi < 4.1h$.

When T and φ are large, they effectively make the bare masses irrelevant, and we shall always pick $m_\phi/m_\chi = 10^2$ in this work, which by the way satisfies (4.67). This choice is motivated by inflationary cosmology where the heavy inflaton decays into radiation. Nevertheless, we emphasise that this will not

³For instance, one could e.g. imagine that $m_\chi \gg m_\chi$ and $\lambda_\phi = \lambda_\chi > h$ such that $\theta(\bar{M}_\eta - 2\bar{M}_\chi) = 1$ only once we go beyond a certain value for φ . One could even potentially imagine pathological situations where the kinematic window $\bar{M}_\eta - 2\bar{M}_\chi > 0$ is open to start with, then closes and reopens again, as T and φ evolve. These cases would clearly display the discontinuous nature of the crab width, due to the kinematic thresholds associated with the (inverse) decays $\phi \leftrightarrow \chi\chi$.

have much influence on $\theta(\bar{M}_\eta - 2\bar{M}_\chi)$ as once T or φ become somewhat significant, say e.g. $T/m_\phi = \varphi/m_\phi = 10$, then the vacuum masses barely affect the effective ones. That said, we are effectively left with 3 parameters, namely $\{\lambda_\phi, \lambda_\chi, h\}$ and we conclude that in order for our crab width to contribute to start with, (4.67) is a necessary condition. Then comes the question whether or not it is a significant contribution to the full thermal width (4.60). In order to try and understand this, we must first evaluate the second term of (4.60), namely the sunset widths.

The sun widths. The contribution from the sunsets to the thermal width (4.60) were evaluated in [17, 62, 76] in the large temperature (vs. thermal mass) regime, $T \gg M_a$, for $a = \phi, \chi$ and they read

$$\Gamma_a^{\text{sun}}(t; \mathbf{p}) = \frac{(\lambda_a^2 + 3h^2) T^2}{1536\pi\bar{\Omega}_a(\mathbf{p})}. \quad (4.68)$$

Those do not involve kinematic thresholds as the finite temperature Cutkosky cut lines can be reoriented, and for the sake of the sunset diagrams, those correspond to $aa \leftrightarrow bb$ scatterings which are always allowed. This is a pure finite temperature effect and as a matter of fact, in vacuum, the sunset widths would vanish because a particle cannot decay into one of its peers, plus two other particles. Therefore, it is well justified to only evaluate the sunset widths when $T \gg M_a$, since they are exponentially Boltzmann suppressed otherwise, as thermal effects always are. For this reason, even though our analytic approximation $T \gg M_a$ breaks down at some point, we expect that our results can be extrapolated to beyond $T \gg M_a$ by interpolating our solution with a Boltzmann-suppressed decaying exponential. Eventually, note that the $1/\bar{\Omega}_a$ factor is physically well-posed to. It indicates that in its rest frame, a particle has a shorter life time. This is due to nothing but relativistic time dilation.

Comparing the crab and sunset widths. It is now interesting to try and compare the parametric dependence of $\Gamma_\phi^{\text{crab}}$ vs. Γ_ϕ^{sun} , as functions of the temperature and the background field. These of course can only be compared if $\Gamma_\phi^{\text{crab}}$, or $\phi \rightarrow \chi\chi$ is not kinematically forbidden to begin with. Therefore, we shall choose model parameters that ensure $M_\phi > M_\chi$, cf. (4.67). In Figs. 4.4 and 4.5 we depict $\Gamma_\phi^{\text{crab}}$ and Γ_ϕ^{sun} as functions of φ , both normalised to $m_\phi = 10^2 m_\chi$, for various temperatures, and for a reference momentum⁴ $|\mathbf{p}| = \langle |\mathbf{p}| \rangle \simeq$

⁴We chose it to be the statistical average momentum $\langle p \rangle$ for a massive scalar, which can be evaluated numerically, and for any mass or temperature with $m < T$, lies within $\langle p \rangle \in [2.7T, 3T]$. This choice is justified for two reasons. First because this tells us what

$3T$, respectively for $\lambda_\phi/\lambda_\chi = \lambda_\phi/h = 10$ and for $\lambda_\phi/\lambda_\chi = \lambda_\phi/h = 10^2$, chosen to ensure $M_\phi > 2M_\chi$ at all times.

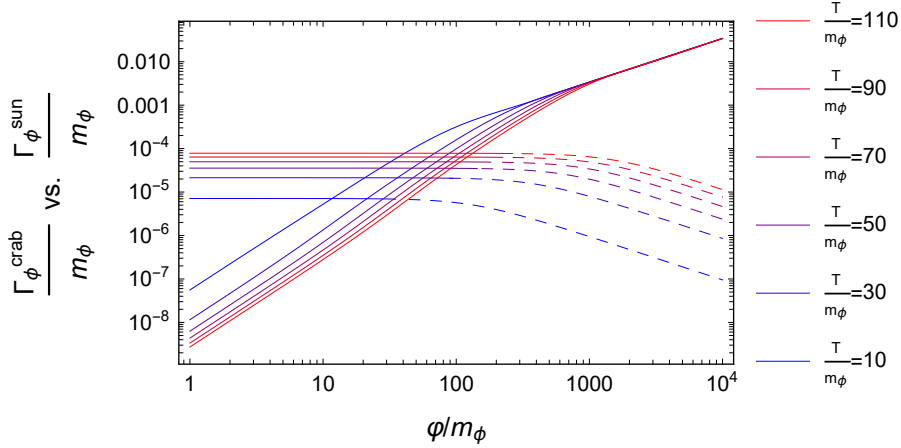


Figure 4.4: The widths $\Gamma_\phi^{\text{crab}}$ and Γ_ϕ^{sun} normalised to the mass m_ϕ vs. the background field φ with a logarithmic scale on both axis, for various temperatures and for the parameter hierarchy $\lambda_\phi/\lambda_\chi = \lambda_\phi/h = 10$. The Γ_ϕ^{sun} lines go from solid to dashed styles when the approximation $T > M_\phi$ breaks down.

These figures display precisely what we expect from just glancing at the parametric dependence of $\Gamma_\phi^{\text{crab}}$ (cf. Eq. (4.62)) and Γ_ϕ^{sun} (cf. Eq. (4.68)). For low field values versus the temperature, the sun width dominates but as φ increases $\Gamma_\phi^{\text{crab}}$ becomes larger than Γ_ϕ^{sun} , primarily because its vertices are φ -enhanced.

The crab width grows polynomially, as a straight line on the logarithmic scale, as expected from Eq. (4.62), except for the intermediate regime where T and φ are comparable. Eventually, all lines collapse to the large-field-valued crab width. Closely looking at Eq. (4.62), only the temperature dependence may be surprising as it decreases with T . This is because we chose $|\mathbf{p}| \simeq 3T$ such that $T/|\mathbf{p}|$ in Eq. (4.62) is constant, and the overall crab width decreases as T grows, because of the remaining $1/\Omega_\phi$ factor.

The sun width decreases polynomially with φ , as expected from the $1/\Omega_\phi$ in Eq. (4.68), though once it becomes dashed, it should actually be more abrupt,

is the crab-lifetime of most particles, since those have momentum $\langle p \rangle$. Second, because we know that the widths evaluated in this section are meant to be plugged in the condensate damping rate Eq. (4.50). Its integrand is peaked around $p \simeq 3T$, because of the hyperbolic cosine, which is nothing but a remnant of the Bose-Einstein distribution.

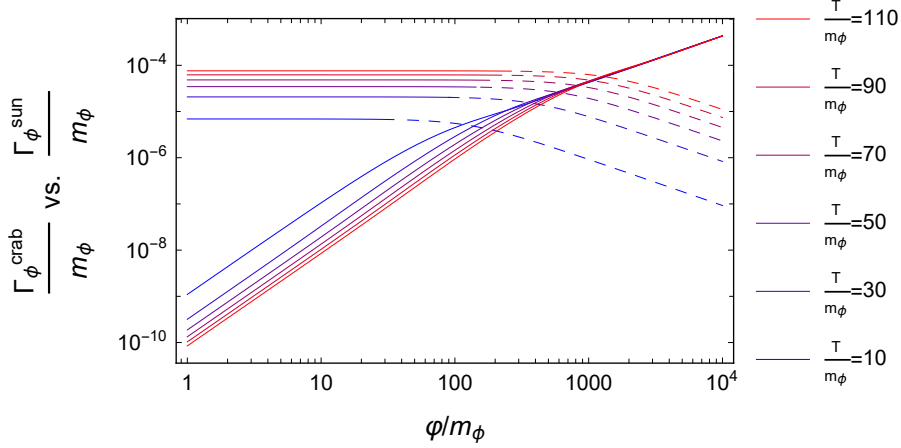


Figure 4.5: The widths $\Gamma_\phi^{\text{crab}}$ and Γ_ϕ^{sun} normalised to the mass m_ϕ vs. the background field φ with a logarithmic scale on both axis, for various temperatures and for $\lambda_\phi/h = 10^2$. The Γ_ϕ^{sun} lines go from solid to dashed styles when the approximation $T > M_\phi$ breaks down.

if not exponentially Boltzmann suppressed. When this suppression starts, the crab widths should always dominate because those are not suppressed.

Comparing Figs. 4.4 and 4.5, we see that increasing λ_ϕ has two major consequences. First, it increases M_ϕ and the approximation $T > M_\phi$ on which Γ_ϕ^{sun} relies, breaks down quicker. Second, it drastically increases the value of φ for which Γ_ϕ^{sun} becomes subdominant. This is not a problem when $h/\lambda_\phi = 10$, i.e. for Fig. 4.5 because the approximation breaks down when the sunset contribution is subdominant. Actually in that case, the presence of the crab width even extends the range of validity of the analytic formula for our total width (4.60) to any value of T . Even more so because when the lines go dashed, they should be exponentially suppressed. However, it is an issue when $h/\lambda_\phi = 10^2$, precisely because the contrary is observed. Therefore, in order to maximise the effect of the crab widths, and in order to extend the range of validity of our (4.60) to beyond the $T > M_\phi$ regime, we shall pick $h/\lambda_\phi \simeq 10$ for the remainder of this work.

That said, let us now move on to the computation of the condensate damping rate (4.50), which is the final quantity that we are after in this work, and the one that plays the most important role when it comes to the feasibility of warm inflation models.

4.4.3 The leading-order damping rate of the condensate

Let us recall our master formula for the leading order damping rate of the condensate (cf. Eq. (4.50)), the latter reads

$$\Gamma_{\varphi}^{\text{LO}} = \sum_{a=\phi,\chi} \frac{g_a^2 \varphi(t)^2}{8T} \int \frac{d^3 \mathbf{p}}{(2\pi)^3} \frac{1}{\Omega_a(t; \mathbf{p})^2 \Gamma_a(t; \mathbf{p}) \left(\cosh \left(\frac{\Omega_a(t; \mathbf{p})}{T} \right) - 1 \right)} \quad (4.69)$$

where $g_{\phi} = \lambda_{\phi}$ and $g_{\chi} = h$, and with our approximate Ω_a and Γ_a which respectively are to be found in (4.53) and (4.60). We now are in a good position to evaluate it. Temporarily forgetting about the obvious time and momentum dependencies, it reads

$$\Gamma_{\varphi}^{\text{LO}} = \sum_{a=\phi,\chi} \frac{g_a^2 \varphi(t)^2}{8T} \int \frac{d^3 \mathbf{p}}{(2\pi)^3} \frac{1}{\Omega_a^2 (\Gamma_a^{\text{crab}} + \Gamma_a^{\text{sun}}) (\cosh (\Omega_a/T) - 1)}, \quad (4.70)$$

where analytic expressions for the crab and sun widths are to be found in the previous section 4.4.2. Unfortunately, the integral in (4.70) cannot be evaluated analytically in the more interesting case where the crab widths or $\phi \leftrightarrow \chi\chi$ are kinematically allowed.⁵

Therefore, let us solve the integral numerically and display in Fig. 4.6 the results under the hierarchy $\lambda_{\phi}/h = \lambda_{\phi}/\lambda_{\chi} = 10$ and $m_{\phi}/m_{\chi} = 10^2$.

First and quite importantly, note the absence of dashed lines because the sunset diagram is subdominant when its analytic approximation is not longer valid, cf. Fig. 4.4, and the presence of the crab width enhances the range of applicability of our analytic results. For low field values, the friction rate displays a polynomial dependence on the background field, as expected from the φ^2 of Eq. (4.70). This is also confirmed by Fig. 4.4, because for those values, the crab has not yet kicked in and the sunset width primarily dominates the integrand. For very large field values, the damping rate abruptly drops down. This is due to a Boltzmann exponential suppression because of the hyperbolic cosine in the denominator of the integrand of Eq. (4.70). The value of φ for which the Boltzmann suppression occurs increases with the temperature. Eventually, we shall comment on the wavy features in the intermediate regime. Those are best understood by studying separately the cases when the crab width is and is not accounted for in the denominator of (4.70). In Fig. 4.7, we depict the leading-order damping rate (4.70), comparing the previous case of Fig. 4.6 and

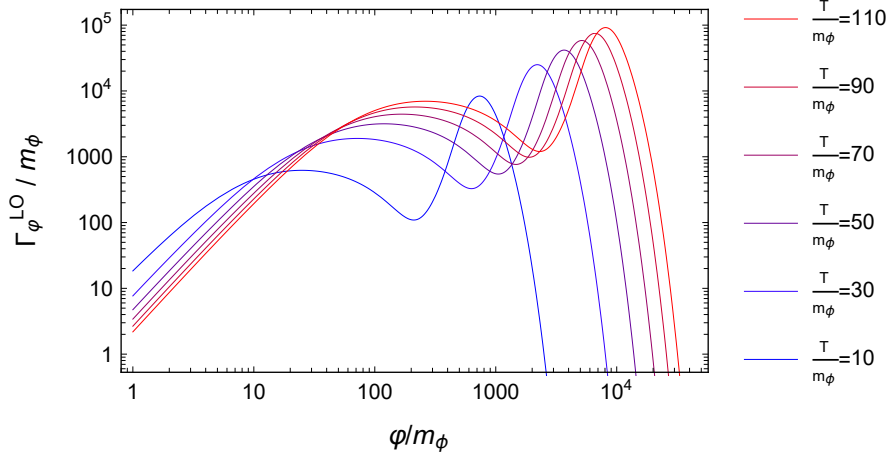


Figure 4.6: The condensate friction rate $\Gamma_\varphi^{\text{LO}}$ of Eq. (4.54) vs. the background field φ , both normalised to the mass m_ϕ , and for various temperature with logarithmic scales on both axis, with $\lambda_\phi/\lambda_\chi = \lambda_\phi/h = m_\phi/m_\chi = 10^2$.

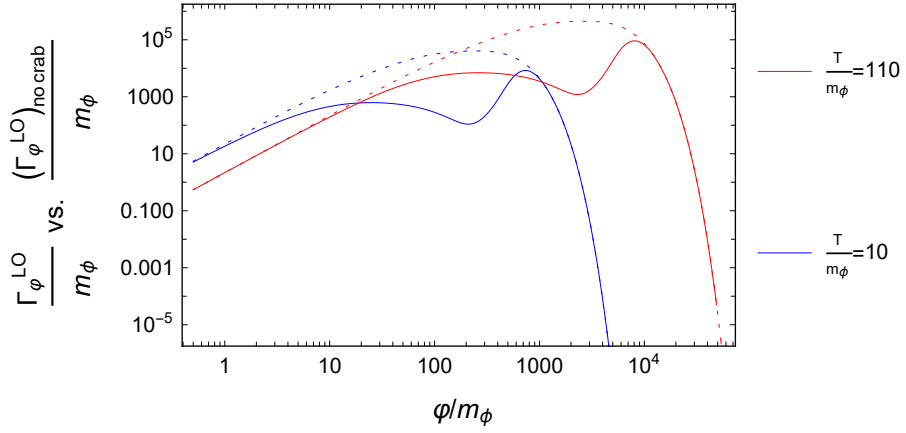


Figure 4.7: The condensate friction rate $\Gamma_\varphi^{\text{LO}}$ of Eq. (4.54) with (solid) and without (dotted) the crab width vs. the background field φ , for various temperatures with logarithmic scales on both axis, with $\lambda_\phi/h = m_\phi/m_\chi = 10^2$.

its counterpart where we by hand removed the contribution of the crab width in (4.70), for the same choice of couplings and two distinct temperatures.

⁵When they are not, our results precisely reproduce those of [62] and we shall not repeat their analysis.

Here a few comments are in order. First, it has now become clear that the wiggly features of Fig. 4.6 are to be attributed to the crab widths. The latter lower the full damping rate by increasing the denominator of the integrand of Eq. (4.70), and the lower the temperature, the lower the field value for which the crab widths matter. To the best of our knowledge and due to the kinematic nature of the crab widths, we believe that the somewhat narrow downward peaks correspond to momentum-dependent kinematically favoured phase space factors that open and close. The finite-temperature kinematic windows are hard to read from e.g. Eq. (4.62) because they are hidden in the logarithms of those expressions. Comparing Figs. 4.6 and 4.7, we see that when it is not Boltzmann suppressed, the crab width dominates in the intermediate and large- φ side of the spectrum (see Fig. (4.4)) and indeed significantly enhances the denominator of our condensate damping rate, hence significantly lowering the latter by several orders of magnitude. This closes the discussion about the numerical integration of (4.69).

4.5 The NLO equation of motion

The leading-order equation of motion (4.48) gets corrected by the two-loop term that is present in (4.20), namely

$$\int_{-\infty}^t dt' \Pi_{\phi}^{-\text{sun}}(t, t'; \mathbf{p} = \mathbf{0}) \varphi(t'), \quad (4.71)$$

and $\Pi_{\phi}^{-\text{sun}}$ is given in Eq. (3.10). We can use the slow-roll approximation $\varphi(t') \simeq \varphi(t) + (t - t')\dot{\varphi}(t)$ to Markovianise this term, and the associated corrections to $V'(\varphi)$ and Γ_{φ} read

$$V'_{\text{sun}}(\varphi) = \varphi(t) \text{Re}\tilde{\Pi}_{\phi}^{\text{sun}}(t, \omega = 0; \mathbf{p} = 0), \quad (4.72)$$

$$\Gamma_{\varphi}^{\text{sun}} = - \lim_{\omega \rightarrow 0} \frac{\text{Im}\tilde{\Pi}_{\phi}^{\text{sun}}(t, \omega; \mathbf{p} = 0)}{\omega}. \quad (4.73)$$

Using diagrammatic arguments, we can see that $V'_{\text{sun}}(\varphi)$ will not qualitatively affect the functional shape of the leading order $V'(\varphi)$ (4.54), rather it will only merely shift the leading order “coefficients of the polynomial expansion”, in a parametrically suppressed manner. Hence, it shall be neglected and we shall just keep (4.54) as our final effective potential. However, using diagrammatic arguments again, $\Gamma_{\varphi}^{\text{sun}}$ is expected to change the qualitative behavior⁶ of the

⁶This is best understood when we realise that the integrals to be solved are very similar to those that determine (4.68) and therefore should go like $\lim_{\mathbf{p} \rightarrow 0} T^2/\Omega = T^2/M$.

full $\Gamma_\varphi^{\text{NLO}} = \Gamma_\varphi^{\text{LO}} + \Gamma_\varphi^{\text{sun}}$, though the former is suppressed by both the loop and coupling constant expansions. The friction rate $\Gamma_\varphi^{\text{sun}}$ which arises from the selfinteracting $\lambda_\phi\phi^4/4!$ and biscalar $h\phi^2\chi^2$ sunset diagrams was studied in the past, see e.g. Ref. [62], wherein they obtained the following high T result^{7,8}

$$\Gamma_\varphi^{\text{sun}} \simeq \frac{h^2 T^2}{(4\pi)^3 M_a} \log\left(\frac{M_a}{M_b}\right), \text{ for } T \gg M_a \gg M_b \text{ and } a \neq b. \quad (4.74)$$

Note the similar structure to (4.68) which simply is due to the fact that the selfenergy that are computed to evaluate the friction rate $\Gamma_\varphi^{\text{sun}}$ (4.73) vs. the thermal width Γ_ϕ^{sun} (4.31) are strictly equivalent, cf. the discussion below (3.10). Actually, the same arguments regarding the range of applicability of (4.68) apply to (4.74). We can slightly extrapolate it and for large φ , it should be exponentially suppressed. Also, note that this NLO contribution to the field damping rate was not studied in Ref. [17], and therefore it will be interesting to see its implications for warm inflation, as we shall do in the next chapter.

In Fig. (4.8), we depict the sunset friction rate $\Gamma_\varphi^{\text{sun}}$ as a function of the background field φ , for various temperatures and for the more interesting case where $\phi \rightarrow \chi\chi$ is kinematically allowed, i.e. when $\lambda_\phi/h = 10 = \lambda_\phi/\lambda_\chi$.

As expected from Eq. (4.74), it grows with the temperature, decreases with the background field, and nonpolynomial behaviours are encountered in the intermediate regime where $\varphi \simeq T$.

At this stage, the full next-to-leading order (NLO) friction rate and effective potential therefore read

$$V'(\varphi) = m_\phi^2 \varphi(t) + \frac{\lambda_\phi}{6} \varphi^3(t) + \varphi(t) T^2 \sum_{a=\phi,\chi} g_b F_b(t) \quad (4.75)$$

$$+ \varphi(t) \sum_{a=\phi,\chi} \frac{g_b}{2(4\pi)^2} (M_b^2(t) \ln(M_b(t)^2/\mu^2) - m_b^2 \ln(m_b^2/\mu^2))$$

$$\Gamma_\varphi^{\text{NLO}} = \Gamma_\varphi^{\text{LO}} + \Gamma_\varphi^{\text{sun}} \quad (4.76)$$

$$= \sum_{a=\phi,\chi} \frac{g_a^2 \varphi(t)^2}{8T} \int \frac{d^3\mathbf{p}}{(2\pi)^3} \frac{1}{\Omega_a^2 (\Gamma_a^{\text{crab}} + \Gamma_a^{\text{sun}}) (\cosh(\Omega_a/T) - 1)} + \Gamma_\varphi^{\text{sun}}$$

⁷For vanishing external four-momenta, the two-to-two scatterings $aa \leftrightarrow bb$ that are described by the imaginary sunset diagrams are nothing but the (inverse) decays $a \rightarrow bb$ or $b \rightarrow aa$. Therefore, that contribution is kinematically forbidden for selfinteractions.

⁸Later we will see that this analytic approximation is more than sufficient because the moment it breaks down takes place in a regime where this term is suppressed by multiple orders of magnitude anyway, cf. Fig. 4.9.

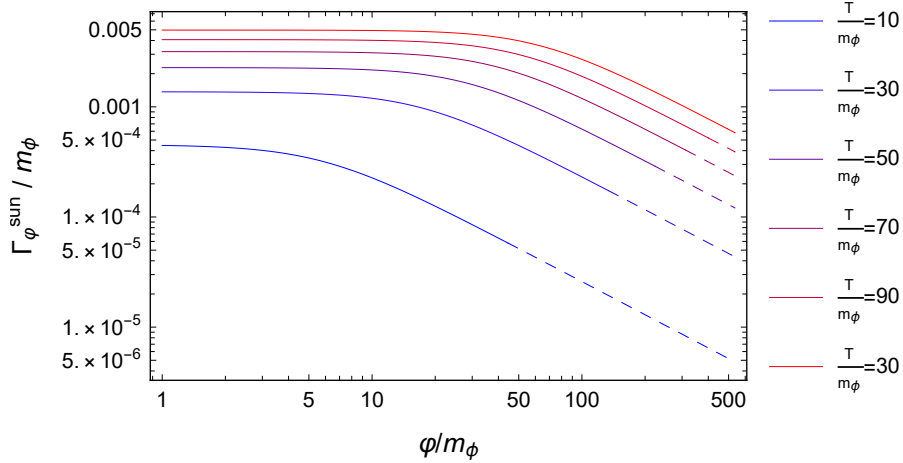


Figure 4.8: The damping rate Γ_ϕ^{sun} of Eq. (4.74) vs. the background field ϕ , both normalised to the mass m_ϕ , for various temperatures and with logarithmic scales on both axis. Choices for the model parameters are identical to Fig. 4.6 and lines go from solid to dashed when the assumption $T > M_a$ breaks down.

where the time- and temperature-dependent frequencies Ω_a and masses M_a are respectively given in Eqs. (4.53)(4.57) and Γ_ϕ^{LO} is the leading order friction rate which was derived in Eq. (4.70), where the thermal widths that appear in its denominator are given in Eqs. (4.61)(4.62)(4.68) and Γ_ϕ^{sun} was just derived in Eq. (4.74). In Fig. 4.9, we separately depict the background field dependence of the two contributions to the NLO damping rate (4.76) for various temperatures and for the more interesting case where $\lambda_\phi/h = \lambda_\phi/\lambda_\chi = 10$ and $m_\phi/m_\chi = 10^2$.

In Fig. 4.9, we can clearly recognise the separate contributions from the leading-order Γ_ϕ^{LO} of Eq. (4.70) and Fig. 4.6 and that of Γ_ϕ^{sun} of Eq. (4.74) and Fig. 4.8. The growing upper lines are the LO damping rates and the decreasing lower ones, which go from solid to dashed when the assumption $T > M_a$ breaks down, are the sunset damping rates. Even though the latter are parametrically suppressed, they strongly dominate the former in the $T \gg \phi$ regime. Then, the LO damping prevails whenever the background field is somewhat significant (even when ϕ is two orders of magnitudes smaller than T , because of the loop and coupling constant suppression of the NLO term $\sim h^2$), up until it gets exponentially Boltzmann suppressed in the very large field limit. Remember that Γ_ϕ^{sun} ought to be Boltzmann suppressed, too, such that in that regime,

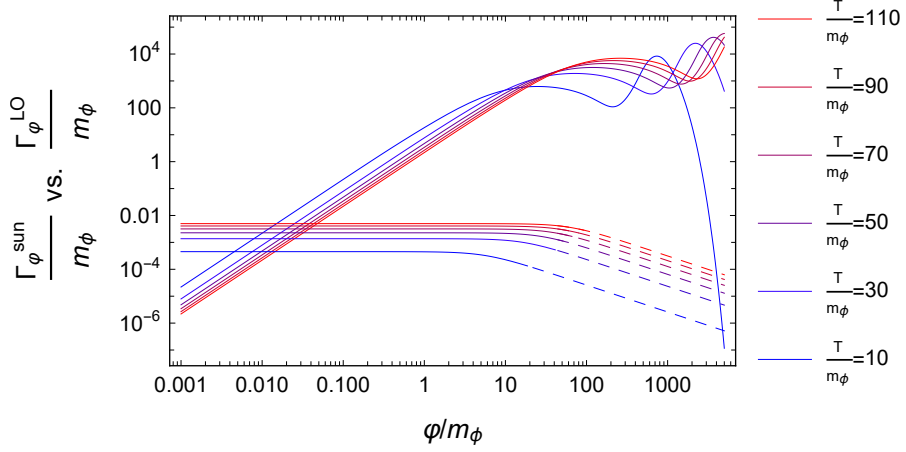


Figure 4.9: The separate contributions to the damping rate Γ_ϕ^{NLO} vs. the background field ϕ , both normalised to the mass m_ϕ , for various temperatures and with logarithmic scales on both axis. Choices for the model parameters are identical to Fig. 4.6 and again, the Γ_ϕ^{sun} lines go from solid to dashed when the assumption $T > M_a$ breaks down.

there is no more condensate damping rate whatsoever, everything is Boltzmann suppressed.

Armed with those expressions, interpretations and knowledge, we are now in good position to question the feasibility of warm inflation within our Z_2 -symmetric two-real-scalar model.

Chapter 5

On the feasibility of warm inflation

In this chapter, we review and introduce the main ingredients to understand the need for (warm) inflation models as solutions of the isotropy, homogeneity, flatness and horizon problems [8] of hot big-bang cosmologies, both from a theoretical and observational perspective. Then, we shall describe how the feasibility of inflation models can be examined via the so-called slow-roll parameters. Eventually, we shall particularise the discussion to the \mathbb{Z}_2 -symmetric scalar theory studied in the previous two chapters to comment on their viability as warm inflation candidates.

5.1 Observational evidence for non-standard cosmology and possible explanations

As a matter of fact, the observational evidence which call for inflation are numerous and rather compelling. They mostly come from measurements of the Cosmic Microwave Background (CMB) temperature power spectrum [1, 9, 77, 78]. That is, the temperature power spectrum of the oldest photons we can detect, dating from a time where the Universe had cooled enough so that neutral elements formed and photons no longer scattered. Of particular relevance for this work are the following properties of our Universe:

- The spatial curvature of the *observable* Universe is flat.

- The angular temperature distribution across the sky is *almost* homogeneous and isotropic, up to tiny distortions across the entire spectrum of wavelengths and in particular, super-Hubble modes¹ are primarily observed in the CMB.
- The spectrum is nearly scale invariant, i.e. there are almost as many large-wavelength fluctuations as short-wavelength perturbations, with a red tilt.
- The fluctuations are nearly Gaussian, i.e. their amplitudes follow a Gaussian distribution e^S , where S is at most quadratic in the fluctuations. As a result, n -point functions in the power spectrum are in good approximation entirely determined by the 2-point functions.

On top of these, the fluctuations are consistent with the hypothesis that they were solely sourced by adiabatic/curvature perturbations, i.e. primordial total density perturbations, which eventually equally perturb all species that constitute the cosmological fluid². Although these have been known for long [78–80], they were more accurately re-discovered and precisely measured by the space-based Planck mission in 2013 [9, 77], and the associated full-sky map of the (CMB) power spectrum, cf. Fig. 5.1.

These peculiarities of our Universe cannot be understood within standard cosmology and they actually all eventually tie to one of the aforementioned three problems of the standard model of cosmology. Therefore, the latter needs to be supplemented by other mechanisms such as cosmic inflation [8] to try and describe those phenomena theoretically.

5.1.1 A simple solution to all problems: cosmic inflation

Cosmic inflation is a simple field-theoretical extension of standard cosmology which naturally accounts for the aforementioned yet-to-be-understood features of our Universe. In its simplest form, it is realised by one (or several) homogeneous scalar field ϕ , the inflaton, of canonical action $S[\phi]$, which rolls down the slope of its potential. For inflation to occur, the scalar potential energy ought to dominate the energy density of the Universe and its kinetic energy ought to

¹Fluctuations which wavelengths exceed the Hubble radius, the distance beyond which objects recede from an observer at a rate faster than the speed of light [1].

²In contradistinction, isocurvature perturbations only excite certain number densities at constant total energy density.

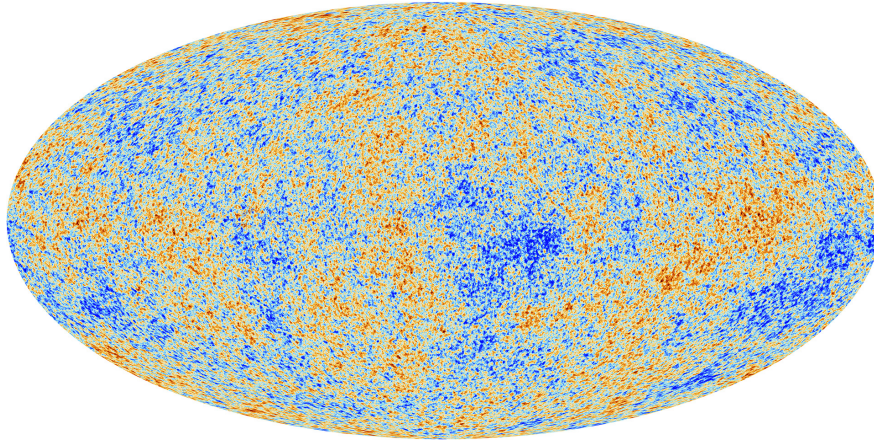


Figure 5.1: Full-sky measurement of the CMB temperature power spectrum – $T = 2.726 \pm 10^{-5} K$ – Planck Mission 2013 results [9].

be subdominant, too. This realises a negative equation of state obtained from the scalar energy-momentum tensor $T_{\mu\nu}$ as

$$\frac{T_{ii}}{T_{00}} = \frac{P}{\rho} \simeq -1. \quad (5.1)$$

The latter in turn triggers an ongoing phase of quasi-exponentially accelerated expansion of the Universe, which, provided that it lasts for long enough, explains the flatness, homogeneity and isotropy and horizon problems of the observable Universe [1,8]. By inflating the scale factor, or the radius of the Universe, by multiple orders of magnitude, the spatial curvature of the Universe is flattened and unseen by an observer which lives in the inflated Universe, just as an ant cannot see the curvature of the earth (flatness problem). Then, it effectively wipes out any matter content in the Universe by diluting it away (homogeneity and isotropy problem). Eventually, it widens the past horizons, hence causally reconnecting structure that would otherwise be disconnected (horizon problem). This phase is commonly referred to as slow-roll inflation, wherein the inflaton must slowly roll down, so as to make it stay sufficiently long at the large-valued side of its potential, where it dominates the energy density of the Universe. As explained in more detail in the introduction, to

the best of our knowledge, there are only two distinguished ways of ensuring that the duration of the inflationary era is long enough. It is either enforced by the flatness of the potential, as was originally proposed in the commonly-accepted standard paradigm [8], or it is dissipation-enforced via quantum and thermal interactions of the inflaton, as was more recently proposed in the theory of “Warm Inflation” [5]. In this thesis, we are particularly interested in the scenario where thermal effects alone enforce the slow-rolling of the field, the potential need not be flat whatsoever.

As we shall explain in detail now, be it cold or warm, inflation naturally enforces the CMB temperature power spectrum perturbations to be adiabatic and scale invariant, and made of super-Hubble modes distributed according to a Gaussian statistics. In the framework of cosmological perturbations [1], the latter are sourced by the scalar quantum fluctuations $\delta\phi$ through metric perturbations in the Einstein equations (which we review in section 6.2), via the associated perturbed energy-momentum tensor $\delta T_{\mu\nu}$. By virtue of ϕ being a canonical scalar, it is well known [1] that its quantised mode functions in an inflating (de Sitter) background evolve as follows:

- Sub-Hubble modes oscillate as their wavelengths are stretched with the expansion of the Universe, until they all eventually become super-Hubble.
- Super-Hubble modes behave as a classical stochastic background noise which amplitudes are distributed according to the nearly Gaussian statistics $e^{S[\phi]}$, up to corrections from quantum interactions.

Therefore, the associated power spectrum of two-point correlation functions is nearly scale-invariant and Gaussian, and since they solely source CMB fluctuations through $T_{\mu\nu}$, they are automatically adiabatic, too. Here, note that quantum corrections may be a source of non-Gaussianities, but these are highly suppressed during standard inflation because the associated potentials are typically very flat and interactions are negligible³.

While this so far sounds ideal as far as cosmological problems are concerned and despite its many successes, cosmic inflation of course has its shortcomings. Despite not everybody agrees on what is a problem and what is not, here we list a few that are considered issues in the community, at least by the critics of inflation. First, cosmic inflation does not provide a complete history of the

³Since warm inflation potentials in principle need not be flat, if a model of warm inflation were shown viable at the background level, it would be very interesting to study whether it releases sizeable non-Gaussianities in the CMB power spectrum, which would potentially make it observationally distinguishable from other models of inflation, as was e.g. claimed in [81–83].

Universe. One may still ask the questions: What happened before? How did it start? Not only that, but also one can formally prove that ever-expanding spacetimes must have an initial spacetime singularity [84, 85]. It goes without saying that many complicated physical and philosophical questions tie to this singularity, starting with the question of the origin of time and space itself. Second it is also proven that successive quantum fluctuations during inflation may in some places in the Universe be so large that inflation would actually never stop there, leading to runaway behaviours and eternal inflation [86, 87]. Hence, ever-inflating causally disconnected patches or multiverses are created. To these eternally-inflating bubbles are associated divergences [88] which come from nothing but the ever-growing sizes of these Universes and the associated volume integration measures. According to [89], when these cannot be regularised, the theory loses its prediction power. Another complication associated with the magnitude of certain quantum fluctuations is known as the trans-Planckian problem for cosmological fluctuations [90]. It is stated as follows. If inflation lasted slightly longer than its minimal duration, then, taking into account inflation and the associated stretching of lengths, all fluctuation wavelengths at the time of inflation would have to be shorter than the Planck length [91]. Since we do not have a fundamental theory that is valid below the Planck scale, people criticise precisely this fact: if wavelengths are sub-Planckian, who knows what theory should be used to describe them to begin with⁴. In order to avoid these complications, inflation models must be fine-tuned to make sure their durations fall right in the window where they solve the cosmological problems (this sets the lower bound), but where their quantum fluctuations are not trans-Planckian (this sets the upper bound). Speaking of fine-tuning, inflation is also criticised because its initial conditions are very specific: it requires an initial slowly-rolling homogeneous field everywhere in a patch that is a billion times bigger than the Planck length [89], and therein, the field value must be large enough that its potential dominates the energy density of the Universe. Based on entropic arguments and the configurations number in the Universe, it has been argued that this is very unlikely [92]. Then, even if it were realised, it is shown that despite inflation is an attractor solution, short inflations which do not solve the flatness and horizon problems are preferred [93]. Eventually, standard inflation is sometimes criticised because the flat potential it requires is hard to embed in natural theories of particle physics.

⁴One may argue that this is not a problem, and simply assume Bunch-Davies initial conditions [1] for the observed modes, which choice can be justified with Ockham's razor principle.

5.1.2 Alternatives to standard cosmic inflation

In light of these issues, the critics of cosmic inflation of course have found alternatives which we wish to briefly comment on. Substitutes to inflation as primordial cosmologies that explain the CMB power spectrum include bouncing cosmologies, e.g. cyclic Ekpyrosis [89,94], matter-bouncing cosmologies [95–97] or string gas cosmologies [98,99], see e.g. [100–102] for detailed reviews, and more importantly for this work, they include warm inflation models.

“Big-Bounce” cosmology. Bouncing cosmologies are typically characterised by scalar-field-driven phases of slow contraction which are continuously connected to the standard cosmological expanding phase. They bounce from a contracting phase to an expanding phase, hence their names. Again, it is the primordial quantum fluctuations of the scalar field during and before the bounce which source fluctuations in the CMB power spectrum. These can be shown to solve the cosmological puzzles in a manner that is consistent with observations, and avoiding the aforementioned inflationary problems. In particular, they resolve the trans-Planckian and multiverse issues, and more importantly they provide a singularity-free and complete history of the Universe, by smoothly connecting the contracting phase to the standard Hubble expansion. Despite their successes, unsurprisingly these bouncing scenarios come with their own shortcomings and challenges, too, in particular when it comes to their modellings at the background level. They typically require us to modify Einstein’s gravity and/or violate the null energy condition $\rho + P \geq 0$, hence giving rise to field degrees of freedom of negative kinetic energy, also known as ghosts, which come accompanied by states of negative norms which violate unitarity. Writing down quantum field theoretical models of bouncing cosmologies which are ghost-free is very challenging and usually summons controversial arguments motivated by string theory and extra spacetime dimensions, theories of quantum gravity or modified theories of Einstein’s General Relativity (both with nonstandard geometric or matter sectors), see e.g. [101] for a review. Other issues of non-singular bouncing cosmologies also relate to the potential unwanted and unstable growth of curvature and anisotropic fluctuations which would spoil their viability as explanations for the CMB power spectrum.

Inflation vs. bouncing cosmologies: the observational differences.

The major differences between cosmic inflation and bouncing alternatives are associated with the Gaussian nature of the spectrum of perturbations, as well as with the generation (or not) of primordial gravity waves. On one hand,

bouncing potentials need not be flat as is the case for inflationary potentials, hence potentially leading to an amount of non-Gaussianities which can be orders of magnitude larger than that observed in standard inflation, see e.g. [89] for a comparison between single-field inflation and a simple two-scalar ekpyrotic model. However, multi-field inflation can accommodate larger non-Gaussianities [103], too, such that we believe these would not constitute a solid smoking-gun signature for bouncing cosmologies. On the other hand, leading-order gravitational waves are not directly sourced by the fluctuations of the scalar field $\delta\phi$, rather they only grow with the size of the Universe. Therefore, bouncing cosmologies present a spectrum of tensor fluctuations that is a lot bluer than that of inflation, as the latter stretched the wavelengths to the darker-red side of the spectrum. Therefore, the detection of a spectrum of primordial gravitational waves potentially constitutes an observational way of discriminating inflation from bouncing cosmologies. As a matter of fact, there are dedicated experiments to the measurements of such primordial gravitational waves, e.g. the BICEP/KECK experiment [104], a ground-based mission in the south pole that focuses on measurements of the B-mode polarisation (typical cross-shaped polarisation of gravity waves) in the CMB. As of today, these together with the Planck collaboration [105, 106] thus far have established rather strong non-observation bounds which quite interestingly already rule out many long-preferred models of inflation, e.g. monomial potentials [91, 106].

Warm inflation cosmology. Warm inflation scenarios solve the cosmological problems as standard inflation does, except it maintains a sufficiently long ongoing phase of slow-roll inflation in the Universe through important quantum and thermal dissipative effects on the inflaton dynamics. If these are strong enough, it is even argued that they could alleviate some of the aforementioned complications of inflationary cosmology. On one hand, warm inflation potentials need not necessarily be flat, hence making them easier to embed in more natural quantum field theoretical models. On the other, it has been claimed in the literature that they may solve the trans-Planckian problem of cosmological fluctuations [107]. The main complications of warm inflation are the following. For one, its feasibility at the background level is highly disputed, as we shall review in detail shortly. Then, even if it were possible, it is not yet clear whether it leaves an observable signature that would make it distinguishable from cold inflation anyway.

Despite we doubt their claims because of the vast landscape of cold inflation models [103], we comment on the smoking guns proposed by the pioneers of warm inflation to distinguish the cold from the warm paradigm. In e.g. [108] or more recently [83], it is argued that the presence of thermal radiation during

warm inflation generically lowers the amount of primordial tensor perturbations. However, we believe that almost any experimentally consistent tensor-to-scalar ratio can be accommodated by other models of cold inflation [103]. Hence, we conclude that this by itself does not constitute a decisive evidence that would discriminate cold from warm inflation. Then, it was claimed in [81] and more formally in [82] that distinct non-Gaussianities appear in the strong dissipative regimes needed for warm inflation, cf. 3. Again, these suffer from the same complaint, cold inflation models can accommodate almost any type of viable non-Gaussianities [103], thus they probably do not constitute discriminating evidence for cold or warm inflation. Eventually, in [109–111], it is argued that baryon asymmetry can be generated through the dissipative effects of warm inflation. This primordial baryon asymmetry in turn generates extra isocurvature/entropy/non-adiabatic CMB fluctuations which are claimed to be potentially measurable by future experiments. As emphasised above, we believe these questions should be addressed if warm inflation is shown viable at the background level, i.e. from first principles of quantum field theory, which is what we turn to next.

5.2 Slow-roll parameters

At the background level, the feasibility of cosmic inflation models, be it warm or cold, is primarily constrained by the duration of the inflationary regime. It ought to last long enough to solve all “problems” of hot big-bang cosmologies, as explained above. The duration of inflation is customarily expressed in terms of a number of e-foldings $N_e(t)$. If $a(t)$ is the so-called scale factor, commonly interpreted as the spatial radius of our Universe, and t_b is the time associated with the beginning of inflation, it characterises the Universe growth by the later time relation given by $a(t > t_b) = a(t_b)e^{N_e(t)}$. It is defined as [1, 17]

$$N_e(t) = \int_{\varphi_b}^{\varphi_t} \frac{d\phi}{\dot{\phi}} H(t), \quad (5.2)$$

where $H(t) = \dot{a}(t)/a(t)$ is the Hubble expansion parameter, the dynamics of which is dictated by Einstein’s equations of General Relativity, and hence the field content under consideration, as we shall review in section 6.2. In order to solve all three homogeneity and isotropy, flatness and horizon problems, the number of e-foldings must at least be of order $N_e \sim 50-70$ [1]. This necessary condition for inflation can be expressed in terms of so-called slow-roll parameters, usually denoted ϵ , η which ensure that the dynamics of the scalar field is slowly evolving and maintains the Universe in its inflation era for a sufficiently

extended period. In a nutshell, maintaining $\epsilon < 1$ guarantees that the equation of state of the Universe is negative as in (5.1), while maintaining $\eta < 1$ ensures the dynamics to be adiabatically evolving. While the slow-roll parameters are well-known for the traditional inflationary dynamics wherein the friction rate we payed so much attention to can be neglected, they are very much less so in the warm inflation scenario [6, 112] where the general shape of the equation of motion reads

$$\ddot{\varphi}(t) + (3H + \Gamma_\varphi)\dot{\varphi}(t) + V'(\varphi) = 0. \quad (5.3)$$

This equation is the curved-spacetime generalisation of the dynamical equation (4.48). In principle, the transport coefficients that govern it ought to be determined from quantum field theory in curved spacetime, too, if we were to remain fully selfconsistent. In the existing literature, see e.g. Refs. [7, 13, 15], it is sometimes argued that the microphysics that governs the transport coefficients unfolds on time scales which are insensitive to spacetime curvature. For the case of warm inflation, the hot temperature and large background field make the quasiparticle effective masses heavier than the Hubble rate, hence curvature corrections are expected to be negligible. In this thesis, we shall work under that assumption too, and leave a more refined treatment of the curvature effects for future work.

In the next sections, we first review the current status of the feasibility of warm inflation and carefully explain to what extent our results are innovative with regards to the existing literature on two-real-scalar models. Then, we derive the flat-space slow-roll parameters of (4.48) and express them in terms of the effective force $V'(\varphi)$ and damping rate Γ_φ . Eventually, we investigate whether or not there exists a corner in parameter space where $V'(\varphi)$ (4.75) and Γ_φ (4.76) at least verify the necessary conditions that the field is slowly rolling for a sizeable amount of time. Were this to be the case, it warrants a more fool-proof investigation of the feasibility of warm inflation, including the derivation and computation of the slow-roll parameter associated with the equation of state of the Universe. The equation of state, or energy-momentum tensor, is tedious to derive and renormalise from first principles of nonequilibrium QFT and we unfortunately have not had the time to study it in detail yet. We shall leave this for future work but comment on our strategy to address this issue.

5.3 The viability of warm inflation: state of the art

Ever since its invention [5] in 1995, the feasibility of warm inflation has been under careful investigation and its viability has been controversial. In particular, quickly after [5], [17] proved from very simple analytic arguments that the simplest quantum field theoretical models can hardly sustain a consistent scenario of warm inflation for a few tens of e-folds. This is primarily because the large quantum and thermal damping coefficient needed for warm inflation is typically accompanied by even larger radiative corrections to the slope of the potential, as we shall carefully explain in the next section. Also, warm inflation has been criticised in e.g. [16], because it relies on fine-tuned models wherein seemingly unrelated quantities (like the temperature and coupling constants) conspire and align at initial time so as to ensure an ongoing inflationary era. Subsequent to those criticisms have followed a cascade of very interesting papers with more complicated models and phenomenological studies, see e.g. [7] that followed [17] in its wake, or the more recent [83, 112–114]. These typically summon a protective symmetry that prevents the inflaton potential from large radiative corrections [83, 113] or complicated off-shell damping mechanisms [14]. What became quickly clear at the time is that warm inflation models were lacking quantum field theoretical rigour in their formulations. Therefore, the pioneers of warm inflation have consequently worked on a series of papers wherein they performed a more fool-proof analysis of the microphysics underlying warm inflation models, see e.g. [6, 13, 14, 55, 115], and the most recent [15].

As far as our two-scalar model is concerned, its viability as warm inflation candidate has been carefully studied in the literature, in particular see e.g. [17] where they perform an analytic study, based on similar assumptions to ours. Using very rough parametric arguments, they concluded that warm inflation can hardly be realised by \mathbb{Z}_2 -symmetric scalar theories, precisely because they showed that it cannot sustain an inflationary regime for $N_e \sim 50$ -70. That conclusion was almost independent of the number of χ fields that the would-be inflaton ϕ couples to, be it very large or just equal to one. However, the analysis of the authors of [17] has the following two shortcomings. First, it is rather rough. They did not compute the effective potential or the damping rate with the degree of precision that we did. Second, this part of the thesis presented two new ingredients that were not accounted for in their work. They omitted:

- I. Thee NLO equation of motion, see section 4.5.
- II. The crab widths (4.61)(4.62) in the LO dissipation coefficient (4.70).

Except for those ingredients, their damping rate and effective potential are qualitatively identical to ours (up to different prefactors), and therefore we shall only carefully investigate the slow-roll parameters in those regimes where the new terms matter, otherwise they will just act as mild corrections to what the authors of [17] studied. We shall precisely determine what hierarchy in the model parameters should be assumed to precisely lie in the regions where I. and II. significantly alter the inflaton dynamics.

In order to study the feasibility of warm inflation in these limiting cases, we will not use the slow-roll conditions obtained in [6] or [17], rather we will first derive our own slow-roll parameters in a more generic differential equation setting.

5.4 Flat-space slow-roll parameters

The η parameter. Let us introduce a formal expansion parameter α into the equation of motion

$$\alpha\ddot{\varphi} + \Gamma_\varphi\dot{\varphi} + V'(\varphi) = 0, \quad (5.4)$$

which controls the smallness of $\ddot{\varphi}$ versus the other terms in the equation. For slow-roll to be justified to start with, $\ddot{\varphi}$ ought to be suppressed. At leading order in α , the solution of this would be

$$\dot{\varphi} \sim -\frac{V'}{\Gamma_\varphi} + \mathcal{O}(\alpha). \quad (5.5)$$

Then, we can use this leading order solution to reduce the derivative order by taking its time derivative, multiplying it by α and equating it to $\alpha\ddot{\varphi}$

$$\alpha\ddot{\varphi} = -\alpha\dot{\varphi}\frac{d}{d\varphi}\left(\frac{V'}{\Gamma}\right) + \mathcal{O}(\alpha^2) = \alpha\frac{V'}{\Gamma_\varphi}\frac{d}{d\varphi}\left(\frac{V'}{\Gamma_\varphi}\right) + \mathcal{O}(\alpha^2). \quad (5.6)$$

Now let us use this to correct the equation (5.4), we find

$$\dot{\varphi} \sim -\frac{V'}{\Gamma_\varphi}\left[1 + \frac{\alpha}{\Gamma_\varphi}\frac{d}{d\varphi}\left(\frac{V'}{\Gamma}\right)\right] + \mathcal{O}(\alpha^2). \quad (5.7)$$

It follows that the condition for slow-roll dynamics reads

$$\eta = \frac{1}{\Gamma_\varphi}\frac{d}{d\varphi}\left(\frac{V'}{\Gamma_\varphi}\right) \ll 1. \quad (5.8)$$

This requirement essentially tells us how strong the condensate damping rate has to be when the inflaton descends the slope of the potential, so as to maintain a slowly rolling dynamics. If slow-roll is to be realised, then the steeper

the slope, the stronger the damping, and (5.8) ought to be viewed as a necessary condition for warm inflation models. However, note that at this point (5.8) has nothing to do with inflation. It only is a statement about adiabatic dynamics and we should bare in mind that while (5.8) is a necessary condition for warm inflation models, it is not a sufficient one. In principle, other slow-roll parameters are to be fulfilled for inflation to occur, e.g. the one that ensures the energy density of the Universe to be precisely dominated by a cosmological-constant-like content which triggers inflation, the so-called ϵ parameter.

The ϵ parameter. The latter ought to be found from the inflaton equation of state by imposing $P_\varphi/\rho_\varphi = -1$, and demand it to generate negative pressure for sufficiently long. Assuming that the effective energy and pressure densities, which descend from the energy-momentum tensor of our scalar theory, can be put under the conventional form

$$\rho_\varphi = \frac{1}{2}\dot{\varphi}^2 + \mathcal{V}_{\text{eff}}, \quad P_\varphi = \frac{1}{2}\dot{\varphi}^2 - \mathcal{V}_{\text{eff}}, \quad (5.9)$$

where \mathcal{V}_{eff} is an effective potential that is *a priori* different from the effective potential V' that drives the condensate dynamics via (5.5). Although we probably already have computed all relevant diagrams, we even expect them to be different because derivatives of the (effective) action with respect to the metric need not be identical to derivatives with respect to the condensate. This is only true at leading order in perturbation theory. That said, imposing $P_\varphi/\rho_\varphi = -1$ yields $\dot{\varphi}^2/2\mathcal{V}_{\text{eff}} \ll 1$, or equivalently, upon using (5.5), this gives

$$\epsilon = \frac{(V')^2}{2\Gamma_\varphi^2 \mathcal{V}_{\text{eff}}} \ll 1, \quad (5.10)$$

which is a second slow-roll parameter to be studied carefully. However, deriving a quantum field theoretical equation of state from first principles, or in this case finding \mathcal{V}_{eff} and the associated slow-roll parameter (5.10), is a very complicated exercise in itself. This will e.g. address the question of a suitable definition for the energy-momentum tensor in a 2PI framework [116]. Then, it is even harder to simultaneously perform a numerical scan and solve the dynamical equations that govern the dynamics of the time-dependent quantities that constitute the slow-roll parameters (5.8) and (5.10), to try and show if those can be maintained low for a few 50-70 e-folds (see e.g. [117, 118] for the dynamical equations).

We should comment that (5.8) and (5.10) are particularly hard to achieve when the interactions that are responsible for the damping of the modes also are responsible for the thermal screening of the particle masses or potentials.

In those cases, typically, large damping rates imply even larger screening effects, as the former arise at higher perturbative orders than the latter. We shall shortly experience precisely these issues for our model and as a matter of fact, it is commonly encountered in quantum field theories. As a consequence, simple models very hardly fulfill (5.8) and (5.10), unless one summons a protective symmetry that prevents the potential from large radiative corrections to. For instance, see the “Warm Little Inflation” papers [112–114], where the inflaton is the Nambu-Goldstone boson of a broken gauge symmetry. See also the very recent and interesting “Minimal Warm Inflation” [83], where the shift symmetry of an axion-like coupling protects the effective potential from too large radiative corrections, and the inflaton damping rate arises from the production of sphalerons, as e.g. computed in Refs. [119, 120].

That said, for the present discussion, we shall proceed step by step and first focus on the slow-roll parameter η of Eq. (5.8). If the latter can be shown smaller than unity for one of those cases that were omitted by [17], then two conclusions can be drawn. On one hand, it will prove that slow-roll can be achieved in flat space for a \mathbb{Z}_2 -symmetric theory of interacting scalars, which is an interesting result in itself. And on the other, it will possibly revive the feasibility of warm inflation in that model, too. Were this to be the case, we leave for future work the more refined analysis of the feasibility of warm inflation, including the first principles derivation of the 2PI effective equation of state for our two-real-scalar model and the investigation of whether conditions (5.10) and (5.11) can be simultaneously satisfied for a few tens of e-folds.

5.5 Slowly rolling with \mathbb{Z}_2 -symmetric scalars

From the previous section, we obtained our slow-roll condition

$$\eta = \frac{1}{\Gamma_\varphi} \frac{d}{d\varphi} \left(\frac{V'}{\Gamma_\varphi} \right) = \frac{1}{\Gamma_\varphi^2} \left(V'' - (\ln \Gamma_\varphi)' \right) < 1, \quad (5.11)$$

and we want to investigate whether our transport coefficients V' of (4.75) and Γ_φ of (4.76) can sustain $\eta < 1$ over a sizeable period of time. In particular, we want to study them in the limiting cases I. and II. (see section 5.3) independently, which both were missed in the analysis of Ref. [17].

5.5.1 Case I.: $\Gamma_\varphi^{NLO} \simeq \Gamma_\varphi^{\text{sun}}$

Closely looking at all relevant equations that feed into (4.76) as well as at Fig.4.9, we see that this limiting case I. is fulfilled by the conditions:

$$\lambda_\chi \gg h \gg \lambda_\phi, \quad T \gg \varphi, M_a \text{ for } a = \phi, \chi, \quad (5.12)$$

wherein we set ourselves in a very high temperature regime and study a very warm inflation scenario. Indeed, the coupling hierarchy is such that $M_\chi > M_\phi$, cf. (4.57), unless the bare masses are fine tuned and hence the crab widths are likely kinematically forbidden. In the pathological case where they are not, they can only be so in the low field regime where they are highly suppressed anyway since $\lambda_\chi \gg h, \lambda_\phi$, and $T \gg \varphi, M_a$, see also Fig. 4.5. Thus, they are neglected in this analysis and in that sense, I. is the antipode of II. in parameter space, since II. wants the crab width to dominate. According to I. thus far, the full damping rate $\Gamma_\varphi^{\text{NLO}}$ is solely composed of two terms, namely $\Gamma_\varphi^{\text{LO}}$ in absence of crab widths and the two-loop sunset contribution (4.74). In a high temperature regime and given our coupling hierarchy the former is suppressed compared to the latter, and indeed, isolating the contribution from I. effectively sets $\Gamma_\varphi^{\text{NLO}} \simeq \Gamma_\varphi^{\text{sun}}$ of (4.74). Under these assumptions regarding the model parameters and associated hierarchies, the one-loop thermal corrections to both the effective masses (4.57) and potential (4.54) take the usual large T value, namely $\lambda T^2/24$ where λ is a generic coupling. Therefore, we obtain the high temperature limit of $\Gamma_\varphi^{\text{sun}}$ of (4.74) and the effective force as⁵

$$V'(\varphi) \simeq m_\phi^2 \varphi + \frac{(\lambda_\phi + h)}{24} T^2 \varphi, \quad (5.13)$$

$$\Gamma_\varphi \simeq \frac{h^2}{(4\pi)^3} \frac{T^2}{M_\chi} \log \left(1 + \frac{\lambda_\chi}{h} \right). \quad (5.14)$$

Plugging these in our slow-roll conditions (5.11), we immediately see that these cannot sustain a high-temperature slow-roll regime, because

$$\eta \propto \frac{(4\pi)^6}{h^2 \log^2(1 + \lambda_\chi/h)} \left(\frac{(\lambda_\phi + h)(\lambda_\chi + h)}{h^2} + \mathcal{O}(m_\phi^2/T^2, (\ln \Gamma_\varphi)'/T^2) \right), \quad (5.15)$$

which makes it impossible to satisfy $\eta < 1$ for our assumptions I. This is simply because I. corresponds to a very high temperature regime, wherein both the damping rate and effective potential grow with a positive power of the temperature. Therefore, it is impossible to generate the large friction needed for

⁵In the high T limit, the terms in the effective force (C.40) that depend on the renormalisation scale essentially behave like the leading-order finite temperature correction $T^2/24$, except they are of second order in the loop and coupling constant expansions, hence parametrically suppressed and neglected.

slow-roll dynamics without simultaneously generating large screening effects on the slope of the potential, which eventually dominate and make the field roll quickly. Not only that, but also the finite temperature corrections to the potential and damping rate arise at different orders in both the loop and coupling constant expansions. Hence, those of the damping rate ($\propto h^2/(4\pi)^3$) are both coupling constant and phase-space suppressed vs. those of the effective potential ($\propto h/24$). We are precisely in the situation commented on at the end of the previous section where large screening effects cannot be avoided when large damping effects are wanted simultaneously. We conclude that in the limiting case I., warm inflation cannot be realised, because even slow-roll cannot.

5.5.2 Case II.: Crab widths dominate

Comparing Γ_a^{crab} and Γ_a^{sun} which respectively are given in Eqs. (4.61)(4.62) and (4.68), we see that a first necessary condition for $\Gamma_a^{\text{crab}} \gg \Gamma_a^{\text{sun}}$ to be fulfilled is the following hierarchy for the effective masses $M_\phi > 2M_\chi$, otherwise Γ_a^{crab} is simply kinematically forbidden. This mass hierarchy can e.g. be arranged by having a large Lagrangian mass for the inflaton and having ultrarelativistic χ fields: $m_\phi \gg m_\chi$, or by tuning the couplings so that the ϕ case of Eq. (4.57) dominates over its χ counterpart. As explained in section (4.4.2), this is best realised by demanding $\varphi > T$ and $\lambda_\phi \gtrsim \lambda_\chi = h$. For consistency with those sections, we shall pick $\lambda_\phi/h = \lambda_\phi/\lambda_\chi = 10$ and $m_\phi/m_\chi = 10^2$, as for Fig. 4.6.

Then, again looking at Eqs. (4.61)(4.62) and (4.68) or even better Fig. 4.4, we note that the requirement $\varphi > T$ readily favors $\Gamma_a^{\text{crab}} \gg \Gamma_a^{\text{sun}}$. Therefore, we set ourselves in case I. by assuming the following very conservative conditions

$$\lambda_\phi \gg \lambda_\chi, h, \quad h^2\varphi \gg \lambda_\phi^2 T / (4\pi)^2, \quad (5.16)$$

such that Γ_a^{crab} is kinematically allowed and strongly dominates Γ_a^{sun} . Note that this regime also tends to favour inflation itself as the latter usually requires a large potential for the energy density of the Universe to be cosmological-constant-like. Also note that this corner in parameter space is precisely the one where case I. is highly suppressed, and the sunset two-loop contribution to $\Gamma_\varphi^{\text{NLO}}$ can be neglected. In Fig. 5.2, we depict the slow-roll parameter η (5.11), as a function of the background field φ and for various temperatures, neglecting the NLO contribution to the friction rate, and the logarithmic derivative in Eq.(5.11) (both of which would just lower η).

We find that η is maintained below unity for a wide range of field values and temperatures and slow-roll, in the sense of (5.11), is achievable for an extended

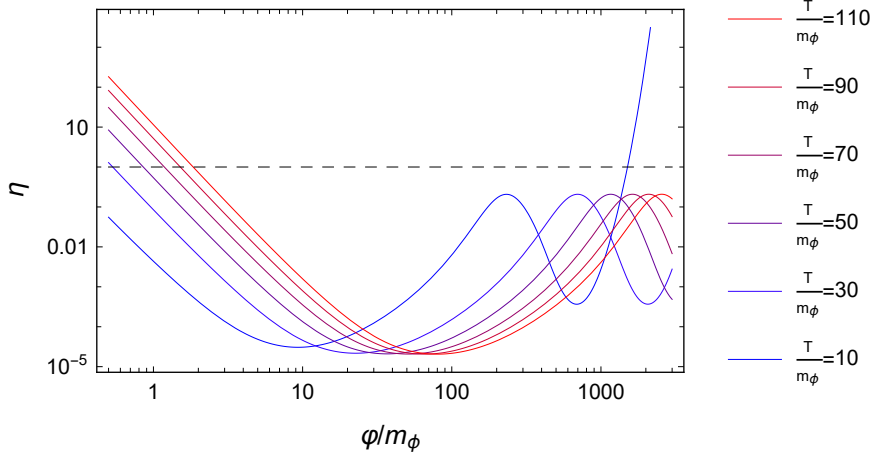


Figure 5.2: The slow-roll parameter η of Eq. (5.11) vs. the background field φ normalised to the mass m_ϕ , and for various temperature with logarithmic scales on both axis. The black dashed line is the unity line.

period⁶, even in flat space. As a matter of fact, varying the couplings λ_ϕ , λ_χ , h , we find that there is always a sizeable window for which the slow-roll condition (5.11) is satisfied, regardless of whether or not the crab widths are kinematically allowed. Only the range of validity is *a priori* reduced when the crab width does not dominate quickly enough, though it can potentially be extended if we by hand introduce a Boltzmann suppressing exponential, cf. section 4.4.2. These results are very comforting because they constitute a solid selfconsistency check and proof that *a posteriori* all approximations used throughout the previous chapter were indeed justified. They are physically interesting too, because we have just proven that a scalar condensate undergoes a phase of overdamped motion, even in flat space, and for a sizeable budget of our model's parameters.

While this does not prove the feasibility of warm inflation in our model, it for sure warrants investigation as to whether our effective potential and damping rate can simultaneously realise (5.8), and a negative equation of state (5.10) for an extended time period. At this stage, we can only say that we unfortunately doubt that it will be viable because the damping rates resulting from the additional cases I. and II. were either shown of NLO and incapable of generating slow-roll to begin with (I.), or they just lower the already existing damping rate (II.). Given that [17] claims warm inflation not to be feasible with our

⁶The wavy features in Fig 5.2 are precisely those we see in Fig. 4.6 and owe their presence to the crab widths. These lower the full damping rate and hence as a result enhance η .

model because the latter cannot sustain inflation for long enough, we believe that lowering further the damping rate (via the crab widths of II.) will not help with this matter, we even expect it to make it worse. However, more closely looking at [17], it appears that the most problematic assumptions are $T \gg M_a$ and $\Gamma_a \gg \dot{\varphi}/\varphi$, both of which are more easily realised thanks to II. Therefore, in order to provide a definitive answer, only a first principles analysis *à la* [17] would do. As emphasised earlier, this requires (a) condition (5.11), (b) the first principles derivation of the equation of state (or 2PI energy-momentum tensor [116]) and the relevant condition (5.10) for our Z_2 -symmetric two-field model, (c) numerically solving the dynamical equations that connect the temperature T , the background φ and the Hubble rate H [117,118], for a window of at least 50-70 e-folds, and (d) check that the range of validity of our results extend to that window. We leave this tedious, yet very interesting, task for future work.

Conclusion and Outlook

Conclusion

In the first part of this thesis, we have studied the nonequilibrium and dissipative dynamics of real scalar fields which interact via \mathbb{Z}_2 symmetric renormalisable interactions, from first principles of the 2PI effective action formalism and the Schwinger-Keldysh formulation of nonequilibrium field theory.

In chapter 2, under the assumption that microphysics time scales are much shorter than those that characterise bulk properties of the system, we have shown in a model- and contour-independent fashion that the equation of motion for a field condensate φ can always be localised and brought into the generic form $\ddot{\varphi} + \sum_{n=1}^{+\infty} \Gamma_{\varphi}^{(n)} \dot{\varphi}^n + V'(\varphi) = 0$. The dissipation coefficients $\Gamma_{\varphi}^{(n)}$ and the effective force $V'(\varphi)$ are computed from Feynman diagrams.

In the next chapters 3-4, we have then computed $\Gamma_{\varphi}^{(1)}$ and $V'(\varphi)$ for our specific \mathbb{Z}_2 -symmetric model, including quantum and thermal corrections to second order in perturbation theory. These computations rely on formal adiabatic solutions of the quantum kinetic equations that govern the nonequilibrium dynamics of quasiparticles, carefully including the backreaction of the condensate. The question of renormalisation in time-dependent backgrounds was scrupulously addressed, too. Our results for the damping rates have a significantly increased range of validity compared to the state-of-the-art computations, because we accounted for contributions that had been omitted in the existing literature, see e.g. [17, 62].

Eventually in the last chapter 5, we have provided a selfconsistency check and proven that slow-roll is indeed realised for a wide subset of the model parameters (even in flat space), hence justifying our assumptions *a posteriori*.

We also reviewed the state of the art of the feasibility of warm inflation and commented on the implications of our results for it. Despite our innovative results, extended range of validity and improved accuracy, we expect warm inflation not to be feasible in the model presented here. However, we emphasise that only a fool-proof analysis of the feasibility of warm inflation that includes the two-scalar equation of state would (in)validate these claims for good.

Outlook

As we just emphasised, among the natural future perspectives to this work of course lies the in-depth study of the feasibility of warm inflation in our two-field model. This requires the first principles derivation of the 2PI energy-momentum tensor, or equation of state, and a numerical scan through the model parameters to determine whether slow-roll inflation can be maintained for a few tens of e-folds. This ought to be not too demanding because we expect the diagrams that constitute the equation of state to be already evaluated and the remainder should be nothing but a numerical analysis based on a readily existing code. Whatever the outcome of this analysis, we also find the “Warm Little Inflation” [112–114] and “Minimal Warm Inflation” [83] models very interesting and it would be a nice continuation to then try and study their viability from first principles. Eventually, repeating all these steps using curved spacetime quantum field theory also is an obvious future prospect of this work.

Another natural extension which we wish to comment on concerns the Breit-Wigner or quasiparticle approximation, heavily used throughout this work. As mentioned in chapter 4, this approximation of course has its limitations whenever off-shell processes are significant. In particular, it has been claimed that off-shell decays and scatterings can be responsible for the overdamped motion of the inflaton, in the so-called two-stage mechanism [13, 14] of warm inflation, wherein the inflaton couples to radiation via a heavy mediator. Checking these claims from first principles and understanding the range of validity of the Breit-Wigner approximation, as well as its role in warm inflation computations, is of great interest and a logical continuation to this work.

Eventually, although primarily motivated by warm inflation, our results potentially have a wider range of applicability than just it. They can likely be applied to study perturbative cosmic reheating or the fate of a scalar in the early Universe, for instance in scenarios where the Higgs couples to the inflaton, see e.g. [121] where the inflaton is natural dark matter candidate, hence constituting a model which interactions resemble the ones studied here.

Part II

Towards a precision computation of N_{eff} in the standard model of particle physics and cosmology

Introduction

The standard model of cosmology, or Λ CDM cosmology very successfully describe the Universe, from its very early times when it was constituted of a hot primordial plasma, to its current content on the largest scale. On top of those that compose Standard Model (SM) of particle physics, Λ CDM cosmologies rely on six fundamental parameters, namely the reduced Hubble expansion parameter h , the dark matter and baryon densities, ω_c and ω_b , the amplitude and spectral index of the primordial curvature power spectrum, A_s and n_s , together with the optical depth to reionisation τ . All these parameters have been measured to better than 1% accuracy by the recent WMAP [78] and Planck [122] missions. Accurately inferring those Λ CDM parameters however crucially relies on one theoretical input: the post- $e^\pm \rightarrow \gamma\gamma$ -annihilation neutrino to photon energy density ratio ρ_ν/ρ_γ . The latter is customarily parametrised by the so-called effective number of cosmological neutrinos N_{eff} . The degree of precision to which the Λ CDM parameters can be inferred from experiments closely ties to the level of accuracy to which N_{eff} is theoretically predicted.

Within the realm of standard model physics, the leading-order value is $N_{\text{eff}} = 3$, which is nothing but the number of massless, left-handed neutrinos in the SM, hence its name. In the SM, δN_{eff} from $N_{\text{eff}} = 3$ come at the percent level and they primarily find their origins in neutrino energy transport and oscillations [123–128], and finite-temperature quantum electrodynamics (FTQED) [129–132]. With improved numerical methods and modelling of the transport equations that govern the neutrino dynamics, together with $\mathcal{O}(e^2)$ FTQED corrections, with e the elementary electric charge, the recently (2019) revised and most quoted theoretical value of value for N_{eff} is $N_{\text{eff}} = 3.044$, to better than per-mille accuracy [133]. While this is currently too small to alter our Λ CDM parameter inference⁷, future experiments are expected to narrow down the uncertainties to subpercent level. For instance, the ground-based CMB-S4 experiment which construction should start in 2021, is expected to improve the 1σ sensitivity to $\sigma(N_{\text{eff}}) \simeq 0.02 \rightarrow 0.03$ [134]. For these reasons, it is timely to beat down the remaining theoretical and computational uncertainties on N_{eff} to below the fourth significant digit. In this part of the thesis, including FTQED effects of unprecedented accuracy and aiming for a four-digit precision, we compute the state-of-the-art SM value of N_{eff} within the instantaneous decoupling approximation, and provide the necessary analytic ingredients to numerically determine it, when including neutrino energy transport and oscillations.

⁷The current best observational constraint on N_{eff} is $N_{\text{eff}} = 2.99^{+0.34}_{-0.33}$ (95% C.I.) [122].

Chapter 6

N_{eff} and cosmological thermodynamics

The effective number of cosmological neutrinos N_{eff} finds its exact definition in the framework of cosmological thermodynamics. In this chapter, following the excellent books [1, 135], we briefly review the main ingredients to describe the thermodynamics of relativistic particles in an expanding Friedmann-Lemaître-Robertson-Walker (FLRW) spacetime, and describe what theoretical inputs enter a precision computation of N_{eff} in the Standard Model of cosmology and particle physics. In particular, we re-evaluate the neutrino decoupling temperature. Eventually, we review the current status of experimental measurements of N_{eff} and comment on future experiments to come.

6.1 Kinematics in FLRW spacetimes

The cosmological principle, which is in very good accordance with observation, stipulates that the Universe we live in is homogeneous and isotropic on large scales. As a result, cosmological spacetimes are described by the so-called Friedmann-Lemaître-Robertson-Walker (FLRW) metric $g_{\mu\nu}$ which reads

$$ds^2 = g_{\mu\nu} dx^\mu dx^\nu = dt^2 - a^2(t) \left(\frac{dr^2}{1 - kr^2} + r^2 d\Omega^2 \right), \quad (6.1)$$

with $a(t)$ the scale factor¹, $k = 0, \pm 1$, the curvature parameter and $d\Omega$ the infinitesimal, three-dimensional solid angle. One distinguishes three qualitatively different spacetimes for three different values of $k = 0$, $k = 1$ and $k = -1$. These respectively correspond to flat, spheric and hyperbolic geometries. Locally, those geometries are all equivalent, and for the present discussion we shall always set $k = 0$, which turns out to also be the experimentally favoured geometry, although all are *a priori* allowed.

The Hubble law. In such spacetimes, denoting $L(t)$ the instantaneously measured physical distance between two point-like observers of same local angular coordinates, we have

$$\dot{L}(t) = H(t)L(t), \quad \text{with } H(t) = \frac{\dot{a}(t)}{a(t)}, \quad (6.2)$$

the Hubble rate, experimentally measured positive $H(t) > 0$ in our Universe. This inevitably leads to the striking observation that not only is our Universe expanding, but also the larger $L(t)$, the speedier the distancing velocity.

The redshift. Also, if a photon is emitted at time t_0 and measured at time $t > t_0$, its emitted and measured frequencies are related by the formula

$$\frac{\omega_0}{\omega} = \frac{a(t)}{a(t_0)} = (1 + r). \quad (6.3)$$

Since the Universe is expanding, $a(t) > a(t_0)$ and the photon's wavelength got stretched to the longer wavelengths of the optical spectrum, hence we define $r > 0$ as the so-called redshift parameter.

The physical momentum. Another physically relevant consequence of the presence of the scale factor in the FLRW metric is the modified mass-shell equation. If p^μ is the four-momentum of a particle, then the latter reads

$$g_{\mu\nu}p^\mu p^\nu = m^2 \Rightarrow (p^0)^2 - a^2\mathbf{p}^2 = m^2, \quad (6.4)$$

and the FLRW energy, as measured by the comoving observer, is given by $\omega = \sqrt{m^2 + a^2\mathbf{p}^2}$, which is valid for both massive and massless particles. From this definition, it is tempting to define the so-called physical momentum $p = a|\mathbf{p}|$, such that ω takes the usual form $\omega = \sqrt{m^2 + p^2}$. Let us try to understand and

¹Though it really is an arbitrary local coordinate, the latter is commonly interpreted as the radius of the spatial size of the Universe. When the scale factor grows (resp. decreases), the Universe expands (resp. contracts).

interpret the meaning of this physical momentum. For this purpose, let λ be an affine parameter along a particle worldline such that, if $q^\mu(\lambda)$ is its position vector, $dq^\mu/d\lambda = p^\mu$, where $p^\mu = (\omega, \mathbf{p})^T$ is its four-momentum. This choice of affine parameter gives a free geodesic equation in terms of p^μ which reads

$$\frac{dp^\mu}{d\lambda} = -\Gamma_{\alpha\beta}^\mu p^\alpha p^\beta \quad (6.5)$$

where the Christoffel symbols are

$$\Gamma_{\alpha\beta}^\mu = \frac{1}{2} g^{\mu\nu} (g_{\nu\beta,\alpha} + g_{\nu\alpha,\beta} - g_{\alpha\beta,\nu}), \quad (6.6)$$

with the usual notation $g_{\alpha\beta,\mu} = \frac{\partial g_{\alpha\beta}}{\partial q^\mu}$. Using the Christoffel symbols of the FLRW metric, the spatial components of the geodesic equation give [135]

$$\frac{d\mathbf{p}^i}{dt} + 2H\mathbf{p}^i = 0 \quad \Rightarrow \quad \begin{cases} |\mathbf{p}| \propto a^{-2}, \\ p \propto a^{-1}. \end{cases} \quad (6.7)$$

For this reason, p is called as the physical momentum because it is the one that redshifts just like the physical energy ω measured by the comoving observer. For massless particles, this also reproduces the redshift of photons (6.3).

6.2 Dynamics in FLRW spacetimes

In order to properly understand the expansion of the Universe which causes structures to move apart and photons to redshift, one has to study the dynamics of particles in the FLRW metric, and the dynamics of the metric itself. In homogeneous and isotropic geometries, the only time-dependent quantity which dictates the spacetime expansion is the scale factor $a(t)$. Its time evolution is governed by the Einstein equations for the metric. In terms of the scale factor $a(t)$, they are the so-called Friedmann equations

$$H^2 = \frac{\Lambda}{3} + \frac{\rho_{\text{tot}}}{3M_{\text{pl}}^2}, \quad (6.8)$$

$$\frac{\ddot{a}}{a} = \frac{\Lambda}{3} - \frac{(\rho_{\text{tot}} + 3P_{\text{tot}})}{6M_{\text{pl}}^2}, \quad (6.9)$$

where $\Lambda > 0$ is the cosmological constant measured positive, ρ_{tot} and P_{tot} are the total energy and pressure densities of the cosmological fluid under consideration, and $M_{\text{pl}} = 2.435 \times 10^8$ GeV is the reduced Planck mass. Those equations are supplemented by the continuity equation in an expanding spacetime

$$\dot{\rho}_{\text{tot}} + 3H(\rho_{\text{tot}} + P_{\text{tot}}) = 0. \quad (6.10)$$

The latter can be solved analytically for barotropic² fluids of equation of state $P = w\rho$ and we find

$$\dot{\rho} + 3(1+w)H\rho = 0 \Rightarrow \rho \propto a^{-3(1+w)}. \quad (6.11)$$

Non-relativistic also known as matter (m) fluids have negligible kinetic energies compared to their mass energies, hence $P_m = 0$ and $w_m = 0$ and they see their energy densities get diluted with the three-dimensional spatial volume

$$\rho_m \propto \frac{1}{a^3}. \quad (6.12)$$

On the other hand, relativistic fluids, also known as radiative (r) fluids, satisfy $P_r = \frac{\rho_r}{3}$, hence $w_r = \frac{1}{3}$ and relativistic energy densities get diluted with the four-dimensional volume

$$\rho_r \propto \frac{1}{a^4}. \quad (6.13)$$

Massless particles (e.g. photons) redshift quicker than massive ones (e.g. electrons) in an expanding FLRW spacetime and the associated energy density dilutes quicker, too.

6.3 Thermodynamics in FLRW spacetimes

Turning the arrow of time, the expansion of the Universe becomes its contraction. Therefore, very early on, our Universe was made of nothing but a hot primordial plasma of Standard Model particles maintained at equilibrium through their gauge interactions. As long as a species interaction rate Γ is larger than the expansion rate H , the associated particles are kept in local (in time) thermal equilibrium and their distribution function can be described by their equilibrium ones (cf. Eqs. (1.41)(1.104))

$$f(t, \omega) = \left(\exp \left(\frac{\omega}{T(t)} \right) \pm 1 \right)^{-1}, \quad (6.14)$$

with $T(t)$ is the time-dependent temperature, adiabatically cooling down with the growth of the scale factor. Indeed, as the Universe expands, its content gets diluted, hence adiabatically lowering the local thermal agitation of the system. As long as this picture holds, the leading order thermodynamic pressure and energy densities are given by Eqs. (1.44)(1.45) for bosons and Eq. (1.112)(1.113)

²Fluids which pressure and density profiles have identical constant-pressure (isobaric) and constant-density (isopycnic) hypersurfaces.

for fermions. The general expressions, weighted with g , the number of relativistic degrees of freedom of the species under consideration and integrated over their physical momenta, read

$$P = g \int \frac{d^3 p}{(2\pi)^3} \frac{p^2}{3\omega} f(t, \omega), \quad \rho = g \int \frac{d^3 p}{(2\pi)^3} \omega f(t, \omega). \quad (6.15)$$

However this smoothly-evolving quasiequilibrium phase unfortunately does not last forever. As the Universe expands and the constituents of the Universe dilute, they start interacting less and less frequently. Their interaction rate Γ decreases with the temperature and becomes lower than the expansion rate $\Gamma < H$, it no longer suffices to maintain species at equilibrium in a rapidly expanding spacetime. The particles undergo a phase of far-from-equilibrium evolution during which species, one by one, decouple from the primordial plasma as their interactions freeze out with the Hubble expansion. Feebly interacting species, e.g. neutrinos, decouple first.

In most cases, the decoupling of species is sufficiently well approximated by the so-called instantaneous decoupling scenario wherein particles instantaneously transit from one equilibrium phase with the primordial plasma to another one where they are entirely decoupled and free-streaming. In that case, the decoupling temperature T_d is usually estimated by demanding

$$\Gamma(T_d) = H(T_d) \quad (6.16)$$

which refers to the instant where the interaction and expansion rates precisely equate. As an exercise of primordial relevance for N_{eff} (which precision computation is the ultimate goal of this part of the thesis) we shall compute the temperature at which weakly interacting neutrinos decouple from a quantum electrodynamical (QED) plasma of interacting (anti)electrons and photons.

Obviously, for certain cosmological observables which ought to be accurately predicted because they are accurately measured, the instantaneous decoupling approximation is unfortunately not sufficient. This is e.g. the case for N_{eff} or the most famous freeze-out relic, the Cosmic Microwave Background (CMB), which is nothing but the free-streaming photon fluid which decoupled from the primordial plasma. The latter is extremely well-measured and in order to theoretically match the level of experimental precision and extract as much information as possible from the CMB, we need to go beyond the instantaneous decoupling limit. We need to be able to accurately track and describe the (non)equilibrium thermodynamic evolution of species as time evolves and the Universe expands, including those moments where distributions are far from equilibrium. We emphasise, many cosmological observables depend on it,

including the CMB and most relevant for this work, the effective number of cosmological neutrinos N_{eff} . This time evolution is encapsulated in the so-called Boltzmann equations for the distribution functions, which we shall describe in the following section.

For this purpose, let $f(q^\mu, p^\mu)$ be the phase space distribution function of a certain particle species and λ be an affine parameter along the particle worldline such that $dq^\mu/d\lambda = p^\mu$, where $q^\mu(\lambda) = (t, \mathbf{x})^T$ is the particle position four-vector and $p^\mu = (\omega, \mathbf{p})^T$ is its four-momentum.

The collisionless Boltzmann equation. If the particle is free-streaming and does not encounter any obstacle along its worldline, then its distribution function satisfies $\frac{df}{d\lambda} = 0$ and the geodesic equation (6.5) holds along that worldline. Therefore, we compute

$$\frac{df}{d\lambda} = 0 \quad \Rightarrow \quad \mathfrak{L}[f] = p^\mu \frac{\partial f}{\partial q^\mu} - \Gamma_{\alpha\beta}^\mu p^\alpha p^\beta \frac{\partial f}{\partial p^\mu} = 0, \quad (6.17)$$

where $\mathfrak{L} = p^\mu \frac{\partial}{\partial q^\mu} - \Gamma_{\alpha\beta}^\mu p^\alpha p^\beta \frac{\partial}{\partial p^\mu}$ is the Liouville operator. In a spatially flat, isotropic and homogeneous spacetime, $f(q^\mu, p^\mu) \rightarrow f(q^0 = t, p^0 = \omega)$ and upon evaluation of the FLRW Christoffel symbols, we find for the previous equation

$$\left(\omega \frac{\partial}{\partial t} - H p^2 \frac{\partial}{\partial \omega} \right) f(t, \omega) = 0 \quad (6.18)$$

Changing variables from $(t, \omega) \rightarrow (a(t), p(\omega) = \sqrt{\omega^2 - m^2})$ where p is the physical momentum, and using the FLRW mass invariant, we find

$$\left(a \frac{\partial}{\partial a} - p \frac{\partial}{\partial p} \right) \tilde{f}(a, p) = 0, \quad (6.19)$$

with $\tilde{f}(a, p) = f(t(a), \omega(p))$. Any solution of this equation must be of the form $\tilde{f}(a, p) = g(a \cdot p)$ and for any reference time \bar{t} of associated $\bar{a} = a(\bar{t})$, this condition gives

$$f(t, \omega) = g(a \cdot p) = g\left(\bar{a} \cdot \frac{a(t)p}{\bar{a}}\right) = f\left(\bar{t}, \omega\left(\frac{a(t)p}{\bar{a}}\right)\right). \quad (6.20)$$

Therefore the form of the phase space distribution function $f(t, \omega)$ does not change along a collisionless worldline, only its spatial momentum gets redshifted.

In particular, assuming that the decoupling of a species i takes place instantaneously and that from the decoupling instant t_d , the species is in thermal

equilibrium, be it a Dirac fermion (+) or a boson (-), we have (cf. Eq. (6.14))

$$f_i(t > t_d, \omega) = \left(\exp \left[\frac{1}{T_d} \omega \left(\frac{a(t)p}{\bar{a}} \right) \right] \pm 1 \right)^{-1}, \quad (6.21)$$

where ω is the FLRW energy $\omega(p) = m_i^2 + p^2$. Using its approximated expression for matter (m) and relativistic fluids (r), respectively $\omega_m(p) \simeq m_i + \frac{p^2}{2m}$ and $\omega_r(p) = p$, we find

$$f_i(t > t_d, \omega_m) = \left(e^{\frac{m_i}{T_d}} \exp \left[\frac{p^2}{2m_i T_m(t)} \right] \pm 1 \right)^{-1}, \quad T_m(t) = \left(\frac{a_d}{a(t)} \right)^2 T_d, \quad (6.22)$$

$$f_i(t > t_d, \omega_r) = \left(\exp \left[\frac{p}{T_r(t)} \right] \pm 1 \right)^{-1}, \quad T_r(t) = \frac{a_d}{a(t)} T_d. \quad (6.23)$$

This suggests that from the moment they decouple, particles follow their equilibrium distribution function with adiabatically evolving temperatures which dynamics depends on their (non)relativistic nature. The temperature of matter particles $T_m(t) \propto \frac{1}{a^2(t)}$ redshifts quicker than that of radiation $T_r(t) \propto \frac{1}{a(t)}$. In particular for ultrarelativistic species, this gives (see Eq. (1.46) for bosons (B) and Eq. (1.114) for Dirac fermions (D))

$$\rho_i = \rho_r = g_i \frac{\pi^2}{30} T_r^4(t) = 3P_i, \text{ if } i \text{ is a boson, and} \quad (6.24)$$

$$\rho_i = \rho_{r,\psi} = g_i \frac{7}{8} \frac{\pi^2}{30} T_r^4(t) = 3P_i, \text{ if } i \text{ is a fermion.} \quad (6.25)$$

Here g_i is the number of relativistic degrees of freedom of the particle species i . In the cosmological literature, it is customary to distinguish a particle from its antiparticle and their contributions to thermodynamic quantities are accounted for separately³. Therefore, g_i here only counts the internal spin degrees of freedom. For spin 1/2 fields, e.g. neutrinos or (anti)electrons, $g_\nu = g_{e^\pm} = 2$. For massless gauge bosons, e.g. for photons $g_\gamma = 2$ and for massive ones, e.g. for the W bosons, $g_{W^\pm} = 3$. Scalars have no spin degrees of freedom, cf. Eq. (1.46). Note that Eqs. (6.24)(6.25) consistently reproduce the conclusions drawn as to how radiative energy densities ought to depend on the FLRW scalar factor, see Eq. (6.13). A similar discussion for nonrelativistic matter particles can be held, too, and we would have recovered the expected behavior (6.12). That said, let us now move on to the more interesting case where the particle under consideration is subject to interactions along its worldline.

³Note however that this is not the case when derived from first principles in quantum field theory, where spin and antiparticles are readily built in features of the formalism, see e.g. Eq. (1.111) and the discussion below.

The Boltzmann equation. However, if the particle does not free-stream and does scatter with other constituents of the Universe, its equation of motion takes the form (see. Eq. (6.17))

$$\mathfrak{L}[f_i] = C[f_i] \quad (6.26)$$

where $C[f_i]$ encapsulates all collision and scattering events that alter the FLRW free-streaming evolution of particles of type i . It is commonly referred to as the collision term and ought to be determined from first principles of quantum field theory, as it arises from the interactions between the particles associated to the fundamental fields. Say the species i is subject to scatterings of the form $i+j \leftrightarrow k+l$, where i is the particle which evolution is tracked by the Boltzmann equation (6.26), and j, k, l are other particles. Then, the full collision term is given by the difference between a production and a destruction rate

$$C[f_i] = C_{k\ell \rightarrow ij}[f_i] - C_{ij \rightarrow k\ell}[f_i], \quad (6.27)$$

such that, in this particular case

$$C[f_i] = (2\pi)^4 \left(\int \prod_{a=j,k,\ell} \frac{g_a d^3 \mathbf{p}_a}{2\omega_{a,\mathbf{p}} (2\pi)^3} \right) \delta^{(4)}(p_k + p_\ell - p_i - p_j) \times \\ \times |\mathcal{M}_{k\ell \leftrightarrow ij}|^2 \left[f_k f_\ell (1 \pm f_i)(1 \pm f_j) - f_i f_j (1 \pm f_k)(1 \pm f_\ell) \right], \quad (6.28)$$

where $|\mathcal{M}_{k\ell \leftrightarrow ij}|^2$ is the squared quantum field theoretical probability amplitude, also known as matrix element, for the process $k\ell \leftrightarrow ij$ and the \pm phase space factor gives either a Pauli blocking factor ($-$) or a Bose-enhanced stimulated emission ($+$) for the particles in the final state. Later in this thesis, we shall precisely derive the relevant Boltzmann equations for this work, from first principles of nonequilibrium quantum field theory.

These last expressions and equations close the general discussion about Boltzmann equations and thermodynamics in FLRW spacetimes. Combining the last two sections together with the Standard Model of particle physics as well as an additional Cold⁴ Dark Matter (CDM) relic, provide a rock solid theoretical description of the thermal history of the Universe, from today ($T \sim 2.7K \sim 2.3 \cdot 10^{-4}$ eV) up to the Planck time, 10^{-43} sec ($T \sim 10^{19}$ GeV) after the big-bang singularity. It is known as the Λ CDM cosmology or standard model of cosmology. Computing accurate predictions from that framework is of great importance if one wants to pinpoint where exactly standard cosmology fails to describe the Universe we live in and where there are deviations from

⁴A relic species is referred to as a cold relic if its mass exceeds its decoupling temperature.

it. The effective number of cosmological neutrinos N_{eff} , amongst others, is one of these cosmological observables one can accurately predict within the theoretical framework presented here. In the coming section, we explain how its definition arises in the context of cosmological thermodynamics and how to compute it efficiently and accurately.

6.4 N_{eff} from FLRW thermodynamics

Within the standard model of cosmology, at temperatures of around 10 MeV, the Universe was constituted of a hot plasma made of QED particles, that is electrons/positrons e^\pm and photons γ , together with three generations of left-handed neutrinos, all maintained at equilibrium through their QED and weak interactions. Starting at around $T \sim 10$ MeV, the Universe expansion which lessens the interaction rates, consequently triggers two physically relevant phenomena as far as N_{eff} is concerned:

- **Neutrino decoupling:** At $T \sim 1$ MeV, the neutrino weak interaction rate drops below the Hubble rate⁵ and the neutrinos decouple from the equilibrium QED plasma and consequently their temperature T_ν evolves independently of T_γ , the temperature of the γ/e^\pm QED sector.
- **Electron/positron $e^+e^- \rightarrow \gamma\gamma$ annihilations:** At $T \sim 0.5$ MeV, lower than the electron mass $m_e = 0.511$ MeV, the electron/positron annihilation into photon pairs, $e^+e^- \rightarrow \gamma\gamma$, is kinematically favoured, hence leading to a nonnegligible net energy transfer from the e^\pm sector to the photon population, effectively reheating the photon fluid.

As a result of these two events, the relic neutrinos end up cooler than the relic photons. How exactly cooler they are is however a tough question to address accurately as it relies on a careful analysis of the quantum out-of-equilibrium dynamics of the ν -QED fluid, all the way from $T \sim 10$ MeV to temperatures that are negligible vs. m_e , i.e. when $T/m_e \rightarrow 0$. As a matter of fact, N_{eff} precisely relies on that, too, as it is defined through

$$\left. \frac{\rho_\nu}{\rho_\gamma} \right|_{T/m_e \rightarrow 0} = N_{\text{eff}} \frac{7}{8} \left(\frac{4}{11} \right)^{4/3}, \quad (6.29)$$

in relation to the post- $e^\pm \rightarrow \gamma\gamma$ -annihilation neutrino to photon energy density ratio. This definition for N_{eff} and the associated prefactors will become crystal

⁵In the next section, we will precisely show at what temperature this neutrino decoupling occurs, which of course will be shown to be consistent with $T_d \sim 1$ MeV.

clear in the next analysis where we explain how to calculate the leading-order value of N_{eff} , from the conservation of the comoving entropy.

6.4.1 N_{eff} in the SM from entropy conservation arguments

For the time being, let us first list the following three approximations:

- (I) **Instantaneous decoupling approximation.** The moment the neutrinos decouple is localised in time and instantaneously occurs at $T = T_d$.
- (II) **Ideal gas approximation.** All particles distribution functions are either exact Bose-Einstein or Fermi-Dirac distributions, cf. Eq. (6.14), and their energy densities and pressures are given by their leading-order ones (6.15).
- (III) **Neutrino-never-coupled approximation.** The electrons (and positrons) are ultrarelativistic at T_d , as if neutrinos were never coupled and decoupled in the infinite past $T_d/m_e \rightarrow \infty$.

Under (I), the QED entropy density⁶ $s(a)$ which we denote as a function of the scale factor, is conserved and fulfills the relation

$$s(a_1)a_1^3 = s(a_2)a_2^3, \quad (6.30)$$

from the moment the neutrinos decouple, i.e. for $a_1, a_2 \geq a_d$.

Now let $a_1 = a_d$ be the scale factor at the decoupling instant and therefore $T_\nu(a_1) = T(a_1) = T_d$. Using Eq. (1.10) and the relativistic energy densities for bosons and fermions (6.24)(6.25), the QED entropy densities read

$$s(a_1) = s^{(0)} \Big|_{T_d/m_e \rightarrow \infty} + \delta s \quad (6.31)$$

where

$$s^{(0)} \Big|_{T_d/m_e \rightarrow \infty} = \left(2 + 2 \cdot 2 \cdot \frac{7}{8}\right) \left(1 + \frac{1}{3}\right) \frac{\pi^2}{30} T_d^3 = \frac{11\pi^2}{45} T_d^3, \quad (6.32)$$

is the QED entropy density of an ideal gas (represented by superscript “(0)”) in the limit where $T_d/m_e \rightarrow \infty$, i.e. under the assumptions (II) and (III). δs captures all deviations from (II) and (III) under the assumption that the entropy density is conserved, which is a consequence of (I).

⁶Unless explicitly labelled by e , γ or ν , all thermodynamic quantities in this section are those of the QED bath.

Then, let a_2 be a certain scale factor well after the neutrinos decoupling, where electrons and positrons are completely nonrelativistic $T(a_2)/m_e \rightarrow 0$. Then, the energy and pressure densities of the electrons and positrons are negligible, as those of matter particles, and the QED entropy density at that time reads

$$s(a_2) = 2 \cdot \frac{2\pi^2}{45} T^3(a_2), \quad (6.33)$$

Now, remembering that after they decouple, the temperature of ultrarelativistic particles, such as that of neutrinos, follows $T_\nu(a) = \frac{a_d}{a} T_d$, (cf. (6.23)). This immediately leads to the relation $T_\nu(a_2) = (a_1/a_2) T_\nu(a_1) = (a_1/a_2) T(a_1)$. Thanks to (I), we can equate (6.31) with (6.33) and it gives

$$\frac{T_\nu(a_2)}{T(a_2)} = \left(\frac{4}{11}\right)^{1/3} \left(1 + \frac{\delta s}{s^{(0)}|_{T_d/m_e \rightarrow \infty}}\right)^{-1/3}, \quad (6.34)$$

which is equivalently rewritten as the energy density ratio

$$\frac{\rho_\nu}{\rho_\gamma} \Big|_{T/m_e \rightarrow 0} = 3 \cdot \left(1 + \frac{\delta s}{s^{(0)}|_{T_d/m_e \rightarrow \infty}}\right)^{-4/3} \frac{7}{8} \left(\frac{4}{11}\right)^{4/3}, \quad (6.35)$$

where the prefactor 3 comes from assuming three generations of neutrinos. This equation is what historically led to the following general definition of N_{eff} as

$$\frac{\rho_\nu}{\rho_\gamma} \Big|_{T/m_e \rightarrow 0} = N_{\text{eff}} \frac{7}{8} \left(\frac{4}{11}\right)^{4/3}, \quad (6.36)$$

since under the assumptions (I)-(III), we can use (6.35) with $\delta s = 0$ and find $N_{\text{eff}} = 3$. Note that the equations established here allow us to go further and relax (II) and (III) but keep (I). Then, we can define $N_{\text{eff}} = 3 + \delta N_{\text{eff}}$, and find

$$\delta N_{\text{eff}} = 3 \left[\left(1 + \frac{\delta s}{s^{(0)}|_{T_d/m_e \rightarrow \infty}}\right)^{-4/3} - 1 \right], \quad (6.37)$$

which is the change in N_{eff} due to refining (II) and (III) within (I). Indeed, (I) is crucial as it ensures entropy conservation (6.30) from T_d onwards and avoids the complications of having to track the out-of-equilibrium time evolution of the neutrino fluid during their decoupling phase. Going beyond (I) requires the numerical solution of generalised Boltzmann equations, also known as quantum kinetic equations, to precisely describe the non-instantaneous decoupling phase of the neutrinos, as well as their mixing through oscillations. In the next discussion, we argue how to do so and estimate N_{eff} by numerically solving the Boltzmann equation for the neutrino sector.

6.4.2 N_{eff} from the continuity equation

When the entropy density is not conserved, N_{eff} is computed by solving and integrating the continuity equation (6.10). Following the notation of Refs. [127, 132], it rewrites

$$\frac{d}{dx} \bar{\rho}_t(x, z(x)) = \frac{1}{x} [\bar{\rho}_t(x, z(x)) - 3\bar{P}_t(x, z(x))], \quad (6.38)$$

where the dimensionless time variable is defined as $x = m_e R(t)$, with $R(t) = a(t)/[a(t_d)T_\nu(t_d)]$ an inverse temperature parameter normalised to the neutrino decoupling temperature T_d ,⁷ $\bar{\rho}_t = \rho_t \cdot (x/m_e)^4$ and $\bar{P}_t = P_t \cdot (x/m_e)^4$ are the dimensionless comoving total energy and pressure densities, where

$$\begin{aligned} \rho_t &= \rho_\gamma + \rho_e + \rho_\nu = \rho + \rho_\nu, \\ P_t &= P_\gamma + P_e + P_\nu = P + P_\nu, \end{aligned} \quad (6.39)$$

sum over all relevant particle species for the neutrino and QED sectors. Associated to those and relevant for this work are the comoving momentum $y = pR(t)$ and rescaled photon temperature $z = T(t)R(t)$.

When it comes to computing N_{eff} , we are after the late time energy density ratio ρ_ν/ρ_γ as $T/m_e \rightarrow 0$ (i.e. as $x \rightarrow \infty$), cf. Eq. (6.36). Assuming that the QED sector remains at equilibrium during the entire time frame of interest, and provided that the distortions to the neutrino phase space distribution are negligible, the latter is fully determined by the temperature ratio T_ν/T . In the instantaneous decoupling limit, this is strictly identical and equivalent to solving the continuity equation (6.38) with the boundary conditions $z_{\text{fin}} = z(x_{\text{fin}} \rightarrow \infty)$ and $z_{\text{ini}} = z(x_{\text{ini}} = m_e/T_d) = 1$. Since z determines the initial and late-time asymptotic boundary conditions under which we solve the continuity equation (6.38), it is suitable to appropriately rewrite it as a dynamical equation of motion for z . Using $d/dx = \partial/\partial x + (dz/dx)\partial/\partial z$, this exercise gives

$$\frac{dz}{dx} = \frac{\frac{1}{2z^3} \left[\frac{1}{x} (\bar{\rho}^{(0)} - 3\bar{P}^{(0)}) - \frac{\partial \bar{\rho}^{(0)}}{\partial x} - \frac{d}{dx} \bar{\rho}_\nu + \frac{1}{x} (\delta \bar{\rho} - 3\delta \bar{P}) - \frac{\partial \delta \bar{\rho}}{\partial x} \right]}{\frac{1}{2z^3} \left(\frac{\partial \bar{\rho}^{(0)}}{\partial z} + \frac{\partial \delta \bar{\rho}}{\partial z} \right)}, \quad (6.40)$$

where we have split the comoving QED energy and pressure densities into an ideal gas component, $\bar{\rho}^{(0)}$ and $\bar{P}^{(0)}$, plus quantum field theoretical corrections

⁷This normalisation is slightly different to that used in e.g. Ref. [133], where $R(t)$ is normalised so as to have $R(t) \rightarrow 1/T$ at times well before neutrino decoupling. Our definition gives $R(t) = 1/T_\nu(t)$ at all times after neutrino decoupling, in the limit of instantaneous decoupling.

$\delta\bar{\rho}$ and $\delta\bar{P}$. Evaluating the ideal gas terms explicitly yields

$$\frac{dz}{dx} = \frac{\left(\frac{x}{z}\right) J(x/z) - \frac{d}{dx}\bar{\rho}_\nu + G_1(x, z)}{\left(\frac{x^2}{z^2}\right) J(x/z) + Y(x/z) + \frac{2\pi^2}{15} + G_2(x, z)}, \quad (6.41)$$

with the special functions

$$\begin{aligned} J(\tau) &= \frac{1}{\pi^2} \int_0^\infty d\omega \omega^2 \frac{\exp(\sqrt{\omega^2 + \tau^2})}{[\exp(\sqrt{\omega^2 + \tau^2}) + 1]^2}, \\ Y(\tau) &= \frac{1}{\pi^2} \int_0^\infty d\omega \omega^4 \frac{\exp(\sqrt{\omega^2 + \tau^2})}{[\exp(\sqrt{\omega^2 + \tau^2}) + 1]^2}, \end{aligned} \quad (6.42)$$

and

$$\begin{aligned} 2z^3 G_1(x, z) &= \frac{1}{x} (\delta\bar{\rho} - 3\delta\bar{P}) - \frac{\partial\delta\bar{\rho}}{\partial x}, \\ 2z^3 G_2(x, z) &= \frac{\partial\delta\bar{\rho}}{\partial z} \end{aligned} \quad (6.43)$$

represent the yet-to-be-specified corrections to the leading-order ideal gas thermodynamic contributions.

The Boltzmann equations kick in Eq. (6.41), via the time-derivative of the neutrino distribution function $d\bar{\rho}_\nu/dx$ which, we note in passing, is the only remaining total derivative. As explained in section 6.3, those Boltzmann equations govern the dynamics of the distribution functions that define bulk thermodynamic quantities, based on the interactions that the corresponding particles are subject to. For the sake of neutrinos, their collisional right hand sides are thus determined from the weakly interacting sector of the Standard Model of particle physics. Under general circumstances, the contributions from the Boltzmann equations cannot ever be neglected, unless interactions are insignificant or if they are argued at equilibrium at all times. This is for instance the case in the instantaneous decoupling limit, where neutrinos very promptly transit between neutrinos at equilibrium with the QED bath, to a QED-independent background of free-streaming neutrinos, and with $d\bar{\rho}_\nu/dx = 0$ at all times. In a realistic scenario, there is of course a transition regime where $d\bar{\rho}_\nu/dx$ is nonvanishing which ought to be accounted for in a precision theoretical prediction of N_{eff} and that requires numerical solutions of the generalised Boltzmann equations in the neutrino sector.

As a cross-check for the validity of this method, one can solve Eq. (6.41) for $d\bar{\rho}_\nu/dx = 0$ (instantaneous decoupling approximation (I)) and $G_1 = G_2 = 0$ (ideal gas approximation (II)) with the initial condition $z_{\text{ini}} = 1$ set at $x_{\text{ini}} = \lim_{T_d/m_e \rightarrow \infty} (m_e/T_d) = 0$ (neutrino-never-coupled approximation (III)). This

exercise yields

$$z_{\text{fin}} = \left(\frac{11}{4}\right)^{1/3} = z_{\text{fin}}^{(0)} \Big|_{x_{\text{ini}}=0}, \quad (6.44)$$

from which we infer the expected $N_{\text{eff}} = 3$ from the previous section. Dropping the aforementioned assumptions, we find the general formula for δN_{eff}

$$\delta N_{\text{eff}} = 3 \left[\left(\frac{z_{\text{fin}}^{(0)} \Big|_{x_{\text{ini}}=0}}{z_{\text{fin}}} \right)^4 - 1 \right]. \quad (6.45)$$

In the limit $d\bar{\rho}_\nu/dx = 0$, equation (6.45) has to precisely reproduce the same result as that of the entropy conservation estimate (6.37), under the same set of assumptions. In the next chapter, we shall go beyond the assumptions (II) and (III), discuss where corrections to them come from, and report the resulting changes to the standard value $N_{\text{eff}} = 3$. That said, let us now evaluate the neutrino decoupling temperature T_d from first principles of nonequilibrium quantum field theory, as we know from past considerations that it enters all theoretical computations of N_{eff} .

6.5 Estimate of the neutrino decoupling temperature T_d

As carefully explained around Eq. (6.16), the decoupling temperature is defined through $\Gamma_\nu(T_d) = H(T_d)$, where $\Gamma_\nu(T)$ is the neutrino weak interaction rate per neutrino with the QED thermal bath from which it decouples, and $H(T)$ is the Hubble expansion rate. The latter is given by Eq. (6.8) and since at the relevant temperatures for N_{eff} , the Universe is solely constituted by a QED bath and neutrinos, it reads

$$H(T)^2 = \frac{1}{3M_{\text{pl}}^2} [\rho(T) + \rho_\nu(T)] \quad (6.46)$$

where within (I), neutrinos always are at equilibrium and ρ_ν reads

$$\rho_\nu = 3 \cdot \frac{7}{8} \frac{\pi^2}{30} g_\nu T_\nu^4. \quad (6.47)$$

Now, just as in the scalar case discussed in section 4.3, it can be shown from first principles of real-time nonequilibrium field theory that the neutrino, or

fermionic in general, distribution functions follow a generalised Boltzmann equation [136, 137], which in absence of oscillations takes the form [33]

$$\frac{df_{\nu, \mathbf{p}}}{dt} = (1 - f_{\nu, \mathbf{p}})\Gamma_{\mathbf{p}}^< - f_{\nu, \mathbf{p}}\Gamma_{\mathbf{p}}^>, \quad (6.48)$$

where⁸

$$\Gamma_{\mathbf{p}}^{\gtrless} = \frac{\mp 1}{2p^0} \text{Tr}[\not{p}\Sigma^{\gtrless}(p)] \Big|_{p^0=\Omega_{\nu, \mathbf{p}}} \quad (6.49)$$

are the production (<; “gain”) and destruction (>; “loss”) terms, respectively, which are functionals of the relevant distribution functions that enter the finite-temperature neutrino Wightman self-energies Σ^{\gtrless} of opposite Schwinger-Keldysh polarities.^{9,10,11}

Note that Eq. (6.48) governs the dynamics of distribution functions, just as the Boltzmann equation (6.26) does and as a matter of fact, we show in Appendix E.1 that they indeed are strictly equivalent in the flat space limit. Eq. (6.48) encapsulates all relevant quantum field theoretical collision terms at all orders in the couplings, provided that perturbation theory can be applied and that bulk properties of the plasma change only adiabatically [33].

For temperatures above T_d , both the neutrino and QED sectors are at thermal equilibrium, hence Σ^{\gtrless} can be computed from equilibrium propagators, and they satisfy the fermionic Kubo-Martin-Schwinger (KMS) relation (1.102)

$$\Sigma^>(p) = -e^{\Omega_{\mathbf{p}}/T} \Sigma^<(p), \quad (6.50)$$

where $\Omega_{\nu, \mathbf{p}}$ is the effective frequency which determines the neutrino dispersion relation. As a result, the production and destruction rates (6.49) obey the detailed balance condition $\Gamma_{\mathbf{p}}^>/\Gamma_{\mathbf{p}}^< = e^{\beta\Omega_{\mathbf{p}}}$, and Eq. (6.48) can be written as

$$\frac{df_{\nu, \mathbf{p}}}{dt} = -\Gamma_{\mathbf{p}} [f_{\nu, \mathbf{p}} - f_D(\Omega_{\nu, \mathbf{p}})], \quad (6.51)$$

where we have defined a mode-dependent interaction rate,

$$\Gamma_{\mathbf{p}} = \Gamma_{\mathbf{p}}^> + \Gamma_{\mathbf{p}}^< = \frac{1}{2p^0 f_D(p^0)} \text{Tr} [\not{p}\Sigma^<(p)] \Big|_{p^0=\Omega_{\nu, \mathbf{p}}}. \quad (6.52)$$

⁸Here, the operator Tr performs the trace over the Dirac matrices.

⁹Note here that this is a flat space result, wherein there is no distinction between the usual spatial momentum and the physical one, and we temporarily went back to the notation of chapter 1, and denoted the full four-momentum $p = (p^0, \mathbf{p})^T$.

¹⁰The Wightman selfenergies are reviewed and presented in Sec. 1.1.9.

¹¹Note the difference in signs between this expression and its scalar counterpart (4.33) in section 4.3, which is due to the difference in signs between bosonic and fermionic KMS relations.

When put under this form, the differential equation (6.51) indicates that the rate at which the distribution function $f_{\nu, \mathbf{p}}$ is driven back to its equilibrium value is dictated by $\Gamma_{\mathbf{p}}$. Therefore, $\Gamma_{\mathbf{p}}$ is the interaction rate per neutrino Γ_{ν} to be equated to the Hubble rate to determine the decoupling temperature¹²

6.5.1 The neutrino–QED plasma interaction rate from Fermi theory

For the sake of neutrino decoupling from a QED plasma, only those weak interactions that connect neutrinos to the QED sector matter. These are

$$\begin{aligned}\nu_e \bar{\nu}_e &\rightarrow e^+ e^-, \\ \nu_e e^\pm &\rightarrow \nu_e e^\pm, \\ \bar{\nu}_e e^\pm &\rightarrow \bar{\nu}_e e^\pm,\end{aligned}\tag{6.54}$$

where we disregard those processes which involve a muon or tau neutrinos. We assumed that they are maintained in thermal equilibrium with the electron neutrinos via large-angle flavour oscillations and neutrino-neutrino scatterings, both of which typically remain efficient beyond T_d , see Ref. [138].

Having in mind the optical theorem and the associated cutting rules, see footnote 12, the relevant selfenergies are depicted in Fig. 6.1. Following SM Feynman rules [139] and integrating out the massive gauge bosons within the Fermi

¹² $\Gamma_{\mathbf{p}}$ can also be related to the spectral selfenergy and retarded selfenergy at the quasiparticle pole using Eqs. (1.71)(1.79), and we find the usual relation

$$\Gamma_{\mathbf{p}} = -\frac{1}{p^0} \text{ImTr} \left[\not{p} \Sigma^R(p) \right] \Big|_{p^0 = \Omega_{\nu, \mathbf{p}}}\tag{6.53}$$

which arises from nothing but the cutting rules and optical theorem at finite temperature, see Refs. [64, 67–69] and section 4.3 for a more refined discussion.

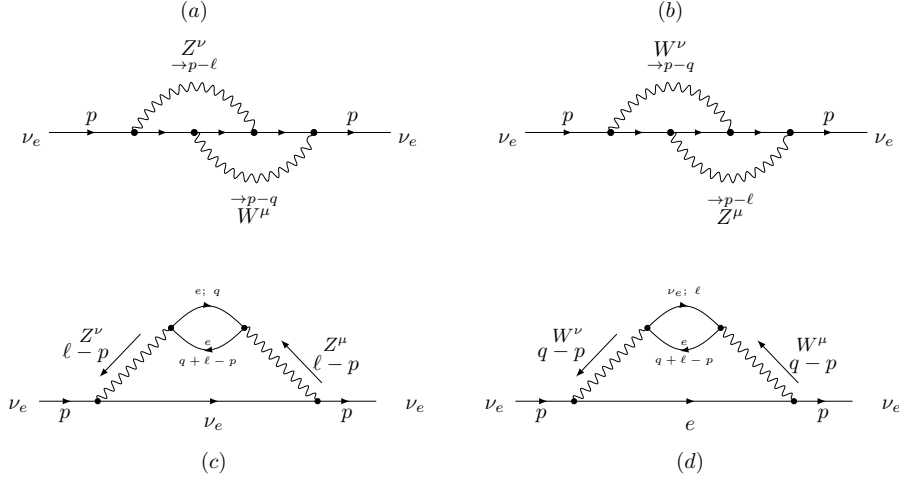


Figure 6.1: Leading-order weak selfenergy diagrams that contribute to the processes listed in (6.54). For notational simplicity we have not labelled every internal fermion line and momentum. The former can be deduced from the bosons connected to the vertices. Momentum is taken to flow in the same direction as the fermion number flow.

effective field theory, we find the associated real-time expressions

$$\begin{aligned} \text{Tr} \left[\not{p} \Sigma_{(a)}^{ba}(p) \right] &= -2 \left(\frac{G_F}{\sqrt{2}} \right)^2 \int \frac{d^4 \ell d^4 q}{(2\pi)^8} \text{Tr} \left[\not{p} \gamma^\mu (1 - \gamma_5) S_e^{ba}(q) \gamma^\nu \right. \\ &\quad \left. \times (g_{V,e} - g_{A,e} \gamma_5) S_e^{ab}(\ell + q - p) \gamma_\mu (1 - \gamma_5) S_\nu^{ba}(\ell) \gamma_\nu (1 - \gamma_5) \right], \end{aligned} \quad (6.55)$$

$$\begin{aligned} \text{Tr} \left[\not{p} \Sigma_{(b)}^{ba}(p) \right] &= -2 \left(\frac{G_F}{\sqrt{2}} \right)^2 \int \frac{d^4 \ell d^4 q}{(2\pi)^8} \text{Tr} \left[\not{p} \gamma^\mu (1 - \gamma_5) S_\nu^{ba}(\ell) \gamma^\nu (1 - \gamma_5) \right. \\ &\quad \left. \times S_e^{ab}(\ell + q - p) \gamma_\mu (g_{V,e} - g_{A,e} \gamma_5) S_e^{ba}(q) \gamma_\nu (1 - \gamma_5) \right], \end{aligned} \quad (6.56)$$

$$\begin{aligned} \text{Tr} \left[\not{p} \Sigma_{(c)}^{ba}(p) \right] &= 4 \left(\frac{G_F}{\sqrt{2}} \right)^2 \int \frac{d^4 \ell d^4 q}{(2\pi)^8} \text{Tr} \left[\not{p} \gamma^\mu (1 - \gamma_5) S_\nu^{ba}(\ell) \gamma^\nu (1 - \gamma_5) \right] \\ &\quad \times \text{Tr} \left[\gamma_\mu (g_{V,e} - g_{A,e} \gamma_5) S_e^{ba}(q) \gamma_\nu (g_{V,e} - g_{A,e} \gamma_5) S_e^{ab}(\ell + q - p) \right], \end{aligned} \quad (6.57)$$

$$\begin{aligned} \text{Tr} \left[\not{p} \Sigma_{(d)}^{ba}(p) \right] &= \left(\frac{G_F}{\sqrt{2}} \right)^2 \int \frac{d^4 \ell d^4 q}{(2\pi)^8} \text{Tr} \left[\not{p} \gamma^\mu (1 - \gamma_5) S_e^{ba}(q) \gamma^\nu (1 - \gamma_5) \right] \\ &\quad \times \text{Tr} \left[\gamma_\mu (1 - \gamma_5) S_\nu^{ba}(\ell) \gamma_\nu (1 - \gamma_5) S_e^{ab}(\ell + q - p) \right], \end{aligned} \quad (6.58)$$

where the superscripts $a, b = \pm$ are Schwinger-Keldysh contour labels, $g_{V,e} = -\frac{1}{4} + \sin^2 \theta_W$, $g_{A,e} = -\frac{1}{4}$, and $g'_{V,e} = g'_{A,e} = \frac{1}{4}$. The Schwinger-Keldysh fermionic propagators are carefully reviewed in section 1.1.10. The loop momenta were chosen so that the internal neutrino always has momentum ℓ and the electrons q and $\ell + q - p$, this will come in handy for the coming calculations. The total selfenergy is the sum of these four contributions.

We want to evaluate $\Sigma^<(p)$. This corresponds to setting the contour indices to $a = -$ and $b = +$, as $\Sigma^{+-}(p) = \Sigma^<(p)$, and only Wightman propagators $S_\psi^{+-} = S_\psi^{\leq}$, where $\psi = \nu_e, e$, contribute in Eqs. (6.55)-(6.58). These Wightman fermionic propagators can be related to the full spectral function in momentum space and the relations read (cf. Eq. (1.103), dropping the (eq) as everything is in equilibrium for the problem at hand anyway)

$$\begin{aligned} S_\psi^>(p) &= (1 - f_D(p^0)) \wp_\psi(p), \\ S_\psi^<(p) &= -f_D(p^0) \wp_\psi(p), \end{aligned} \quad (6.59)$$

where $\wp_\psi(p)$ is the spectral density. For the present calculation we use the leading-order spectral density detailed in section 1.1.10, and the spectral density of a free fermion of mass m_ψ reads

$$\wp_{\psi,0}(p) = (2\pi) \text{sgn}(p^0) (\not{p} + m_\psi) \delta(p^2 - m_\psi^2), \quad (6.60)$$

which has only one sharp peak at $p^2 = m_\psi^2$, at the vacuum particle mass shell. These delta functions put the internal fermion lines of the selfenergy diagrams on shell. The associated Wightman propagators also involve the delta functions and read

$$S_{\psi,0}^{\leq}(p) = -(f_D(|p^0|) - \theta(\mp p^0)) (2\pi) (\not{p} + m_\psi) \delta(p^2 - m_\psi^2), \quad (6.61)$$

where $\theta(p^0)$ denotes a Heaviside step function. Putting internal particles precisely on their mass shells through the delta functions effectively cuts through all internal fermion lines, as shown in Fig. 6.2 and the products of these cuts

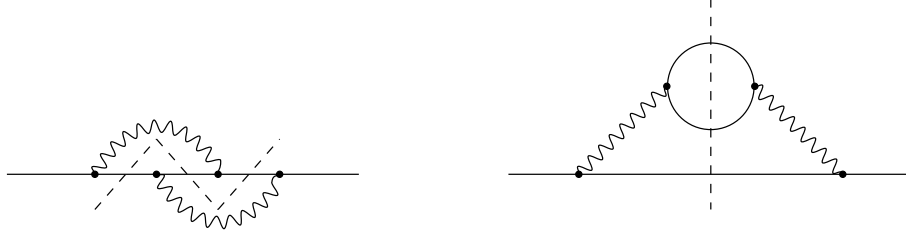


Figure 6.2: Finite temperature Cutkosky cuts of the self-energies.

are nothing but the $2 \rightarrow 2$ scattering processes of (6.54) and their complex conjugates, just as demands the optical theorem.

In other words, the scattering rate obtained here from first principles of nonequilibrium field theory is precisely that usually presented in textbooks [1], following the approach of kinetic theory and collisional integrals. In appendix E.1, we demonstrate in detail the correspondence between the two approaches at *leading-order*. The advantage of our first principles method over the usual $2 \rightarrow 2$ scattering approach is that it provides a more self-consistent and systematic tool to implement higher order corrections, e.g. relevant for precision computations of N_{eff} .

6.5.2 The neutrino decoupling temperature

Evaluating the selfenergy contributions (6.55) to (6.58) assuming a free fermion-spectral density (6.60) for both $\psi = \nu_e, e$, we find the interaction rate

$$\begin{aligned}
\Gamma_{\mathbf{p}}(T) &= \frac{(e^{|\mathbf{p}|/T} + 1)}{2|\mathbf{p}|} \sum_{i=a,b,c,d} \frac{\mathcal{C}_i G_F^2}{4(2\pi)^4} \int \int_0^\infty d|\mathbf{p}| d|\boldsymbol{\ell}| \frac{|\mathbf{p}|^2 |\boldsymbol{\ell}|}{E_q} \int_{-1}^{+1} d \cos \alpha \\
&\times \sum_{\epsilon, \tau = \pm 1} \left\{ \frac{\pi \theta(\tilde{b}^2 - 4\tilde{a}\tilde{c})}{\sqrt{|\tilde{a}|}} \left[f_D(|\ell^0|) - \theta(-\ell^0) \right] \left[f_D(|q^0|) - \theta(-q^0) \right] \right. \\
&\times \left. \left[f_D(|\ell^0 + q^0 - p^0|) - \theta(\ell^0 + q^0 - p^0) \right] \right. \\
&\times \left. \sum_{(mn)} A_{(mn)}^i \left[G_{(mn)}^0 + \frac{\tilde{b}}{2|\tilde{a}|} G_{(mn)}^1 + \left(\frac{3\tilde{b}^2 + 4\tilde{c}|\tilde{a}|}{8\tilde{a}^2} \right) G_{(mn)}^2 \right] \right\} \Bigg|_{\substack{q^0 = \epsilon \omega_{\mathbf{q}} \\ \ell^0 = \tau |\boldsymbol{\ell}|}}.
\end{aligned} \tag{6.62}$$

The definitions of the coefficients \mathcal{C}_i , $A_{(mn)}^i$, and $G_{(mn)}^i$ are gathered in Tables E.1 and E.2, and \tilde{a} , \tilde{b} , and \tilde{c} are ϵ - and τ -dependent functions of $|\mathbf{p}|$, $|\mathbf{q}|$, $|\boldsymbol{\ell}|$,

with $\cos \alpha$ given in Eqs. (E.30) to (E.32). We detail the full calculation of $\Gamma_{\mathbf{p}}(T)$ in appendix E.2.

To estimate the interaction rate per neutrino from the momentum-dependent $\Gamma_{\mathbf{p}}$ to the interaction rate per neutrino Γ_{ν} , we evaluate $\Gamma_{\mathbf{p}}$ at some representative mean momentum $\langle |\mathbf{p}| \rangle \simeq 3.15T$. Fig. 6.3 shows the interaction rate $\Gamma_{\nu}(T) = \Gamma_{\langle |\mathbf{p}| \rangle}$ as a function of T , together with the Hubble expansion rate $H(T)$ as a function of T as well, assuming the QED plasma to be an ideal gas. The neutrino decoupling temperature is obtained when the lines cross and solving $\Gamma_{\nu}(T_d) - H(T_d) = 0$ for T_d , we obtain

$$T_d = 1.3453 \text{ MeV}. \quad (6.63)$$

This neutrino decoupling temperature is consistent with the state-of-the-art findings of Ref. [140] to about 5%, the difference being attributed to their different definition of Γ_{ν} and approximations¹³ to estimate it. In this work, Γ_{ν} is the mode-dependent rate $\Gamma_{\mathbf{p}}$ evaluated at $|\mathbf{p}| = \langle |\mathbf{p}| \rangle \simeq 3.15T$, while in Ref. [140], they defined Γ_{ν} as the momentum-averaged destruction rate $\langle \Gamma_{\mathbf{p}}^{\nu} \rangle$.

Finite temperature QED corrections to the decoupling temperature.

Relevant for a precision computation of N_{eff} are corrections to this value of T_d , which is sensitive to higher-order corrections to the selfenergy diagrams of Fig. 6.1 and to the Hubble rate (6.46). The leading-order corrections relevant for N_{eff} are FTQED corrections to $\Gamma_{\mathbf{p}}$ and H .

On one hand, H gets modified through a QED-corrected equation of state which alters the total pressure and energy density and consequently H , cf. (6.46). We shall examine that in detail in section 7.3, and therefore do not repeat the analysis here. For the time being, we shall just plot the associated thermally (“th”) corrected H_{th} as a function of the temperature in Fig. 6.3.

On the other, we distinguish two types of FTQED corrections to the interaction rate $\Gamma_{\mathbf{p}}$ that describes $2 \rightarrow 2$ neutrino–electron scattering at leading order: (a) modification to the dispersion relation, and (b) vertex corrections. These are illustrated diagrammatically in Fig. 6.4.

Contributions of the type (a) amount to dressing the fermionic QED-charged propagator with a photon [141], which can be effectively implemented by replacing free propagators by partially resummed ones, wherein the (vacuum) particle

¹³The authors of Ref. [140] averaged out the final state Pauli blocking factors before performing the phase space integrals whereas we did not make any approximation to perform them. Therefore, our computations should be more realistic.

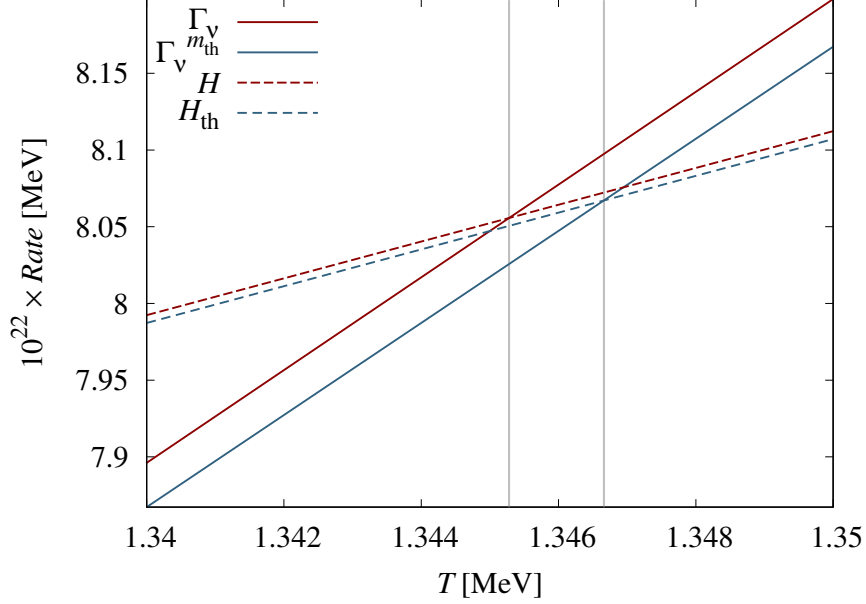


Figure 6.3: Interaction rate per neutrino with the QED plasma Γ_ν (solid lines) versus the Hubble expansion rate H (dashed lines) as functions of the temperature of the QED plasma T . Rates without FTQED corrections are indicated in red, while those with FTQED corrections are in blue.

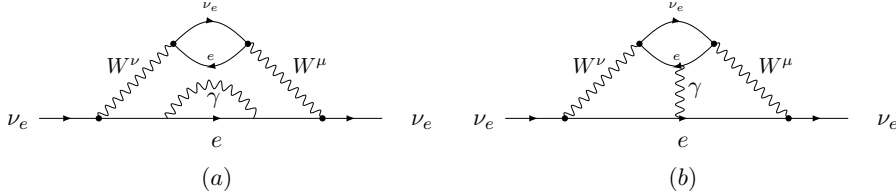


Figure 6.4: The only two qualitatively different finite-temperature QED corrections to the weak scattering rates, (a) dispersion relation modifications due to selfinteractions, and (b) vertex corrections due to photon exchanges.

mass is shifted to its thermal counterpart. For the problem at hand, this can be implemented by replacing all occurrences of m_e^2 in the mode-dependent interaction rate $\Gamma_{\mathbf{p}}$ by its thermal counterpart $m_e^2 + \delta m_{e,T}^2(p)$, where we take $\delta m_{e,T}^2(p)$ to be the $\mathcal{O}(e^2)$, one-loop selfenergy-induced mass given by [140, 142]

$$\delta m_{e,T}^2(p) = \frac{e^2 T^2}{6} + \frac{e^2}{\pi^2} \int_0^\infty d\tilde{p} \frac{\tilde{p}^2}{\omega_{\tilde{p}}} \tilde{f}_D - \frac{m_e^2 e^2}{2\pi^2 p} \int_0^\infty d\tilde{p} \frac{\tilde{p}}{\omega_{\tilde{p}}} \ln \left| \frac{p + \tilde{p}}{p - \tilde{p}} \right| \tilde{f}_D, \quad (6.64)$$

where $\tilde{f}_D = f_D(\omega_{\tilde{p}})$. This is particularly straightforward if we discard the momentum-dependent piece in $\delta m_{e,T}^2(p)$, which on average constitutes less than 10% of the total $\delta m_{e,T}^2(p)$. Indeed, in that case, the analytic reduction of all loop integrals in $\Gamma_{\mathbf{p}}$ proceeds identically as in the case with bare propagators.

Contributions of the type (b) can unfortunately not be dealt with similarly, they would require an explicit computation of each individual diagram involving a photon exchange, a very demanding task that we leave for future work.

Fig. 6.3 shows the thermal-mass-corrected interaction rate $\Gamma_\nu^{m_{\text{th}}}(T)$ as a function of the QED plasma temperature, together with the thermally-corrected Hubble expansion rate $H_{\text{th}}(T)$. Solving $\Gamma_\nu^{m_{\text{th}}}(T_d^{m_{\text{th}}}) - H_{\text{th}}(T_d^{m_{\text{th}}}) = 0$ for the thermal-mass-corrected neutrino decoupling temperature $T_d^{m_{\text{th}}}$, we find

$$T_d^{m_{\text{th}}} = 1.3467 \text{ MeV}, \quad (6.65)$$

that is a deviation of 0.1% from the uncorrected T_d , which is consistent with the findings of [140]¹⁴. Before moving to our precision computations of N_{eff} , we shall first review the past, current and future status of experimental measurements on N_{eff} , which will set an accuracy goal for our theoretical predictions for the deviations from $N_{\text{eff}} = 3$.

6.6 Measuring N_{eff} in the Standard Model: a quick overview

In this section, we briefly review the different measurements and experimental bounds obtained on the value of N_{eff} in the Standard Model today, and what will hopefully be achieved in the future.

6.6.1 Measuring N_{eff} : the state of the art

Past measurements. The number of light neutrino species in the Standard Model has been known to be 3 for a long time, e.g. from the LEP experiment

¹⁴Note that [140] always assumed ideal gases when evaluating $H(T)$. Their thermally-corrected neutrino decoupling temperature therefore corresponds to the intersection of the red dashed and blue solid lines in figure 6.3, which generally returns a higher value of T_d than the intersection of the two blue lines.

in the 90s [143] and more accurately since the precision measurement of the Z pole in 2012 [144]. Prior to that, cosmology alone was only able to put bounds from primordial big-bang nucleosynthesis (BBN) [145–148], i.e. from the formation of light elements. The main idea behind these bounds is the following. If neutrinos exist, they are abundantly produced in the early Universe, hence they contribute to its total energy density via Eq. (6.8) and speed up its expansion. Increasing the expansion of the Universe e.g. increases the abundance of Helium that is created during BBN, thus the more numerous the neutrinos, the more important the helium abundance. Therefore, measuring the amount of Helium in the early Universe puts bounds on the effective number of neutrinos in the cosmos. These serve as powerful independent bounds on N_{eff} that supplements the current best N_{eff} measurements, rely on less assumptions and overcome parameter degeneracies, as we shall comment on later in more detail.

Nowadays, measurements of N_{eff} are best obtained from the matter and CMB power spectrum, i.e. using combined data from BOSS [149] which measures the matter power spectrum, and Planck [77] or WMAP [78] missions which both measure the CMB power spectrum anisotropies. Therefore, in order to understand how N_{eff} is currently determined, we need to understand in detail how N_{eff} and neutrinos in general affect the matter and CMB power spectra.

CMB physics in a nutshell. At temperatures relevant for neutrino-CMB physics, four major events occur, neutrino decoupling, recombination, matter-radiation equality (EQ) and photon decoupling or photon last scattering surface (LSS). As the scale factor $a(t)$ grows, the Universe expands and the temperature T cools down. Neutrinos decouple first at around $T_d \simeq 1.35$ MeV during the radiation era. During the same epoch, the $e^\pm \rightarrow \gamma\gamma$ recombination occurs at around $T \simeq m_e = 0.511$ MeV. Then the Universe switches from the radiation-dominated era ($\rho_t \simeq \rho_r \propto a^{-4}$) to the matter-dominated one ($\rho_t \simeq \rho_m \propto a^{-3}$) at equality $\rho_r = \rho_m$, when $T_{\text{EQ}} \simeq 0.7$ eV [135], and eventually photons decouple at $T_{\text{LSS}} \simeq 0.26$ eV and free-stream in a curved background.

From recombination onwards, the cosmological fluid is essentially made of photons and baryons (matter), hence referred to as the photon-baryon (p-b) fluid. Neutrinos and cold dark matter have decoupled. Roughly speaking, the p-b fluid behaves according to two competing effects. The gravitational attraction developed by the baryons/matter, vs. the radiation pressure exerted by the photons which try and escape the baryonic gravitational pull. In the inhomogeneous overdense region seeded by inflation or alternatives, the pressure is higher than outside, and spherical outward-propagating sound waves escape these at the sound speed c_s , just as sound waves arise from pressure differences

in the air. The sound speed

$$c_s^2 = \frac{1}{3(1 + 3\rho_b/4\rho_\gamma)} \quad (6.66)$$

is much higher in the radiation than in the matter era, because most of the pressure and density is made of photons there. In the matter era, the sound speed eventually drops to zero, as $3\rho_b/4\rho_\gamma \rightarrow \infty$.

These acoustic oscillations in the plasma are nothing but p-b density waves that propagate to equilibrate the cosmological fluid and are precisely what give rise to CMB and matter fluctuations, also known as baryon acoustic oscillations (BAO). In practice the degrees of freedom of the perturbations are decomposed in spherical harmonics of certain amplitudes, wave numbers $k \sim 1/\lambda$ and multipoles ℓ . These quantities and their dynamics coupled to metric perturbations are what determine the CMB and matter power spectra. They are described by a set of coupled Boltzmann and Einstein equations derived in the framework of cosmological perturbation theory [1]. Solving and understanding these is of the greatest importance to understand the shape of the power spectra, but doing it in detail is very tedious. It involves a very complicated interplay between many gravitational, geometric, quantum and thermal effects that compete across a broad range of temperatures. It is even more complicated to try and isolate the effects of neutrinos alone [135, 150, 151]. However, since neutrinos are not coupled to the p-b fluid, they will only affect CMB physics through changes in the pre-recombination history, or changes in the (perturbed) Einstein/Friedmann equations, and these can be organised into *background* and *perturbation* effects. The former directly alter the evolution of the scale factor, and the latter directly impact the CMB anisotropies by modifications of the linearised Einstein equations for the metric perturbations, which in turn backreact on the p-b fluid fluctuations. *Background* effects are usually hard to associate to one species in particular. *Perturbation* effects, however, can be peculiar to a certain species.

Matter-radiation equality. The most significant (*background*) N_{eff} -induced effect on the CMB and matter power spectrum has to do with the matter-radiation equality. More precisely, it relates to the way acoustic waves propagate during the radiation and matter eras, and how N_{eff} has an effect on that. First, clearly the sound speed is different in these two epochs: it is $1/\sqrt{3}$ during the radiation era, while it continuously drops down to zero in the matter era. This affects the phase shifts and locations of the peaks in the CMB

power spectrum by modifications of the sound horizon¹⁵ at the last scattering surface [135, 150, 151]. Then, in the radiation era, fluctuations of wavelengths within the sound horizon oscillate and propagate with an almost constant amplitude. Super-sound-horizon modes barely propagate, they just stay frozen to their initial state. Metric perturbations and gravitational potential wells decay over time. In the matter era the p-b fluid starts coupling more and more to gravity keeping the same amount of total pressure: structure formation and clustering start. From equality to decoupling, matter density perturbations grow while radiative pressure waves escape less and their amplitudes lessen, they get gravitationally damped. Eventually, beyond the LSS, photons and their remaining perturbations free-stream in the perturbed metric background.

As a result of these two distinguished phases, the overall amplitude, phase shifts and peak locations of the CMB power spectrum crucially depends on the amount of time or temperature $\Delta T_{\text{EQ}}^{\text{LSS}} = T_{\text{EQ}} - T_{\text{LSS}}$ that the matter era lasts for, before photons eventually decouple and their fluctuations free-stream. Determining $\Delta T_{\text{EQ}}^{\text{LSS}}$ accurately requires the precise computations of matter-radiation equality and photon decoupling. The photon decoupling temperature is very well known from both theory and experiments [1], hence $\Delta T_{\text{EQ}}^{\text{LSS}}$ actually solely depends on the precise moment of the matter-radiation equality which itself is defined by $\rho_m|_{T_{\text{EQ}}} = \rho_r|_{T_{\text{EQ}}}$. Now since $T_{\text{EQ}} \ll m_e$, and using the definition of N_{eff} in Eq. (6.36), we find that

$$\rho_m|_{T_{\text{EQ}}} = \rho_r|_{T_{\text{EQ}}} = \rho_\gamma \left(1 + N_{\text{eff}} \frac{7}{8} \left(\frac{4}{11} \right)^{4/3} \right), \quad (6.67)$$

hence N_{eff} plays a major role in determining the matter-radiation instant. This is how N_{eff} primarily affects the CMB and matter power spectra, and hence structure formation [135, 150–153], i.e. via modifications of the matter-radiation Eq. (6.67). Striking consequences of varying N_{eff} and the time of matter-radiation equality are direct and significant changes in the location of the turnover point of the matter power spectrum [154], or in the CMB power spectrum amplitudes (this depends on the duration of the matter vs. radiation eras before decoupling), peak locations and phase shifts (these are directly related to the physical sound speed and horizon at LSS).

Silk damping. N_{eff} then affects the power spectra via a *perturbation* effect called Silk or diffusion damping [155]. It is the fact that random photon scatterings in the p-b fluid tend to erase fluctuations which wavelengths are below the

¹⁵The distance travelled by an acoustic wave front since some initial time deep in the radiation era. Provided that the initial is far enough in the past, the sound horizon is independent of its exact value.

photon mean free path. The more scattering events, the more these fluctuations are damped. Neutrinos scatter with electrons and photons, in particular before recombination, hence they contribute to Silk damping, and in particular, the higher N_{eff} and the more neutrino species, the more scatterings and the more Silk damping. As emphasised above, this mechanism is particularly effective before and around the time of recombination where interactions and scatterings between electrons and photons are kinematically highly favoured. This eventually results in a reduction of the photon power spectrum in its high multipole side [150, 151], in the so-called damping tail. The contributions of neutrinos there can very well be isolated [151], hence this constitutes a smoking-gun for the contributions of neutrinos to the CMB power spectrum.

Anisotropic stress. Collisionless neutrinos cannot be treated as a perfect fluid of vanishing anisotropic stress, simply because they have no interactions and collisions which over time kill the initial anisotropies, as e.g. Compton scatterings do for the p-b($-e^\pm$) fluid [1]. A careful analysis of the evolution of neutrino perturbations [150] shows that these neutrino anisotropic stresses produce a *perturbation* effect that reduces the amplitude and shift the peaks of the high- ℓ CMB anisotropy spectrum [156]. In particular, it affects the third peak most significantly. In standard Λ CDM cosmologies, there is no other species that releases such an anisotropic stress tensor¹⁶, this hence constitutes a direct probe of the neutrino sector through CMB measurements.

The free-streaming length, weak lensing and neutrino masses. Decoupled species, as e.g. neutrinos, free-stream and are characterised by their free-streaming length: $\lambda_{\text{fs}}(t) \sim c_\nu(t)/H(t)$, where $t_H = H^{-1}$ is the Hubble time. This determines what length scale in the p-b- ν perturbed equations are not influenced by the free-streaming neutrinos at a given time¹⁷. Wavelengths below $\lambda_{\text{fs}}(t)$ are effectively not influenced by the perturbations of free-streaming neutrinos. For instance, potential wells which widths exceed λ_{fs} will capture and interact neutrinos whereas these would just fly by thinner potential wells. The same goes for other perturbations. In practice, these effects of the free-streaming length are observed through weak lensing effects¹⁸. CMB measurements can distinguish the gravitational potential wells which were sensitive

¹⁶For instance, one may wonder about cold dark matter is a collisionless decoupled species too, but it is nonrelativistic matter and it hence generates no pressure whatsoever.

¹⁷A similar but better quantity to evaluate this is the integrated free-streaming horizon $h_{\text{fs}}(t)$ which tells which wavelengths scale never were affected by the free-streaming neutrinos.

¹⁸These geometric effects bend the geodesic of CMB photons towards the line of sight of an observer, simply because there is gravitating matter between the place where the photon was emitted and the position of the observer.

to neutrinos from the others through precision measurements of weak lensing effects in the angular distribution of the CMB power spectrum.

Since a species' free-streaming length depends on its mass, this also provides a way for precision cosmology to put bounds on the sum of the neutrino masses. If neutrinos are massless, their free-streaming speed is 1, hence $\lambda_{\text{fs}} \simeq H^{-1}$. If they are massive, their speed is lower and they become nonrelativistic when their masses exceed their average momentum $\langle p \rangle = 3.15T_\nu$. For sub-eV masses, as e.g. is the case for active left-handed neutrinos, this nonrelativistic transition happens in the matter dominated era and the neutrino free-streaming speed and Hubble rate take well-defined forms in terms of the matter energy density [1, 135]. This precisely determines which modes and potential wells are affected by neutrinos and which are not, and gives a way to probe the neutrino masses from their imprints on certain specific modes in the CMB spectrum of anisotropies.

Expansion rate modifications. Another way that neutrinos and N_{eff} can affect the evolution of perturbations is via modifications of the expansion rate. This can be achieved with both *background* or *perturbation* effects.

On one hand, they induce changes on the *background* scale factor itself, by modifying the expansion rate through the unperturbed Einstein equations. The neutrino energy density increases the expansion rate. This has an impact on the way both the p-b fluid and its fluctuations evolve. First, it further cools down the overall CMB temperatures via the integrated Sachs-Wolfe (ISW) effect [157]. The ISW effect is a geometric and gravitational effect on the CMB temperature due to the expansion of the Universe and time dilation on an observer of the CMB. Starting at LSS, and all along its geodesic or line of sight, a photon observed today was continuously redshifted by the expanding metric background in a time-dependent manner as the background changes over time according to Einstein's equations. In order to fully account for these cumulated effects, one must integrate the gravitational contributions of time dilation and temperature shifts all along the geodesic, from the last scattering surface, all the way to today. Second, increasing the background expansion rate also decreases the baryonic gravitational pull on the photon perturbations, because physical distances between gravitating objects is stretched quicker. In the same way, this affects any length scale defined with the integrated Hubble rate, as e.g. the sound horizon. These *background* effects can typically not be attributed to neutrinos alone and do not constitute a discriminating smoking-gun.

On the other, neutrinos can have a direct *perturbation* effect on the metric fluctuations (respecting the free-streaming length condition) which in turn back-reacts on the fluctuations of the p-b fluid via the equations of cosmological

perturbations. These can lead to all sorts of distortions, both cumulatively redshifting and blueshifting the final CM power spectrum.

N_{eff} and degeneracies. A problem with N_{eff} measurements from the CMB is its degeneracy with other cosmological parameters. First and foremost, it is degenerate with the matter energy density fraction $\omega_m = \omega_b + \omega_{dm}$ [128, 156]. This is because observations of CMB anisotropies, in particular the ratio of the first to the third acoustic peaks, only fixes the matter-to-radiation energy density, cf. Eq. (6.67). Then, N_{eff} is degenerate with the age of the Universe or the present-day Hubble rate H_0 [156, 158, 159], which is not ideal given the current H_0 tension in the community [160]. These were potential problems for WMAP [156], because they did not have access to precision measurements of higher N_{eff} -sensitive peaks in the CMB anisotropies¹⁹. However, it is argued that the peculiar anisotropic stresses and Silk damping effects left by neutrinos in the CMB anisotropies (cf. the previous paragraphs), as measured by WMAP [161, 162] or Planck [156] can already provide an independent handle on N_{eff} and overcome these degeneracies by WMAP or Planck [122] data alone. The anisotropic stress puts the lower bound, and the Silk damping the upper one. Moreover, the Atacama Cosmology Telescope (ACT) and South Pole Telescope (SPT) also provide independent measurements of N_{eff} [156] due to neutrino Silk damping in the high- ℓ spectrum [151].

Other N_{eff} degeneracies include the primordial Helium $Y_{\mathcal{P}}$ [151, 156] and the couplings and masses of WIMPs (weakly interacting massive particles) dark matter candidates. Again, independent measurements of BBN light abundances [163] and of WIMP properties [164] would break these degeneracies.

Because of these degeneracies, certain combinations of degenerate parameters are experimentally undistinguishable from a single data set and therefore isolating effects of N_{eff} alone on the CMB is very hard and one has to be careful when reading strong statements about the effect of N_{eff} on the power spectrum. One has to make sure what other parameters are being played with simultaneously. In this context, one physically interesting question that can be addressed easily is the following: *What happens if we vary N_{eff} but keep all other cosmological parameters constant?* The answer is that it increases the overall amplitude in the CMB peaks, slightly shift their locations and their phases, as can e.g. be seen in Fig. 5.3 of Ref. [135]. The explanation for that is fairly simple and rather illuminating. If all parameters are kept constant, then increasing N_{eff} primarily increases the radiative energy density. This has

¹⁹Unlike WMAP, Planck does have access to the N_{eff} -sensitive higher peaks and provides independent measurements of N_{eff} which break these degeneracies.

the the following effects. It increases the expansion rate via the Friedmann equations, delays matter-radiation equality and reduces gravitational effects in the entire history of the Universe, as explained above. As a result, it widens physical distances between gravitating objects, shortens the duration of the matter era before photon decoupling and thus the amplitude of CMB fluctuations are less damped and less trapped by gravity, they escape more. As a result, the amplitudes of the CMB anisotropies are bigger. Unfortunately, this is an effect that cannot be attributed to N_{eff} alone, precisely because of the above-mentioned $N_{\text{eff}} - \omega_m$ and $N_{\text{eff}} - H_0$ degeneracies. What really is an N_{eff} smoking-gun signature in the CMB is the phase shift in the third peak from the anisotropic stress release from the free-streaming neutrinos, and the Silk damping of neutrinos in the CMB damping tail.

These types of changes in the CMB and matter power spectra are precisely what experiments are after when doing cosmological parameter inference, and, from a very simplified perspective, this is how N_{eff} is determined from observing the CMB and matter power spectrum.

Most recent and precise measurement of N_{eff} in the standard model.

To this date, the most precise measurement of N_{eff} , considering it a free parameter in a standard Λ CDM cosmology, was performed by the data of both the CMB Planck [122] and the BAO BOSS [149] missions. They obtained

$$N_{\text{eff}} = 2.99^{+0.34}_{-0.33} \text{ (95\% C.I.)}, \quad (6.68)$$

that is $N_{\text{eff}} = 3$, plus decimal corrections. This value is obtained under the assumptions that we live in a Λ CDM cosmology coupled to the Standard Model of Particle Physics. Obviously BSM cases are worth investigating too, both theoretically and experimentally. We shall comment on them when discussing deviations from $N_{\text{eff}} = 3$ in the next chapter.

6.6.2 Measuring N_{eff} : the future

The most promising upcoming experiment that would improve on the precision at which N_{eff} is measured is the ground-based CMB-S4 mission [134,165] which construction should start in 2021. In short, the goals of this experiment is to perform measurements of the CMB power spectrum and anisotropies of unprecedented accuracy to put constraints on deviations of the thermal and gravitational history of the Universe as predicted from the Standard Model. Most relevant for this work is the expected precision they will achieve on N_{eff} , which in its most conservative version reaches $\sigma(N_{\text{eff}}) = 0.02 - 0.03$ [134,165],

that is, they will resolve percent level corrections. That said, it is timely to beat down the remaining theoretical uncertainties on N_{eff} to below the fourth significant digit, so that these are negligible in the error progression. These are precisely what we turn to next.

Chapter 7

Corrections to $N_{\text{eff}} = 3$

In the previous chapter, we discussed and studied in detail the standard value $N_{\text{eff}} = 3$, which we recall is a result of a standard-model computation, and of making the three assumptions: (I) the instantaneous decoupling approximation, (II) the ideal gas approximation and (III) the neutrino-never-coupled approximation, cf. section 6.4.1. Therefore we distinguish two types of corrections to $N_{\text{eff}} = 3$, beyond the Standard-Model (BSM) corrections, and deviations from dropping (I)-(III).

BSM corrections. Any BSM ingredient that modifies the radiative energy density, distorts the distribution functions of the relativistic plasma or changes the expansion history, be it at tree or loop level, will eventually alter N_{eff} via

$$\rho_{\text{rad}} = \rho_{\gamma} + \rho_{\nu} + (\text{BSM physics}) = \frac{\pi^2}{15} T^2 \left(1 + N_{\text{eff}} \frac{7}{8} \left(\frac{4}{11} \right)^{4/3} \right). \quad (7.1)$$

In the first section of this chapter, we discuss some BSM effects which impact N_{eff} and hence also comment on which are experimentally (dis)favoured if a change in N_{eff} were observed.

Deviations from (I)-(III). Any deviation from (I)-(III) leads to a change δN_{eff} in the effective number of cosmological neutrinos N_{eff} , which brings it away from its standard value 3. Eqs. (6.37) and (6.45) are our master formulae to compute δN_{eff} , when adopting (I) in the computations. In this chapter, we shall step by step drop (III) and (II). For both, the resulting δN_{eff} is computed

using Eqs. (6.37) and (6.45), however, we also provide the necessary ingredients to fully estimate from solving the Boltzmann equations. Indeed we know that once (I) is dropped, Eqs. (6.37) and (6.45) no longer hold. Therefore, simultaneously relaxing all three conditions and studying their interplay, which we ultimately ought to do to consistently predict N_{eff} , must be performed using the method explained in section 6.4.2, and the associated analytic G -functions are computed here. Eventually, we comment on the errors made on N_{eff} due to the uncertainties on the measured parameters that potentially feed into our computations.

7.1 BSM corrections: a theoretical and experimental overview

As argued in Eq. (7.1), N_{eff} can serve as a way of parametrising BSM effects in the thermal history of the Universe. Of course, the list of BSM effects that alter N_{eff} is infinite, because literally anything that modifies the expansion rate, modifies the radiative energy density, and distorts the equilibrium distribution functions will eventually alter it. Here, we list a few well-motivated and well-studied BSM particles and models that affect N_{eff} and comment on their viability based on current and future experimental bounds.

N_{eff} and neutrino masses and oscillations. The most obvious and well-established BSM ingredient that corrects N_{eff} is the effect of neutrino masses and oscillations, which is not part of the SM strictly speaking. In fact, accounting for neutrino masses and oscillations in the transport equations that determine N_{eff} is a well-established field [123–128] and these corrections can lower N_{eff} by as much as $\delta N_{\text{eff}}^{\text{osc}} \simeq -0004$ [127] or in the fifth significant digit [166].

N_{eff} and right-handed neutrinos. In order to explain the tiny masses and oscillations of the active left-handed neutrinos, probably the most natural and popular explanation is that they come accompanied by one or several sterile right-handed counterparts, which explain the light active neutrino masses via a seesaw mechanism [167–171], and see e.g. [156, 172–174] and references therein for detailed theoretical, phenomenological and experimental reviews and introductions on right-handed neutrinos. Their mixing with active neutrinos augment N_{eff} and as such, they can be constrained by cosmological data and must be consistent with them.

The original high-scale seesaw mechanism [167–171] proposed very heavy Majorana right-handed neutrinos with masses well above the electroweak scale (~ 200 GeV), just below the Grand Unified Theories (GUT) scale (10^{16} GeV). These can explain the baryon asymmetry in the Universe (BAU) through thermal leptogenesis and CP-violating decays of the right-handed neutrinos [175]. These very heavy particles are not present in the Universe at all times relevant for N_{eff} and CMB physics, and hence do not affect them at all. This makes them experimentally inaccessible from cosmology.

Then, low-scale seesaw models were proposed wherein right-handed neutrinos have masses below the TeV scale. These are particularly interesting because they can realise leptogenesis (via CP-violating decays and/or resonant oscillations) [176–179], and their properties can be probed at laboratory experiments, see e.g. [180] for a summary of bounds. Sub-GeV masses are parametrically allowed and these would eventually affect N_{eff} slightly [181–185], through nonequilibrium distortions and entropy injections during, before and after BBN as follows.

The production rate and lifetime of the heavy neutrinos are both proportional to the square of their mixing angles with ordinary neutrinos. The lifetime is proportional to the fifth power of their mass. This implies that seesaw right-handed neutrinos with masses below 100 MeV are ruled out by a combination of neutrino oscillation data, direct searches, BBN and N_{eff} [182]. For mixing angles that are large enough to explain the masses of the heavier two SM neutrinos, such sterile neutrinos necessarily come into equilibrium in the early universe. Upper bounds on their mixing angles obtained from experiments then imply that their lifetime is long enough to either disturb BBN or affect the primordial plasma after BBN in a way that is visible in the light element abundances and/or N_{eff} . Assuming a standard cosmological history, the only ways to avoid this is to either give the right-handed neutrinos a very tiny mixing angle (in which case they cannot explain the SM neutrino masses alone) or to suppress their production in the primordial plasma with new interactions. In the keV mass range, right-handed neutrinos with tiny mixings give rise to stable long-lived right-handed neutrinos which constitute viable dark matter candidates [186]. These contribute as relativistic particles to N_{eff} around BBN and neutrino decoupling, and act as matter at times relevant for CMB physics. However, their number densities at BBN and neutrino decoupling are so low that their effect on N_{eff} falls within current bounds on N_{eff} , see e.g. [187] for a review.

Eventually, even lighter eV-mass right-handed neutrinos are highly constrained by N_{eff} . If they are in equilibrium around BBN and neutrino decoupling, they

are simply ruled out by Planck data [156], because they would increase the amount of hot dark matter by too much [188, 189], and more importantly any extra relativistic species at that time contributes $\delta N_{\text{eff}} = 1$. Therefore, extra interactions must bring them out of equilibrium and/or highly depopulate their number densities at the relevant temperatures. Low-mass right-handed neutrinos are actually motivated by the excess signal for $\bar{\nu}_\mu \rightarrow \bar{\nu}_e$ and $\nu_\mu \rightarrow \nu_e$ flavor conversions, respectively in the LSND [190] and more recently MiniBooNE experiments [191]. If interpreted by flavor oscillations through sterile states, these anomalies (and others, see e.g. sections 3.1, 4.2 and 4.3 in [173]) could indeed be explained by low-mass right-handed neutrinos [173, 174, 192]. However, these require large mixing angles that would bring the sterile neutrinos in thermal equilibrium early in the Universe, hence causing the above-mentioned tensions with precision cosmology. These can precisely be resolved if the sterile neutrinos have non-standard interactions [193], or if cosmology itself is modified by e.g. additional radiation [188, 189]. The experimental neutrino research program DUNE [194] initially designed to measure CP violation in the neutrino mixing matrix is sensitive to these non-standard interactions of right-handed neutrinos and hence can potentially probe them.

N_{eff} and other additional light species. As emphasised above, additional light particles increase the radiation energy density, and hence they increase N_{eff} and the authors of [195] carefully study the possibility that the Planck mission [122] probes or rules out the associated deviations in N_{eff} . As argued there, only thermal light particles which decouple at $T \lesssim 200$ MeV are within the reach of the Planck mission, cf. Fig. 3 in [195], hence [195] focuses on these species which have been in equilibrium with the SM through the QCD phase transition ($T \simeq 200$ MeV), see e.g. [196]. Prior to that, the quarks constitute most of the relativistic degrees of freedom in the Universe, hence bringing N_{eff} to a much larger value that is insensitive to small changes. The results of [195] are summarised in table 1 therein, and we shall briefly review them throughout the next paragraphs.

N_{eff} and axion-like particles. Light spin 0 Goldstone bosons that are in equilibrium with the SM through the QCD phase transition, e.g. axion-like particles (ALPs) which were also studied in Ref. [197], are highly constrained by non-observation bounds obtained from star and supernovae cooling [198–200]. Indeed, if they existed, these ALPs would be produced in star cores and interact weakly enough to actually escape them, hence we should see them. As a consequence of these astrophysical bounds, their effects on the CMB either fall well below Planck sensitivity [195, 197], or their couplings to muons and

taus are fine-tuned and much stronger than their couplings to any other SM fields. In that case, they can lead to a change in N_{eff} of as much as $\Delta N_{\text{eff}} = 0.2\text{--}0.6$ [195, 197].

N_{eff} and dark photons. Massless spin 1 gauge bosons A'_μ are consistent with Planck, because their long-range forces/couplings to SM fermions are greatly restricted to be too weak to significantly alter N_{eff} [201]. Typically, only tiny kinetic mixings $\mathcal{L} \supset -\epsilon F'_{\mu\nu} F^{\mu\nu}$ between the new and SM gauge bosons are allowed, as e.g. is the case for a dark photon [202], and corrections to N_{eff} arise from a new fermionic content, say χ , a potential dark matter candidate, see [203] and references therein. For a massless dark photon, the parameters of these models are constrained by Planck and astrophysical data [195], and must comply to $\epsilon < 10^{-8}$ and $10 \text{ MeV} < m_\chi < 150 \text{ MeV}$. Lower m_χ are restricted from astrophysics and higher masses cause the dark photon to decouple before the QCD phase transition, hence bringing it below Planck's sensitivity.

Higher MeV masses of freeze-in dark photons have been studied in [202]. These do not couple to neutrinos directly and only heat up the $e^\pm\text{-}\gamma$ fluid after neutrino decoupling, hence reducing N_{eff} cf. Eq. (6.36). Planck already constrains their masses to $m_{A'} > 8.5 \text{ MeV}$ and their kinetic mixings to SM gauge bosons to below $\epsilon \lesssim 10^{-9.5}$. The maximal induced change in N_{eff} reads $\delta N_{\text{eff}}^{d\gamma} \simeq -0.3$ and decreases with the dark photon mass, cf. Fig. 3 in [202]. The CMB S-4 experiment [134] is expected to increase the sensitivity to dark photon masses to 17 MeV [202], cf. Fig. 3 in [202].

N_{eff} and modified theories of gravity. Massless higher spins usually summoned in modified theories of gravity, as e.g. the gravitino (3/2) in supergravity [204] and gravitons (2). Both decouple at very high temperatures. The effects of massive gravitinos on N_{eff} are studied in [205] wherein constraints on N_{eff} put bounds on the gravitino-to-photons decays (which lower N_{eff}) rates. According to [195], current (Planck) and near-future (CMB-S4) CMB experiments will not resolve the induced changes in N_{eff} . Eventually, it has recently been suggested in [159] that scalar-tensor theories help reduce the H_0 tension [160] and lead to smaller values of N_{eff} down to $N_{\text{eff}} = 2.8$. These are experimentally disfavoured.

N_{eff} and thermal freeze-out dark matter. Weakly Interacting Massive Particles (WIMPs) are well-motivated dark matter candidates [206] which generically decouple from the cosmological plasma at $T \sim m_{\text{WIMP}}/20 \text{ MeV}$, i.e. they are nonrelativistic. Therefore, as soon as $m_{\text{WIMP}} \lesssim 20 \text{ MeV}$, they contribute

to neutrino decoupling and alter N_{eff} and their impact was studied in [128,207]. Using CMB and BBN constraints on N_{eff} , they show that $m_{\text{WIMP}} \gtrsim 3.7$ MeV and future CMB missions will improve the bounds up to $m_{\text{WIMP}} \gtrsim 10 - 15$ MeV.

Having covered a wide range of BSM effects that could potentially impact N_{eff} , let study the deviations from N_{eff} that come from dropping (I)-(III) within the Standard Model alone, bearing in mind that we have a four significant digit accuracy goal.

7.2 The neutrino-never-coupled (NNC) approximation

The ‘‘neutrino-never-coupled’’ (NNC) assumption (III) approximates $T_d/m_e \rightarrow \infty$. This approximation is very rough since neutrino decoupling is expected to occur around $T_d \sim 1$ MeV and $m_e = 0.511$ MeV. As a result, the deviation δs^{NNC} from dropping this assumption is the most significant source of changes in N_{eff} studied in this work.

As explained previously, a finite T_d/m_e enters the standard estimate of N_{eff} by changing the QED entropy density at the time of neutrino decoupling by the amount (cf. Eqs. (1.10)(6.15))

$$\delta s^{\text{NNC}} = \frac{g_e}{2\pi^2 T_d} \int_0^\infty dp p^2 \left(\omega_e + \frac{p^2}{3\omega_e} \right) f_D(\omega_e) \Big|_{T_d/m_e \rightarrow \infty}^{T_d/m_e}, \quad (7.2)$$

where we recall $f_D(\omega) = [\exp(\omega/T) + 1]^{-1}$ is the Fermi–Dirac distribution, $\omega_e^2 = p^2 + m_e^2$ is the electron energy, and p is the physical momentum which scales as $p \propto a^{-1}$. It is straightforward to evaluate (7.2) numerically for any neutrino decoupling temperature T_d . With our estimate $T_d = 1.3453$ MeV from Sec. 6.5, we find $\delta s^{\text{NNC}}/s^{(0)}|_{T_d/m_e \rightarrow \infty} \simeq -0.009859$. Plugging it in Eq. (6.37) gives the correction to N_{eff}

$$\delta N_{\text{eff}}^{\text{NNC}} \simeq 0.039895 \quad (7.3)$$

from dropping the NNC approximation (III). Figure 7.1 depicts $\delta N_{\text{eff}}^{\text{NNC}}$ versus the neutrino decoupling temperature T_d .

In terms of the continuity equation (6.40) and the method of Sec. 6.4.2, dropping (III) corresponds to not having $x_{\text{ini}} \equiv m_e/T_d = 0$ anymore, but still keeping $G_1 = G_2 = 0$ and $d\bar{\rho}_\nu/dx = 0$ as those arise from relaxing (II) and (I).

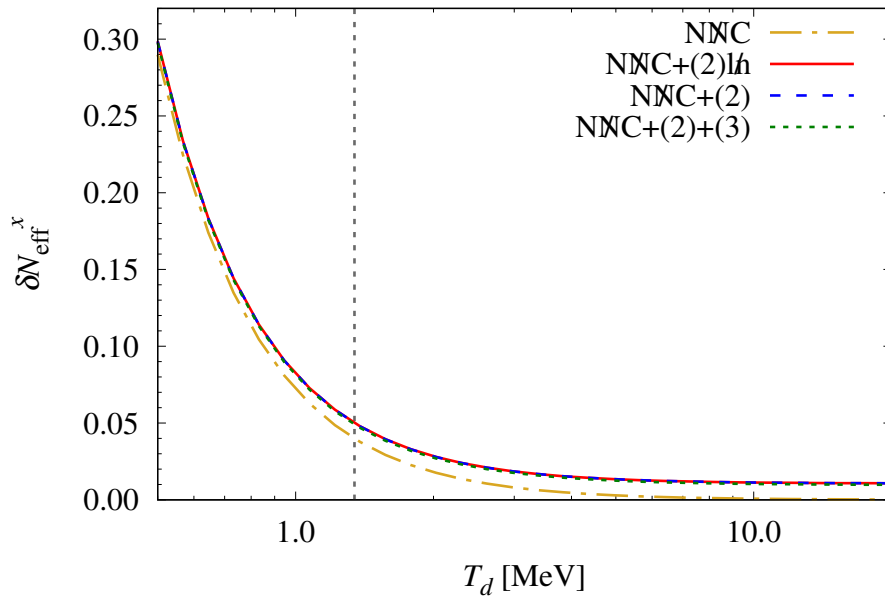


Figure 7.1: Corrections to $N_{\text{eff}} = 3$ due to relaxing various assumptions, as a function of the neutrino decoupling temperature T_d . The gold/dot-dash line denotes dropping the neutrino-never-coupled approximation ($x = \text{NNC}$), the red/solid line includes in addition the log-independent $\mathcal{O}(e^2)$ FTQED correction to the QED equation of state ($x = \text{NNC} + (2)\ln$), the blue/dashed line includes the full $\mathcal{O}(e^2)$ FTQED correction ($x = \text{NNC} + (2)$), and the green/dotted line contains FTQED corrections up to and including $\mathcal{O}(e^3)$ ($x = \text{NNC} + (2) + (3)$). The vertical grey/dotted line marks $T_d = 1.3453$ MeV.

7.3 Finite-temperature corrections to the QED equation of state

Finite temperature field theory enters a theoretical computation of N_{eff} in many different instances, including the QED equation of state, the neutrino interaction rate and collision integrals, etc. We here focus on finite-temperature corrections to the QED equation of state which is expected to be the correction that dominates δN_{eff} next. In this section, we investigate the departure from the ideal gas behaviour which originates from the interactions amongst its constituents, and relax (II) in the QED sector .

These corrections have been widely considered in the literature, see e.g. [130–132,208], wherein the deviations from the ideal gas picture had been unfailingly attributed to the acquisition of thermal masses by the QED particles. While this interpretation is correct to some degree, it has led to misinterpretations when it comes to computations of thermodynamic bulk quantities [209].

As we know very well from section 1.1 (more precisely sections 1.1.7 and 1.1.8), a more fool-proof calculation starts with the partition function Z for QED at finite temperature, for which a systematic expansion of $\ln Z$ in powers of the QED coupling constant e (i.e., the elementary electric charge) can be consistently formulated in the framework of real-time equilibrium field theory as

$$\ln Z = \ln Z^{(0)} + \ln Z^{(2)} + \ln Z^{(3)} + \dots \quad (7.4)$$

where $\ln Z^{(n)} \propto e^n$. This expansion is well established up to $n = 3$ for non-vanishing electron mass m_e and chemical potential μ [22] and to $n = 5$ in the limit where $m_e = \mu = 0$ [210,211]. At each order n in the power expansion, standard thermodynamics relations (1.8)-(1.10) hold and are used to go from $\ln Z^{(n)}$ to the corresponding pressure $P^{(n)}$, energy density $\rho^{(n)}$, and entropy density $s^{(n)}$

$$P^{(n)} = \frac{T}{V} \ln Z^{(n)}, \quad (7.5)$$

$$\rho^{(n)} = \frac{T^2}{V} \frac{\partial \ln Z^{(n)}}{\partial T} = -P^{(n)} + T \frac{\partial P^{(n)}}{\partial T}, \quad (7.6)$$

$$s^{(n)} = \frac{1}{V} \frac{\partial [T \ln Z^{(n)}]}{\partial T} = \frac{\rho^{(n)} + P^{(n)}}{T}, \quad (7.7)$$

where T and V are the temperature and volume of the system respectively. At zeroth order, the QED pressure and energy density are

$$P^{(0)} = \frac{T}{\pi^2} \int_0^\infty dp p^2 \ln \left[\frac{(1 + e^{-\omega_e/T})^2}{(1 - e^{-\omega_\gamma/T})} \right], \quad (7.8)$$

$$\rho^{(0)} = \frac{1}{\pi^2} \int_0^\infty dp p^2 \left[\frac{2\omega_e}{e^{\omega_e/T} + 1} + \frac{\omega_\gamma}{e^{\omega_\gamma/T} - 1} \right], \quad (7.9)$$

cf. Eqs. (6.15), which describe nothing but an ideal gas of photons and electrons/positrons, with $\omega_\gamma = p$ and $\omega_e^2 = p^2 + m_e^2$.

7.3.1 $\mathcal{O}(e^2)$ FTQED

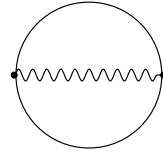
$$\ln Z^{(2)} = -\frac{1}{2} \left(\text{Diagram} \right)$$


Figure 7.2: The $\mathcal{O}(e^2)$ correction to the partition function $\ln Z$.

The lowest order correction to the QED partition function comes at order $\mathcal{O}(e^2)$ and is diagrammatically given by the two-loop diagram depicted in Fig. 7.2. Its contribution to the partition function is well-known and the corresponding $\ln Z^{(2)}$ is e.g. given in Eq.(5.58) of Ref. [22]. For an isotropic and CP -symmetric medium such as that under consideration, the chemical potentials vanish, the angular integral can be performed and the expression simplifies to

$$P^{(2)} = \frac{T}{V} \ln Z^{(2)} = -\frac{e^2 T^2}{12\pi^2} \int_0^\infty dp \frac{p^2}{\omega_p} n_D - \frac{e^2}{8\pi^4} \left(\int_0^\infty dp \frac{p^2}{\omega_p} n_D \right)^2 + \frac{e^2 m_e^2}{16\pi^4} \int_0^\infty dp \int_0^\infty d\tilde{p} \frac{p\tilde{p}}{\omega_p \omega_{\tilde{p}}} \ln \left| \frac{p + \tilde{p}}{p - \tilde{p}} \right| n_D \tilde{n}_D, \quad (7.10)$$

where we have introduced $n_D = 2f_D(\omega_p)$, and $\tilde{n}_D = 2f_D(\omega_{\tilde{p}})$. Under (III), i.e. $T/m_e \rightarrow \infty$, Eq. (7.10) evaluates to $P^{(2)} = -5e^2 T^4/288$.

Putting Ref. [208] aside, state-of-the-art theory predictions of N_{eff} have only implemented the first two, “log-independent” terms of Eq. (7.10), following Ref. [132], itself based on Ref. [130]. The “log-dependent” term is usually disregarded, due to it being shown too insignificant to warrant a detailed investigation on its contribution to N_{eff} , see e.g. Ref. [131, 132]. We study both in what follows.

Log-independent contribution (lh). Solely considering the first two “log-independent” terms of equation (7.10), we find the energy and entropy density corrections

$$\rho^{(2)\text{lh}} = -\frac{e^2 T^2}{12\pi^2} \int_0^\infty dp \frac{p^2}{\omega_p} (n_D + T \partial_T n_D) + \frac{e^2}{8\pi^4} \left(\int_0^\infty dp \frac{p^2}{\omega_p} n_D \right)^2 - \frac{e^2}{4\pi^4} \left(\int_0^\infty dp \frac{p^2}{\omega_p} n_D \right) \left(\int_0^\infty dp \frac{p^2}{\omega_p} T \partial_T n_D \right), \quad (7.11)$$

$$s^{(2)\text{lh}} = -\frac{e^2 T}{12\pi^2} \int_0^\infty dp \frac{p^2}{\omega_p} (2n_D + T \partial_T n_D) - \frac{e^2}{4\pi^4} \left(\int_0^\infty dp \frac{p^2}{\omega_p} n_D \right) \left(\int_0^\infty dp \frac{p^2}{\omega_p} \partial_T n_D \right). \quad (7.12)$$

In general, those need to be evaluated numerically. In the limit where $T/m_e \rightarrow \infty$, they analytically evaluate to $\rho^{(2)\text{lh}} = -5e^2 T^4/96$ and $s^{(2)\text{lh}} = -5e^2 T^3/72$, respectively.

Let us now compute the associated δN_{eff} from entropy conservation arguments, and first read off the δs of Eq. (6.37) with the definition

$$\delta s = \delta s^{\text{N}\ddot{\text{N}}\text{C}} + s^{(2)\text{lh}} \Big|_{T=T_d}, \quad (7.13)$$

where $\delta s^{\text{N}\ddot{\text{N}}\text{C}}$ is the change in the QED entropy density at $T = T_d$ from dropping (III), which is given in Eq. (7.2). Evaluating δs from our estimated $T_d = 1.3453$ MeV, we obtain $\delta s / s^{(0)} \Big|_{T_d/m_e \rightarrow \infty} \simeq -0.012324$, and hence

$$\delta N_{\text{eff}}^{\text{N}\ddot{\text{N}}\text{C}+(2)\text{lh}} \simeq 0.050015, \quad (7.14)$$

where the fine structure constant value is $\alpha = e^2/4\pi = 1/137$. Subtracting the correction (7.3) from (7.14) due to dropping (III), we find a net $\mathcal{O}(e^2)$ log-independent FTQED correction of the following significant magnitude

$$\delta N_{\text{eff}}^{(2)\text{lh}} = \delta N_{\text{eff}}^{\text{N}\ddot{\text{N}}\text{C}+(2)\text{lh}} - \delta N_{\text{eff}}^{\text{N}\ddot{\text{N}}\text{C}} \simeq 0.010121 \quad (7.15)$$

for $T_d = 1.3453$ MeV, which ought to be compared with the often-quoted $\delta N_{\text{eff}}^{(2)\text{lh}} \simeq 0.010594$ from Ref. [131] calculated from the same FTQED correction but within (III). Fig. 7.1 displays $\delta N_{\text{eff}}^{\text{N}\ddot{\text{N}}\text{C}+(2)\text{lh}}$ for a range of neutrino decoupling temperatures and Fig. 7.3 shows the correction $\delta N_{\text{eff}}^{(2)\text{lh}}$ alone (i.e., with the N $\ddot{\text{N}}$ C contribution deduced from $\delta N_{\text{eff}}^{\text{N}\ddot{\text{N}}\text{C}+(2)\text{lh}}$).

Then, keeping in mind that we should eventually drop (I) for which entropy conservation arguments cannot be applied, we read off $\delta \bar{\rho} = \rho^{(2)\text{lh}} \times (x/m_e)^4$

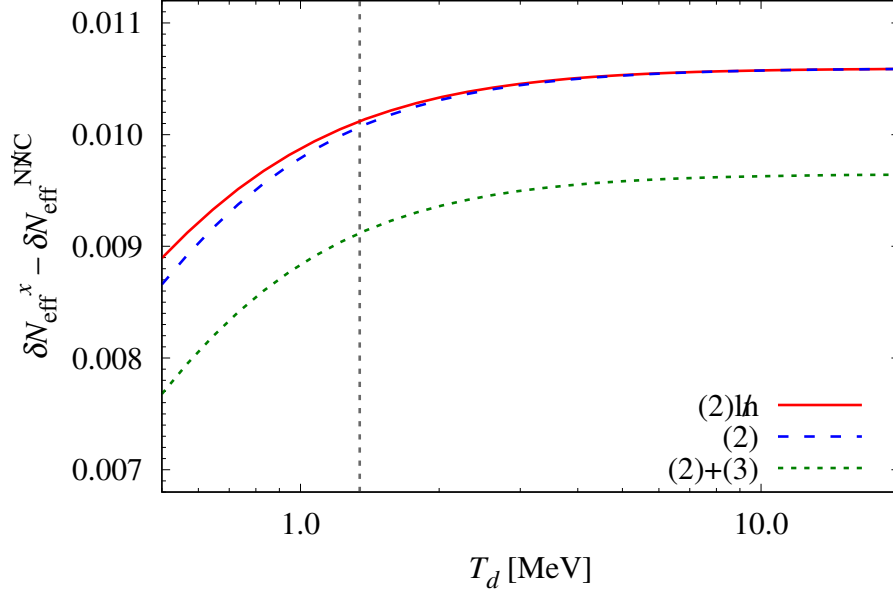


Figure 7.3: Effective corrections to $N_{\text{eff}} = 3$ due to FTQED effects on the QED equation of state alone (i.e., with the $N\cancel{C}$ contribution subtracted), as a function of the neutrino decoupling temperature T_d . The red/solid line denotes the log-independent $\mathcal{O}(e^2)$ contribution ($x = N\cancel{C} + (2)\ln$), the blue/dashed line the full $\mathcal{O}(e^2)$ correction ($x = N\cancel{C} + (2)$), and the green/dotted line includes corrections up to and including $\mathcal{O}(e^3)$ ($x = N\cancel{C} + (2) + (3)$). The vertical grey/dotted line marks $T_d = 1.3453$ MeV.

and $\delta\bar{P} = P^{(2)\ln} \times (x/m_e)^4$ from our corresponding log-independent terms and Eq. (6.43) gives the associated $G_1(x/z)$ and $G_2(x/z)$ functions for the

continuity equation (6.40)

$$G_1^{(2)\text{lh}}(\tau) = \frac{e^2}{2} \left[\frac{1}{\tau} \left(\frac{K(\tau)}{3} + 2K(\tau)^2 - \frac{J(\tau)}{6} - J(\tau)K(\tau) \right) + \frac{K'(\tau)}{6} - K(\tau)K'(\tau) + \frac{J'(\tau)}{6} + J'(\tau)K(\tau) + J(\tau)K'(\tau) \right], \quad (7.16)$$

$$G_2^{(2)\text{lh}}(\tau) = \frac{e^2}{2} \left[2J(\tau)K(\tau) - J(\tau)^2 - \frac{(K(\tau) + J(\tau))}{3} + \left(\tau J'(\tau) + \frac{1}{\tau} Y'(\tau) \right) \left(K(\tau) + \frac{1}{6} \right) \right], \quad (7.17)$$

where $(\dots)' = \partial_\tau(\dots)$, and the newly defined function $K(\tau)$ reads

$$K(\tau) = \frac{1}{\pi^2} \int_0^\infty d\omega \frac{\omega^2}{\sqrt{\omega^2 + \tau^2}} \frac{1}{\exp\{(\sqrt{\omega^2 + \tau^2})\} + 1}, \quad (7.18)$$

while $J(\tau)$ and $Y(\tau)$ are given in Eq. (6.42).

Observe that (7.16) is strictly identical to Eq.(18) of Ref. [132]. Our expression for $G_2^{(2)\text{lh}}$, on the other hand, is analytically different from the result reported in Eq.(19) of Ref. [132], but numerically equivalent to within machine precision for a range of τ values. With the exception of Ref. [208], all recent precision calculations of N_{eff} , see e.g. [127, 133, 166, 212] implement FTQED effects on the QED equation of state by solving the continuity equation (6.40) modified with Eqs. (7.16)(7.17) (or their numerically equivalent counterparts presented in Ref. [132])¹.

Logarithmic contribution (ln). The energy and entropy density corrections corresponding to the third, log-dependent term of Eq. (7.10) read

$$\rho^{(2)\text{ln}} = \frac{e^2 m_e^2}{16\pi^4} \iint_0^\infty dp \, d\tilde{p} \frac{p\tilde{p}}{\omega_p \omega_{\tilde{p}}} \ln \left| \frac{p + \tilde{p}}{p - \tilde{p}} \right| n_D (2T \partial_T \tilde{n}_D - \tilde{n}_D), \quad (7.19)$$

$$s^{(2)\text{ln}} = \frac{e^2 m_e^2}{8\pi^4} \iint_0^\infty dp \, d\tilde{p} \frac{p\tilde{p}}{\omega_p \omega_{\tilde{p}}} \ln \left| \frac{p + \tilde{p}}{p - \tilde{p}} \right| n_D \partial_T \tilde{n}_D, \quad (7.20)$$

both of which vanish in the limit $T/m_e \rightarrow \infty$. It is usually argued that even at a finite T/m_e , the significance of these terms amounts to less than 10% of the

¹The often-quoted $\delta N_{\text{eff}}^{(2)\text{lh}} \simeq 0.010594$ corresponds to $z_{\text{fin}} \simeq 1.39979$ through Eq. (6.45), and can be obtained from a numerical solution of the continuity equation (6.40) with the initial conditions set at $x_{\text{ini}} = 0$. The number cited in Ref. [132, 166], i.e. $z_{\text{fin}} = 1.39975$, corresponds to setting the initial conditions at $x_{\text{ini}} = 0.0341$, or, equivalently, $T_d = 15$ MeV.

log-independent term from previous discussion, see e.g. Ref. [132]. As such, they are usually discarded.

To assess this claim and estimate the corresponding correction to N_{eff} , we identify the entropy deviation at neutrino decoupling with

$$\delta s = \delta s^{\text{N}\ddot{\text{K}}\text{C}} + s^{(2)\text{ln}} \Big|_{T=T_d} + s^{(2)\text{ln}} \Big|_{T=T_d}. \quad (7.21)$$

Then, for a decoupling temperature $T_d = 1.3453$ MeV, we find $\delta s / s^{(0)} \Big|_{T_d/m_e \rightarrow \infty} \simeq -0.012312$, leading to a correction to N_{eff} of

$$\delta N_{\text{eff}}^{\text{N}\ddot{\text{K}}\text{C}+(2)} \simeq 0.049965, \quad (7.22)$$

or, equivalently, a net $\mathcal{O}(e^2)$ FTQED contribution of

$$\delta N_{\text{eff}}^{(2)} = \delta N_{\text{eff}}^{\text{N}\ddot{\text{K}}\text{C}+(2)} - \delta N_{\text{eff}}^{\text{N}\ddot{\text{K}}\text{C}} \simeq 0.010070, \quad (7.23)$$

of which

$$\delta N_{\text{eff}}^{(2)\text{ln}} = \delta N_{\text{eff}}^{(2)} - \delta N_{\text{eff}}^{(2)\text{ln}} \simeq -0.000050, \quad (7.24)$$

and about 0.5% of $\delta N_{\text{eff}}^{(2)}$, comes from the $\mathcal{O}(e^2)$ logarithmic term on its own. Thus, the logarithmic contribution appears to be even less significant than previously envisaged.

Nevertheless, for completeness we report here the associated would-be G_1 and G_2 functions to be used in the continuity equation

$$\begin{aligned} G_1^{(2)\text{ln}}(\tau) &= \frac{e^2 x}{16\pi^4 z^3} \iint_0^\infty dy \, d\tilde{y} \frac{y}{\sqrt{y^2 + x^2}} \frac{\tilde{y}}{\sqrt{\tilde{y}^2 + x^2}} \ln \left| \frac{y + \tilde{y}}{y - \tilde{y}} \right| \times \\ &\quad \times \left\{ -n_D \tilde{n}_D - z n_D \partial_z \tilde{n}_D \right. \\ &\quad \left. - x [z (\partial_x n_D \partial_z \tilde{n}_D + n_D \partial_x \partial_z \tilde{n}_D) - n_D \partial_x \tilde{n}_D] \right. \\ &\quad \left. + \frac{x^2(y^2 + x^2 + \tilde{y}^2 + x^2)}{2(y^2 + x^2)(\tilde{y}^2 + x^2)} (2z n_D \partial_z \tilde{n}_D - n_D \tilde{n}_D) \right\}, \end{aligned} \quad (7.25)$$

$$\begin{aligned} G_2^{(2)\text{ln}}(\tau) &= \frac{e^2 x^2}{16\pi^4 z^2} \iint_0^\infty dy \, d\tilde{y} \frac{y}{\sqrt{y^2 + x^2}} \frac{\tilde{y}}{\sqrt{\tilde{y}^2 + x^2}} \ln \left| \frac{y + \tilde{y}}{y - \tilde{y}} \right| \times \\ &\quad \times \partial_z (n_D \partial_z \tilde{n}_D). \end{aligned} \quad (7.26)$$

We solved the continuity equation including these corrections for a range of neutrino decoupling temperatures and shown the results in Figs. 7.1 and 7.3. They again confirm the irrelevance of the $\mathcal{O}(e^2)$ logarithmic term as compared with both the total $\mathcal{O}(e^2)$ FTQED contribution, and our four-significant-digit accuracy goal. As a conclusion, the logarithmic $\mathcal{O}(e^2)$ finite temperature QED correction to the QED equation of state can indeed be disregarded.

7.3.2 $\mathcal{O}(e^3)$ FTQED

The next-to-leading-order QED correction to the ideal gas partition function is of a noninteger power of the QED fine structure constant. It is of order $\mathcal{O}(e^3)$ and comes from resumming the infinitely many insertions of the so-called ring diagrams, depicted on Fig. 7.4. The ring diagrams are the 1PI finite temperature QED selfenergies for the photons and they effectively shift the pole of the photon propagators in a temperature-dependent fashion. The photon acquires a thermal mass, or Debye-mass, from screening effects in the plasma, which regularises the infrared divergence of its associated thermal propagator, due to the presence of an extra power of e in its denominator.

$$\ln Z^{(3)} = \frac{1}{2} \left[\frac{1}{2} \text{ring}_2 - \frac{1}{3} \text{ring}_3 + \frac{1}{4} \text{ring}_4 + \dots \right]$$

Figure 7.4: Diagrammatic expression for the $\mathcal{O}(e^3)$ correction to the FTQED partition function. Filled black circles denote the 1PI photon selfenergy.

At that order in the QED coupling constant expansion, the pressure is well-known and was e.g. computed in Ref. [22], it reads

$$P^{(3)} = \frac{T}{V} \ln Z^{(3)} = \frac{e^3 T}{12\pi^4} I^{3/2}(T), \quad (7.27)$$

with

$$I(T) = \int_0^\infty dp \left(\frac{p^2 + \omega_p^2}{\omega_p} \right) n_D. \quad (7.28)$$

In the nonrelativistic limit where the Fermi-Dirac distribution can be replaced by its Maxwell-Boltzmann counterpart, $P^{(3)}$ is nothing but the Debye-Hückel pressure correction due to the screening of the static Coulomb potential [22, 130] in a thermal plasma. The associated energy and entropy corrections are

$$\rho^{(3)} = \frac{e^3 T^2}{8\pi^4} I^{1/2} \partial_T I, \quad (7.29)$$

$$s^{(3)} = \frac{e^3}{24\pi^4} \left(2I^{3/2} + 3I^{1/2} T \partial_T I \right). \quad (7.30)$$

In the limit $T/m_e \rightarrow \infty$, these expressions evaluate to $P^{(3)} = e^3 T^4 / (36\sqrt{3}\pi)$, $\rho^{(3)} = e^3 T^4 / (12\sqrt{3}\pi)$, and $s^{(3)} = e^3 T^3 / (9\sqrt{3}\pi)$.

Following the same spirit as for the previously analysed corrections and writing the full entropy correction as

$$\delta s = \delta s^{\text{N}\ddot{\text{N}}\text{C}} + s^{(2)\text{ln}} \Big|_{T=T_d} + s^{(2)\text{ln}} \Big|_{T=T_d} + s^{(3)} \Big|_{T=T_d}, \quad (7.31)$$

we find $\delta s / s^{(0)} \Big|_{T_d/m_e \rightarrow \infty} \simeq -0.012081$ for $T_d = 1.3453$ MeV. Then, Eq. (6.37) yields a correction

$$\delta N_{\text{eff}}^{\text{N}\ddot{\text{N}}\text{C}+(2)+(3)} \simeq 0.049013, \quad (7.32)$$

or, equivalently, a net $\mathcal{O}(e^2) + \mathcal{O}(e^3)$ FTQED contribution of magnitude

$$\delta N_{\text{eff}}^{(2)+(3)} = \delta N_{\text{eff}}^{\text{N}\ddot{\text{N}}\text{C}+(2)+(3)} - \delta N_{\text{eff}}^{\text{N}\ddot{\text{N}}\text{C}} \simeq 0.009119, \quad (7.33)$$

of which

$$\delta N_{\text{eff}}^{(3)} = \delta N_{\text{eff}}^{\text{N}\ddot{\text{N}}\text{C}+(2)+(3)} - \delta N_{\text{eff}}^{\text{N}\ddot{\text{N}}\text{C}+(2)} \simeq -0.000952 \quad (7.34)$$

stems from the $\mathcal{O}(e^3)$ correction of this section. The associated G_1 and G_2 functions, relevant for solving the continuity equation, are given by

$$\begin{aligned} G_1^{(3)}(\tau) &= \frac{e^3}{4\pi} \left(K + \frac{\tau^2}{2} k \right)^{1/2} \left[\frac{1}{\tau} (2J - 4K) - 2J' - \tau^2 j' \right. \\ &\quad \left. - \tau (2k + j) - \frac{(2J + \tau^2 j)(\tau(k - j) + K')}{2(2K + \tau^2 k)} \right], \\ G_2^{(3)}(\tau) &= \frac{e^3}{4\pi} \left(K + \frac{\tau^2}{2} k \right)^{1/2} \left[\frac{(2J + \tau^2 j)^2}{2(2K + \tau^2 k)} - \frac{2}{\tau} Y' - \tau (3J' + \tau^2 j') \right], \end{aligned}$$

with the special functions

$$\begin{aligned} k(\tau) &= \frac{1}{\pi^2} \int_0^\infty d\omega \frac{1}{\sqrt{\omega^2 + \tau^2}} \frac{1}{\exp\{(\sqrt{\omega^2 + \tau^2})\} + 1}, \\ j(\tau) &= \frac{1}{\pi^2} \int_0^\infty d\omega \frac{\exp(\sqrt{\omega^2 + \tau^2})}{(\exp(\sqrt{\omega^2 + \tau^2}) + 1)^2}, \end{aligned} \quad (7.35)$$

and $J(\tau)$, $Y(\tau)$, and $K(\tau)$ given in Eqs. (6.42) and (7.18). Figures 7.1 and 7.3, as before, display the correction to N_{eff} as a function of the neutrino decoupling temperature T_d .

Here a few comments are in order. First and most notably, the change in N_{eff} from $\mathcal{O}(e^3)$ FTQED is negative. As a result, it goes in the opposite direction to the $\mathcal{O}(e^2)$ and balances them out to a small extent. The $\mathcal{O}(e^3)$

FTQED contributions lessen the correction to N_{eff} obtained from the lower order corrections. The microphysical reasons for it are unclear and to the best of our knowledge, we can only attribute them to the regularisation of infrared-sensitive loop corrections, since they arise from the resummation of the ring diagrams of Fig. 7.4 which gave the photons an effective thermal mass.

Second, having in mind our four-significant-digit accuracy goal, we conclude that our $\mathcal{O}(e^3)$ FTQED corrections not only are sizeable and should not be disregarded, but also they are comparable to the neutrino-oscillations-induced change in N_{eff} , if not larger. Indeed, Ref. [127] reports a correction of up to $\delta N_{\text{eff}}^{\text{osc}} \simeq -0.0004$ when neutrino oscillations are consistently included in the energy transport calculation, while Ref. [166] finds a shift in the fifth significant digit. Therefore, while neutrino oscillations invariably have been acknowledged as key ingredients in standard N_{eff} computations, we here have shown that $\mathcal{O}(e^3)$ FTQED corrections should have been, too. For all these reasons, we insist that any future precision computation of N_{eff} with a four-significant-digit accuracy goal should consider the latter as a standard input.

7.3.3 $\mathcal{O}(e^4)$ FTQED

For the sake of completeness and to provide a measure of the theoretical uncertainty, we study the $\mathcal{O}(e^4)$ FTQED correction to the equation of state and its impact on N_{eff} in the limit $T/m_e \rightarrow \infty$. The $\mathcal{O}(e^4)$ pressure correction reads [210]:

$$P^{(4)} \Big|_{T/m_e \rightarrow \infty} = \frac{T}{V} \ln Z^{(4)} \Big|_{T/m_e \rightarrow \infty} \simeq -0.0611 \frac{e^4}{\pi^6} T^4, \quad (7.36)$$

where, we discarded a 5% uncertainty in the numerical prefactor and taken the renormalisation scale at that of the temperature. We obtain the associated energy and entropy densities using the usual standard thermodynamic relations, and find $\rho^{(4)} \simeq -0.1833 e^4 T^4 / \pi^6$ and $s^{(4)} \simeq -0.2444 e^4 T^3 / \pi^6$. Using Eq. (6.37), we estimate the resulting change in N_{eff} and find

$$\delta N_{\text{eff}}^{(4)} \simeq 3.5 \times 10^{-6}. \quad (7.37)$$

Putting aside Hubble-volume surveys, which in the most idealised and optimistic circumstances may have the accuracy to resolve N_{eff} at the level of 10^{-6} corrections [213], such a change in N_{eff} will not be probed in the near future. We therefore conclude that the $\mathcal{O}(e^4)$ FTQED correction to the QED equation of state is, for the time-being, unnecessary.

7.3.4 Finite temperature correction to T_d

In section 6.5.2, we studied the change in T_d from those FTQED corrections to the neutrino decoupling temperature (and the weak rates) that could simply be implemented by shifting the electron mass to its thermal counterpart and computing the Hubble rate using the $\mathcal{O}(e^2)$ equation of state. This of course affects N_{eff} and reading off Figs. 7.1 and 7.3, it merely shifts the final N_{eff} by

$$\delta N_{\text{eff}}^{m_{\text{th}}} \simeq -0.000080. \quad (7.38)$$

Though larger than the $\mathcal{O}(e^2)$ logarithmic correction to the QED equation of state discussed in section 7.3.1, it still is an order of magnitude smaller than the $\mathcal{O}(e^3)$ correction of section 7.3.2 which demonstrates that, on its own, this contribution has an irrelevant impact on N_{eff} .

7.4 Results within the instantaneous decoupling approximation (I)

Let us summarise the results for δN_{eff} obtained from entropy conservation arguments, i.e. only valid within the instantaneous decoupling approximation (I). They ought to be interpreted as estimates of how large corrections will be in the more realistic computation where (I) is dropped too. In table 7.1 are gathered the δN_{eff} changes obtained from dropping (III) the neutrino-never-coupled (NNC) and (II) the ideal gas approximations for the QED equation of state, within the instantaneous decoupling limit (I).

A few comments are in order. As expected and emphasised before, the dominant deviation from $N_{\text{eff}} = 3$ comes from relaxing (II) which allows for some entropy of the e^\pm -annihilation to be transferred between the QED and neutrino sectors for a longer time than within (II). Then, the finite temperature QFT effects come into play when (III) is relaxed and alter the QED equation of state via a power coupling expansion in the QED coupling constant e . At order $\mathcal{O}(e^2)$, the corrections to N_{eff} are of the same order of magnitude as those obtained from letting go of (II) and are primarily obtained from the log-independent part. The log-dependent bit is almost negligible, it falls below the order $\mathcal{O}(e^3)$ correction which is however of particular relevance. Indeed, the latter provides a sizeable contribution to N_{eff} across a broad range of possible decoupling temperatures, which we estimated more significant than the effect of including neutrino oscillations, always considered as a standard input in

x	$\delta N_{\text{eff}}^x (T_d = 1.3453 \text{ MeV})$	$\delta N_{\text{eff}}^x (T_d^{m_{\text{th}}} = 1.46 \text{ MeV})$
	QED equation of state corrections	
N \cancel{X} C	0.039895	0.033903
(2) \cancel{h}	0.010121	0.010173
(2) ln	-0.000050	-0.000043
(3)	-0.000952	-0.000951
(4)	$\simeq 3.5 \times 10^{-6}$	$\simeq 3.5 \times 10^{-6}$
	Weak rate corrections	
m_{th}	-0.000080	-0.000067
Total	0.048937	0.043019

Table 7.1: Summary of the various SM contributions to N_{eff} considered thus far, within the instantaneous decoupling approximation (I). The (instantaneous) neutrino decoupling temperature $T_d = 1.3453 \text{ MeV}$ is that established in section 6.5, while $T_d^{m_{\text{th}}} = 1.46 \text{ MeV}$ has been obtained from matching $\delta N_{\text{eff}}^{\text{N}\cancel{X}\text{C}+(2)\cancel{h}} + \delta N_{\text{eff}}^{m_{\text{th}}}$ to 0.044 [133].

N_{eff} computations. On the contrary, FTQED corrections of order $\mathcal{O}(e^3)$ so far never were and one major consequence of this piece of work within (I) is that we demonstrated that they should be. Analytic ingredients to implement them when including neutrino energy transport and oscillations have been computed, too. By matching known corrections $\delta N_{\text{eff}}^{\text{N}\cancel{X}\text{C}+(2)\cancel{h}} + \delta N_{\text{eff}}^{m_{\text{th}}}$ to the most recent such calculation [133], we infer that in comparison to $N_{\text{eff}} = 3.044$ [133], the new FTQED corrections studied in this work lower it to

$$N_{\text{eff}} = 3.043. \quad (7.39)$$

Higher order FTQED corrections and their impact on N_{eff} on the other hand, is too low to be resolved in near-future experiments. Before moving to the final conclusions regarding this part of the thesis, we wish to comment on the potential experimental errors that tarnish all theoretical computations of N_{eff} .

7.5 Theoretical uncertainties from errors on measurements

Of course, to all theory predictions which rely on experimentally measured parameters, e.g. the QED coupling constant e or the Fermi constant G_F , are associated uncertainties which eventually impact the theory predictions. We

	Parameter [Units]	Value $\pm 1\sigma$ uncertainty	Reference
Weak	$\sin^2 \theta_W$	0.23122 ± 0.00004	[215]
	$G_F [10^{-5} \text{GeV}^{-2}]$	1.1663787 ± 0.0000006	[215]
	$m_W [\text{GeV}]$	80.379 ± 0.012	[215]
Neutrino	$\sin^2 \theta_{12}/10^{-1}$	$3.20^{+0.20}_{-0.16}$	[216]
	$\sin^2 \theta_{13}/10^{-2}$	$2.160^{+0.083}_{-0.069}$	[216]
	$\sin^2 \theta_{23}/10^{-1}$	$5.47^{+0.20}_{-0.30}$	[216]
	$\Delta m_{21}^2 [10^{-5} \text{eV}^2]$	$7.55^{+0.20}_{-0.16}$	[216]
	$ \Delta m_{31}^2 [10^{-3} \text{eV}^2]$ (NO)	2.50 ± 0.03	[216]
	$ \Delta m_{31}^2 [10^{-3} \text{eV}^2]$ (IO)	$2.42^{+0.03}_{-0.04}$	[216]

Table 7.2: Central values and 1σ uncertainties of the weak sector physical constants. The neutrino parameter values have been derived in the global fit [216] assuming a normal mass ordering (NO), with the exception of the last entry marked which assumes an inverted mass ordering (IO). Inverting the mass hierarchy induces variations in the global best-fit values which are statistically insignificant ($< 1\sigma$) [216, 217].

briefly review how large these uncertainties potentially are in the context of neutrino cosmology, and more precisely N_{eff} which is primarily sensitive to the QED and weak sectors of the Standard Model.

Measurement errors in the QED sector. Relevant for N_{eff} are the electron mass m_e and the fine structure constant $\alpha = e^2/4\pi$. These are experimentally measured to nine significant digits [214], and are in that sense infinitely well-known, as far as N_{eff} computations are concerned.

Measurement errors in the weak sector. Unlike the QED sector, physical constants in the weak sector, which we summarise in table 7.2, are far less well-measured. As far as we work under the instantaneous decoupling approximation, and neglect neutrino masses and oscillations, the weak sector is, again, very well-known, cf. the first three rows of table 7.2. Once neutrino oscillations are turned on, the neutrino mass splittings Δm_{ij}^2 are relatively well-known and the least well-measured parameters are the solar neutrino mixing angle $\sin^2 \theta_{12}$ and the atmospheric one $\sin^2 \theta_{23}$, each have a 1σ -uncertainty of about 6%.

Resulting uncertainties on computations of N_{eff} . As emphasised above, instantaneous decoupling computations are merely affected by experimental

uncertainties, because they do not depend on the poorly-measured oscillation parameters. In particular, QED parameters are infinitely well-known and only the Fermi constant and W and Z boson masses affect N_{eff} through the neutrino weak rates and decoupling temperature. As a rule of thumb, we know from our previous analysis and e.g. Fig. 7.1 that changing the neutrino decoupling temperature T_d by an amount $\sim 10^{-3}$ induces a shift of $|\delta N_{\text{eff}}| \lesssim 10^{-4}$. Then, we evaluate from power counting that changing $\sin^2 \theta_W$ and G_F , within their 3σ measurement error bands, that is to say relative changes of $\sim \pm 5 \times 10^{-4}$ and $\sim \pm 10^{-6}$ respectively (see table 7.2), cannot modify T_d fractionally by more than $\sim 10^{-4}$, and hence N_{eff} by more than $|\delta N_{\text{eff}}| \sim 10^{-5}$. The impact of varying the W boson mass is even less significant. Therefore, errors on measurements are insignificant as far as instantaneous decoupling computations of N_{eff} are concerned.

As we very well know, dropping the instantaneous decoupling approximation is a complicated exercise that includes solving the neutrino Boltzmann equations numerically. This is currently under investigation, with the help of our colleagues S. Pastor, P. de Salas and S. Gariazzo who provide expertise on the numerical side². We already have studied dependence of N_{eff} on these uncertainties for the measurements of physical constants in the weak sector and here, we only shortly present the results and underlying physics. We leave the presentation of the more refined analysis for a future publication.

In a nutshell, our results are the following. First and foremost, numerical instability and uncertainties dominate the errors that result from measurements of physical constants. Then, despite the large errors on the mass splittings, these do not affect N_{eff} much. This is simply because the typical neutrino oscillation frequencies $\Delta m_{ij}^2/2\langle p \rangle$ are much faster than the Hubble rate around neutrino decoupling [218]. Hence, since the integration of Boltzmann equations is performed over a Hubble time (or more) around neutrino decoupling, these effects are averaged out and N_{eff} solely effectively depends on the relative mixing angles $\sin^2 \theta_{ij}$. Second, we find no strong dependence on $\sin^2 \theta_{23}$, despite the large 1σ error bar. Physically, this is simply because that mixing angle only affects the μ and τ neutrino populations alone, and effectively swaps them around. These populations enter N_{eff} computations in an identical manner [219], hence varying the $\nu_\mu \leftrightarrow \nu_\tau$ swapping rate $\sin^2 \theta_{23}$ does not change the final outcome of the N_{eff} computations by much. Eventually, we do obtain that N_{eff} presents a sensitivity on $\sin^2 \theta_{12}$, and to a smaller extent, on $\sin^2 \theta_{13}$ as well. Physically, this is because these mixing angles govern the conversion rates between electron neutrinos and the other two neutrino populations. Since the electrons

²They are the developers of `FortEPiANO` [133], a fully momentum-dependent decoupling code that accepts up to 3 active + 3 sterile neutrino flavours.

neutrinos are in direct contact with the $e^\pm - \gamma$ QED plasma, swapping electron neutrinos for other neutrino species changes the QED interactions between the neutrino and QED sectors, hence affecting N_{eff} directly. For $\sim \pm 20\%$ variations in $\sin^2 \theta_{12}$, i.e. a 3σ error band, N_{eff} can change by $\pm 10^{-4}$. For similar variations in $\sin^2 \theta_{13}$, the resulting changes in N_{eff} are an order of magnitude smaller, but that is simply because $\sin^2 \theta_{13}$ itself is already an order of magnitude smaller than $\sin^2 \theta_{12}$. Again, we emphasise that while these uncertainties are sizeable, the final uncertainties on N_{eff} still primarily stem from numerics.

Conclusion and Outlook

Conclusion

In the second part of this thesis, we first reviewed the theoretical inputs needed to properly define N_{eff} in the context of cosmological thermodynamics.

Then, we addressed the question of the departure from $N_{\text{eff}} = 3$, within the Standard Model of particle physics and cosmology. The prominent reason for this arises from dropping the assumption that electrons and photons are relativistic at neutrino decoupling, i.e. from dropping the “neutrino-never-coupled” (NNC) approximation.

From first principles of real-time finite-temperature field theory, we then studied corrections to the QED equation of state starting from the QED partition function, including effects of up to $\mathcal{O}(e^4)$. We have accurately quantified their impact on N_{eff} , i.e. we evaluated to which degree they drive it away from 3 within the instantaneous decoupling approximation (I). At leading-order $\mathcal{O}(e^2)$, we recovered the state-of-the-art result $\delta N_{\text{eff}}^{(2)\text{lh}} \simeq 0.01$. We even went further, and studied a so-far-neglected $\mathcal{O}(e^2)$ logarithmic contribution, and found its contribution to N_{eff} , namely $\delta N_{\text{eff}}^{(2)\text{ln}} \simeq -5 \times 10^{-5}$, to be even more negligible than initially expected. With a four-significant-digit precision goal, this $\mathcal{O}(e^2)$ logarithmic correction and the $\mathcal{O}(e^4)$ correction (which $\delta N_{\text{eff}}^{(4)} \simeq 3 \times 10^{-6}$) can be considered optional to unnecessary in future calculations.

In contradistinction, the $\mathcal{O}(e^3)$ correction to the QED equation of state is of great relevance, as it contributes $\delta N_{\text{eff}}^{(3)} \simeq 0.001$ across a wide range of realistic neutrino decoupling temperatures. The magnitude of this correction to $N_{\text{eff}} = 3$ is not only sizeable with respect to our four-significant-digit accuracy goal, but also with respect to the change in N_{eff} obtained from the neutrino oscillations

(up to $\delta N_{\text{eff}}^{\text{osc}} \simeq -0.0004$, depending on decoupling code). As a result, the $\mathcal{O}(\epsilon^3)$ correction to the QED equation of state should be considered a necessary input in future precision computations of N_{eff} .

Eventually, we provided estimates for the neutrino decoupling temperature T_d from first principles of real-time nonequilibrium field theory. At leading order, we obtained $T_d = 1.3453$ MeV, which is consistent with the results of [140] to 5%.

Outlook

A natural continuation of this work is a more fully fledged investigation of the impact on N_{eff} of the different effects considered in this work, one that would include neutrino energy transport and oscillations. This is achieved by numerically solving the quantum kinetic equations, or Boltzmann equations, that govern the nonequilibrium dynamics of the distribution functions, as e.g. presented in [133, 166].

As a matter of fact, joining forces with S. Pastor, P. de Salas and S. Gariazzo who provide expertise on the numerical side, we are on the verge of announcing a state-of-the-art SM benchmark N_{eff} , in a very-near-future publication that includes the interplay between the above mentioned FTQED effects together with neutrino energy transport and oscillations. This will also include a careful examination of the remaining uncertainties on our SM benchmark N_{eff} , as a result of observational error bars in the physical constants (e.g. the Fermi constant), approximations in the weak collision integrals that feed in the Boltzmann equations, and the current numerical precision.

Appendices

Appendix **A**

The 2PI effective action at 1-loop order

Let us first calculate the so-called 1PI one-loop effective action for a single real scalar field degree of freedom $\phi(x)$. The associated one-loop 2PI effective action can then be determined from Eqs. (1.119)(1.121).

As far as 1PI computations are concerned, $R(x, y)$ can temporarily be disregarded and set to zero. Indeed, all our results are determined from the action functional. As discussed above Eq. (1.119), at the level of the 1PI effective action, $R(x, y)$ can just be interpreted as a spacetime dependent mass shift. Thus we can neglect it for the time being and reinsert it at the end of the day by making the replacement

$$S[\phi] \rightarrow S[\phi, R] = S[\phi] + \frac{1}{2} \int_{x,y} R(x, y) \phi(x) \phi(y). \quad (\text{A.1})$$

This means that we can restrict ourselves to the usual 1PI effective action

$$\Gamma[\varphi] = W[J] - \int_x J(x) \varphi(x) \quad \Leftrightarrow \quad W[J] = \Gamma[\varphi] + \int_x J(x) \varphi(x) \quad (\text{A.2})$$

and generating functional

$$Z[J] = \int \mathcal{D}\phi \exp \frac{i}{\hbar} \left[S[\phi] + \int_x J(x) \phi(x) \right] = \exp \left[\frac{i}{\hbar} W[J] \right]. \quad (\text{A.3})$$

Though called the one-loop effective action, it actually is the effective action at order \hbar , hence we explicitly account for the presence of \hbar in this appendix.

The connection between quantum power expansions in \hbar and the diagrammatic loop expansion will be explained, too.

Let us study leading (LO) and next-to-leading order (NLO) quantum deviations around the classical path ϕ_{cl} and their associated effective actions. By definition ϕ_{cl} satisfies the stability condition

$$\left. \frac{\delta S[\phi]}{\delta \phi(x)} \right|_{\phi_{cl}} = -J(x). \quad (\text{A.4})$$

Strictly speaking, this equation makes ϕ_{cl} a functional of J , i.e. $\phi_{cl}[J]$. *A priori*, it is to be distinguished from $\varphi = \langle \phi \rangle$. ϕ_{cl} is that path that dominates the functional integral in the limit where $\hbar \rightarrow 0$. It satisfies the classical equation of motion. φ is the full one-point function, the quantum and statistical average of the full quantum field ϕ . It satisfies

$$\left. \frac{\delta \Gamma[\varphi]}{\delta \varphi(x)} \right|_{\varphi} = -J(x), \quad (\text{A.5})$$

with the usual abuses of notation.

A.1 Leading order 1PI effective action

At lowest order in \hbar , i.e. neglecting quantum fluctuations about ϕ_{cl} , we simply evaluate the functional integral within $Z[J]$ in the limit where $\hbar \rightarrow 0$, ϕ_{cl} extremises the exponential and we obtain the leading order generating functional

$$Z^{\text{LO}}[J] = e^{\frac{i}{\hbar}(S[\phi_{cl}] + \int_x J(x)\phi_{cl}(x))} = e^{\frac{i}{\hbar}(\Gamma^{\text{LO}}[\varphi] + \int_x J(x)\varphi^{\text{LO}}(x))} \quad (\text{A.6})$$

such that

$$W^{\text{LO}}[J] = \Gamma^{\text{LO}}[\varphi] + \int_x J(x)\varphi^{\text{LO}}(x) = S[\phi_{cl}] + \int_x J(x)\phi_{cl}(x). \quad (\text{A.7})$$

In the particular case of the lowest order approximation, using Eq. (A.4), we evaluate

$$\begin{aligned} \varphi^{\text{LO}}(x) &= \frac{\delta W^{\text{LO}}[J]}{\delta J(x)} = \frac{\delta}{\delta J(x)} \left[S[\phi_{cl}] + \int_y J(y)\phi_{cl}(y) \right] \\ &= \int_y \frac{\delta S[\phi_{cl}]}{\delta \phi_{cl}(y)} \frac{\delta \phi_{cl}(y)}{\delta J(x)} + \phi_{cl}(x) + \int_y J(y) \frac{\delta \phi_{cl}(y)}{\delta J(x)} = \phi_{cl}(x). \end{aligned}$$

This being reintroduced in the previous equation yields

$$\Gamma^{\text{LO}}[\varphi] = S[\varphi], \quad \varphi^{\text{LO}} = \phi_{cl}. \quad (\text{A.8})$$

A.2 Next-to-leading order 1PI effective action

The next-to-leading order (NLO) contribution in \hbar is found by expanding around ϕ_{cl} , i.e. we write $\phi(x) = \phi_{cl}(x) + \sqrt{\hbar} \eta(x)$ and $\eta(x)$ describes the dimensionless functional quantum fluctuations around ϕ_{cl} . Expanding the action functional about $\phi_{cl}(x)$ to order \hbar thus gives

$$S[\phi] = S[\phi_{cl}] + \sqrt{\hbar} \int_x \frac{\delta S[\phi]}{\delta \phi(x)} \Big|_{\phi_{cl}} \eta(x) + \frac{\hbar}{2} \int_{xy} \frac{\delta^2 S[\phi]}{\delta \phi(x) \delta \phi(y)} \Big|_{\phi_{cl}} \eta(x) \eta(y) + \mathcal{O}(\sqrt[3]{\hbar}) \quad (\text{A.9})$$

which, using the stability condition (A.4) implies linear order in \hbar

$$S[\phi] + \int_x J(x) \phi(x) \simeq S[\phi_{cl}] + \int_x J(x) \phi_{cl}(x) + \frac{\hbar}{2} \int_{xy} \frac{\delta^2 S}{\delta \phi(x) \delta \phi(y)} \Big|_{\phi_{cl}} \eta(x) \eta(y). \quad (\text{A.10})$$

There is no contribution proportional to $\sqrt{\hbar}$ because of the stability condition (A.4). Hence, the next-to-leading order generating functional is given by

$$Z^{\text{NLO}}[J] = e^{\frac{i}{\hbar} (S[\phi_{cl}] + \int_x J(x) \phi_{cl}(x))} \int \mathcal{D}(\sqrt{\hbar} \eta) \exp \left[\frac{i}{2} \int_{xy} \frac{\delta^2 S}{\delta \phi(x) \delta \phi(y)} \Big|_{\phi_{cl}} \eta(x) \eta(y) \right]. \quad (\text{A.11})$$

The path integral can be evaluated using the following functional Gaussian integral theorem, which we prove first.

Digression on Gaussian functional integrals. Let A be a real symmetric matrix, then we will show

$$\int_{-\infty}^{\infty} \left(\prod_{i=1}^N d\eta_i \right) \exp \left(\frac{i}{2} \sum_{i,j=1}^N \eta_i A_{ij} \eta_j \right) = \frac{(2\pi)^N}{\sqrt{\det(-iA)}} \quad (\text{A.12})$$

where $\{\eta\}$ is a set of real variables.

Since A is symmetric, it is diagonalizable,

$$\sum_{i,j=1}^N \eta_i A_{ij} \eta_j = \eta^T A \eta = (O\xi)^T A (O\xi) = \sum_{i=1}^N \xi_i^2 D_{ii}, \quad (\text{A.13})$$

and O performs the linear transformation from $\{\xi\}$ to $\{\eta\}$ with the elements of the diagonal matrix $D = O^T A O$ being the eigenvalues of A . Since the

transformation is linear, one can switch from $\{\xi\}$ to $\{\eta\}$ in the integration variables and the price to pay is just a constant Jacobian $J = \left| \det \left(\frac{\partial \xi_i}{\partial \eta_j} \right) \right| = |\det O| = 1$, such that

$$\begin{aligned} \int_{-\infty}^{\infty} \left(\prod_{i=1}^N d\eta_i \right) \exp \frac{i}{2} \sum_{i,j=1}^N \eta_i A_{ij} \eta_j &= \int_{-\infty}^{\infty} \left(\prod_{i=1}^N d\xi_i \right) \exp \left(\frac{i}{2} \sum_{i=1}^N \xi_i^2 D_{ii} \right) \\ &= \prod_{i=1}^N \int_{-\infty}^{\infty} d\xi_i \exp \left(\frac{i}{2} \xi_i^2 D_{ii} \right) \\ &= \sqrt{\frac{(2\pi)^N}{\prod_{i=1}^N -iD_{ii}}} \end{aligned}$$

because $\int_{-\infty}^{\infty} d\xi_i \exp \left(\frac{i}{2} \xi_i^2 D_{ii} \right) = \sqrt{\frac{2\pi}{-iD_{ii}}}$ provided that $\text{Im}(D_{ii}) > 0$. If $\text{Im}(D_{ii}) = 0$, the convergence of the integral is ensured by $D_{ii} \rightarrow D_{ii} + i\epsilon$.

Back to the calculation. Now let us define $A(x, y) = \frac{\delta^2 S[\phi]}{\delta \phi(x) \delta \phi(y)} \Big|_{\phi_{cl}}$ where x and y act as matrix indices. By definition, A is diagonal as our action functional is local, hence $A = D$. On the CTP, the convergence of the Gaussian functional integral is piecewise ensured with the requirements that $\text{Im} D(x, x) > 0$ on the forward contour and $\text{Im} D(x, x) < 0$ on the backward contour. Those amount to nothing but demanding that $A = iG_0^{-1}$ is the contour-ordered Green's function (1.125). Then, we can perform the functional Gaussian integral in (A.11) and the result, up to a normalisation factor, reads

$$\begin{aligned} Z^{\text{NLO}}[J] &= \exp \left[\frac{i}{\hbar} \left(S[\phi_{cl}] + \int_x J(x) \phi_{cl}(x) \right) \right] \det [G_0^{-1}]^{-1/2} \\ &= \exp \left[\frac{i}{\hbar} \left(S[\phi_{cl}] + \int_x J(x) \phi_{cl}(x) \right) \right] \exp \left[-\frac{1}{2} \text{Tr} \ln G_0^{-1} \right] \\ &= \exp \left[\frac{i}{\hbar} \left(S[\phi_{cl}] + \int_x J(x) \phi_{cl}(x) + \frac{i\hbar}{2} \text{Tr} \ln G_0^{-1} \right) \right]. \end{aligned}$$

The Tr operator here performs integrals \int_{xy} as the entries of the matrices under consideration here are specified by spacetime arguments x and y . Up to an additive constant, we find for the next-to-leading order effective action

$$\Gamma^{\text{NLO}}[\varphi] + \int_x J(x) \varphi(x) = S[\phi_{cl}] + \int_x J(x) \phi_{cl}(x) + \frac{i\hbar}{2} \text{Tr} \ln G_0^{-1}. \quad (\text{A.14})$$

From these past equations we know that we can parametrise $\varphi = \phi_{cl} + \hbar\varphi^{(1)} + \mathcal{O}(\sqrt{\hbar})$ as there is no $\sqrt{\hbar}$ correction to the effective action and $\varphi^{\text{LO}} = \phi_{cl}$. Now we compute the right hand side of the previous equation using Eq. (A.4)

$$S[\varphi(x) - \hbar\varphi^{(1)}(x)] + \int_x J(x)(\varphi(x) - \hbar\varphi^{(1)}(x)) + \frac{i\hbar}{2} \text{Tr} \ln G_0^{-1}[\varphi - \hbar\varphi^{(1)}]$$

$$= S[\varphi] + \frac{i\hbar}{2} \text{Tr} \ln G_0^{-1}[\varphi] + \int_x J(x)\varphi(x) + \mathcal{O}(\hbar^2)$$

to finally arrive at

$$\Gamma^{\text{NLO}}[\varphi] = S[\varphi] + \frac{i\hbar}{2} \text{Tr} \ln G_0^{-1}[\varphi]. \quad (\text{A.15})$$

Though this really is the next-to-leading order effective action Γ^{NLO} in \hbar , it is known as the one-loop effective action. This terminology comes from the diagrammatic interpretation of the contribution $\text{Tr} \ln G_0^{-1}[\varphi]$. It is a closed loop which resums infinitely vertex insertions made of couplings to the background φ . Using Eqs. (1.49)(1.125), we find the one-loop truncated 1PI effective action

$$\begin{aligned} \Gamma^{\text{NLO}}[\varphi] &= S[\varphi] + \frac{i\hbar}{2} \text{Tr} \ln G_f^{-1} + \frac{i\hbar}{2} \text{Tr} \ln \left[\mathbb{I} - G_f \frac{i\delta^2 \mathcal{L}_{\text{int}}[\phi]}{\delta\phi^2} \Big|_{\varphi} \delta_{\mathcal{C}} \right] \\ &= S[\varphi] + \frac{i\hbar}{2} \text{Tr} \ln G_f^{-1} - \frac{i\hbar}{2} \sum_{n=1}^{\infty} \frac{1}{n} \text{Tr} \left[\left(G_f \frac{i\delta^2 \mathcal{L}_{\text{int}}[\phi]}{\delta\phi^2} \Big|_{\varphi} \delta_{\mathcal{C}} \right)^n \right], \end{aligned}$$

making the diagrammatic interpretation explicit.

A.3 The one-loop 2PI effective action.

In order to find the associated one-loop 2PI effective action (1.124), we first start from Eq. (A.15) and make the replacement $S[\phi] \rightarrow S[\phi, R]$ using Eq. (1.119), hence computing the R -dependent 1PI effective action. We find

$$\Gamma^{\text{NLO}}[\varphi, R] = S[\varphi, R] + \frac{i}{2} \text{Tr} \ln [G_0^{-1}[\varphi] - iR]. \quad (\text{A.16})$$

Now using Eqs. (1.121)(1.123) and explicitly injecting Eq. (1.119), we find the one-loop 2PI effective action

$$\mathbf{\Gamma}^{\text{NLO}}[\varphi, \Delta] = S[\varphi] + \frac{i}{2} \text{Tr} \ln [G_0^{-1}[\varphi] - iR] - \frac{1}{2} \text{Tr}[\Delta R]. \quad (\text{A.17})$$

At this order, the solution of the equation of motion for the propagator is $\Delta^{-1} = G_0^{-1} - iR$. Plugging this back into the previous equation, we obtain

$$\mathbf{\Gamma}^{\text{NLO}}[\varphi, \Delta] = S[\varphi] + \frac{i}{2} \text{Tr} \ln [\Delta^{-1}] + \frac{i}{2} \text{Tr}[\Delta G_0^{-1}] - \frac{i}{2} \text{Tr}[\Delta \Delta^{-1}], \quad (\text{A.18})$$

where $-\frac{i}{2} \text{Tr}[\Delta \Delta^{-1}]$ is an irrelevant constant when it comes to 2PI equations of motion. Higher order contribution to the full effective action are then

parametrised by $\Gamma_2[\varphi, \Delta]$, where 2 stands for two or more loops. Up to an irrelevant additive constant, the full 2PI effective action reads

$$\begin{aligned}\mathbf{\Gamma}[\varphi, \Delta] &= \mathbf{\Gamma}^{\text{NLO}}[\varphi, \Delta] + \Gamma_2[\varphi, \Delta], \\ &= S[\varphi] + \frac{i}{2} \text{Tr} \ln [\Delta^{-1}] - \frac{i}{2} \text{Tr} [\Delta G_0^{-1}] + \Gamma_2[\varphi, \Delta]\end{aligned}\quad (\text{A.19})$$

from where one can read off Eq. (1.124) using Eq. (1.123).

Adiabatic propagators

Under the assumption that the breaking of time-translation invariance is only driven by $\varphi(t)$ which itself is slowly rolling, it seems sensible to assume that the out-of-equilibrium time-dependence of the propagators is mild and adiabatic. In the next two sections, we comment and derive the main conclusions one can draw from assuming an adiabatic time evolution of the time-dependent quantities that enter the description of (quasi)particles through the associated propagators. In particular, one solves the Kadanoff-Baym equations, and interpret their solutions in terms of quasiparticles, which we then connect to the kinetic theory.

B.1 Wentzel-Kramers-Brillouin solutions: derivation

In this section, we provide a derivation for the solutions of the KBEs (4.21) and (4.22) in the WKB approximation, analogously to Ref. [33]. We start with the first KBE (4.21). Given the boundary conditions $\Delta^-(t_1, t_2; \mathbf{p})|_{t_1=t_2} = 0$ and $\partial_{t_1} \Delta^-(t_1, t_2; \mathbf{p})|_{t_1=t_2} = 1$, the WKB ansatz for the spectral function in the mixed representation reads

$$\Delta^-(t_1, t_2; \mathbf{p}) \simeq \frac{\sin\left(\int_{t_2}^{t_1} dt' \Omega_{t'}\right) e^{-\frac{1}{2} \left| \int_{t_2}^{t_1} dt' \Gamma_{t'} \right|}}{\sqrt{\Omega_{t_1} \Omega_{t_2}}}, \quad (\text{B.1})$$

where we simplified the notation for $\Omega_a(t; \mathbf{p}) \rightarrow \Omega_t$ and similarly for Γ . Starting out with that Ansatz, we then employ the following assumptions:

- 1) adiabaticity, i.e. $|\dot{\Omega}_t/\Omega_t^2| \ll 1$ and $|\dot{\Gamma}_t/\Gamma_t^2| \ll 1$
- 2) weak damping, i.e. $|\Gamma_t/\Omega_t| \ll 1$ due to weak coupling.
- 3) $\Pi^-(t_1, t_2; \mathbf{p})$ and $\Pi^+(t_1, t_2; \mathbf{p})$ have a finite support, i.e., they quickly approach zero for $|t_1 - t_2| \gtrsim \tau_{\text{int}}$ with τ_{int} being some characteristic time scale of microscopic physics e.g. that of quantum scattering events.
- 4) Ω_t and Γ_t can be approximately regarded as constants over the support of $\Pi^-(t_1, t_2; \mathbf{p})$ and $\Pi^+(t_1, t_2; \mathbf{p})$.

Here Ω_t and Γ_t are to be found such that Eq. (B.1) solves Eq. (4.21), i.e.

$$\left(\partial_{t_1}^2 + \omega_a(t_1; \mathbf{p})^2\right) \Delta_a^-(t_1, t_2; \mathbf{p}) = - \int_{t_2}^{t_1} dt' \Pi_a^-(t_1, t'; \mathbf{p}) \Delta_a^-(t', t_2; \mathbf{p}) \quad (\text{B.2})$$

under such assumptions. To determine Ω_t and Γ_t , it is convenient to decompose $\Delta^-(t_1, t_2; \mathbf{p})$ as

$$\Delta^-(t_1, t_2; \mathbf{p}) = -\frac{i}{2}(\rho^+(t_1, t_2; \mathbf{p}) - \rho^-(t_1, t_2; \mathbf{p})), \quad (\text{B.3})$$

where

$$\rho^\alpha(t_1, t_2; \mathbf{p}) = \frac{e^{\alpha i \int_{t_2}^{t_1} dt' \Omega_{t'}} e^{-\frac{\alpha}{2} \left| \int_{t_2}^{t_1} dt' \Gamma_{t'} \right|}}{\sqrt{\Omega_{t_1} \Omega_{t_2}}}, \quad (\text{B.4})$$

with $\alpha = \pm$. If $\rho^+(t_1, t_2; \mathbf{p})$ and $\rho^-(t_1, t_2; \mathbf{p})$ solve Eq. (B.2) separately, then so does $\Delta^-(t_1, t_2; \mathbf{p})$. Let's consider the case of $t_1 > t_2$. Using Eqs. (B.3) and (B.4) into Eq. (B.2), we obtain

$$\omega_{t_1}^2 - \Omega_{t_1}^2 - i\alpha\Omega_{t_1}\Gamma_{t_1} \simeq - \int_0^{t_1-t_2} dz \Pi^-(t_1, t_1-z) e^{\int_{t_1}^{t_1-z} dt' (i\alpha\Omega_{t'} - \frac{1}{2}\Gamma_{t'})} \quad (\text{B.5})$$

$$= - \int_0^\infty dz \theta(t_1 - t_2 - z) \Pi^-(t_1, t_1 - z) e^{\int_{t_1}^{t_1-z} dt' (i\alpha\Omega_{t'} - \frac{1}{2}\Gamma_{t'})}. \quad (\text{B.6})$$

by neglecting $\Gamma_{a;t_1}/\Omega_{a;t_1}$ and $\dot{\Omega}_{a;t_1}/\Omega_{a;t_1}^2$ terms. Inserting the step function into the integrand in the RHS of Eq. (B.6), we were able to extend the upper

limit of the integral to the infinity.¹ By using integral representation of the step function, the RHS of Eq. (B.6) becomes

$$\begin{aligned}
& - \int_0^\infty dz \int_{-\infty}^\infty \frac{d\omega'}{2\pi} \frac{e^{-i\omega'(t_1-t_2-z)}}{\omega' + i\eta} \Pi^-(t_1, t_1 - z; \mathbf{p}) e^{\int_{t_1}^{t_1-z} dt' (i\alpha\Omega_{t'} - \frac{1}{2}\Gamma_{t'})} \\
& \simeq - \int_0^\infty dz \int_{-\infty}^\infty \frac{d\omega'}{2\pi} \frac{e^{-i\omega'(t_1-t_2-z)}}{\omega' + i\eta} \Pi^-(t_1, t_1 - z; \mathbf{p}) e^{(-i\alpha\Omega_{t_1} + \frac{1}{2}\Gamma_{t_1})z} \\
& = - \int_{-\infty}^\infty \frac{d\omega'}{2\pi} \frac{e^{-i\omega'(t_1-t_2)}}{\omega' + i\eta} \int_0^\infty dz \Pi^-(t_1, t_1 - z; \mathbf{p}) e^{i(\omega' - \alpha\Omega_{t_1} - \frac{1}{2}\Gamma_{t_1})z} \\
& = - \int_{-\infty}^\infty \frac{d\omega'}{2\pi} \frac{e^{-i\omega'(t_1-t_2)}}{\omega' + i\eta} \tilde{\Pi}^-(t_1, \omega' + \hat{\Omega}_{t_1}^\alpha) \\
& = - \tilde{\Pi}^-(t_1, \hat{\Omega}_{t_1}^\alpha)
\end{aligned} \tag{B.7}$$

with $\hat{\Omega}_t^\alpha = -\alpha\Omega_t - \frac{i}{2}\Gamma_t$. $\hat{\Omega}_t$ in the main text corresponds to $\hat{\Omega}_t^-$, i.e. $\hat{\Omega}_t = \hat{\Omega}_t^-$. To get the second line we used that $\Omega_{t'}$ and $\Gamma_{t'}$ are approximately constant over the support of Π^- and in the fourth line we introduced the one-sided Fourier transform of $\Pi^-(t_1, t_2)$ expressed as

$$\tilde{\Pi}^-(t, \omega; \mathbf{p}) = \int_0^\infty dz e^{iz\omega} \Pi^-(t, t - z; \mathbf{p}). \tag{B.8}$$

Note that we introduced tilded quantities when one deals with one-sided Fourier transform. To pass to the last line, the residue theorem was employed. From Eq. (B.8) we see that

$$\tilde{\Pi}^-(t, \hat{\Omega}_t^+; \mathbf{p}) = (\tilde{\Pi}^-(t, \hat{\Omega}_t^-; \mathbf{p}))^*. \tag{B.9}$$

Plugging back Eq. (B.7) into Eq. (B.6) and using the relation (B.9), we obtain

$$\Omega_t = \sqrt{\omega^2(t; \mathbf{p}) + \text{Re}(\tilde{\Pi}^-(t, \hat{\Omega}_t^-; \mathbf{p}))}, \tag{B.10}$$

$$\Gamma_t = -\frac{\text{Im}(\tilde{\Pi}^-(t, \hat{\Omega}_t^-; \mathbf{p}))}{\Omega_t}. \tag{B.11}$$

The case of $t_2 > t_1$ can be investigated analogously leading to the same results as above. Eq. (B.1) with Eqs. (B.10) and (B.11) then determine $\Delta^-(t_1, t_2; \mathbf{p})$.

¹Ref. [33] separately considered the two cases when the time separation $|t_1 - t_2|$ is smaller and larger than τ_{int} , see remarks below Eq. (9) of Ref. [33]. But this is not necessary when one uses the step function in Eq. (B.6).

The solution to the second KBE ($t_i \rightarrow -\infty$)

$$\begin{aligned} \left(\partial_{t_1}^2 + \omega_a(t_1; \mathbf{p})^2\right) \Delta_a^+(t_1, t_2; \mathbf{p}) &= - \int_{-\infty}^{t_1} dt' \Pi_a^-(t_1, t'; \mathbf{p}) \Delta_a^+(t', t_2; \mathbf{p}) \\ &\quad + \int_{-\infty}^{t_2} dt' \Pi_a^+(t_1, t'; \mathbf{p}) \Delta_a^-(t', t_2; \mathbf{p}) \end{aligned} \quad (\text{B.12})$$

is given by

$$\Delta^+(t_1, t_2; \mathbf{p}) = \int_{-\infty}^{t_1} dt'_1 \int_{-\infty}^{t_2} dt'_2 \Delta^-(t_1, t'_1; \mathbf{p}) \Pi^+(t'_1, t'_2; \mathbf{p}) \Delta^-(t'_2, t_2; \mathbf{p}), \quad (\text{B.13})$$

which can be directly verified by plugging it into the second KBE (B.12). Define $t_{max} = \max(t_1, t_2)$ and rewrite (B.13) as²

$$\int_{-\infty}^{t_{max}} dt'_1 \int_{-\infty}^{t_{max}} dt'_2 \theta(t_1 - t'_1) \theta(t_2 - t'_2) \Delta^-(t_1, t'_1; \mathbf{p}) \Pi^+(t'_1, t'_2; \mathbf{p}) \Delta^-(t'_2, t_2; \mathbf{p}). \quad (\text{B.14})$$

$\Delta^+(t_1, t_2; \mathbf{p})$ given above is apparently symmetric under $t_1 \leftrightarrow t_2$ as it should be. Therefore, one can symmetrise the integrand of Eq. (B.14) as

$$\frac{1}{2} \left[\theta(t_1 - t'_1) \theta(t_2 - t'_2) \Delta^-(t_1, t'_1; \mathbf{p}) \Pi^+(t'_1, t'_2; \mathbf{p}) \Delta^-(t'_2, t_2; \mathbf{p}) + (t_1 \leftrightarrow t_2) \right].$$

Then the integrand above is symmetric under $t'_1 \leftrightarrow t'_2$ due to the symmetry and antisymmetry of the real-time Π^+ and Δ^- , and the spectral propagator thus far reads

$$\begin{aligned} \int_{-\infty}^{t_{max}} dt'_1 \int_{-\infty}^{t'_1} dt'_2 \theta(t_1 - t'_1) \theta(t_2 - t'_2) \Delta^-(t_1, t'_1; \mathbf{p}) \Pi^+(t'_1, t'_2; \mathbf{p}) \Delta^-(t'_2, t_2; \mathbf{p}) \\ + (t_1 \leftrightarrow t_2) \end{aligned}$$

By substituting (B.3), the latter can be further decomposed as

$$\Delta^+(t_1, t_2; \mathbf{p}) = F^+(t_1, t_2; \mathbf{p}) + F^-(t_1, t_2; \mathbf{p}). \quad (\text{B.15})$$

Here $F^+(t_1, t_2; \mathbf{p})$ contains the contributions from the integrand of Eq. (B.15) proportional to $\rho^\alpha \rho^\alpha$, while $F^-(t_1, t_2; \mathbf{p})$ contains the rest of the contributions,

²Note that the approach adopted here does not require the split of the integration region that was made in [33], which led to \mathcal{D} in Eq.(12) thereof, hence we have no \mathcal{D} term and there is no need to show that the \mathcal{D} term is negligible.

i.e. coming from $\rho^\alpha \rho^{-\alpha}$ terms. Assuming $\Gamma_t \geq 0$, $F^-(t_1, t_2; \mathbf{p})$ becomes (whenever WKB assumptions 1)-4) are employed, we use \simeq instead of $=$)

$$\begin{aligned}
F^-(t_1, t_2; \mathbf{p}) &= - \int_{-\infty}^{t_{max}} dt'_1 \int_{-\infty}^{t'_1} dt'_2 \theta(t_1 - t'_1) \theta(t_2 - t'_2) \Pi^+(t'_1, t'_2; \mathbf{p}) \\
&\times \left(\frac{i}{2}\right)^2 \frac{e^{i \int_{t'_1}^{t_1} dt' \Omega_{t'} - \frac{1}{2} \left| \int_{t'_1}^{t_1} \Gamma_{t'} \right|}}{\sqrt{\Omega_{t_1} \Omega_{t'_1}}} \frac{e^{-i \int_{t'_2}^{t_2} dt' \Omega_{t'} - \frac{1}{2} \left| \int_{t'_2}^{t_2} \Gamma_{t'} \right|}}{\sqrt{\Omega_{t'_2} \Omega_{t_2}}} + c.c. + (t_1 \leftrightarrow t_2) \\
&= - \int_{-\infty}^{t_{max}} dt'_1 \int_{-\infty}^{t'_1} dt'_2 \theta(t_1 - t'_1) \theta(t_2 - t'_2) \Pi^+(t'_1, t'_2; \mathbf{p}) \\
&\times \left(\frac{i}{2}\right)^2 \frac{e^{i \int_{t'_1}^{t_1} dt' \Omega_{t'} - \frac{1}{2} \int_{t'_1}^{t_1} \Gamma_{t'}}}{\sqrt{\Omega_{t_1} \Omega_{t'_1}}} \frac{e^{-i \int_{t'_2}^{t_2} dt' \Omega_{t'} - \frac{1}{2} \int_{t'_2}^{t_2} \Gamma_{t'}}}{\sqrt{\Omega_{t'_2} \Omega_{t_2}}} + c.c. + (t_1 \leftrightarrow t_2) \\
&= \frac{1}{4\sqrt{\Omega_{t_1} \Omega_{t_2}}} \int_{-\infty}^{t_{max}} dt'_1 \int_{-\infty}^{t'_1} dt'_2 \theta(t_1 - t'_1) \theta(t_2 - t'_2) \Pi^+(t'_1, t'_2; \mathbf{p}) \\
&\times \frac{e^{i \left(\int_{t'_1}^{t_{min}} + \int_{t_{min}}^{t_1} + \int_{t'_2}^{t_{min}} + \int_{t_{min}}^{t_2} \right) dt' (\Omega_{t'} + \frac{i}{2} \Gamma_{t'})}}{\sqrt{\Omega_{t'_1} \Omega_{t'_2}}} + c.c. + (t_1 \leftrightarrow t_2)
\end{aligned}$$

where into account the Heaviside step functions, in the second line we removed the absolute value $||$ as we assume that $\Gamma_{t'}$ is positive. Then, introducing $t_{min} = \min(t_1, t_2)$, we have

$$\begin{aligned}
&= \frac{1}{4\sqrt{\Omega_{t_1} \Omega_{t_2}}} \int_{-\infty}^{t_{max}} dt'_1 \int_{-\infty}^{t'_1} dt'_2 \theta(t_1 - t'_1) \theta(t_2 - t'_2) \Pi^+(t'_1, t'_2; \mathbf{p}) \\
&\times \frac{e^{i \left(\int_{t_{min}}^{t_1} + \int_{t_{min}}^{t_2} + 2 \int_{t'_1}^{t_{min}} + \int_{t'_2}^{t_{min}} \right) dt' (\Omega_{t'} + \frac{i}{2} \Gamma_{t'})}}{\sqrt{\Omega_{t'_1} \Omega_{t'_2}}} + c.c. + (t_1 \leftrightarrow t_2) \\
&= \frac{e^{i \left(\int_{t_{min}}^{t_1} + \int_{t_{min}}^{t_2} \right) dt' (\Omega_{t'} + \frac{i}{2} \Gamma_{t'})}}{4\sqrt{\Omega_{t_1} \Omega_{t_2}}} \int_{-\infty}^{t_{max}} dt'_1 \int_{-\infty}^{t'_1} dt'_2 \theta(t_1 - t'_1) \theta(t_2 - t'_2) \\
&\times \Pi^+(t'_1, t'_2; \mathbf{p}) \frac{e^{i \left(2 \int_{t'_1}^{t_{min}} + \int_{t'_2}^{t_{min}} \right) dt' (\Omega_{t'} + \frac{i}{2} \Gamma_{t'})}}{\sqrt{\Omega_{t'_1} \Omega_{t'_2}}} + c.c. + (t_1 \leftrightarrow t_2).
\end{aligned}$$

Now changing variables to $\tau = t'_1$ and $z = (\tau - t'_2)$, and using that Ω is positive, too, we have

$$\begin{aligned}
&= \frac{e^{i \int_{t_2}^{t_1} dt' \Omega_{t'} | - \frac{1}{2} \int_{t_2}^{t_1} dt' \Gamma_{t'} |}}{4 \sqrt{\Omega_{t_1} \Omega_{t_2}}} \int_{-\infty}^{t_{max}} d\tau \int_0^{\tau - \infty} dz \theta(t_1 - \tau) \theta(t_2 - \tau + z) \\
&\times \frac{e^{2i \int_{\tau}^{t_{min}} dt' \hat{\Omega}_{t'}^* + i \int_{\tau-z}^{\tau} dt' \hat{\Omega}_{t'}^*}}{\sqrt{\Omega_{\tau} \Omega_{\tau-z}}} \Pi^+(\tau, \tau - z; \mathbf{p}) + c.c. + (t_1 \leftrightarrow t_2) \\
&= \frac{e^{i \int_{t_2}^{t_1} dt' \Omega_{t'} | - \frac{1}{2} \int_{t_2}^{t_1} dt' \Gamma_{t'} |}}{4 \sqrt{\Omega_{t_1} \Omega_{t_2}}} \int_{-\infty}^{t_{max}} d\tau \theta(t_1 - \tau) \int_0^{\infty} dz \int_{-\infty}^{+\infty} \frac{i}{2\pi} d\omega' \times \\
&\frac{e^{-i\omega'(t_2 - \tau + z)}}{\omega' + i\eta} \frac{e^{2i \int_{\tau}^{t_{min}} dt' \hat{\Omega}_{t'}^* + i \int_{\tau-z}^{\tau} dt' \hat{\Omega}_{t'}^*}}{\sqrt{\Omega_{\tau} \Omega_{\tau-z}}} \Pi^+(\tau, \tau - z; \mathbf{p}) + c.c. + (t_1 \leftrightarrow t_2) \\
&= \frac{e^{i \int_{t_2}^{t_1} dt' \Omega_{t'} | - \frac{1}{2} \int_{t_2}^{t_1} dt' \Gamma_{t'} |}}{4 \sqrt{\Omega_{t_1} \Omega_{t_2}}} \int_{-\infty}^{t_{max}} d\tau \theta(t_1 - \tau) e^{2i \int_{\tau}^{t_{min}} dt' \hat{\Omega}_{t'}^*} \int_{-\infty}^{+\infty} \frac{i}{2\pi} d\omega' \\
&\times \frac{e^{-i\omega'(t_2 - \tau)}}{\omega' + i\eta} \int_0^{\infty} dz \frac{e^{i(\int_{\tau-z}^{\tau} dt' \hat{\Omega}_{t'}^* - \omega' z)}}{\sqrt{\Omega_{\tau} \Omega_{\tau-z}}} \Pi^+(\tau, \tau - z; \mathbf{p}) + c.c. + (t_1 \leftrightarrow t_2) \\
&\simeq \frac{e^{i \int_{t_2}^{t_1} dt' \Omega_{t'} | - \frac{1}{2} \int_{t_2}^{t_1} dt' \Gamma_{t'} |}}{4 \sqrt{\Omega_{t_1} \Omega_{t_2}}} \int_{-\infty}^{t_{max}} d\tau \theta(t_1 - \tau) e^{2i \int_{\tau}^{t_{min}} dt' \hat{\Omega}_{t'}^*} \int_{-\infty}^{+\infty} \frac{i}{2\pi} d\omega' \\
&\times \frac{e^{-i\omega'(t_2 - \tau)}}{\omega' + i\eta} \int_0^{\infty} dz \frac{e^{i(\hat{\Omega}_{\tau}^* - \omega')z}}{\Omega_{\tau}} \Pi^+(\tau, \tau - z; \mathbf{p}) + c.c. + (t_1 \leftrightarrow t_2).
\end{aligned}$$

Now recalling the definition of the one-sided Fourier transform (B.8)

$$\begin{aligned}
&= \frac{e^{i \int_{t_2}^{t_1} dt' \Omega_{t'} | - \frac{1}{2} \int_{t_2}^{t_1} dt' \Gamma_{t'} |}}{4 \sqrt{\Omega_{t_1} \Omega_{t_2}}} \int_{-\infty}^{t_{max}} d\tau \theta(t_1 - \tau) e^{2i \int_{\tau}^{t_{min}} dt' \hat{\Omega}_{t'}^*} \\
&\times \int_{-\infty}^{+\infty} \frac{i}{2\pi} d\omega' \frac{e^{-i\omega'(t_2 - \tau)}}{\omega' + i\eta} \frac{\tilde{\Pi}^+(\tau, \hat{\Omega}^* - \omega'; \mathbf{p})}{\Omega_{\tau}} + c.c. + (t_1 \leftrightarrow t_2) \\
&= \frac{e^{i \int_{t_2}^{t_1} dt' \Omega_{t'} | - \frac{1}{2} \int_{t_2}^{t_1} dt' \Gamma_{t'} |}}{4 \sqrt{\Omega_{t_1} \Omega_{t_2}}} \left(\int_{-\infty}^{t_2} + \int_{t_2}^{t_{max}} \right) d\tau \theta(t_1 - \tau) e^{2i \int_{\tau}^{t_{min}} dt' \hat{\Omega}_{t'}^*} \\
&\times \int_{-\infty}^{+\infty} \frac{i}{2\pi} d\omega' \frac{e^{-i\omega'(t_2 - \tau)}}{\omega' + i\eta} \frac{\tilde{\Pi}^+(\tau, \hat{\Omega}^* - \omega'; \mathbf{p})}{\Omega_{\tau}} + c.c. + (t_1 \leftrightarrow t_2).
\end{aligned}$$

Using the residue theorem, the second term vanishes and, using the symmetry of our integrands, we finally evaluate

$$\begin{aligned}
&= \frac{e^{i\left|\int_{t_2}^{t_1} dt' \Omega_{t'}\right| - \frac{1}{2}\left|\int_{t_2}^{t_1} dt' \Gamma_{t'}\right|}}{4\sqrt{\Omega_{t_1}\Omega_{t_2}}} \int_{-\infty}^{t_2} d\tau \theta(t_1 - \tau) e^{2i\int_{\tau}^{t_{min}} dt' \hat{\Omega}_{t'}} \frac{\tilde{\Pi}^+(\tau, \hat{\Omega}^*; \mathbf{p})}{\Omega_{\tau}} \\
&+ c.c. + (t_1 \leftrightarrow t_2) \\
&= \frac{e^{i\left|\int_{t_2}^{t_1} dt' \Omega_{t'}\right| - \frac{1}{2}\left|\int_{t_2}^{t_1} dt' \Gamma_{t'}\right|}}{4\sqrt{\Omega_{t_1}\Omega_{t_2}}} \int_{-\infty}^{t_{min}} d\tau e^{2i\int_{\tau}^{t_{min}} dt' \hat{\Omega}_{t'}} \frac{\tilde{\Pi}^+(\tau, \hat{\Omega}^*; \mathbf{p})}{\Omega_{\tau}} \\
&+ c.c. + (t_1 \leftrightarrow t_2),
\end{aligned}$$

and therefore

$$F_{t_1 t_2}^- = \frac{e^{i\left|\int_{t_2}^{t_1} dt' \Omega_{t'}\right| - \frac{1}{2}\left|\int_{t_2}^{t_1} dt' \Gamma_{t'}\right|}}{2\sqrt{\Omega_{t_1}\Omega_{t_2}}} \int_{-\infty}^{t_{min}} d\tau e^{2i\int_{\tau}^{t_{min}} dt' \hat{\Omega}_{t'}} \frac{\tilde{\Pi}^+(\tau, \hat{\Omega}^*)}{\Omega_{\tau}} + c.c., \quad (\text{B.16})$$

where *c.c.* stands for complex conjugate and $\hat{\Omega}_{\tau} = \Omega_{\tau} - \frac{i}{2}\Gamma_{\tau}$. A somewhat long but similar derivation gives for $F^+(t_1, t_2; \mathbf{p})$

$$F_{t_1 t_2}^+ \simeq \frac{-\cos\left(\int_{t_2}^{t_1} dt' \Omega_{t'}\right) e^{-\frac{1}{2}\left|\int_{t_2}^{t_1} dt' \Gamma_{t'}\right|}}{\sqrt{\Omega_{t_1}\Omega_{t_2}}} \int_{-\infty}^{t_{min}} d\tau e^{-\int_{\tau}^{t_{min}} dt' \Gamma_{t'}} \frac{\text{Re}\tilde{\Pi}^+(\tau, \hat{\Omega}^*)}{\Omega_{\tau}}. \quad (\text{B.17})$$

Comparing Eq. (B.16) and Eq. (B.17), we see that Eq. (B.16) is suppressed, since it contains a rapidly oscillating term in the integrand which frequency is $\Omega_{t'}$. Hence, we ignore the contribution from $F^-(t_1, t_2; \mathbf{p})$ and find from (B.15)

$$\Delta^+(t_1, t_2; \mathbf{p}) \simeq \frac{-\cos\left(\int_{t_2}^{t_1} \Omega_{t'}\right) e^{-\frac{1}{2}\left|\int_{t_2}^{t_1} dt' \Gamma_{t'}\right|}}{\sqrt{\Omega_{t_1}\Omega_{t_2}}} \int_{-\infty}^{t_B} d\tau \frac{\text{Re}\tilde{\Pi}^+(\tau, \hat{\Omega}_{\tau}^*; \mathbf{p})}{\Omega_{\tau}} e^{-\int_{\tau}^{t_B} dt' \Gamma_{t'}} \quad (\text{B.18})$$

where t_B is the Boltzmann time defined as

$$t_B = t_{min} = \min(t_1, t_2), \quad (\text{B.19})$$

which is the time variable for which a generalised Boltzmann holds, as we shall show in the next discussion.

B.2 The Boltzmann equation from QFT

Building on our previous experience of equilibrium field theory, let us define the would-be out-of-equilibrium distribution function $f(t_B; \mathbf{p})$ through the relation

$$1 + 2f(t_B; \mathbf{p}) = - \int_{-\infty}^{t_B} d\tau \frac{2\text{Re}\tilde{\Pi}^+(\tau, \hat{\Omega}_\tau^*; \mathbf{p})}{\Omega_\tau} e^{-\int_\tau^{t_B} dt' \Gamma_{t'}}, \quad (\text{B.20})$$

such that

$$\Delta^+(t_1, t_2; \mathbf{p}) \simeq \frac{\cos\left(\int_{t_2}^{t_1} \Omega_{t'}\right) e^{-\frac{1}{2}\left|\int_{t_2}^{t_1} dt' \Gamma_{t'}\right|}}{\sqrt{\Omega_{t_1} \Omega_{t_2}}} (1 + 2f(t; \mathbf{p})) \quad (\text{B.21})$$

which is the WKB propagator quoted in Eq. (4.26). From these, together with $\Gamma = \Gamma^> - \Gamma^<$ and

$$2\text{Re}\tilde{\Pi}^+(t, \hat{\Omega}; \mathbf{p}) = -\Omega(t; \mathbf{p})(\Gamma^>(t; \mathbf{p}) + \Gamma^<(t; \mathbf{p})), \quad (\text{B.22})$$

taking the derivative of the distribution function shows that it must obey the local Boltzmann equation

$$\frac{df(t_B; \mathbf{p})}{dt} = (1 + f(t_B; \mathbf{p}))\Gamma_{t_B}^< - f(t_B; \mathbf{p})\Gamma_{t_B}^> \quad (\text{B.23})$$

which is equivalently written as

$$\frac{df(t_B; \mathbf{p})}{dt} = -\Gamma_t(f(t_B; \mathbf{p}) - \bar{f}(t_B; \mathbf{p})), \quad (\text{B.24})$$

where $\bar{f}(t; \mathbf{p})$ is defined as

$$\bar{f} = (\Gamma^>/\Gamma^< - 1)^{-1}. \quad (\text{B.25})$$

This closes the discussion regarding the adiabatic WKB propagators and the associated Boltzmann equation as we just proved all relevant equations for section 4.3. The physics discussion is established there.

B.3 The iterative solution of the Boltzmann equation

Here we provide an alternative proof of Eq. (4.38) which is the leading-order adiabatic approximation to the Boltzmann equation. In terms of $\bar{f}(t)$ defined

in Eq. (4.39), the statistical propagator (4.26) or (B.18) can be rewritten as

$$\begin{aligned} & \frac{\cos\left(\int_{t_2}^{t_1} dt' \Omega_{t'}\right) e^{-\frac{1}{2}\left|\int_{t_2}^{t_1} dt' \Gamma_{t'}\right|}}{2\sqrt{\Omega_{t_1}\Omega_{t_2}}} \int_{-\infty}^{t_B} d\tau \Gamma_\tau (1 + 2\bar{f}(\tau)) e^{-\int_\tau^{t_B} dt' \Gamma_{t'}}, \\ & \simeq \frac{\cos\left(\int_{t_2}^{t_1} dt' \Omega_{t'}\right) e^{-\frac{1}{2}\left|\int_{t_2}^{t_1} dt' \Gamma_{t'}\right|}}{2\sqrt{\Omega_{t_1}\Omega_{t_2}}} \left(1 + 2 \int_{-\infty}^{t_B} d\tau \Gamma_\tau \bar{f}(\tau) e^{-\int_\tau^{t_B} dt' \Gamma_{t'}}\right). \end{aligned} \quad (\text{B.26})$$

where we used

$$\int_{-\infty}^t d\tau \Gamma_\tau e^{-\int_\tau^t dt' \Gamma_{t'}} = e^{-\int_\tau^t dt' \Gamma_{t'}} \Big|_{\tau=-\infty}^{\tau=t} = 1 - e^{-\int_{-\infty}^t dt' \Gamma_{t'}} \simeq 1, \quad (\text{B.27})$$

assuming $e^{-\int_{-\infty}^t dt' \Gamma_{t'}} \ll 1$ (or $\int_{-\infty}^t dt' \Gamma_{t'} \gg 1$). Let us focus on the integral in Eq. (B.26) (sending $t_B \rightarrow t$ for the time-being, for notational simplicity), and define

$$f(t) = \int_{-\infty}^t d\tau \Gamma_\tau \bar{f}(\tau) e^{-\int_\tau^t dt' \Gamma_{t'}}. \quad (\text{B.28})$$

Applying a slow-roll condition to the distribution function³, similar to that applied to φ , we get $\bar{f}(\tau) \simeq \bar{f}(t) + (\tau - t)\dot{\bar{f}}(t)$ and again using Eq. (B.27),

$$f(t) \simeq \bar{f}(t) + \dot{\bar{f}}(t) \int_{-\infty}^t d\tau (\tau - t) \Gamma_\tau e^{-\int_\tau^t dt' \Gamma_{t'}}. \quad (\text{B.29})$$

Integrating by parts, the above becomes

$$\begin{aligned} \int_{-\infty}^t d\tau (\tau - t) \Gamma_\tau e^{-\int_\tau^t dt' \Gamma_{t'}} &= \int_{-\infty}^t d\left(e^{-\int_\tau^t dt' \Gamma_{t'}}\right) (\tau - t) \\ &= (\tau - t) e^{-\int_\tau^t dt' \Gamma_{t'}} \Big|_{\tau=-\infty} - \int_{-\infty}^t d\tau e^{-\int_\tau^t dt' \Gamma_{t'}}. \end{aligned} \quad (\text{B.30})$$

Now assuming $\lim_{\tau \rightarrow -\infty} \tau e^{-\int_\tau^t dt' \Gamma_{t'}} \rightarrow 0$, which is always the case provided that the integral $\int_{-\infty}^t d\tau e^{-\int_\tau^t dt' \Gamma_{t'}}$ is finite, then we get

$$\int_{-\infty}^t d\tau (\tau - t) \Gamma_\tau e^{-\int_\tau^t dt' \Gamma_{t'}} \simeq - \int_{-\infty}^t d\tau e^{-\int_\tau^t dt' \Gamma_{t'}}. \quad (\text{B.31})$$

³From Eq. (4.35) it follows that this approximation is justified as far as we assume an adiabatic evolution for Γ_τ , i.e. $|\dot{\Gamma}_\tau/\Gamma_\tau^2| \ll 1$, which was used for the WKB solution to KBEs to begin with.

Finally using the fact that the memory integral in the last equation is dominated by the most recent past time interval (as the integrand is peaked at $\tau = t$), during which the time dependence of Γ can be neglected⁴, we get

$$\int_{-\infty}^t d\tau (\tau - t) \Gamma_\tau e^{-\int_\tau^t dt' \Gamma_{t'}} \simeq - \int_{-\infty}^t d\tau e^{-\Gamma_t \int_\tau^t dt'} = -\frac{1}{\Gamma_t}. \quad (\text{B.32})$$

Thus, Eq. (B.28) becomes

$$f(t) \simeq \bar{f}(t) - \frac{\dot{\bar{f}}(t)}{\Gamma_t}. \quad (\text{B.33})$$

B.4 Gradient expansion of the distribution function

In this Appendix, we determine what constrains the requirement

$$\frac{\dot{\bar{f}}}{\bar{f}} < \bar{f} \Leftrightarrow \frac{\dot{\bar{f}}}{\bar{f}} < \Gamma \quad (\text{B.34})$$

imposes on our model's parameters, assuming we are in thermal equilibrium. In that case, we have

$$\bar{f}_a = f_B(\Omega_a) = (e^{\Omega_a/T} - 1)^{-1} \quad (\text{B.35})$$

such that $\dot{\bar{f}} = \frac{df_B}{d\Omega_a} \frac{d\Omega_a}{dt}$, where, as a first order approximation, we only consider the effective frequency $\Omega_a = \sqrt{m_a^2 + \mathbf{p}^2 + g_a \varphi^2/2 + \mathcal{F}(\varphi, T)(\lambda_a + h)T^2}$, where one can find identify the function $\mathcal{F}(\varphi, T)$, which arises from the one-loop temperature correction, i.e. that of Eq. (4.56) but its precise form does not really matter as it will cancel with itself later on. We compute

$$|\dot{\bar{f}}_a| = \frac{f_B^2(\Omega_a) e^{\Omega_a/T} g_a |\varphi \dot{\varphi}|}{T 2\Omega_a}. \quad (\text{B.36})$$

Taking the two-loop finite temperature width $\Gamma_a = \frac{\lambda_a^2 T^2}{256\pi^3 \Omega_a}$ of Eq. (4.68) (assuming the masses are such that there is no one-loop width, for kinematic reasons, as explained in Sec.4.4.2), we get to the requirement

$$\frac{f_B(\Omega_a) e^{\Omega_a/T} g_a |\varphi \dot{\varphi}|}{T 2} < \frac{\lambda_a^2 T^2}{256\pi^3} \quad (\text{B.37})$$

⁴We expect this to be a good approximation when Γ_t is varying slowly with time (i.e. when Γ satisfies the adiabatic condition $|\dot{\Gamma}|/\Gamma^2 \ll 1$), which, again, we know was assumed in the derivation of the WKB solutions.

We study two limiting cases which we refer to as soft modes ($\Omega < T$) and hard modes ($\Omega > T$), and Taylor expanding in the relevant small quantity, we find

$$|\varphi\dot{\varphi}| < \frac{\lambda_a^2}{g_a} \frac{\Omega_a T^2}{128\pi^3}, \quad \text{for soft modes,} \quad (\text{B.38})$$

$$|\varphi\dot{\varphi}| < \frac{\lambda_a^2}{g_a} \frac{T^3}{128\pi^3}, \quad \text{for hard modes.} \quad (\text{B.39})$$

If the requirement for soft modes holds, it automatically holds for hard modes too. Therefore we only study further the soft condition. Now regardless whether you are in a high φ or high T regime, if the field oscillates harmonically $\varphi(t) = \Phi \cos(\omega_\varphi t)$, its oscillation frequency is dominated by whatever dominates the particles frequencies, too, such that

$$\omega_\varphi \simeq \sqrt{\frac{(\lambda_\phi + h)}{(\lambda_a + h)}} \Omega_a, \quad \text{if } T \text{ dominates,} \quad (\text{B.40})$$

$$\omega_\varphi \simeq \sqrt{\frac{\lambda_\phi}{3g_a}} \Omega_a, \quad \text{if } \varphi \text{ dominates.} \quad (\text{B.41})$$

While for the temperature dominated part, the aforementioned prefactor $\mathcal{F}(\varphi, T)$ exactly appears in both ω_φ and Ω_a , there is a $\frac{1}{3}$ factor difference when it comes to the condensate dominated regime (see Eq. (??) vs. Eqs. (4.21)(4.22)). As a result, starting from the soft mode condition, we get the following constrain for the initial field value

$$\Phi^2 < \sqrt{\frac{(\lambda_a + g_a)}{(\lambda_\phi + h)}} \frac{\lambda_a^2}{g_a} \frac{T^2}{128\pi^3 \sin(\omega_\varphi t) \cos(\omega_\varphi t)}, \quad \text{if } T \text{ dominates } \Omega, \quad (\text{B.42})$$

$$\Phi^2 < \sqrt{\frac{3g_a}{\lambda_\phi}} \frac{\lambda_a^2}{g_a} \frac{T^2}{128\pi^3 \sin(\omega_\varphi t) \cos(\omega_\varphi t)}, \quad \text{if } \varphi \text{ dominates } \Omega, \quad (\text{B.43})$$

which lead to the most conservative constrains

$$\Phi^2 < \sqrt{\frac{(\lambda_a + g_a)}{(\lambda_\phi + h)}} \frac{\lambda_a^2}{g_a} \frac{T^2}{64\pi^3}, \quad \text{if } T \text{ dominates } \Omega, \quad (\text{B.44})$$

$$\Phi^2 < \sqrt{\frac{3g_a}{\lambda_\phi}} \frac{\lambda_a^2}{g_a} \frac{T^2}{64\pi^3}, \quad \text{if } \varphi \text{ dominates } \Omega. \quad (\text{B.45})$$

As a conclusion, for a sufficiently large temperature, the gradient expansion of the distribution function is justified, and if need be, even the couplings can be adjusted so as to have $\Phi \gg T$. Of course, a more realistic treatment would be that of a damped harmonic oscillator, but in that case, we expect the conditions to be less constraining.

Appendix C

Renormalising the 2PI equations of motion

With this Appendix we provide details regarding the self-consistent renormalisation (at finite temperature and non vanishing time-dependent background φ) of the 2PI effective equations of motion and the corresponding divergences appearing in the context of our \mathbb{Z}_2 -symmetric model, under the approximation scheme explained in chapter 4. In particular, we want to show that time-dependent divergences can be consistently absorbed at all times, with time-independent counterterms. We shall present it in detail at one-loop level.

C.1 Counterterms in the 2PI effective action

Expliciting the dependences on the model parameters, the classical action reads

$$S[\phi, \chi; \{p_a\}] = \int_x -\frac{1}{2}\phi(\square+m_\phi^2)\phi - \frac{\lambda_\phi}{4!}\phi^4 - \frac{1}{2}\chi(\square+m_\chi^2)\chi - \frac{\lambda_\chi}{4!}\chi^4 - \frac{h}{4}\chi^2\phi^2, \quad (\text{C.1})$$

where $\{p_a\} = \{m_\phi, m_\chi, \lambda_\phi, \lambda_\chi, h\}$ denotes the set of parameters of our model. For the sake of the renormalisation procedure, we introduce the renormalised

field strengths, masses and couplings as well as their associated counterterms

$$\phi = Z_\phi^{1/2} \phi_r, \quad (\text{C.2})$$

$$\chi = Z_\chi^{1/2} \chi_r, \quad Z_a = 1 + \delta Z_a, \quad (\text{C.3})$$

$$Z_a m_a^2 = m_{a,r}^2 + \delta m_a^2, \quad (\text{C.4})$$

$$Z_a^2 \lambda_a = \lambda_{a,r} + \delta \lambda_a, \quad (\text{C.5})$$

$$Z_\phi Z_\chi h = h_r + \delta h_r. \quad (\text{C.6})$$

where $a = \{\phi, \chi\}$. In terms of those parameters the classical action becomes a functional of the renormalised fields and parameters and rewrites

$$\begin{aligned} S[\phi, \chi; \{g_a\}] &= S[\phi_r, \chi_r; \{g_{a,r}\}] + \int_x -\frac{1}{2} \phi_r (\delta Z_\phi \square + \delta m_\phi^2) \phi_r - \frac{\delta \lambda_\phi}{4!} \phi_r^4 \\ &+ \int_x -\frac{1}{2} \chi_r (\delta Z_\chi \square + \delta m_\chi^2) \chi_r - \frac{\delta \lambda_\chi}{4!} \chi_r^4 - \frac{\delta h}{4} \chi_r^2 \phi_r^2 = S_r + \delta S \end{aligned} \quad (\text{C.7})$$

The terms that add to the renormalised classical action $S[\phi, \chi; \{g_a\}]$ will be referred to as classical counterterms in the coming computations.

We want to absorb the divergences which appear in the 2PI EOM for the propagators Δ_{ab} and φ and therefore want to express the 2PI effective action in terms of the renormalised parameters. First, we note

$$\varphi = \langle \phi \rangle = Z_\phi^{1/2} \langle \phi_r \rangle = Z_\phi^{1/2} \varphi_r, \quad (\text{C.8})$$

$$\Delta_{ab}(x, y) = \langle \phi_a(x) \phi_b(y) \rangle - \varphi_a(x) \varphi_b(y) = Z_a^{1/2} Z_b^{1/2} \Delta_{ab,r}(x, y). \quad (\text{C.9})$$

Then, we recall that the 2PI effective action is given by

$$\Gamma[\varphi, \Delta; \{p_a\}] = S[\varphi, 0; \{p_a\}] + \frac{i}{2} \text{Tr} \ln \Delta^{-1} + \frac{i}{2} \text{Tr} G_0^{-1}[\varphi] \Delta + \Gamma_2[\varphi, \Delta; \{p_a\}], \quad (\text{C.10})$$

which terms will be studied one by one. First, we find

$$S[\varphi, 0; \{p_a\}] = S[\varphi_r, 0; \{p_{a,r}\}] + \int_x \left[-\frac{1}{2} \varphi_r (\delta Z_\phi \square + \delta m_\phi^2) \varphi_r - \frac{\delta \lambda_\phi}{4!} \varphi_r^4 \right]. \quad (\text{C.11})$$

Second, it is immediate to see that

$$\frac{i}{2} \text{Tr} \ln \Delta^{-1} = \frac{i}{2} \text{Tr} \ln \Delta_r^{-1} + (\text{const}). \quad (\text{C.12})$$

Third, the one-loop terms are found using

$$iG_{0,a}^{-1}[\varphi](x, y) = \frac{1}{Z_a} \frac{\delta^2}{\delta \phi_r(x) \delta \phi_r(y)} \left[S_r + \delta S \right] \Bigg|_{(\varphi_r, 0)}$$

$$= \frac{1}{Z_a} \left[\underbrace{-(\square + m_{a,r}^2 + \frac{g_{a,r}}{2} \varphi_r^2) \delta_C(x-y)}_{=iG_{0,a,r}^{-1}[\varphi_r](x,y)} - \underbrace{(\delta Z_\phi \square + \delta m_a^2 + \frac{\delta g_a}{2} \varphi_r^2) \delta_C(x-y)}_{=i\delta G_{0,a,r}^{-1}[\varphi_r](x,y)} \right].$$

Eventually, at second order in the coupling constant, the 2PI effective action of two- or more-loop diagrams reads

$$\begin{aligned} \Gamma_2[\varphi, \Delta; \{g_a\}] &\sim \lambda_a \Delta_{aa}^2 + h \Delta_\phi \Delta_\chi + \varphi^2 \lambda_\phi^2 \Delta_\phi^3 + \varphi^2 h^2 \Delta_\phi \Delta_\chi^2 \\ &= \frac{(\lambda_{a,r} + \delta \lambda_a)}{Z_a^2} Z_a^2 \Delta_{aa,r}^2 + \frac{(h_r + \delta h)}{Z_\phi Z_\chi} Z_\phi \Delta_{\phi,r} Z_\chi \Delta_{\chi,r} \\ &\quad + (Z_\phi^{1/2} \varphi_r)^2 \left(\frac{\lambda_{\phi,r} + \delta \lambda_\phi}{Z_\phi^2} \right)^2 (Z_\phi \Delta_{\phi,r})^3 \\ &\quad + (Z_\phi^{1/2} \varphi_r)^2 \left(\frac{h_r + \delta h}{Z_\phi Z_\chi} \right)^2 (Z_\phi \Delta_{\phi,r}) (Z_\chi \Delta_{\chi,r})^2 \end{aligned} \quad (\text{C.13})$$

from which we conclude that $\Gamma_2[\varphi, \Delta; \{g_a\}] = \Gamma_2[\varphi_r, \Delta_r; \{g_{a,r} + \delta g_a\}]$, which actually holds at all order. This result is crucial because it show that the structure of the diagram in terms of the renormalised propagators is identical, only the vertices get a counterterm counterpart. In the end, in terms of the renormalised parameters and counterterms and up to an additive constant, the 2PI effective action splits as

$$\begin{aligned} \Gamma[\varphi_r, \Delta_r, \{g_{a,r} + \delta g_a\}] &= S[\varphi_r, 0, \{g_{a,r}\}] + \frac{i}{2} \text{Tr} \ln \Delta_r^{-1} + \frac{i}{2} \text{Tr} G_{0,r}^{-1}[\varphi_r] \Delta_r \\ &+ \int_x -\frac{1}{2} \varphi_r (\delta Z_\phi \square + \delta m_\phi^2) \varphi_r - \frac{\delta \lambda_\phi}{4!} \varphi_r^4 + \frac{i}{2} \text{Tr} \delta G_{0,r}^{-1}[\varphi_r] \Delta_r + \Gamma_2[\varphi_r, \Delta_r, \{g_{a,r} + \delta g_a\}]. \end{aligned}$$

C.2 Renormalising at one-loop

Renormalisation conditions usually are imposed on the propagators and n -point functions (e.g. using an $\overline{\text{MS}}$ scheme) because they usually are the quantities of interest in standard vacuum QFT. In this work, what we are after are the (spatially homogeneous and isotropic) EOMs for φ and Δ_{ab} . Therefore, we naturally are led to impose renormalisation conditions on the divergences which appear in those EOMs themselves and not on the n -point functions.

At the level of the EOMs level at second order in the coupling constant expansion, only two quantities require renormalisation, namely the effective dispersion relations of the KBEs which determine the propagators (see Eq. (4.30)),

and the φ_r -effective potential (which appears in the φ_r -EOM (4.49))¹

$$\begin{aligned} \Omega_{a,r}^2(t; \mathbf{p}) &= \mathbf{p}^2 + m_{a,r}^2 + \delta m_a^2 + \frac{(g_{a,r} + \delta g_a)}{2} \varphi_r^2(t) + \text{Re} \tilde{\Pi}_{a,r}^{-\text{crab}}(t, \Omega_{a,r}; \mathbf{p}) \\ &+ \sum_{b=\phi, \chi} \frac{(c_{ab,r} + \delta c_{ab})}{2} \int \frac{d^3 \mathbf{q}}{(2\pi)^3} \left(\frac{1 + 2f_B(\Omega_{b,r}(t; \mathbf{q}))}{2\Omega_{b,r}(t; \mathbf{q})} \right), \end{aligned} \quad (\text{C.14})$$

$$\begin{aligned} V'(\varphi_r) &= m_{\phi,r}^2 \varphi_r + \delta m_{\phi}^2 \varphi_r + \frac{(\lambda_{\phi,r} + \delta \lambda_{\phi})}{6} \varphi_r^3 \\ &+ \varphi_r \sum_{a=\phi, \chi} \frac{(g_{a,r} + \delta g_a)}{2} \int \frac{d^3 \mathbf{p}}{(2\pi)^3} \frac{(1 + 2f_B(\Omega_{a,r}(t; \mathbf{p})))}{2\Omega_{a,r}(t; \mathbf{p})} \end{aligned} \quad (\text{C.15})$$

where $g_{\phi} = \lambda_{\phi}$, $g_{\chi} = h$ and c_{ab} is a 2×2 matrix of couplings such that $c_{aa} = \lambda_a$ and $c_{ab} = h$, cf. (3.13)(3.14). The nonlocal self-energies shall be evaluated as explained in section 4.4.2, wherein we neglect the time dependence of φ within the loops integrals and restore time-translation invariance to find $\tilde{\Pi}_a^-(t, \omega; \mathbf{p}) \simeq \int_0^{\infty} dz e^{i\omega z} \Pi_a^-(z)$, where $z = t - t'$. The time-translation invariant selfenergies read (cf. Eqs. (3.23) and (3.25))

$$\Pi_{a,r}^-(z) = -\tilde{\varphi}_r^2 \sum_{b,c} \ell_{abc,r}^2 \int \frac{d^3 \mathbf{q}}{(2\pi)^3} \int_{-\infty}^{+\infty} dz e^{i\tilde{\Omega}_{a,r}(\mathbf{p})z} \bar{\Delta}_{b,r}^+(z; \mathbf{q}) \bar{\Delta}_{c,r}^-(z; -\mathbf{q}),$$

and ℓ_{abc} is a $2 \times 2 \times 2$ matrix of couplings such that $\ell_{\phi bc} = (\lambda_{\phi} \delta_{b\phi} + h \delta_{b\chi}) \delta_{bc}$, $\ell_{\chi bb} = 0$ and $\ell_{\chi\chi\phi} = \ell_{\chi\phi\chi} = h$.² From now on we shall first identify the counterterms to ensure the finiteness of Eq. (C.14) i.e. that of the Kadanoff-Baym equations (KBE) at all times, and then show that the counterterms identified for it also ensure Eq. (C.15) to be finite at all times. *A priori*, this is a very complicated exercise as they form a set of coupled transcendental equations that ought to be renormalised simultaneously. In the coming sections, we shall show its renormalisability under the assumption that $\Omega_{a,r}$ on the right hand sides of these equations can be written as³

$$\Omega_{a,r}^2(t; \mathbf{p}) = \mathbf{p}^2 + M_{a,r}^2(t), \quad (\text{C.16})$$

¹*A priori* these expressions should also involve the field strength renormalisation parameters δZ_a but we will show that for the theory under consideration here, there is no momentum-dependent divergence, such that we can freely put $\delta Z_a = 1$.

²At second order in the coupling constant expansion $\mathcal{O}(g^2)$, we have $\ell_{abc}^2 = \ell_{abc,r}^2$ as we shall demonstrate that $\delta \ell_{abc} \sim \mathcal{O}(g^2)$.

³This form for the effective frequency is only valid in two cases. Either when solely local corrections are included and computed from the tree-level frequencies, e.g. those of the tadpoles as Eq. (C.14) or when the nontrivial momentum dependence (which can typically not be packed into the form of (C.16)) of the nonlocal corrections are neglected.

with

$$M_{a,r}^2(t) = m_{a,r}^2 + \frac{g_{a,r}}{2} \varphi_r^2(t) + \sum_{b=\phi,\chi} c_{ab,r} T^2 \mathcal{F}_b(g_{b,r} \varphi_r(t); T) \quad (\text{C.17})$$

a loop-induced time-dependent mass which potentially includes both the condensate backreaction and thermal corrections to its mass-shell, through the dimensionless function $\mathcal{F}_b(g_b \varphi_r(t); T)$. Its time-dependence only arises from that of $g_b \varphi_r^2(t)$, either through the effective dimensionful vertices, or through the tree-level backreaction $g_b \varphi_r^2(t)$ on the masses of the particles that run in the loops, see Eq. (4.24). The point here is that it is accompanied by yet another coupling constant, which will be of crucial importance later, when discussing renormalisation at a given order in perturbation theory.

This form of the effective mass is encompassing because it includes both the case where we approximate $\Omega_{a,r}^2(t; \mathbf{p})$ by $\omega_{a,r}^{\text{tree}}(t; \mathbf{p})^2$ (cf. (4.24)) but also goes beyond just that as it allows for thermal corrections to be included as well. In particular, the very high temperature limit of \mathcal{F}_b is known and is given by $\mathcal{F}_b = 1/24$ [21]. Let us now focus on the Kadanoff-Baym equations (KBE) first, and renormalise the associated effective frequency (C.14).

C.3 Computations of the loops diagrams in the KBE

There are two expressions to be computed at the level of the KBE

$$\frac{(c_{ab,r} + \delta c_{ab})}{2} \int \frac{d^3 \mathbf{q}}{(2\pi)^3} \left(\frac{1 + 2f_B(\Omega_{b,r}(t; \mathbf{q}))}{2\Omega_{b,r}(t; \mathbf{q})} \right), \quad (\text{C.18})$$

and

$$\Pi_{a,r}^-(z) = -\bar{\varphi}_r^2 \sum_{b,c} \ell_{abc,r}^2 \int \frac{d^3 \mathbf{q}}{(2\pi)^3} \int_{-\infty}^{+\infty} dz e^{i\bar{\Omega}_{a,r}(\mathbf{p})z} \bar{\Delta}_{b,r}^+(z; \mathbf{q}) \bar{\Delta}_{c,r}^-(z; -\mathbf{q}). \quad (\text{C.19})$$

The divergences come from the f_B -independent part, because the Bose-Einstein regularises the potential ultraviolet divergences and we therefore shall focus on the divergent f_B -independent part first, before moving to the finite f_B -dependent bits.

C.3.1 Tadpole divergence.

For the divergent f_B -independent part of the tadpole, we will employ dimensional regularisation as $4 \rightarrow D \rightarrow 4 - 2\epsilon$ and $d^4q \rightarrow d^D q \mu^{2\epsilon}$ and

$$\begin{aligned} \frac{c_{ab}\mu^{2\epsilon}}{2} \int \frac{d^{D-1}\mathbf{q}}{(2\pi)^{D-1}} \frac{1}{2\Omega_{b,r}(t, \mathbf{q})} &= \frac{c_{ab}\mu^{2\epsilon}}{2} \frac{2\sqrt{\pi}^{-D-1}}{(2\pi)^{D-1}\Gamma(\frac{D-1}{2})} \int_0^\infty dq \frac{q^{D-2}}{2\sqrt{q^2 + M_{b,r}(t)^2}} \\ &= \frac{c_{ab}M_{b,r}(t)^2}{2(4\pi)^2} (N_\epsilon + \ln(M_{b,r}(t)^2/\mu^2) + \mathcal{O}(\epsilon)), \end{aligned} \quad (\text{C.20})$$

where $N_\epsilon = -1 - \epsilon^{-1} - \ln(4\pi) + \gamma_E$ where γ_E is the Euler-Mascheroni constant, and the divergent contribution comes from ϵ^{-1} .

C.3.2 Crab divergence.

Let us now compute the real part of the crab diagram, under the approximation scheme presented in section 4.4.2. We evaluate

$$\begin{aligned} \text{Re}\tilde{\Pi}_{a,r}^{-\text{crab}}(\Omega_{a,r}) &= \frac{1}{2} \left[\int_0^\infty dz (e^{i\Omega_{a,r}z} + e^{-i\Omega_{a,r}z}) \Pi_{a,r}^{-\text{crab}}(z) \right] \\ &= \int_0^\infty dz \cos(\Omega_{a,r}z) \Pi_{a,r}^{-\text{crab}}(z) \\ &= -\varphi_r^2(t) \sum_{b,c} \ell_{abc,r}^2 \int \frac{d^3\mathbf{q}}{(2\pi)^3} \frac{(\frac{1}{2} + f_B(\Omega_{b,r}(t, \mathbf{q})))}{\Omega_{b,r}(t, \mathbf{q})\Omega_{c,r}(t, -\mathbf{q})} \\ &\quad \times \underbrace{\int_0^\infty dz \cos(\Omega_{a,r}(t, \mathbf{p})z) \sin(\Omega_{c,r}(t, -\mathbf{q})z) \cos(\Omega_{b,r}(t, \mathbf{q})z)}_{=I_{abc}} \end{aligned} \quad (\text{C.21})$$

where ℓ_{abc} is a $2 \times 2 \times 2$ matrix of couplings such that $\ell_{\phi bc} = (\lambda_\phi \delta_{b\phi} + h\delta_{b\chi})\delta_{bc}$, $\ell_{\chi bb} = 0$ and $\ell_{\chi\chi\phi} = \ell_{\chi\phi\chi} = h$, cf. Eqs. (3.23)(3.25). Introducing an upper cut-off C (this is not a renormalisation cut-off, rather it helps evaluate I_{abc} analytically), we can then calculate I_{abc} explicitly

$$\begin{aligned} I_{abc} &= \lim_{C \rightarrow +\infty} \frac{1}{4} \left[\frac{1}{\omega_{a \ b \ c}_{+-+}} + \frac{1}{\omega_{a \ b \ c}_{+++}} - \frac{1}{\omega_{a \ b \ c}_{++-}} - \frac{1}{\omega_{a \ b \ c}_{+--}} \right] \rightarrow I_{abc}^{\neq 0} \quad (\text{C.22}) \\ &+ \frac{1}{4} \left[-\frac{\cos\left(C\omega_{a \ b \ c}_{+-+}\right)}{\omega_{a \ b \ c}_{+-+}} - \frac{\cos\left(C\omega_{a \ b \ c}_{+++}\right)}{\omega_{a \ b \ c}_{+++}} + \frac{\cos\left(C\omega_{a \ b \ c}_{++-}\right)}{\omega_{a \ b \ c}_{++-}} + \frac{\cos\left(C\omega_{a \ b \ c}_{+--}\right)}{\omega_{a \ b \ c}_{+--}} \right] \end{aligned}$$

(C.23)

where $\omega_{\alpha\beta\gamma}^{a,b,c}(t, \mathbf{p}, \mathbf{q}) = \alpha\Omega_{a,r}(t, \mathbf{p}) + \beta\Omega_{b,r}(t, \mathbf{q}) + \gamma\Omega_{c,r}(t, \mathbf{q})$. The first line is made of nonnegligible contributions but the second of very quickly oscillating cosines with infinite frequencies, which, once integrated w.r.t. \mathbf{q} , effectively cancel. With that expression, we can evaluate the divergent part of the crab selfenergy using dimensional regularisation. We find

$$\begin{aligned} & \frac{\ell_{abc,r}^2}{2} \int \frac{d^3\mathbf{q}}{(2\pi)^3} \frac{I_{abc}^{\neq 0}(\mathbf{p}, \mathbf{q})}{\Omega_{b,r}(t, \mathbf{q})\Omega_{c,r}(t, -\mathbf{q})} \\ & \stackrel{4 \rightarrow D-2\epsilon}{=} \frac{\ell_{abc,r}^2 \mu^{2\epsilon}}{2} \frac{2\sqrt{\pi}^{D-1}}{(2\pi)^{D-1}\Gamma(\frac{D-1}{2})} \int_0^\infty dq \frac{q^{D-2} I_{abc}^{\neq 0}(\mathbf{q})}{\Omega_{b,r}(t, \mathbf{q})\Omega_{c,r}(t, -\mathbf{q})} \\ & = -\frac{\ell_{abc,r}^2}{2(4\pi)^2} \left(\frac{\Omega_{a,r}(t; \mathbf{p})^2 + M_{b,r}(t)^2 - M_{c,r}(t)^2}{\Omega_{a,r}(t; \mathbf{p})^2} \right) N_\epsilon + (\text{finite})_{abc}. \end{aligned} \quad (\text{C.24})$$

The finite $(\text{finite})_{abc}$ terms will be discussed shortly and at this point, we focus on the divergence, which reads

$$\text{Div} \left[\text{Re}\tilde{\Pi}_{a,r}^{-\text{crab}} \right] = \varphi_r^2(t) \sum_{b,c} \frac{\ell_{abc,r}^2}{2(4\pi)^2} \left(\frac{\Omega_{a,r}(t; \mathbf{p})^2 + M_{b,r}(t)^2 - M_{c,r}(t)^2}{\Omega_{a,r}(t; \mathbf{p})^2} \right) N_\epsilon$$

Recalling Eqs. (3.23)(3.25), the sum over field indices can be performed for the divergent contributions and in both cases the b, c -dependent contributions cancel and so does the momentum dependence on \mathbf{p} , (hence proving that we could indeed require $\delta Z_a = 1$, cf. footnote 1). We find

$$\text{Div} \left[\text{Re}\tilde{\Pi}_a^{-\text{crab}}(\Omega_a) \right] = \frac{\varphi_r^2(t)}{2(4\pi)^2} (g_{a,r}^2 + h_r^2) N_\epsilon. \quad (\text{C.25})$$

Again, we end up with time-dependent divergences.

C.3.3 Finite tadpole

The finite contributions from the tadpole diagrams have two origins. On one hand, there is the finite remainder of the f_B -independent divergent integral, that is the logarithmic contribution in Eq. (C.20), i.e.

$$\frac{c_{ab}M_{b,r}(t)^2}{2(4\pi)^2} \ln(M_{b,r}(t)^2/\mu^2). \quad (\text{C.26})$$

On the other, there are the finite temperature-dependent corrections one has to calculate from

$$\frac{(c_{ab,r} + \delta c_{ab})}{2} \int \frac{d^3\mathbf{q}}{(2\pi)^3} \frac{f_B(\Omega_{b,r}(t; \mathbf{q}))}{\Omega_{b,r}(t; \mathbf{q})} = (c_{ab,r} + \delta c_{ab}) T^2 F_{b,r}(t), \quad (\text{C.27})$$

where we introduced a formal function $F_{b,r}(t)$ which is finite and can be analytically approximated⁴ as

$$F_{b,r}(t) = \frac{1}{(2\pi)^2} \left(\text{Li}_2 \left(e^{-M_{b,r}(t)/T} \right) - \frac{M_{b,r}(t)}{T} \log \left(1 - e^{-M_{b,r}(t)/T} \right) \right), \quad (\text{C.28})$$

where $\text{Li}_2(x)$ is the polylogarithm of order 2 or dilogarithm. In particular, note that in the limit where $M_b^{\text{tree}}(t)/T \rightarrow 0$, this precisely reproduces the standard high temperature result since $F_{b,r}(t)|_{M_{b,r}/T \rightarrow 0} = 1/24$. Also, note that this very function is a perfect candidate to try and selfconsistently implement thermal corrections to the effective frequency (C.16) and mass (C.17), to solve the transcendental equation (C.14), hence the similar notation.

C.3.4 Finite crab

The finite contributions from the crab diagrams have two origins too. On one hand, there is the finite remainder of the f_B -independent divergent integral, that is the $(\text{finite})_{\text{abc}}$ in Eq. (C.24). Those can be evaluated analytically and read

$$\begin{aligned} (\text{finite})_{\text{abc}} &= \frac{\varphi_e^2 \ell_{abc,r}^2 K_{abc}^2}{2(4\pi)^2 \Omega_a^2} \ln \left(-\frac{\Omega_a^2 M_b^2}{K_{abc}^4} \right) \\ &\quad - \frac{\varphi_r^2 \ell_{abc,r}^2 (\Omega_a^2 + M_b^2 - M_c^2)}{2(4\pi)^2 \Omega_a^2} \ln \left(\frac{M_b^2}{\mu^2} \right) \\ &\quad - \frac{\varphi_r^2 \ell_{abc,r}^2 2M_b^2}{2(4\pi)^2 K_{abc}^2} {}_2F_1^{(0,0,1,0)} \left(\frac{1}{2}, 1, 2, -\frac{4\Omega_a^2 M_b^2}{K_{abc}^4} \right) \\ &\quad - \frac{\varphi_r^2 \ell_{abc,r}^2 2M_b^2}{2(4\pi)^2 K_{abc}^2} {}_2F_1^{(0,1,0,0)} \left(\frac{1}{2}, 1, 2, -\frac{4\Omega_a^2 M_b^2}{K_{abc}^4} \right) \end{aligned}$$

where ${}_2F_1$ are hypergeometric functions and

$$K_{abc}^2 = \sqrt{\Omega_a^4 + (M_b^2 - M_c^2)^2 - 2\Omega_a^2(M_b^2 + M_c^2)},$$

and $\Omega_a = \Omega_a(t; \mathbf{p})$.

On the other hand, there are the finite, temperature-dependent f_B -contribution from integrating I_{abc} with the Bose-Einstein distribution function in Eq. (C.21). Those were studied in Ref. [62]. The resulting corrections are finite and of the generic form $-\ell_{abc,r}^2 T \varphi_r^2(t)/32\pi M_{c,r}(t)$.

⁴At worst this analytic approximation overestimates the result by an amount of order $\sim 0.15\%$ in the narrow regime where $M_{b,r}$ and T are precisely comparable.

Both these finite contributions from the crab diagrams are suppressed (compared to the tree-level and local corrections computed above) from both the loop and coupling constant expansion viewpoints and display no qualitatively new parametric dependence on φ or T , hence will be neglected for the remainder of this work.

C.4 Renormalising the Kadanoff-Baym equations

The effective frequencies (C.14), including the divergences and computations of the above finite terms and neglecting the crab ones, read

$$\begin{aligned} \Omega_{a,r}^2(t; \mathbf{p}) &= \mathbf{p}^2 + m_{a,r}^2 + \delta m_a^2 + (g_{a,r} + \delta g_a) \frac{\varphi_r^2(t)}{2} + \frac{\varphi_r^2(t)}{2(4\pi)^2} (g_{a,r}^2 + h_r^2) N_\epsilon \\ &+ \sum_{b=\phi,\chi} (c_{ab,r} + \delta c_{ab}) \left(\frac{M_{b,r}(t)^2}{2(4\pi)^2} (N_\epsilon + \ln(M_{b,r}(t)^2/\mu^2)) + T^2 F_{b,r}(t) \right) \end{aligned}$$

and we now have bring it to a finite value by properly adjusting the Lagrangian parameters or counterterms. The nontrivial, however crucial issues of this formula are the time-dependent contributions that multiply N_ϵ . The Lagrangian parameters have to be adjusted so as to have a finite effective frequency at all times. Let us recall the generic form for the time-dependence of the effective masses (C.17)

$$M_{b,r}^2(t) = m_{b,r}^2 + \frac{g_{b,r}}{2} \varphi_r^2(t) + \sum_{d=\phi,\chi} c_{bd,r} T^2 \mathcal{F}_d(g_{d,r} \varphi_r(t); T).$$

Whenever they multiply a divergence, the time-dependent functions \mathcal{F}_d have to be Taylor expanded in $g_{d,r} \varphi_r(t)$ at the desired order in perturbation theory, because we know that renormalisation only consistently works at each individual order of perturbation theory. For the problem at hand, the leading order time-dependence obtained from this expansion is accompanied by yet another coupling constant and can hence be neglected.⁵ Therefore, we realise that if we wish to cancel the time-dependence of the divergences in Ω_a^2 , a minimal prescription is obtained by solving the following set of linear equations

$$\delta g_a = - \frac{(g_{a,r}^2 + h_r^2)}{(4\pi)^2} N_\epsilon - \sum_{b=\phi,\chi} \frac{(c_{ab,r} + \delta c_{ab})}{2(4\pi)^2} g_{b,r} N_\epsilon, \quad \text{for } a = \phi, \chi. \quad (\text{C.29})$$

This is a set of two equations that connect three variables, namely $\delta\lambda_\phi$, h and $\delta\lambda_\chi$. *A priori*, it ought to be supplemented by a third equation in order to

⁵While this is not valid if the temperature were not constant, it is straightforward to modify (C.29) in that more general case.

be solved exactly. The missing third equation would precisely come from the renormalisation of the Makovian equation of motion for the background of χ and therefore, for the sake of this analysis, we can just set $\delta\lambda_\chi = 0$ because we assumed $\langle\chi\rangle = 0$. Thus, the relations above completely fix δg_a .

That said, a few comments readily are in order at this point. First, closely looking at Eq. (C.29), we can assure that coupling counterterms $\delta g_a = \delta\lambda_\phi, \delta h$ which satisfy it must be of second order in the renormalised coupling constants. This has two crucial consequences. On one hand, as argued in footnote 2, this ensures that $\ell_{abc}^2 = \ell_{abc,r}^2$ at second order in the coupling constants and on the other, the time-dependent divergences coming from $\delta c_{ab} \cdot M_{b,r}(t)^2$ are neglected at second order in the coupling constants. As a result, we can conclude that the time-dependence of the divergences in $\Omega_{a,r}^2(t; \mathbf{p})$ have been taken care of and, baring in mind that we work at second order in perturbation theory, we find

$$\begin{aligned} \Omega_{a,r}^2(t; \mathbf{p}) &= \mathbf{p}^2 + m_{a,r}^2 + \delta m_a^2 + g_{a,r} \frac{\varphi_r^2(t)}{2} \\ &+ \sum_{b=\phi,\chi} \frac{c_{ab,r}}{2(4\pi)^2} \left(\frac{g_{b,r}\varphi_r^2(t)}{2} + \sum_{d=\phi,\chi} c_{bd,r} T^2 \mathcal{F}_d(t) \right) \ln(M_{b,r}^2(t)/\mu^2) \\ &+ \sum_{b=\phi,\chi} c_{ab,r} \left(\frac{m_{b,r}^2}{2(4\pi)^2} (N_\epsilon + \ln(M_{b,r}(t)^2/\mu^2)) + T^2 F_{b,r}(t) \right) \\ &+ \sum_{b=\phi,\chi} \delta c_{ab} \left(\frac{m_{b,r}^2}{2(4\pi)^2} (N_\epsilon + \ln(m_{b,r}^2/\mu^2)) + T^2 F_{b,r}|_{\varphi=0} \right) \end{aligned} \quad (\text{C.30})$$

where we only kept terms at second order in the coupling constants in the products of δc_{ab} with $M_b(t)^2$ and $F_b(t)$. The remaining time-independent divergences are now controlled via mass renormalisation, by fixing δm_a^2 at given $\varphi_0 = \varphi_r(t_0)$, T_0 and renormalisation scale μ . A minimal, and physically well motivated subtraction scheme would e.g. require

$$\begin{aligned} \delta m_a^2 &= -g_{a,r} \frac{\varphi_0^2}{2} \\ &- \sum_{b=\phi,\chi} \frac{c_{ab,r}}{2(4\pi)^2} \left(\frac{g_{b,r}\varphi_0^2}{2} + \sum_{d=\phi,\chi} c_{bd,r} T_0^2 \mathcal{F}_d(t_0) \right) \ln(M_{b,r}^2(t_0)/\mu^2) \\ &- \sum_{b=\phi,\chi} c_{ab,r} \left(\frac{m_{b,r}^2}{2(4\pi)^2} (N_\epsilon + \ln(M_{b,r}(t_0)^2/\mu^2)) + T_0^2 F_{b,r}(t_0) \right) \\ &- \sum_{b=\phi,\chi} \delta c_{ab} \left(\frac{m_{b,r}^2}{2(4\pi)^2} (N_\epsilon + \ln(m_{b,r}^2/\mu^2)) + T_0^2 F_{b,r}|_{\varphi=0} \right). \end{aligned} \quad (\text{C.31})$$

This choice defines $m_{a,r} = m_a^{\text{phys}}(\varphi_0, T_0)$ as the physical mass of particles of type a at certain reference background φ_0 , temperature T_0 and renormalisation scale μ . The renormalised effective frequency then reads

$$\begin{aligned} \Omega_{a,r}^2(t; \mathbf{p}) &= \mathbf{p}^2 + m_{a,r}^2 + \frac{1}{2}g_{a,r}(\varphi_r^2(t) - \varphi_0^2) & (\text{C.32}) \\ &+ \sum_{b=\phi,\chi} \frac{c_{ab,r}g_{b,r}}{4(4\pi)^2} (\varphi_r^2(t) \ln(M_{b,r}(t)^2/\mu^2) - \varphi_0^2 \ln(M_{b,r}(t_0)^2/\mu^2)) \\ &+ \sum_{b,d=\phi,\chi} \frac{c_{ab,r}c_{bd,r}}{2(4\pi)^2} (T^2 \mathcal{F}_d(t) \ln(M_{b,r}(t)^2/\mu^2) - T_0^2 \mathcal{F}_d(t_0) \ln(M_{b,r}(t_0)^2/\mu^2)) \\ &+ \sum_{b=\phi,\chi} c_{ab,r} \left(\frac{m_{b,r}^2}{2(4\pi)^2} \ln(M_{b,r}(t)^2/M_{b,r}(t_0)^2) + T^2 F_{b,r}(t) - T_0^2 F_{b,r}(t_0) \right). \end{aligned}$$

where we used $\ln(M_{b,r}(t)/M_{b,r}(t_0)) = \ln(M_{b,r}(t)^2/\mu) - \ln(M_{b,r}(t_0)^2/\mu^2)$. Renormalising at vanishing background and temperature $\varphi_0 = T_0 = 0$

$$\begin{aligned} \Omega_{a,r}^2(t; \mathbf{p}) &= \mathbf{p}^2 + m_{a,r}^2 + \frac{1}{2}g_{a,r}\varphi_r^2(t) + \sum_{b=\phi,\chi} c_{ab,r}T^2 F_{b,r}(t) & (\text{C.33}) \\ &+ \sum_{b=\phi,\chi} \frac{c_{ab,r}}{2(4\pi)^2} (M_{b,r}^2(t) \ln(M_{b,r}(t)^2/\mu^2) - m_{b,r}^2 \ln(m_{b,r}^2/\mu^2)), \end{aligned}$$

and $m_{a,r} = m_a^{\text{phys}}$ is the vacuum physical mass for particle excitations of the field species a . Defining $\Omega_{a,r}^{\text{eff}}(t; \mathbf{p}) = \mathbf{p}^2 + M_{a,r}^{\text{eff}}(t)^2$, we have a definition for a physical, effective thermal mass given by the following expression

$$\begin{aligned} M_{a,r}^{\text{eff}}(t)^2 &= m_{a,r}^2 + \frac{1}{2}g_{a,r}\varphi_r^2(t) + \sum_{b=\phi,\chi} c_{ab,r}T^2 F_{b,r}(t) & (\text{C.34}) \\ &+ \sum_{b=\phi,\chi} \frac{c_{ab,r}}{2(4\pi)^2} (M_{b,r}^2(t) \ln(M_{b,r}(t)^2/\mu^2) - m_{b,r}^2 \ln(m_{b,r}^2/\mu^2)). \end{aligned}$$

C.5 Renormalised Markovian equation of motion

At the level of the equation of motion for the background field (C.15), we have to evaluate the following one-loop integrals

$$\varphi_r(t) \sum_{a=\phi,\chi} \frac{(g_{a,r} + \delta g_a)}{2} \int \frac{d^3\mathbf{p}}{(2\pi)^3} \frac{(1 + 2f_B(\Omega_{a,r}(t; \mathbf{p})))}{2\Omega_{a,r}(t; \mathbf{p})}. \quad (\text{C.35})$$

The structure of those is identical to the one-loop tadpoles that contributed to the effective frequency (C.14) and we already have evaluated them. Therefore, following the notation introduced in the previous sections, we obtain

$$\begin{aligned} & \varphi_r(t) \sum_{a=\phi,\chi} (g_{a,r} + \delta g_a) \left(\frac{M_{a,r}(t)^2}{2(4\pi)^2} (N_\epsilon + \ln(M_{a,r}(t)^2/\mu^2)) + T^2 F_{a,r}(t) \right) \\ &= \varphi_r(t) \sum_{a=\phi,\chi} g_{a,r} \left(\frac{M_{a,r}(t)^2}{2(4\pi)^2} (N_\epsilon + \ln(M_{a,r}(t)^2/\mu^2)) + T^2 F_{a,r}(t) \right) \\ &+ \varphi_r(t) \sum_{a=\phi,\chi} \delta g_a \left(\frac{m_{a,r}^2}{2(4\pi)^2} (N_\epsilon + \ln(m_{a,r}^2/\mu^2)) + T^2 F_{a,r}(t)|_{\varphi=0} \right). \end{aligned}$$

At this point, the effective potential (C.15) rewrites

$$\begin{aligned} V'(\varphi_r) &= m_{\phi,r}^2 \varphi_r + \delta m_\phi^2 \varphi_r + \frac{(\lambda_{\phi,r} + \delta\lambda_\phi)}{6} \varphi_r^3 \tag{C.36} \\ &+ \varphi_r(t) \sum_{a=\phi,\chi} g_{a,r} \left(\frac{M_{a,r}(t)^2}{2(4\pi)^2} (N_\epsilon + \ln(M_{a,r}(t)^2/\mu^2)) + T^2 F_{a,r}(t) \right) \\ &+ \varphi_r(t) \sum_{a=\phi,\chi} \delta g_a \left(\frac{m_{a,r}^2}{2(4\pi)^2} (N_\epsilon + \ln(m_{a,r}^2/\mu^2)) + T^2 F_{a,r}(t)|_{\varphi=0} \right). \end{aligned}$$

The crucial point here is that the coupling and mass counterterms, respectively $\delta\lambda_\phi$ and δm_ϕ , have respectively already been fixed in Eqs. (C.29) and (C.31). Particularising Eq. (C.29) for $a = \phi$, for which $c_{\phi b,r} = g_{b,r}$, this equation only ever summons δh and $\delta\lambda_\phi$ which are of second order in the couplings, therefore

$$\delta\lambda_\phi = -\frac{3(\lambda_{\phi,r}^2 + h_r^2)}{2(4\pi)^2} N_\epsilon = -\sum_{a=\phi,\chi} \frac{3g_{a,r}^2}{2(4\pi)^2} N_\epsilon \tag{C.37}$$

which, once divided by 6 (cf. (C.36)) exactly cancel the time-dependent divergence of the above expression and the 2PI equations of motion conspire to simultaneously be finite at all times, despite the coupling counterterms are divided by different prefactors. Plugging $\delta\lambda_\phi$ in the above effective potential, we

have

$$\begin{aligned}
V'(\varphi_r) &= m_{\phi,r}^2 \varphi_r + \delta m_{\phi}^2 \varphi_r + \frac{\lambda_{\phi,r}}{6} \varphi_r^3 \\
&+ \varphi_r \sum_{a=\phi,\chi} \frac{g_{a,r}}{2(4\pi)^2} \left(\frac{g_{a,r} \varphi_r(t)}{2} + \sum_b c_{ab,r} T^2 \mathcal{F}_b(t) \right) \ln(M_{a,r}^2(t)/\mu^2) \\
&+ \varphi_r \sum_{a=\phi,\chi} g_{a,r} \left(\frac{m_{a,r}^2}{2(4\pi)^2} (N_\epsilon + \ln(M_{a,r}(t)^2/\mu^2)) + T^2 F_{a,r}(t) \right) \\
&+ \varphi_r \sum_{a=\phi,\chi} \delta g_a \left(\frac{m_{a,r}^2}{2(4\pi)^2} (N_\epsilon + \ln(m_{a,r}^2/\mu^2)) + T^2 F_{a,r}(t)|_{\varphi=0} \right). \quad (C.38)
\end{aligned}$$

Then, using $c_{\phi b,r} = g_{b,r}$ in Eq. (C.31), we find for δm_{ϕ}^2

$$\begin{aligned}
\delta m_{\phi}^2 &= -\lambda_{\phi,r} \frac{\varphi_0^2}{2} \\
&- \sum_{b=\phi,\chi} \frac{g_{b,r}}{2(4\pi)^2} \left(\frac{g_{b,r} \varphi_0^2}{2} + \sum_d c_{bd,r} T_0^2 \mathcal{F}_d(t_0) \right) \ln(M_{b,r}^2(t_0)/\mu^2) \\
&- \sum_{b=\phi,\chi} g_{b,r} \left(\frac{m_{b,r}^2}{2(4\pi)^2} (N_\epsilon + \ln(M_{b,r}(t_0)^2/\mu^2)) + T_0^2 F_{b,r}(t_0) \right) \\
&- \sum_{b=\phi,\chi} \delta g_b \left(\frac{m_{b,r}^2}{2(4\pi)^2} (N_\epsilon + \ln(m_{b,r}^2/\mu^2)) + T_0^2 F_{b,r}|_{\varphi=0} \right). \quad (C.39)
\end{aligned}$$

This precisely takes care of all divergences that appear in the effective potential and again renormalising at vanishing background and temperature, we find

$$\begin{aligned}
V'(\varphi_r) &= m_{\phi,r}^2 \varphi_r(t) + \frac{\lambda_{\phi,r}}{6} \varphi_r^3(t) + \varphi_r(t) T^2 \sum_{b=\phi,\chi} g_{b,r} F_{b,r}(t) \\
&+ \sum_{b=\phi,\chi} \frac{g_{b,r}}{2(4\pi)^2} (M_{b,r}^2(t) \ln(M_{b,r}(t)^2/\mu^2) - m_{b,r}^2 \ln(m_{b,r}^2/\mu^2)). \quad (C.40)
\end{aligned}$$

This last expression closes the discussion on the renormalisation of the 2PI equations of motion in a time-dependent background $\varphi_r(t)$ and Eqs. (C.34) and (C.40) provide the effective mass or frequency, together with the effective potential, including quantum and thermal corrections in the 2PI framework which allows for a consistent treatment of resummation and backreactions of the time-dependent background.

Appendix D

Evaluating the crab diagram

We here evaluate the crab diagram under the assumptions described in section 4.4.2 needed for the thermal width. Using (3.23) and (3.25), together with the approximate WKB propagators (4.58) of section 4.4.2, we evaluate the Fourier transforms as

$$\begin{aligned}
 \Pi_a^{-\text{crab}}(p^0, \mathbf{p}) &= \int_{-\infty}^{+\infty} dz e^{izp^0} \Pi_a^{-\text{crab}}(z; \mathbf{p}) \\
 &= -\bar{\varphi}^2 \sum_{b,c=\phi,\chi} \ell_{abc}^2 \int_{-\infty}^{+\infty} dz e^{izp^0} \int \frac{d^3\mathbf{q}}{(2\pi)^3} \bar{\Delta}_b^+(z; \mathbf{q}) \bar{\Delta}_c^-(z; \mathbf{p} - \mathbf{q}) \\
 &= -\bar{\varphi}^2 \sum_{b,c=\phi,\chi} \ell_{abc}^2 \int \frac{d^3\mathbf{q}}{(2\pi)^3} \int_{-\infty}^{+\infty} dz e^{izp^0} \bar{\Delta}_b^+(z; \mathbf{q}) \bar{\Delta}_c^-(z; \mathbf{p} - \mathbf{q}), \quad (\text{D.1})
 \end{aligned}$$

where t_{abc} is a $2 \times 2 \times 2$ matrix of couplings such that $t_{\phi bc} = (\lambda_\phi \delta_{b\phi} + h \delta_{b\chi}) \delta_{bc}$, $t_{\chi bb} = 0$ and $t_{\chi\chi\phi} = t_{\chi\phi\chi} = h$. Overbarred quantities are time-dependent quantities considered as constant only within loop integrals, and then evaluated at the relevant reference time set by the quantity of interest, e.g. the thermal width $\Gamma_a(t; \mathbf{p}) = \Pi^-(\bar{\Omega}_a(\mathbf{p}); \mathbf{p})/2i\bar{\Omega}_a(\mathbf{p})$, as explained in section 4.4.2. The

z -integral can be performed using Eq. (4.58) and we find

$$\begin{aligned}
& \int_{-\infty}^{+\infty} dz e^{izp^0} \Delta_b^+(z; \mathbf{q}) \Delta_c^-(z; \mathbf{p} - \mathbf{q}) = \\
& = \int_{-\infty}^{+\infty} dz e^{izp^0} \frac{\cos(\bar{\Omega}_b(\mathbf{q}) \cdot z) \sin(\bar{\Omega}_c(\mathbf{p} - \mathbf{q}) \cdot z)}{\bar{\Omega}_b(\mathbf{q}) \bar{\Omega}_c(\mathbf{p} - \mathbf{q})} \left(\frac{1}{2} + f_B(\bar{\Omega}_b(\mathbf{q})) \right) \\
& = \frac{(\frac{1}{2} + f_B(\bar{\Omega}_b(\mathbf{q})))}{\bar{\Omega}_b(\mathbf{q}) \bar{\Omega}_c(\mathbf{p} - \mathbf{q})} \int_{-\infty}^{+\infty} dz e^{izp^0} \cos(\bar{\Omega}_b(\mathbf{q}) \cdot z) \sin(\bar{\Omega}_c(\mathbf{p} - \mathbf{q}) \cdot z) \\
& = \frac{-\pi i (1 + 2f_B(\bar{\Omega}_b(\mathbf{q})))}{4 \bar{\Omega}_b(\mathbf{q}) \bar{\Omega}_c(\mathbf{p} - \mathbf{q})} \left[\delta(p^0 + \bar{\Omega}_b(\mathbf{q}) + \bar{\Omega}_c(\mathbf{p} - \mathbf{q})) \right. \\
& \quad + \delta(-p^0 + \bar{\Omega}_b(\mathbf{q}) - \bar{\Omega}_c(\mathbf{p} - \mathbf{q})) \\
& \quad - \delta(p^0 + \bar{\Omega}_b(\mathbf{q}) - \bar{\Omega}_c(\mathbf{p} - \mathbf{q})) \\
& \quad \left. - \delta(p^0 - \bar{\Omega}_b(\mathbf{q}) - \bar{\Omega}_c(\mathbf{p} - \mathbf{q})) \right]. \quad (\text{D.2})
\end{aligned}$$

In light of Eqs. (D.2) and (D.1), let us consider the following abstract \mathbf{q} -integral

$$I_{abc}^{(\alpha, \beta)}(p^0, \mathbf{p}) = \int \frac{d^3 \mathbf{q}}{(2\pi)^3} \frac{(1 + 2f_B(\bar{\Omega}_b(\mathbf{q})))}{\bar{\Omega}_b(\mathbf{q}) \bar{\Omega}_c(\mathbf{p} - \mathbf{q})} \delta(\alpha p^0 + \beta \bar{\Omega}_b(\mathbf{q}) - \bar{\Omega}_c(\mathbf{p} - \mathbf{q})), \quad (\text{D.3})$$

where $\alpha, \beta = \pm 1$. Then Eq. (D.1) can be written as

$$\Pi_a^{\text{-crab}}(p^0, \mathbf{p}) = \frac{i\pi \bar{\varphi}^2}{4} \sum_{b, c = \phi, \chi} \ell_{abc}^2 \left(I_{abc}^{(-1, -1)} + I_{abc}^{(-1, 1)} - I_{abc}^{(1, 1)} - I_{abc}^{(1, -1)} \right). \quad (\text{D.4})$$

One angle integral in Eq. (D.3) can be performed to yield ($q = |\mathbf{q}|$)

$$\begin{aligned}
I_{abc}^{(\alpha, \beta)} & = \int_0^\infty \frac{q^2 dq}{(2\pi)^2} \int_{-1}^1 dx \frac{(1 + 2f_B(\bar{\Omega}_b(q)))}{\bar{\Omega}_b(q) \bar{\Omega}_c(|\mathbf{p} - \mathbf{q}|)} \delta(\alpha p^0 + \beta \bar{\Omega}_b(q) - \bar{\Omega}_c(|\mathbf{p} - \mathbf{q}|)) \\
& = \int_0^\infty \frac{q^2 dq}{(2\pi)^2} \frac{(1 + 2f_B(\bar{\Omega}_b(q)))}{\bar{\Omega}_b(q)} \int_{-1}^1 dx \frac{\delta(\alpha p^0 + \beta \bar{\Omega}_b(q) - \bar{\Omega}_c(|\mathbf{p} - \mathbf{q}|))}{\bar{\Omega}_c(|\mathbf{p} - \mathbf{q}|)}, \quad (\text{D.5})
\end{aligned}$$

where we replaced $\mathbf{q} \rightarrow q$ (similarly for $\mathbf{p} \rightarrow p$) and $\mathbf{p} - \mathbf{q} \rightarrow |\mathbf{p} - \mathbf{q}|$ in the argument for Ω and x is defined by $x = \frac{\mathbf{p} \cdot \mathbf{q}}{|\mathbf{p}| |\mathbf{q}|}$ (so that $|\mathbf{p} - \mathbf{q}| = \sqrt{p^2 + q^2 - 2pqx}$). The x -integral in Eq. (D.5) is

$$\int_{-1}^1 dx \frac{\delta(\alpha p^0 + \beta \bar{\Omega}_b(q) - \bar{\Omega}_c(|\mathbf{p} - \mathbf{q}|))}{\bar{\Omega}_c(|\mathbf{p} - \mathbf{q}|)} = \frac{\theta(\alpha p^0 + \beta \bar{\Omega}_b(q)) \theta(1 - x_0^2)}{[\alpha p^0 + \beta \bar{\Omega}_b(q)] |\partial_x \bar{\Omega}_c(|\mathbf{p} - \mathbf{q}|)|_{x=x_0}}, \quad (\text{D.6})$$

where x_0 is the solution of $\alpha p^0 + \beta \bar{\Omega}_b(\mathbf{q}) - \bar{\Omega}_c(|\mathbf{p} - \mathbf{q}|) = 0$, i.e. (using Eq. (4.23))

$$x_0 = \frac{\bar{M}_c^2(t) - \xi_a^2 - \bar{M}_b^2(t) - 2\alpha\beta p^0 \bar{\Omega}_b(\mathbf{q})}{2pq}, \quad (\text{D.7})$$

where the tree-level mass is defined in Eq. (3.2) where we defined

$$\xi_a^2 = p_0^2 - \mathbf{p}^2 \quad (\text{D.8})$$

which determines whether the external particle is on- or off-shell and thus carries the species label a . We now calculate

$$|\partial_x \bar{\Omega}_c(|\mathbf{p} - \mathbf{q}|)|_{x=x_0} = \frac{pq}{|\bar{\Omega}_c(|\mathbf{p} - \mathbf{q}|)|_{x=x_0}} = \frac{pq}{|\alpha p^0 + \beta \bar{\Omega}_b(\mathbf{q})|}. \quad (\text{D.9})$$

Then x -integral (D.6) becomes

$$\int_{-1}^1 dx \frac{\delta(\alpha p^0 + \beta \bar{\Omega}_b(\mathbf{q}) - \bar{\Omega}_c(|\mathbf{p} - \mathbf{q}|))}{\bar{\Omega}_c(|\mathbf{p} - \mathbf{q}|)} = \frac{\theta(\alpha p^0 + \beta \bar{\Omega}_b(\mathbf{q})) \theta(1 - x_0^2)}{pq} \quad (\text{D.10})$$

and Eq. (D.5) becomes (using Eq. (4.23))

$$\begin{aligned} I_{abc}^{(\alpha,\beta)}(p^0, \mathbf{p}) &= \frac{1}{p} \int_0^\infty \frac{qdq}{(2\pi)^2} \frac{(1 + 2f_B(\bar{\Omega}_b(\mathbf{q})))}{\bar{\Omega}_b(\mathbf{q})} \theta(\alpha p^0 + \beta \bar{\Omega}_b(\mathbf{q})) \theta(1 - x_0^2) \\ &= \frac{1}{p} \int_{\bar{M}_b}^\infty \frac{d\omega_b}{(2\pi)^2} (1 + 2f_B(\omega_b)) \theta(\alpha p^0 + \beta \omega_b) \theta(1 - x_0^2). \end{aligned} \quad (\text{D.11})$$

Due to the step functions and the lower limit of the integral, the above integral is non-vanishing when there exists a range of ω_b that satisfies

$$\omega_b > \bar{M}_b(t), \quad (\text{D.12})$$

$$\alpha p^0 + \beta \omega_b > 0, \quad (\text{D.13})$$

$$\frac{(\bar{M}_c^2(t) - \xi_a^2 - \bar{M}_b^2(t) - 2\alpha\beta p^0 \omega_b)^2}{4p^2 (\omega_b^2 - \bar{M}_b^2(t))} < 1. \quad (\text{D.14})$$

The inequality (D.14) can be rewritten as

$$4\xi_a^2 \omega_b^2 - 4\alpha\beta p^0 (\bar{M}_c^2 - \xi_a^2 - \bar{M}_b^2) \omega_b + (\bar{M}_c^2 - \xi_a^2 - \bar{M}_b^2)^2 + 4p^2 \bar{M}_b^2 < 0, \quad (\text{D.15})$$

This is equivalent to the inequality

$$\omega_b \in]\omega_{abc}^{(\alpha\beta)-}, \omega_{abc}^{(\alpha\beta)+}[, \text{ if } \xi_a^2 \geq 0 \quad (\text{D.16})$$

$$\omega_b \notin]\omega_{abc}^{(\alpha\beta)-}, \omega_{abc}^{(\alpha\beta)+}[, \text{ if } \xi_a^2 \leq 0, \quad (\text{D.17})$$

with (for $\alpha\beta = \pm 1$)

$$\omega_{abc}^{(\alpha\beta)\pm} = \frac{-\alpha\beta(\xi_a^2 + \bar{M}_b^2 - \bar{M}_c^2) p^0 \pm p \sqrt{(\xi_a^2 - (\bar{M}_b + \bar{M}_c)^2) (\xi_a^2 - (\bar{M}_b - \bar{M}_c)^2)}}{2\xi_a^2}. \quad (\text{D.18})$$

The quantities $\omega_{abc}^{(\alpha\beta)\pm}$ given in Eq. (D.18) can be real only when the term inside the square root in Eq. (D.18) is real and positive, i.e. when

$$(\xi_a^2 - (\bar{M}_b + \bar{M}_c)^2) (\xi_a^2 - (\bar{M}_b - \bar{M}_c)^2) \geq 0. \quad (\text{D.19})$$

The on-shell case $\xi_a^2 = \bar{M}_a^2$ or $p^0 = \bar{\Omega}_a(\mathbf{p})$. Let us examine Eq. (D.19) in the case where $\xi_a^2 = \bar{M}_a^2$. The equality clearly excludes the case $a = b = c$. The inequality (D.19) also tells us that $a = b \neq c$ (or $a = c \neq b$) is also excluded unless $\bar{M}_c > 2\bar{M}_a$ (or $\bar{M}_b > 2\bar{M}_a$). The case $a \neq b \neq c$ need not be treated because we are in a two-field system. Now let us investigate the following relevant cases :

- Case $a = b = c$: This cannot contribute due to inequality (D.19).
- Case $a = b \neq c$: This can contribute when

$$\bar{M}_c > 2\bar{M}_a. \quad (\text{D.20})$$

- Case $a = c \neq b$: This can contribute when

$$\bar{M}_b > 2\bar{M}_a. \quad (\text{D.21})$$

- Case $a \neq b = c$: This can contribute when

$$\bar{M}_a > 2\bar{M}_b. \quad (\text{D.22})$$

To summarise, $I_{abc}^{(\alpha,\beta)}$ given in Eq. (D.11) (also in Eq. (D.3)) is non-vanishing when there exists an interval of ω_b , which simultaneously satisfies the inequalities (D.12), (D.13) and (D.16) provided that the inequality (D.19) is satisfied. Let us denote such an interval by (ω^-, ω^+) . For given (α, β) , one can find ω^- and ω^+ by working out inequalities (D.12), (D.13) and (D.16) with Eq. (D.18), and the result is shown in Table D.1. Note that for a given choice of (a, b, c) , only one choice of (α, β) can allow for such a non-empty interval.

Case (α, β)	$a = b = c$	$a = b \neq c$	$a \neq b = c$	$b \neq a = c$
(1, 1)	×	$\omega^\pm = \omega_{abc}^{(1)\pm}$	×	×
(1, -1)	×	×	$\omega^\pm = \omega_{abc}^{(-1)\pm}$	×
(-1, 1)	×	×	×	$\omega^\pm = \omega_{abc}^{(-1)\pm}$

Table D.1: Values of ω^\pm for which the interval (ω^-, ω^+) that satisfies inequalities (D.12), (D.13) and (D.16) allow for non-vanishing $I_{abc}^{(\alpha, \beta)}$. Here \times denotes that such an interval does not exist. $\omega_{abc}^{(\alpha, \beta)\pm}$ are given in Eq. (D.18) and they are meant to be used only for those cases where the inequality (D.19) (i.e. inequalities (D.20)-(D.22)) is satisfied.

Once one has found ω^- and ω^+ given in table D.1, the integral (D.11) becomes

$$\begin{aligned}
I_{abc}^{(\alpha, \beta)}(\mathbf{p}) &= \frac{1}{\mathfrak{p}} \int_{\omega^-}^{\omega^+} \frac{d\omega_b}{(2\pi)^2} (1 + 2f_B(\omega_b)) \\
&= \frac{1}{\mathfrak{p}(2\pi)^2} \left[\omega^- - \omega^+ + 2T \log \left(\frac{f_B(\omega^-)}{f_B(\omega^+)} \right) \right] \quad (\text{D.23})
\end{aligned}$$

with a product of a proper Heaviside step function such as $\theta(\bar{M}_a - 2\bar{M}_b)$ implied (see inequalities (D.20)-(D.22)). Then, using (D.4), (D.23) and Table D.1, one can compute $\Pi_\chi^{\text{-crab}}$ and $\Pi_\phi^{\text{-crab}}$ using (3.23) and (3.25). $\Pi_\chi^{\text{-crab}}$ is given by

$$\begin{aligned}
\Pi_\chi^{\text{-crab}}(\bar{\Omega}_\chi(\mathbf{p}), \mathbf{p}) &= \int_{-\infty}^{+\infty} dz e^{iz\bar{\Omega}_\chi(\mathbf{p})} \Pi_\chi^{\text{-crab}}(z; \mathbf{p}) \\
&= i \frac{\pi h^2 \bar{\varphi}^2}{4} \left(I_{\chi bc}^{(-1,1)} - I_{\chi bc}^{(1,1)} - I_{\chi bc}^{(1,-1)} \right)_{(b=\chi, c=\phi)} + (b \leftrightarrow c) \\
&= -i \frac{\pi h^2 \bar{\varphi}^2}{4} \left(I_{\chi\chi\phi}^{(1,1)} - I_{\chi\phi\chi}^{(-1,1)} \right) \\
&= -i \theta(\bar{M}_\phi - 2\bar{M}_\chi) \frac{h^2 \bar{\varphi}^2}{16\pi\mathfrak{p}} \left[\omega_{\chi\chi\phi}^{(1)-} - \omega_{\chi\chi\phi}^{(1)+} + 2T \log \left(\frac{f_B(\omega_{\chi\chi\phi}^{(1)-})}{f_B(\omega_{\chi\chi\phi}^{(1)+})} \right) \right. \\
&\quad \left. - \omega_{\chi\phi\chi}^{(-1)-} + \omega_{\chi\phi\chi}^{(-1)+} - 2T \log \left(\frac{f_B(\omega_{\chi\phi\chi}^{(-1)-})}{f_B(\omega_{\chi\phi\chi}^{(-1)+})} \right) \right] \\
&= -i \theta(\bar{M}_\phi - 2\bar{M}_\chi) \frac{h^2 \bar{\varphi}^2 T}{8\pi\mathfrak{p}} \log \left(\frac{f_B(\omega_{\chi\chi\phi}^{(1)-}) f_B(\omega_{\chi\phi\chi}^{(-1)+})}{f_B(\omega_{\chi\chi\phi}^{(1)+}) f_B(\omega_{\chi\phi\chi}^{(-1)-})} \right). \quad (\text{D.24})
\end{aligned}$$

Here $\omega_{\chi\chi\phi}^{(1)\pm}$ and $\omega_{\chi\phi\chi}^{(-1)\pm}$ are obtained from Eq. (D.18) by setting $\{a = b = \chi, c = \phi, \alpha\beta = 1\}$ and $\{a = c = \chi, b = \phi, \alpha\beta = -1\}$, respectively, i.e.

$$\omega_{\chi\chi\phi}^{(1)\pm} = \frac{(\bar{M}_\phi^2 - 2\bar{M}_\chi^2)\sqrt{p^2 + \bar{M}_\chi^2} \pm p\bar{M}_\phi\sqrt{\bar{M}_\phi^2 - 4\bar{M}_\chi^2}}{2\bar{M}_\chi^2}, \quad (\text{D.25})$$

$$\omega_{\chi\phi\chi}^{(-1)\pm} = \frac{\bar{M}_\phi^2\sqrt{p^2 + \bar{M}_\chi^2} \pm p\bar{M}_\phi\sqrt{\bar{M}_\phi^2 - 4\bar{M}_\chi^2}}{2\bar{M}_\chi^2}. \quad (\text{D.26})$$

In the same way as for $\Pi_\chi^{-\text{crab}}$ we obtain $\Pi_\phi^{-\text{crab}}$ as

$$\begin{aligned} \Pi_\phi^{-\text{crab}}(\bar{\Omega}_\phi(\mathbf{p}), \mathbf{p}) &= \int_{-\infty}^{+\infty} dz e^{iz\bar{\Omega}_\phi(\mathbf{p})} \Pi_\phi^{-\text{crab}}(z; \mathbf{p}) \\ &= -i \frac{\pi \bar{\varphi}^2}{4} h^2 I_{\phi\chi\chi}^{(1,-1)}(\mathbf{p}) \\ &= -i \frac{\bar{\varphi}^2}{16\pi p} h^2 \theta(\bar{M}_\phi - 2\bar{M}_\chi) \left[\omega_{\phi\chi\chi}^{(-1)-} - \omega_{\phi\chi\chi}^{(-1)+} + 2T \log \left(\frac{f_B(\omega_{\phi\chi\chi}^{(-1)-})}{f_B(\omega_{\phi\chi\chi}^{(-1)+})} \right) \right] \end{aligned} \quad (\text{D.27})$$

$$= -i \frac{\bar{\varphi}^2 T}{16\pi p} h^2 \theta(\bar{M}_\phi - 2\bar{M}_\chi) \log \left(\frac{f_B(\omega_{\phi\chi\chi}^{(-1)-}) f_B(-\omega_{\phi\chi\chi}^{(-1)-})}{f_B(\omega_{\phi\chi\chi}^{(-1)+}) f_B(-\omega_{\phi\chi\chi}^{(-1)+})} \right) \quad (\text{D.28})$$

with $\omega_{\phi\chi\chi}^{(-1)\pm}$ being

$$\omega_{\phi\chi\chi}^{(-1)\pm} = \frac{\bar{M}_\phi^2\sqrt{p^2 + \bar{M}_\phi^2} \pm p\bar{M}_\phi\sqrt{\bar{M}_\phi^2 - 4\bar{M}_\chi^2}}{2\bar{M}_\phi^2}. \quad (\text{D.29})$$

In the last equality of Eq. (D.28), we used $\omega = T \log \left(\frac{-f_B(-\omega)}{f_B(\omega)} \right)$. Eq. (D.28) is consistent with the on-shell part of the result of Ref. [71].

Appendix E

The neutrino-QED interaction rate

E.1 Connection of the damping rate to the Boltzmann collision term

We demonstrate in this section the correspondence, at leading order, between the neutrino damping rate calculated from the retarded selfenergy represented by figure 6.1, and the usual Boltzmann collision term for the $2 \rightarrow 2$ scattering processes (6.54).

For brevity we illustrate in detail only the selfenergy diagram (b) in figure 6.1, or, equivalently, equation (6.56); the correspondence between the two approaches for the other three selfenergy terms can be easily established in the same manner. For $a = -$ and $b = +$ (hence $ba = <$ and $ab = >$) and plugging into equation (6.56) the Wightman propagators (6.59), we have

$$\begin{aligned} \text{Tr} \left[\not{p} \Sigma_{(b)}^<(p) \right] &= -2 \left(\frac{G_F}{\sqrt{2}} \right)^2 \int \frac{d^4 \ell d^4 q}{(2\pi)^8} f_D(\ell^0) (1 - f_D(\ell^0 + q^0 - p^0)) f_D(q^0) \times \\ &\text{Tr} \left[\not{p} \gamma^\mu (1 - \gamma_5) \rho_\nu(\ell) \gamma^\nu (1 - \gamma_5) \rho_e(\ell + q - p) \gamma_\mu (g_{V,e} - g_{A,e} \gamma_5) \rho_e(q) \gamma_\nu (1 - \gamma_5) \right], \end{aligned} \quad (\text{E.1})$$

which is generally valid for any spectral density $\rho_\psi(p)$. At leading order we use the free spectral density (6.60), so that equation (E.1) reduces to

$$\begin{aligned} \text{Tr} \left[\not{p} \Sigma_{(b)}^<(p) \right] &= -G_F^2 \int \frac{d^4\ell d^4q}{(2\pi)^5} f_D(\ell^0)(1 - f_D(\ell^0 + q^0 - p^0)) f_D(q^0) \\ &\times \text{sgn}(\ell^0) \text{sgn}(\ell^0 + q^0 - p^0) \text{sgn}(q^0) \delta(\ell^2) \delta((\ell + q - p)^2 - m_e^2) \delta(q^2 - m_e^2) \text{Tr}_b, \end{aligned} \quad (\text{E.2})$$

where we have defined

$$\text{Tr}_b = \text{Tr} \left[\not{p} \gamma^\mu (1 - \gamma_5) \not{\ell} \gamma^\nu (1 - \gamma_5) (\not{\ell} + \not{q} - \not{p} + m_e) \gamma_\mu (g_{V,e} - g_{A,e} \gamma_5) (\not{q} + m_e) \gamma_\nu (1 - \gamma_5) \right], \quad (\text{E.3})$$

which contains all of the Dirac algebra of the problem at hand. Using resummed spectral densities in (E.1) would correspond to dressing all particles into quasiparticles with thermal masses and widths, which is a convenient way to introduce some higher order FTQED corrections, in particular (but not only) those assigned to thermal masses [70].

In order to connect to kinetic theory and the Boltzmann collision term, we introduce a 4-dimensional Dirac delta distribution in u and then integrate over u :

$$\begin{aligned} \text{Tr} \left[\not{p} \Sigma_{(b)}^<(p) \right] &= -G_F^2 \int \frac{d^4\ell d^4q d^4u}{(2\pi)^9} (2\pi)^4 \delta^{(4)}(u - q - \ell + p) f_D(\ell^0) (1 - f_D(u^0)) \\ &\times f_D(q^0) \text{sgn}(\ell^0) \text{sgn}(u^0) \text{sgn}(q^0) \delta(\ell^2) \delta(u^2 - m_e^2) \delta(q^2 - m_e^2) \text{Tr}_b. \end{aligned} \quad (\text{E.4})$$

Note that this step does not change the physics of the expression; it merely recasts the expression in a more convenient form for our purposes. Then,

cycling through all possible sign combinations of ℓ^0 , u^0 , and q^0 yields

$$\begin{aligned}
\text{Tr} \left[\not{p} \Sigma_{(b)}^<(p) \right] = & -G_F^2 \int \frac{d^3 \ell d^3 \mathbf{q} d^3 \mathbf{u}}{(2\pi)^9 8\omega_\ell \omega_q \omega_u} (2\pi)^4 \delta^{(3)}(\mathbf{u} - \mathbf{q} - \boldsymbol{\ell} + \mathbf{p}) \\
& \times \left[f_\ell (1 - f_u) f_q \delta(\omega_u - \omega_q - \omega_\ell + p^0) \text{Tr}_b^{+++} \right. \\
& \quad - f_\ell (1 - f_u) (1 - f_q) \delta(\omega_u + \omega_q - \omega_\ell + p^0) \text{Tr}_b^{++-} \\
& \quad - f_\ell f_u f_q \delta(-\omega_u - \omega_q - \omega_\ell + p^0) \text{Tr}_b^{+-+} \\
& \quad - (1 - f_\ell) (1 - f_u) f_q \delta(\omega_u - \omega_q + \omega_\ell + p^0) \text{Tr}_b^{-++} \\
& \quad + f_\ell f_u (1 - f_q) \delta(-\omega_u + \omega_q - \omega_\ell + p^0) \text{Tr}_b^{+--} \\
& \quad + (1 - f_\ell) f_u f_q \delta(-\omega_u - \omega_q + \omega_\ell + p^0) \text{Tr}_b^{-+-} \\
& \quad + (1 - f_\ell) (1 - f_u) (1 - f_q) \delta(\omega_u + \omega_q + \omega_\ell + p^0) \text{Tr}_b^{-+-} \\
& \quad \left. - (1 - f_\ell) f_u (1 - f_q) \delta(-\omega_u + \omega_q + \omega_\ell + p^0) \text{Tr}_b^{---} \right], \tag{E.5}
\end{aligned}$$

where we have defined

$$\text{Tr}_b^{ijk} = \text{Tr}_b |_{\ell^0=i\omega_\ell, u^0=j\omega_u, q^0=k\omega_q}, \tag{E.6}$$

and used the vacuum dispersion relations $\omega_\ell = |\boldsymbol{\ell}|$, $\omega_u^2 = |\mathbf{u}|^2 + m_e^2$, and $\omega_q^2 = |\mathbf{q}|^2 + m_e^2$. The particle phase space distributions are labelled by their 4-momenta in the subscript, $f_x = f_D(\omega_x)$, and we have used the relation $f_D(-\omega) = 1 - f_D(\omega)$.

In the form (E.5), the physics of the selfenergy is immediately discernible: the processes corresponding to each term can be identified by their initial and final state particles. Specifically, initial state phase space distributions always appear simply as a factor f_x , while final state phase space distributions come in the form of a Pauli-blocking factor $(1 - f_x)$. Furthermore, because we are computing $\text{Tr} \left[\not{p} \Sigma_{(b)}^<(p) \right]$, which is associated with the production rate $\Gamma^<$ and hence accompanied by a Pauli-blocking factor $(1 - f_p)$ in the generalised Boltzmann equation (6.48), the neutrino that carries the 4-momentum p should also be interpreted as a final state particle. Then, the eight processes corresponding to the eight terms of equation (E.5) are simply those shown in figure E.1 (read from left to right, top to bottom).

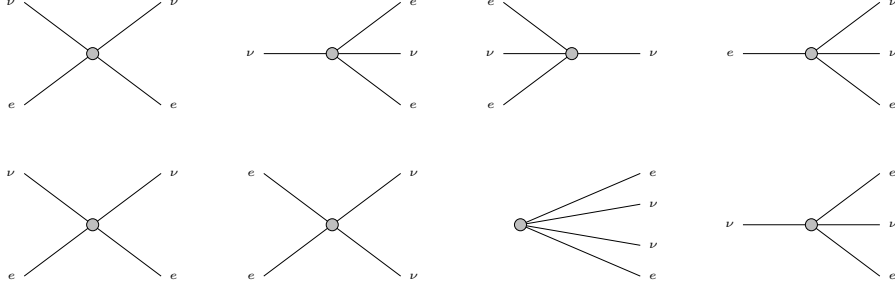


Figure E.1: Scattering processes corresponding to the eight terms in equation (E.5), read from left to right, top to bottom. Only the $2 \rightarrow 2$ processes are kinematically allowed.

Clearly, not all of the processes of figure E.1 are allowed. Throwing away those processes that are kinematically forbidden, we are left with

$$\begin{aligned}
\text{Tr} \left[\not{p} \Sigma_{(b)}^<(p) \right] = & -G_F^2 \int \frac{d^3 \ell d^3 \mathbf{q} d^3 \mathbf{u}}{(2\pi)^9 8 \omega_\ell \omega_q \omega_u} (2\pi)^4 \delta^{(3)}(\mathbf{u} - \mathbf{q} - \boldsymbol{\ell} + \mathbf{p}) \\
& \times \left[f_\ell (1 - f_u) f_q \delta(\omega_u - \omega_q - \omega_\ell + p^0) \text{Tr}_b^{+++} \right. \\
& + f_\ell f_u (1 - f_q) \delta(-\omega_u + \omega_q - \omega_\ell + p^0) \text{Tr}_b^{+--} \\
& \left. + (1 - f_\ell) f_u f_q \delta(-\omega_u - \omega_q + \omega_\ell + p^0) \text{Tr}_b^{--+} \right]. \tag{E.7}
\end{aligned}$$

Repeating the calculation for the remaining three selfenergy contributions (6.55), (6.57), and (6.58), we always find the same phase space structure, the differences being entirely contained in the trace terms and the coupling constant. Then, collecting all contributions, the total mode-dependent production rate can now be written as

$$\begin{aligned}
\Gamma_{\mathbf{p}}^< = & \frac{1}{2p^0} \text{Tr} \left[\sum_{i'=a,b,c,d} \not{p} \Sigma_{(i')}^<(p) \right] \\
= & -\frac{G_F^2}{2p^0} \int \frac{d^3 \ell d^3 \mathbf{q} d^3 \mathbf{u}}{(2\pi)^9 8 \omega_\ell \omega_q \omega_u} (2\pi)^4 \delta^{(3)}(\mathbf{u} - \mathbf{q} - \boldsymbol{\ell} + \mathbf{p}) \\
& \times \left[f_\ell (1 - f_u) f_q \delta(\omega_u - \omega_q - \omega_\ell + p^0) \text{Tr}^{+++} \right. \\
& + f_\ell f_u (1 - f_q) \delta(-\omega_u + \omega_q - \omega_\ell + p^0) \text{Tr}^{+--} \\
& \left. + (1 - f_\ell) f_u f_q \delta(-\omega_u - \omega_q + \omega_\ell + p^0) \text{Tr}^{--+} \right], \tag{E.8}
\end{aligned}$$

where $\text{Tr}^{ijk} = \sum_{i'=a,b,c,d} \lambda_{i'} \text{Tr}_{i'}^{ijk}$, with coefficients $\lambda_a = \lambda_b = 1$, $\lambda_c = -2$, and $\lambda_d = -1/2$. The traces have been evaluated to be

$$\begin{aligned} \text{Tr}_a &= \text{Tr} \left[\not{p} \gamma^\mu (1 - \gamma_5) (\not{q} + m_e) \gamma^\nu (g_{V,e} - g_{A,e} \gamma_5) \right. \\ &\quad \left. \times (\not{\psi} + m_e) \gamma_\mu (1 - \gamma_5) \not{\ell} \gamma_\nu (g_{V,e} - g_{A,e} \gamma_5) \right] \\ &= -128(g_{V,e} + g_{A,e})(p \cdot u)(\ell \cdot q) + 64m_e^2(g_{V,e} - g_{A,e})(p \cdot \ell), \end{aligned} \quad (\text{E.9})$$

$$\begin{aligned} \text{Tr}_b &= \text{Tr} \left[\not{p} \gamma^\mu (1 - \gamma_5) \not{\ell} \gamma^\nu (1 - \gamma_5) (\not{\psi} + m_e) \gamma_\mu (g_{V,e} - g_{A,e} \gamma_5) (\not{q} + m_e) \gamma_\nu (1 - \gamma_5) \right] \\ &= -128(g_{V,e} + g_{A,e})(p \cdot u)(\ell \cdot q) + 64m_e^2(g_{V,e} - g_{A,e})(p \cdot \ell) = \text{Tr}_a, \end{aligned} \quad (\text{E.10})$$

$$\begin{aligned} \text{Tr}_c &= \text{Tr} \left[\not{p} \gamma^\mu (1 - \gamma_5) \not{\ell} \gamma^\nu (1 - \gamma_5) \right. \\ &\quad \left. \text{quad} \times \text{Tr} \left[\gamma_\mu (g_{V,e} - g_{A,e} \gamma_5) (\not{q} + m_e) \gamma_\nu (g_{V,e} - g_{A,e} \gamma_5) (\not{\psi} + m_e) \right] \right] \\ &= 64(g_{V,e}^2 + g_{A,e}^2) \left((p \cdot q)(\ell \cdot u) + (p \cdot u)(\ell \cdot q) \right) - 64m_e^2(g_{V,e}^2 - g_{A,e}^2)(p \cdot \ell) \\ &\quad - 128g_{V,e}g_{A,e} \left((p \cdot q)(\ell \cdot u) - (p \cdot u)(\ell \cdot q) \right), \end{aligned} \quad (\text{E.11})$$

$$\begin{aligned} \text{Tr}_d &= \text{Tr} \left[\not{p} \gamma^\mu (1 - \gamma_5) (\not{q} + m_e) \gamma^\nu (1 - \gamma_5) \right] \text{Tr} \left[\gamma_\mu (1 - \gamma_5) \not{\ell} \gamma_\nu (1 - \gamma_5) (\not{\psi} + m_e) \right] \\ &= 256(p \cdot u)(\ell \cdot q), \end{aligned} \quad (\text{E.12})$$

from which we conclude that the selfenergy diagrams (a) and (b) contribute identically to the interaction rate.

The corresponding mode-dependent destruction rate $\Gamma_{\mathbf{p}}^>$ can be easily deduced from $\Gamma_{\mathbf{p}}^<$ by (i) noting that, to turn $\text{Tr} [\not{p} \Sigma^<(p)]$ into $\text{Tr} [\not{p} \Sigma^>(p)]$, we need simply to replace the Wightman propagators $S_\psi^\lessgtr \rightarrow S_\psi^\gtrless$, which, through equation (6.59), amounts to swapping $(1 - f_x) \leftrightarrow -f_x$, and (ii) introducing an

overall sign flip via the definition (6.49). Then,

$$\begin{aligned}
\Gamma_{\mathbf{p}}^{\gt} &= -\frac{1}{2p^0} \text{Tr} \left[\sum_{i'=a,b,c,d} \not{p} \Sigma_{(i')}^{\gt}(p) \right] \\
&= -\frac{G_F^2}{2p^0} \int \frac{d^3\ell d^3\mathbf{q} d^3\mathbf{u}}{(2\pi)^9 8\omega_\ell \omega_q \omega_u} (2\pi)^4 \delta^{(3)}(\mathbf{u} - \mathbf{q} - \boldsymbol{\ell} + \mathbf{p}) \\
&\quad \times \left[(1 - f_\ell) f_u (1 - f_q) \delta(\omega_u - \omega_q - \omega_\ell + p^0) \text{Tr}^{+++} \right. \\
&\quad \quad + (1 - f_\ell)(1 - f_u) f_q \delta(-\omega_u + \omega_q - \omega_\ell + p^0) \text{Tr}^{+-+} \\
&\quad \quad \left. + f_\ell(1 - f_u)(1 - f_q) \delta(-\omega_u - \omega_q + \omega_\ell + p^0) \text{Tr}^{-++} \right],
\end{aligned} \tag{E.13}$$

which together with $\Gamma_{\mathbf{p}}^{\lt}$ can be used to construct a collision term for f_p ,

$$C[f_p] = (1 - f_p) \Gamma_{\mathbf{p}}^{\lt} - f_p \Gamma_{\mathbf{p}}^{\gt}, \tag{E.14}$$

based on the generalised Boltzmann equation (6.48).

In order to match the existing results in the literature, e.g, equation (8) and table I of [208], we change the 4-momentum variables to $P_i = (\omega_i, \mathbf{p}_i)$, $i = 1, \dots, 4$. Then, for $f_1 = f_p$, we find the collision term

$$C[f_1] = \frac{1}{2\omega_1} \int \frac{d^3\mathbf{p}_2 d^3\mathbf{p}_3 d^3\mathbf{p}_4}{(2\pi)^9 8\omega_2 \omega_3 \omega_4} (2\pi)^4 \delta^{(4)}(P_1 + P_2 - P_3 - P_4) F_r S_r \langle |\mathcal{M}_r|^2 \rangle, \tag{E.15}$$

where $F_r = (1 - f_1)(1 - f_2)f_3f_4 - f_1f_2(1 - f_3)(1 - f_4)$ is a phase space factor, and the symmetrised squared matrix elements

$$S_r \langle |\mathcal{M}_r|^2 \rangle = S_1 \langle |\mathcal{M}_{\nu_e + e^- \leftrightarrow e^- + \nu_e}|^2 \rangle + S_2 \langle |\mathcal{M}_{\nu_e + e^+ \leftrightarrow e^+ + \nu_e}|^2 \rangle \tag{E.16}$$

$$+ S_3 \langle |\mathcal{M}_{\nu_e + \bar{\nu}_e \leftrightarrow e^- + e^+}|^2 \rangle \tag{E.17}$$

can be mapped to the traces of equations (E.8) and (E.13) via

$$\begin{aligned}
G_F^{-2} S_1 \langle |\mathcal{M}_{\nu_e + e^- \leftrightarrow e^- + \nu_e}|^2 \rangle &= -\text{Tr}^{+--} \Big|_{P_2=(\omega_q, -\mathbf{q}), P_3=(\omega_u, -\mathbf{u}), P_4=(\omega_\ell, \boldsymbol{\ell})}, \\
G_F^{-2} S_2 \langle |\mathcal{M}_{\nu_e + e^+ \leftrightarrow e^+ + \nu_e}|^2 \rangle &= -\text{Tr}^{+++} \Big|_{P_2=(\omega_u, \mathbf{u}), P_3=(\omega_q, \mathbf{q}), P_4=(\omega_\ell, \boldsymbol{\ell})}, \\
G_F^{-2} S_3 \langle |\mathcal{M}_{\nu_e + \bar{\nu}_e \leftrightarrow e^- + e^+}|^2 \rangle &= -\text{Tr}^{-++} \Big|_{P_2=(\omega_\ell, -\boldsymbol{\ell}), P_3=(\omega_q, \mathbf{q}), P_4=(\omega_u, -\mathbf{u})}.
\end{aligned} \tag{E.18}$$

Thus, we have demonstrated that the neutrino damping rate calculated from the two-loop retarded selfenergy at the (quasi)particle pole is indeed equivalent at leading order to the usual Boltzmann collision term for $2 \rightarrow 2$ scattering from kinetic theory.

E.2 Leading-order calculation of the damping rate

We show in this section how to reduce the selfenergy expressions (6.55) to (6.58) to the leading-order mode-dependent interaction rate (6.62). Plugging into equations (6.55) to (6.58) the free-fermion Wightman propagators (6.61) and the traces (E.9) to (E.12) with $u = \ell - p + q$, the selfenergy contributions can be written as

$$\begin{aligned} \text{Tr} \left[\not{p} \Sigma_{(i)}^{\leq}(p) \right] &= \frac{\mathcal{C}_i G_F^2}{(2\pi)^5} \int d^4\ell d^4q \mathcal{F}(p^0, q^0, \ell^0) \delta(\ell^2) \delta(q^2 - m_e^2) \delta((\ell - p + q)^2 - m_e^2) \\ &\times \left[A_{(p\ell)}^i m_e^2 (p \cdot \ell) + A_{(pq)(\ell p)}^i (p \cdot q)(\ell \cdot p) + A_{(pq)^2}^i (p \cdot q)^2 + A_{(p\ell)^2}^i (p \cdot \ell)^2 \right], \end{aligned} \quad (\text{E.19})$$

where $\mathcal{F}(p^0, q^0, \ell^0)$ reads

$$\mathcal{F} = \left[f_D(|\ell^0 + q^0 - p^0|) - \theta(\ell^0 + q^0 - p^0) \right] \left[f_D(|\ell^0|) - \theta(-\ell^0) \right] \left[f_D(|q^0|) - \theta(-q^0) \right], \quad (\text{E.20})$$

and the various coefficients (\mathcal{C}_i , $A_{(p\ell)}^i$, etc.) are given in table E.1.

	$i = a, b$	$i = c$	$i = d$
\mathcal{C}_i	64	-128	-128
$A_{(p\ell)}^i$	$g_{V,e} - g_{A,e}$	$-(g_{V,e}^2 - g_{A,e}^2)$	0
$A_{(pq)(\ell p)}^i$	$-4(g_{V,e} + g_{A,e})$	$2(g_{V,e} + g_{A,e})^2$	2
$A_{(pq)^2}^i$	$-2(g_{V,e} + g_{A,e})$	$2(g_{V,e}^2 + g_{A,e}^2)$	1
$A_{(p\ell)^2}^i$	$-2(g_{V,e} + g_{A,e})$	$(g_{V,e} + g_{A,e})^2$	1

Table E.1: Coefficients appearing in the weak-rate and selfenergy integrals (6.62), (E.19), and (E.35).

To simplify equation (E.19), observe that it is of the form

$$\begin{aligned} I &= \int d^4q d^4\ell f(q, \ell, p) \delta(\ell^2) \delta(q^2 - m_e^2) \delta((\ell + q - p)^2 - m_e^2) \\ &= \int \frac{d^3\ell d^3\mathbf{q}}{4|\ell|\omega_q} \sum_{\epsilon, \tau = \pm 1} f(q, \ell, p) \delta((\ell + q - p)^2 - m_e^2) \Big|_{\substack{q^0 = \epsilon\omega_q \\ \ell^0 = \tau|\ell|}}, \end{aligned} \quad (\text{E.21})$$

where $\omega_q^2 = |\mathbf{q}|^2 + m_e^2$, $f(q, \ell, p)$ is a scalar function independent of the Lorentz contraction $\ell \cdot q$, and the second equality follows from the fact that the first two

Dirac deltas in ℓ^2 and q^2 simply put the corresponding particles on their mass shells. To evaluate the remaining Dirac delta distribution, we first parametrise the 3-momenta in spherical coordinates,

$$\begin{aligned}\mathbf{p} &= |\mathbf{p}|(0, 0, 1)^T, \\ \ell &= |\ell|(0, \sin \alpha, \cos \alpha)^T, \\ \mathbf{q} &= |\mathbf{q}|(\sin \theta \sin \beta, \sin \theta \cos \beta, \cos \theta)^T,\end{aligned}\tag{E.22}$$

so that the integral (E.21) becomes

$$\begin{aligned}I &= \frac{2\pi}{4} \iint_0^\infty d|\ell|d|\mathbf{q}| \int_0^{2\pi} d\beta \int_{-1}^{+1} d\cos \alpha d\cos \theta \\ &\quad \times \frac{|\mathbf{q}|^2|\ell|}{\omega_q} \sum_{\epsilon, \tau = \pm 1} f(q, \ell, p) \delta((\ell + q - p)^2 - m_e^2) \Bigg|_{\substack{q^0 = \epsilon\omega_q \\ \ell^0 = \tau|\ell|}}.\end{aligned}\tag{E.23}$$

Similarly, the Lorentz contractions can now be written as

$$\begin{aligned}\ell \cdot p &= \tau|\ell||\mathbf{p}| - |\mathbf{p}||\ell| \cos \alpha, \\ p \cdot q &= \epsilon\omega_q|\mathbf{p}| - |\mathbf{p}||\mathbf{q}| \cos \theta, \\ \ell \cdot q &= \epsilon\tau\omega_q|\ell| - |\ell||\mathbf{q}|(\sin \alpha \sin \theta \cos \beta + \cos \alpha \cos \theta),\end{aligned}\tag{E.24}$$

from which we immediately deduce that the integrand (E.23) depends on β only through the Dirac delta distribution $\delta((\ell + q - p)^2 - m_e^2)$.

Then, following [220], we can solve the β -integral in (E.23) by first identifying $\delta((\ell + q - p)^2 - m_e^2) = \delta(g(\beta))$, which can be further decomposed to

$$\delta(g(\beta)) = \sum_i \frac{1}{|g'(\beta_i)|} \delta(\beta - \beta_i) = \frac{\delta(\beta - \beta_1) + \delta(\beta - \beta_2)}{2|\ell||\mathbf{q}| \sin \theta \sin \alpha \sin \beta_0}.\tag{E.25}$$

Here, β_i denotes the roots of the function $g(\beta)$: in this case, there are two, β_1 and $\beta_2 = 2\pi - \beta_1$, on the interval $\beta \in [0, 2\pi]$, given by

$$\cos \beta_i = \frac{|\mathbf{q}||\mathbf{p}| \cos \theta - \epsilon\omega_q|\mathbf{p}| + |\ell||\mathbf{p}| \cos \alpha - \tau|\ell||\ell| + \epsilon\tau|\ell|\omega_q - |\ell||\mathbf{q}| \cos \alpha \cos \theta}{|\ell||\mathbf{q}| \sin \theta \sin \alpha},\tag{E.26}$$

and $|\sin \beta_1| = |\sin \beta_2| = |\sin \beta_0|$; the derivative $g'(\beta_i)$ is given by $\partial_\beta g|_{\beta_i} = -2|\ell||\mathbf{q}| \sin \theta \sin \alpha \sin \beta_i$. Then, substituting equation (E.25) into equation (E.23), yields

$$I = \frac{2\pi}{4} \iint_0^\infty d|\ell|d|\mathbf{q}| \int_{-1}^{+1} d\cos \alpha d\cos \theta \frac{|\mathbf{q}|^2|\ell|}{\omega_q} \sum_{\epsilon, \tau = \pm 1} \frac{f(q, \ell, p) \theta(1 - \cos^2 \beta_0)}{|\ell||\mathbf{q}| \sin \theta \sin \alpha \sin \beta_0} \Bigg|_{\substack{q^0 = \epsilon\omega_q \\ \ell^0 = \tau|\ell|}}$$

(E.27)

where we have inserted a Heaviside step function $\theta(1 - \cos^2 \beta_0)$ to ensure that the condition $\cos^2 \beta_0 \leq 1$ is respected.

The next step is to recognise that, in equation (E.27), the following two expressions are functionally equivalent:

$$\frac{\theta(1 - \cos^2 \beta_0)}{|\boldsymbol{\ell}||\mathbf{q}|\sin \theta \sin \alpha \sin \beta_0} = \frac{\theta(|\boldsymbol{\ell}|^2|\mathbf{q}|^2 \sin^2 \theta \sin^2 \alpha (1 - \cos^2 \beta_0))}{\sqrt{|\boldsymbol{\ell}|^2|\mathbf{q}|^2 \sin^2 \theta \sin^2 \alpha (1 - \cos^2 \beta_0)}}, \quad (\text{E.28})$$

where the r.h.s. expression has the desirable property that the Heaviside step function and the square root take the same argument that is quadratic in $z = \cos \theta$, i.e.,

$$|\boldsymbol{\ell}|^2|\mathbf{q}|^2(1 - z^2) \sin^2 \alpha (1 - \cos^2 \beta_0) = \tilde{a}z^2 + \tilde{b}z + \tilde{c}, \quad (\text{E.29})$$

with coefficients

$$\tilde{a} = -|\mathbf{q}|^2|\boldsymbol{\ell} - \mathbf{p}|^2 \leq 0, \quad (\text{E.30})$$

$$\begin{aligned} \tilde{b} = -2 \Big[& -|\boldsymbol{\ell}|^2|\mathbf{p}||\mathbf{q}| \cos^2 \alpha + (|\boldsymbol{\ell}||\mathbf{p}|^2|\mathbf{q}| + \epsilon\omega_q|\boldsymbol{\ell}||\mathbf{p}||\mathbf{q}| + \tau|\boldsymbol{\ell}|^2|\mathbf{p}||\mathbf{q}| \\ & - \epsilon\tau\omega_q|\boldsymbol{\ell}|^2|\mathbf{q}|) \cos \alpha - \epsilon\omega_q|\mathbf{p}|^2|\mathbf{q}| - \tau|\boldsymbol{\ell}||\mathbf{p}|^2|\mathbf{q}| + \epsilon\tau\omega_q|\boldsymbol{\ell}||\mathbf{p}||\mathbf{q}| \Big], \end{aligned} \quad (\text{E.31})$$

$$\begin{aligned} \tilde{c} = & -|\boldsymbol{\ell}|^2(|\mathbf{p}|^2 + |\mathbf{q}|^2) \cos^2 \alpha + 2(\epsilon\omega_q|\boldsymbol{\ell}||\mathbf{p}|^2 + \tau|\boldsymbol{\ell}|^2|\mathbf{p}|^2 - \epsilon\tau\omega_q|\boldsymbol{\ell}|^2|\mathbf{p}|) \cos \alpha \\ & + |\boldsymbol{\ell}|^2(|\mathbf{q}|^2 - |\mathbf{p}|^2) - \omega_q^2(|\boldsymbol{\ell}|^2 + |\mathbf{p}|^2) + 2\epsilon\omega_q|\boldsymbol{\ell}|^2|\mathbf{p}| + 2\tau\omega_q^2|\boldsymbol{\ell}||\mathbf{p}| - 2\epsilon\tau\omega_q|\boldsymbol{\ell}||\mathbf{p}|^2. \end{aligned} \quad (\text{E.32})$$

Because $\tilde{a} \leq 0$, the quadratic (E.29) represents a downward parabola with two real and non-degenerate roots z_{\pm} ,

$$z_{\pm} = \frac{\tilde{b}}{2|\tilde{a}|} \pm \sqrt{\left(\frac{\tilde{b}}{2\tilde{a}}\right)^2 + \frac{\tilde{c}}{|\tilde{a}|}}, \quad (\text{E.33})$$

whenever $\tilde{b}^2 - 4\tilde{a}\tilde{c} > 0$ is satisfied. This also means that the Heaviside step function is nonzero only in the region between non-degenerate z_{\pm} . Then, rewriting the quadratic (E.29) in terms of its roots (E.33), equation (E.27) can now be recast as

$$\begin{aligned} I = \frac{2\pi}{4} \int_0^{\infty} d|\boldsymbol{\ell}|d|\mathbf{q}| \frac{|\mathbf{q}|^2|\boldsymbol{\ell}|}{\omega_q} \int_{-1}^{+1} d \cos \alpha \frac{\theta(\tilde{b}^2 - 4\tilde{a}\tilde{c})}{\sqrt{|\tilde{a}|}} \\ \times \int_{z_-}^{z_+} dz \sum_{\epsilon, \tau = \pm 1} \frac{f(q, \ell, p)}{\sqrt{(z - z_-)(z_+ - z)}} \Big|_{\substack{q^0 = \epsilon\omega_q \\ \ell^0 = \tau|\boldsymbol{\ell}|}}. \end{aligned} \quad (\text{E.34})$$

	$j = 0$	$j = 1$	$j = 2$
$G_{(p\ell)}^j$	$m_e^2(\tau \ell \mathbf{p} - \ell \mathbf{p} \cos\alpha)$	0	0
$G_{(pq)(\ell p)}^j$	$\epsilon\omega_q \mathbf{p} (\tau \ell \mathbf{p} - \ell \mathbf{p} \cos\alpha)$	$ \mathbf{q} \mathbf{p} (\ell \mathbf{p} \cos\alpha - \tau \ell \mathbf{p})$	0
$G_{(pq)^2}^j$	$\omega_q^2 \mathbf{p} ^2$	$-2\epsilon\omega_q \mathbf{p} ^2 \mathbf{q} $	$ \mathbf{q} ^2 \mathbf{p} ^2$
$G_{(p\ell)^2}^j$	$(\tau \ell \mathbf{p} - \ell \mathbf{p} \cos\alpha)^2$	0	0

Table E.2: Coefficients appearing in the weak-rate and selfenergy integrals (6.62) and (E.36).

To further reduce the number of integrals, we apply (E.34) to the selfenergy (E.19)

$$\begin{aligned} \text{Tr} \left[\not{p} \Sigma_{(i)}^{\leq}(p) \right] &= \frac{C_i G_F^2}{4(2\pi)^4} \int_0^\infty d|\ell| d|\mathbf{q}| \frac{|\mathbf{q}|^2 |\ell|}{\omega_q} \int_{-1}^{+1} d\cos\alpha \sum_{\epsilon, \tau = \pm 1} \left[\frac{\theta(\tilde{b}^2 - 4\tilde{a}\tilde{c})}{\sqrt{|\tilde{a}|}} \times \right. \\ &\left. \mathcal{F}(p^0, q^0, \ell^0) \left(A_{(p\ell)}^i I_{(p\ell)}^z + A_{(pq)(\ell p)}^i I_{(pq)(\ell p)}^z + A_{(pq)^2}^i I_{(pq)^2}^z + A_{(p\ell)^2}^i I_{(p\ell)^2}^z \right) \right] \Bigg|_{\substack{q^0 = \epsilon\omega_q \\ \ell^0 = \tau|\ell|}} \end{aligned} \quad (\text{E.35})$$

where, for $(mn) = (p\ell), (pq)(\ell p), (pq)^2, (p\ell)^2$, we have defined

$$\begin{aligned} I_{(mn)}^z &= \int_{z_-}^{z_+} dz \left(\frac{G_{(mn)}^0 + zG_{(mn)}^1 + z^2G_{(mn)}^2}{\sqrt{(z - z_-)(z_+ - z)}} \right) \\ &= \pi \left[G_{(mn)}^0 + \frac{\tilde{b}}{2|\tilde{a}|} G_{(mn)}^1 + \left(\frac{3\tilde{b}^2 + 4\tilde{c}|\tilde{a}|}{8\tilde{a}^2} \right) G_{(mn)}^2 \right], \end{aligned} \quad (\text{E.36})$$

with the z -independent coefficients $G_{(mn)}^j$, $j = 0, 1, 2$, given in table E.2.

Putting it all back into equation (E.35), and noting that the mode-dependent interaction rate, as defined in equation (6.52), is equivalently

$$\Gamma_{\mathbf{p}} = \frac{(e^{p^0/T} + 1)}{2p^0} \sum_i \text{Tr} \left[\not{p} \Sigma_{(i)}^{\leq}(p) \right], \quad (\text{E.37})$$

we obtain the final result (6.62) for $p^0 = |\mathbf{p}|$.

Bibliography

- [1] Patrick Peter and Jean-Philippe Uzan, *Primordial cosmology*, Oxford Graduate Texts. Oxford Univ. Press, Oxford, 2009.
- [2] Katherine Freese, “Review of Observational Evidence for Dark Matter in the Universe and in upcoming searches for Dark Stars”, *EAS Publ. Ser.*, vol. 36, pp. 113–126, 2009.
- [3] Matts Roos, “Dark matter: The evidence from astronomy, astrophysics and cosmology”, 2010.
- [4] Dragan Huterer and Daniel L Shafer, “Dark energy two decades after: Observables, probes, consistency tests”, *Rept. Prog. Phys.*, vol. 81, no. 1, pp. 016901, 2018.
- [5] Arjun Berera, “Warm inflation”, *Phys. Rev. Lett.*, vol. 75, pp. 3218–3221, 1995.
- [6] Arjun Berera, Ian G. Moss, and Rudnei O. Ramos, “Warm Inflation and its Microphysical Basis”, *Rept. Prog. Phys.*, vol. 72, pp. 026901, 2009.
- [7] Arjun Berera, Marcelo Gleiser, and Rudnei O. Ramos, “A First principles warm inflation model that solves the cosmological horizon / flatness problems”, *Phys. Rev. Lett.*, vol. 83, pp. 264–267, 1999.
- [8] Alan H. Guth, “The Inflationary Universe: A Possible Solution to the Horizon and Flatness Problems”, *Phys. Rev.*, vol. D23, pp. 347–356, 1981, [Adv. Ser. Astrophys. Cosmol.3,139(1987)].
- [9] P.A.R. Ade et al., “Planck 2013 results. I. Overview of products and scientific results”, *Astron. Astrophys.*, vol. 571, pp. A1, 2014.

-
- [10] Alexei A. Starobinsky, “A New Type of Isotropic Cosmological Models Without Singularity”, *Phys. Lett.*, vol. 91B, pp. 99–102, 1980, [,771(1980)].
- [11] Andrei D. Linde, “A New Inflationary Universe Scenario: A Possible Solution of the Horizon, Flatness, Homogeneity, Isotropy and Primordial Monopole Problems”, *Phys. Lett.*, vol. 108B, pp. 389–393, 1982, [Adv. Ser. Astrophys. Cosmol.3,149(1987)].
- [12] C. Armendariz-Picon, T. Damour, and Viatcheslav F. Mukhanov, “k -inflation”, *Phys. Lett.*, vol. B458, pp. 209–218, 1999.
- [13] Arjun Berera and Rudnei O. Ramos, “Construction of a robust warm inflation mechanism”, *Phys. Lett. B*, vol. 567, pp. 294–304, 2003.
- [14] Mar Bastero-Gil, Arjun Berera, Rudnei O. Ramos, and Joao G. Rosa, “General dissipation coefficient in low-temperature warm inflation”, *JCAP*, vol. 01, pp. 016, 2013.
- [15] Mar Bastero-Gil, Arjun Berera, Rudnei O. Ramos, and João G. Rosa, “Towards a reliable effective field theory of inflation”, 7 2019.
- [16] Ian G. Moss and Chun Xiong, “On the consistency of warm inflation”, *JCAP*, vol. 11, pp. 023, 2008.
- [17] Junichi Yokoyama and Andrei D. Linde, “Is warm inflation possible?”, *Phys. Rev. D*, vol. 60, pp. 083509, 1999.
- [18] Jørgen Rammer, *Quantum Field Theory of Non-equilibrium States*, Cambridge University Press, 2007.
- [19] Juergen Berges, “Introduction to nonequilibrium quantum field theory”, *AIP Conf. Proc.*, vol. 739, no. 1, pp. 3–62, 2004.
- [20] Ashok K. Das, *Finite Temperature Field Theory*, World Scientific, New York, 1997.
- [21] Michel Le Bellac, *Thermal Field Theory*, Cambridge Monographs on Mathematical Physics. Cambridge University Press, 1996.
- [22] J.I. Kapusta and Charles Gale, *Finite-temperature field theory: Principles and applications*, Cambridge Monographs on Mathematical Physics. Cambridge University Press, 2011.
- [23] Julian S. Schwinger, “Brownian motion of a quantum oscillator”, *J. Math. Phys.*, vol. 2, pp. 407–432, 1961.

-
- [24] L. V. Keldysh, “Diagram technique for nonequilibrium processes”, *Zh. Eksp. Teor. Fiz.*, vol. 47, pp. 1515–1527, 1964, [Sov. Phys. JETP20,1018(1965)].
- [25] Murray Gell-Mann and Francis Low, “Bound states in quantum field theory”, *Phys. Rev.*, vol. 84, pp. 350–354, Oct 1951.
- [26] M.E. Peskin and D.V. Schroeder, *An Introduction To Quantum Field Theory*, Frontiers in Physics. Avalon Publishing, 1995.
- [27] Richard MacKenzie, “Path integral methods and applications”, in *6th Vietnam International School on Physics Vung-Tau, Vietnam, 27 December 1999 - 9 January 2000*, 1999.
- [28] Mathias Garny and Markus Michael Muller, “Kadanoff-Baym Equations with Non-Gaussian Initial Conditions: The Equilibrium Limit”, *Phys. Rev. D*, vol. 80, pp. 085011, 2009.
- [29] Marco Drewes, “Novel collective excitations in a hot scalar field theory”, *Phys. Lett.*, vol. B732, pp. 127–136, 2014.
- [30] Sidney R. Coleman and Erick J. Weinberg, “Radiative Corrections as the Origin of Spontaneous Symmetry Breaking”, *Phys. Rev.*, vol. D7, pp. 1888–1910, 1973.
- [31] Tomislav Prokopec, Michael G. Schmidt, and Steffen Weinstock, “Transport equations for chiral fermions to order \hbar and electroweak baryogenesis. Part 1”, *Annals Phys.*, vol. 314, pp. 208–265, 2004.
- [32] A. Anisimov, W. Buchmuller, M. Drewes, and S. Mendizabal, “Nonequilibrium Dynamics of Scalar Fields in a Thermal Bath”, *Annals Phys.*, vol. 324, pp. 1234–1260, 2009.
- [33] Marco Drewes, Sebastian Mendizabal, and Christoph Weniger, “The Boltzmann Equation from Quantum Field Theory”, *Phys. Lett.*, vol. B718, pp. 1119–1124, 2013.
- [34] Bjorn Garbrecht and Mathias Garny, “Finite Width in out-of-Equilibrium Propagators and Kinetic Theory”, *Annals Phys.*, vol. 327, pp. 914–934, 2012.
- [35] L. D. Landau, “On the theory of phase transitions”, *Zh. Eksp. Teor. Fiz.*, vol. 7, pp. 19–32, 1937, [Ukr. J. Phys.53,25(2008)].
- [36] W Lenz, “Beitrag zum Verständnis der magnetischen Erscheinungen in festen Körpern”, *Z. Phys.*, vol. 21, pp. 613–615, 1920.

-
- [37] Ernst Ising, “Contribution to the Theory of Ferromagnetism”, *Z. Phys.*, vol. 31, pp. 253–258, 1925.
- [38] V. L. Ginzburg and L. D. Landau, “On the Theory of superconductivity”, *Zh. Eksp. Teor. Fiz.*, vol. 20, pp. 1064–1082, 1950.
- [39] F. Englert and R. Brout, “Broken Symmetry and the Mass of Gauge Vector Mesons”, *Phys. Rev. Lett.*, vol. 13, pp. 321–323, 1964, [,157(1964)].
- [40] G. S. Guralnik, C. R. Hagen, and T. W. B. Kibble, “Global Conservation Laws and Massless Particles”, *Phys. Rev. Lett.*, vol. 13, pp. 585–587, 1964, [,162(1964)].
- [41] Peter W. Higgs, “Broken Symmetries and the Masses of Gauge Bosons”, *Phys. Rev. Lett.*, vol. 13, pp. 508–509, 1964, [,160(1964)].
- [42] R. D. Peccei and Helen R. Quinn, “CP Conservation in the Presence of Instantons”, *Phys. Rev. Lett.*, vol. 38, pp. 1440–1443, 1977, [,328(1977)].
- [43] John McDonald, “Gauge singlet scalars as cold dark matter”, *Phys. Rev.*, vol. D50, pp. 3637–3649, 1994.
- [44] C. P. Burgess, Maxim Pospelov, and Tonnis ter Veldhuis, “The Minimal model of nonbaryonic dark matter: A Singlet scalar”, *Nucl. Phys.*, vol. B619, pp. 709–728, 2001.
- [45] M. C. Bento, O. Bertolami, R. Rosenfeld, and L. Teodoro, “Selfinteracting dark matter and invisibly decaying Higgs”, *Phys. Rev.*, vol. D62, pp. 041302, 2000.
- [46] Paola Arias, Davide Cadamuro, Mark Goodsell, Joerg Jaeckel, Javier Redondo, and Andreas Ringwald, “WISPy Cold Dark Matter”, *JCAP*, vol. 1206, pp. 013, 2012.
- [47] C. Wetterich, “Cosmology and the Fate of Dilatation Symmetry”, *Nucl. Phys.*, vol. B302, pp. 668–696, 1988.
- [48] C. Armendariz-Picon, Viatcheslav F. Mukhanov, and Paul J. Steinhardt, “A Dynamical solution to the problem of a small cosmological constant and late time cosmic acceleration”, *Phys. Rev. Lett.*, vol. 85, pp. 4438–4441, 2000.
- [49] Jin U Kang, Vitaly Vanchurin, and Sergei Winitzki, “Attractor scenarios and superluminal signals in k-essence cosmology”, *Phys. Rev.*, vol. D76, pp. 083511, 2007.

- [50] Edmund J. Copeland, M. Sami, and Shinji Tsujikawa, “Dynamics of dark energy”, *Int. J. Mod. Phys.*, vol. D15, pp. 1753–1936, 2006.
- [51] Stefano Profumo, Michael J. Ramsey-Musolf, and Gabe Shaughnessy, “Singlet Higgs phenomenology and the electroweak phase transition”, *JHEP*, vol. 08, pp. 010, 2007.
- [52] Hiren H. Patel and Michael J. Ramsey-Musolf, “Baryon Washout, Electroweak Phase Transition, and Perturbation Theory”, *JHEP*, vol. 07, pp. 029, 2011.
- [53] Jose R. Espinosa, Thomas Konstandin, and Francesco Riva, “Strong Electroweak Phase Transitions in the Standard Model with a Singlet”, *Nucl. Phys.*, vol. B854, pp. 592–630, 2012.
- [54] David E. Morrissey and Michael J. Ramsey-Musolf, “Electroweak baryogenesis”, *New J. Phys.*, vol. 14, pp. 125003, 2012.
- [55] Arjun Berera, Ian G. Moss, and Rudnei O. Ramos, “Local Approximations for Effective Scalar Field Equations of Motion”, *Phys. Rev. D*, vol. 76, pp. 083520, 2007.
- [56] Florian Gautier and Julien Serreau, “On the Langevin description of nonequilibrium quantum fields”, *Phys. Rev. D*, vol. 86, pp. 125002, 2012.
- [57] Masahiro Morikawa, “Classical Fluctuations in Dissipative Quantum Systems”, *Phys. Rev.*, vol. D33, pp. 3607, 1986.
- [58] Fabrizio Cametti, Giovanni Jona-Lasinio, Carlo Presilla, and Fabio Toninelli, “Comparison between quantum and classical dynamics in the effective action formalism”, in *Proceedings, International School of Physics “Enrico Fermi”, 143rd Course, “New Directions in Quantum Chaos”: Varenna, Italy, July 20-30, 1999*, 1999, pp. 431–448.
- [59] Dražen Glavan, “Perturbative reduction of derivative order in EFT”, *JHEP*, vol. 02, pp. 136, 2018.
- [60] E. Calzetta and B. L. Hu, “Dissipation of Quantum Fields From Particle Creation”, *Phys. Rev.*, vol. D40, pp. 656–659, 1989.
- [61] D. Boyanovsky, K. Davey, and Chiu Man Ho, “Particle abundance in a thermal plasma: Quantum kinetics vs. Boltzmann equation”, *Phys. Rev.*, vol. D71, pp. 023523, 2005.
- [62] Yeuk-Kwan E. Cheung, Marco Drewes, Jin U Kang, and Jong Chol Kim, “Effective Action for Cosmological Scalar Fields at Finite Temperature”, *JHEP*, vol. 08, pp. 059, 2015.

- [63] Kyohei Mukaida, Kazunori Nakayama, and Masahiro Takimoto, “Fate of Z_2 Symmetric Scalar Field”, *JHEP*, vol. 12, pp. 053, 2013.
- [64] H. Arthur Weldon, “Simple Rules for Discontinuities in Finite Temperature Field Theory”, *Phys. Rev.*, vol. D28, pp. 2007, 1983.
- [65] R. L. Kobes and G. W. Semenoff, “Discontinuities of Green Functions in Field Theory at Finite Temperature and Density”, *Nucl. Phys.*, vol. B260, pp. 714–746, 1985.
- [66] R. L. Kobes and G. W. Semenoff, “Discontinuities of Green Functions in Field Theory at Finite Temperature and Density. 2”, *Nucl. Phys.*, vol. B272, pp. 329–364, 1986.
- [67] P. V. Landshoff, “Simple physical approach to thermal cutting rules”, *Phys. Lett.*, vol. B386, pp. 291–296, 1996.
- [68] Francois Gelis, “Cutting rules in the real time formalisms at finite temperature”, *Nucl. Phys.*, vol. B508, pp. 483–505, 1997.
- [69] Paulo F. Bedaque, Ashok K. Das, and Satchidananda Naik, “Cutting rules at finite temperature”, *Mod. Phys. Lett.*, vol. A12, pp. 2481–2496, 1997.
- [70] Marco Drewes, “On the Role of Quasiparticles and thermal Masses in Nonequilibrium Processes in a Plasma”, 2010.
- [71] Marco Drewes and Jin U Kang, “The Kinematics of Cosmic Reheating”, *Nucl. Phys.*, vol. B875, pp. 315–350, 2013, [Erratum: *Nucl. Phys.*B888,284(2014)].
- [72] Rajesh R. Parwani, “Resummation in a hot scalar field theory”, *Phys. Rev.*, vol. D45, pp. 4695, 1992, [Erratum: *Phys. Rev.*D48,5965(1993)].
- [73] Björn Garbrecht, Frank Glowna, and Pedro Schwaller, “Scattering Rates For Leptogenesis: Damping of Lepton Flavour Coherence and Production of Singlet Neutrinos”, *Nucl. Phys.*, vol. B877, pp. 1–35, 2013.
- [74] Marco Drewes and Jin U Kang, “Sterile neutrino Dark Matter production from scalar decay in a thermal bath”, *JHEP*, vol. 05, pp. 051, 2016.
- [75] Gilles Buldgen, Marco Drewes, Jin U. Kang, and Ui Ri Mun, “General Markovian Equation for Scalar Fields in a Slowly Evolving Background”, 12 2019.

- [76] Per Elmfors, Kari Enqvist, and Iiro Vilja, “Thermalization of the Higgs field at the electroweak phase transition”, *Nucl. Phys. B*, vol. 412, pp. 459–478, 1994.
- [77] Planck Collaboration, “Planck 2018 results. i. overview and the cosmological legacy of planck”, 2018.
- [78] G. Hinshaw et al., “Nine-Year Wilkinson Microwave Anisotropy Probe (WMAP) Observations: Cosmological Parameter Results”, *Astrophys. J. Suppl.*, vol. 208, pp. 19, 2013.
- [79] D.J. Fixsen, E.S. Cheng, J.M. Gales, John C. Mather, R.A. Shafer, and E.L. Wright, “The Cosmic Microwave Background spectrum from the full COBE FIRAS data set”, *Astrophys. J.*, vol. 473, pp. 576, 1996.
- [80] E L Wright, “Wmap first year results”, , no. astro-ph/0306132, Jun 2003.
- [81] Ian G. Moss and Timothy Yeomans, “Non-gaussianity in the strong regime of warm inflation”, *JCAP*, vol. 08, pp. 009, 2011.
- [82] Mar Bastero-Gil, Arjun Berera, Ian G. Moss, and Rudnei O. Ramos, “Theory of non-Gaussianity in warm inflation”, *JCAP*, vol. 12, pp. 008, 2014.
- [83] Kim V. Berghaus, Peter W. Graham, and David E. Kaplan, “Minimal Warm Inflation”, *JCAP*, vol. 03, pp. 034, 2020.
- [84] Arvind Borde, Alan Guth, and Alexander Vilenkin, “Inflationary spacetimes are incomplete in past directions”, *Physical review letters*, vol. 90, pp. 151301, 05 2003.
- [85] Arvind Borde and Alexander Vilenkin, “Eternal inflation and the initial singularity”, *Phys. Rev. Lett.*, vol. 72, pp. 3305–3309, 1994.
- [86] P. J. Steinhardt, “Natural inflation”, in *Very Early Universe*, January 1983, pp. 251–266.
- [87] Alexander Vilenkin, “The Birth of Inflationary Universes”, *Phys. Rev. D*, vol. 27, pp. 2848, 1983.
- [88] Jaume Garriga and Alexander Vilenkin, “Watchers of the multiverse”, *JCAP*, vol. 05, pp. 037, 2013.
- [89] Angelika Fertig, *Alternatives to Inflation – non-minimal ekpyrosis and conflation*, PhD thesis, Humboldt U., Berlin, 2016.

-
- [90] Jerome Martin and Robert H. Brandenberger, “The TransPlanckian problem of inflationary cosmology”, *Phys. Rev. D*, vol. 63, pp. 123501, 2001.
- [91] Andrei D. Linde, “Chaotic Inflation”, *Phys. Lett. B*, vol. 129, pp. 177–181, 1983.
- [92] ROGER PENROSE, “Difficulties with inflationary cosmology”, *Annals of the New York Academy of Sciences*, vol. 571, pp. 249 – 264, 12 2006.
- [93] G.W. Gibbons and Neil Turok, “The Measure Problem in Cosmology”, *Phys. Rev. D*, vol. 77, pp. 063516, 2008.
- [94] Justin Khoury, Burt A. Ovrut, Paul J. Steinhardt, and Neil Turok, “Ekpyrotic universe: Colliding branes and the origin of the hot big bang”, *Physical Review D*, vol. 64, no. 12, Nov 2001.
- [95] Laura E. Allen and David Wands, “Cosmological perturbations through a simple bounce”, *Physical Review D*, vol. 70, no. 6, Sep 2004.
- [96] Patrick Peter and Nelson Pinto-Neto, “Cosmology without inflation”, *Phys. Rev. D*, vol. 78, pp. 063506, 2008.
- [97] Patrick Peter and Nelson Pinto-Neto, “Primordial perturbations in a nonsingular bouncing universe model”, *Physical Review D*, vol. 66, no. 6, Sep 2002.
- [98] Robert H. Brandenberger, “Looking beyond inflationary cosmology”, *Can. J. Phys.*, vol. 84, pp. 437, 2006.
- [99] Robert H. Brandenberger, “Alternatives to the inflationary paradigm of structure formation”, *Int. J. Mod. Phys. Conf. Ser.*, vol. 01, pp. 67–79, 2011.
- [100] M NOVELLO and S BERGLIAFFA, “Bouncing cosmologies”, *Physics Reports*, vol. 463, no. 4, pp. 127–213, Jul 2008.
- [101] Diana Battfeld and Patrick Peter, “A critical review of classical bouncing cosmologies”, *Physics Reports*, vol. 571, pp. 1–66, Apr 2015.
- [102] Anna Ijjas and Paul J Steinhardt, “Bouncing cosmology made simple”, *Classical and Quantum Gravity*, vol. 35, no. 13, pp. 135004, Jun 2018.
- [103] Jerome Martin, Christophe Ringeval, and Vincent Vennin, “Encyclopædia Inflationaris”, *Phys. Dark Univ.*, vol. 5-6, pp. 75–235, 2014.

-
- [104] The BICEP/Keck Collaboration et al., “Measurements of degree-scale b-mode polarization with the bicep/keck experiments at south pole”, 2018.
- [105] P. A. R. Ade, N. Aghanim, Z. Ahmed, R. W. Aikin, K. D. Alexander, M. Arnaud, J. Aumont, C. Baccigalupi, A. J. Banday, D. Barkats, and et al., “Joint analysis of bicep2/keck array and planck data”, *Physical Review Letters*, vol. 114, no. 10, Mar 2015.
- [106] Planck Collaboration et al., “Planck 2018 results. x. constraints on inflation”, 2018.
- [107] Arjun Berera and Jaime R. Calderón, “Trans-planckian censorship and other swampland bothers addressed in warm inflation”, *Physical Review D*, vol. 100, no. 12, Dec 2019.
- [108] Sam Bartrum, Arjun Berera, and João G Rosa, “Warming up for planck”, *Journal of Cosmology and Astroparticle Physics*, vol. 2013, no. 06, pp. 025–025, Jun 2013.
- [109] Robert H. Brandenberger and Masahide Yamaguchi, “Spontaneous baryogenesis in warm inflation”, *Phys. Rev. D*, vol. 68, pp. 023505, 2003.
- [110] Mar Bastero-Gil, Arjun Berera, Rudnei O. Ramos, and João G. Rosa, “Warm baryogenesis”, *Physics Letters B*, vol. 712, no. 4-5, pp. 425–429, Jun 2012.
- [111] Mar Bastero-Gil, Arjun Berera, Rudnei O. Ramos, and Joao G. Rosa, “Adiabatic out-of-equilibrium solutions to the Boltzmann equation in warm inflation”, *JHEP*, vol. 02, pp. 063, 2018.
- [112] Mar Bastero-Gil, Sukannya Bhattacharya, Koushik Dutta, and Mayukh Raj Gangopadhyay, “Constraining Warm Inflation with CMB data”, *JCAP*, vol. 02, pp. 054, 2018.
- [113] Mar Bastero-Gil, Arjun Berera, Rudnei O. Ramos, and Joao G. Rosa, “Warm Little Inflaton”, *Phys. Rev. Lett.*, vol. 117, no. 15, pp. 151301, 2016.
- [114] Yang-yang Wang, Jian-Yang Zhu, and Xiao-Min Zhang, “Observational Constraints on Two-field Warm Inflation”, *Phys. Rev. D*, vol. 99, no. 10, pp. 103529, 2019.
- [115] Mar Bastero-Gil and Arjun Berera, “Warm inflation model building”, *Int. J. Mod. Phys. A*, vol. 24, pp. 2207–2240, 2009.

-
- [116] Matti Herranen, Tommi Markkanen, and Anders Tranberg, “Quantum corrections to scalar field dynamics in a slow-roll space-time”, *JHEP*, vol. 05, pp. 026, 2014.
- [117] Jerome Martin, Christophe Ringeval, and Vincent Vennin, “Observing Inflationary Reheating”, *Phys. Rev. Lett.*, vol. 114, no. 8, pp. 081303, 2015.
- [118] Marco Drewes, “What can the CMB tell about the microphysics of cosmic reheating?”, *JCAP*, vol. 03, pp. 013, 2016.
- [119] Guy D. Moore and Marcus Tassler, “The Sphaleron Rate in SU(N) Gauge Theory”, *JHEP*, vol. 02, pp. 105, 2011.
- [120] Mikko Laine and Aleksi Vuorinen, *Basics of Thermal Field Theory*, vol. 925, Springer, 2016.
- [121] Juan P. Beltrán Almeida, Nicolás Bernal, Javier Rubio, and Tommi Tenkanen, “Hidden Inflaton Dark Matter”, *JCAP*, vol. 03, pp. 012, 2019.
- [122] N. Aghanim et al., “Planck 2018 results. VI. Cosmological parameters”, 2018.
- [123] Steen Hannestad and Jes Madsen, “Neutrino decoupling in the early universe”, *Phys. Rev.*, vol. D52, pp. 1764–1769, 1995.
- [124] A. D. Dolgov, S. H. Hansen, and D. V. Semikoz, “Nonequilibrium corrections to the spectra of massless neutrinos in the early universe”, *Nucl. Phys.*, vol. B503, pp. 426–444, 1997.
- [125] A. D. Dolgov, S. H. Hansen, and D. V. Semikoz, “Nonequilibrium corrections to the spectra of massless neutrinos in the early universe: Addendum”, *Nucl. Phys.*, vol. B543, pp. 269–274, 1999.
- [126] S. Esposito, G. Miele, S. Pastor, M. Peloso, and O. Pisanti, “Nonequilibrium spectra of degenerate relic neutrinos”, *Nucl. Phys.*, vol. B590, pp. 539–561, 2000.
- [127] Gianpiero Mangano, Gennaro Miele, Sergio Pastor, Teguyco Pinto, Ofelia Pisanti, and Pasquale D. Serpico, “Relic neutrino decoupling including flavor oscillations”, *Nucl. Phys.*, vol. B729, pp. 221–234, 2005.
- [128] Miguel Escudero, “Neutrino decoupling beyond the Standard Model: CMB constraints on the Dark Matter mass with a fast and precise N_{eff} evaluation”, *JCAP*, vol. 1902, pp. 007, 2019.

- [129] Duane A. Dicus, Edward W. Kolb, A. M. Gleeson, E. C. G. Sudarshan, Vigdor L. Teplitz, and Michael S. Turner, “Primordial Nucleosynthesis Including Radiative, Coulomb, and Finite Temperature Corrections to Weak Rates”, *Phys. Rev.*, vol. D26, pp. 2694, 1982.
- [130] A. F. Heckler, “Astrophysical applications of quantum corrections to the equation of state of a plasma”, *Phys. Rev.*, vol. D49, pp. 611–617, 1994.
- [131] Robert E. Lopez and Michael S. Turner, “An Accurate Calculation of the Big Bang Prediction for the Abundance of Primordial Helium”, *Phys. Rev.*, vol. D59, pp. 103502, 1999.
- [132] G. Mangano, G. Miele, S. Pastor, and M. Peloso, “A Precision calculation of the effective number of cosmological neutrinos”, *Phys. Lett.*, vol. B534, pp. 8–16, 2002.
- [133] S. Gariazzo, P. F. de Salas, and S. Pastor, “Thermalisation of sterile neutrinos in the early Universe in the 3+1 scheme with full mixing matrix”, *JCAP*, vol. 1907, no. 07, pp. 014, 2019.
- [134] Kevork N. Abazajian et al., “CMB-S4 Science Book, First Edition”, 2016.
- [135] Julien Lesgourgues, Gianpiero Mangano, Gennaro Miele, and Sergio Pastor, *Neutrino Cosmology*, Cambridge University Press, 2013.
- [136] Vincenzo Cirigliano, Christopher Lee, Michael J. Ramsey-Musolf, and Sean Tulin, “Flavored Quantum Boltzmann Equations”, *Phys. Rev.*, vol. D81, pp. 103503, 2010.
- [137] Christian Fidler, Matti Herranen, Kimmo Kainulainen, and Pyry Matti Rahkila, “Flavoured quantum Boltzmann equations from cQPA”, *JHEP*, vol. 02, pp. 065, 2012.
- [138] A. D. Dolgov, “Neutrinos in cosmology”, *Phys. Rept.*, vol. 370, pp. 333–535, 2002.
- [139] Jorge C. Romao and Joao P. Silva, “A resource for signs and Feynman diagrams of the Standard Model”, *Int. J. Mod. Phys.*, vol. A27, pp. 1230025, 2012.
- [140] N. Fornengo, C. W. Kim, and J. Song, “Finite temperature effects on the neutrino decoupling in the early universe”, *Phys. Rev.*, vol. D56, pp. 5123–5134, 1997.

-
- [141] V. P. Silin, “On the electromagnetic properties of a relativistic plasma”, *Sov. Phys. JETP*, vol. 11, no. 5, pp. 1136–1140, 1960, [Zh. Eksp. Teor. Fiz.38,1577(1960)].
- [142] H. Arthur Weldon, “Covariant Calculations at Finite Temperature: The Relativistic Plasma”, *Phys. Rev.*, vol. D26, pp. 1394, 1982.
- [143] O. Adriani et al., “Results from the L3 experiment at LEP”, *Phys. Rept.*, vol. 236, pp. 1–146, 1993.
- [144] J. et al. Beringer, “Review of particle physics”, *Phys. Rev. D*, vol. 86, pp. 010001, Jul 2012.
- [145] V. F. Shvartsman, “Density of relict particles with zero rest mass in the universe.”, *Soviet Journal of Experimental and Theoretical Physics Letters*, vol. 9, pp. 184–186, January 1969.
- [146] Gary Steigman, David N. Schramm, and James E. Gunn, “Cosmological limits to the number of massive leptons”, *Physics Letters B*, vol. 66, no. 2, pp. 202–204, January 1977.
- [147] O. Pisanti, A. Cirillo, S. Esposito, F. Iocco, G. Mangano, G. Miele, and P.D. Serpico, “PARthENoPE: Public Algorithm Evaluating the Nucleosynthesis of Primordial Elements”, *Comput. Phys. Commun.*, vol. 178, pp. 956–971, 2008.
- [148] Ryan Cooke, Max Pettini, Regina A. Jorgenson, Michael T. Murphy, and Charles C. Steidel, “Precision measures of the primordial abundance of deuterium”, *Astrophys. J.*, vol. 781, no. 1, pp. 31, 2014.
- [149] Kyle S. Dawson, David J. Schlegel, Christopher P. Ahn, Scott F. Anderson, Éric Aubourg, Stephen Bailey, Robert H. Barkhouser, Julian E. Bautista, Alessandra Beifiori, Andreas A. Berlind, and et al., “The baryon oscillation spectroscopic survey of sdss-iii”, *The Astronomical Journal*, vol. 145, no. 1, pp. 10, Dec 2012.
- [150] Sergei Bashinsky and Uros Seljak, “Neutrino perturbations in CMB anisotropy and matter clustering”, *Phys. Rev. D*, vol. 69, pp. 083002, 2004.
- [151] Zhen Hou, Ryan Keisler, Lloyd Knox, Marius Millea, and Christian Reichardt, “How massless neutrinos affect the cosmic microwave background damping tail”, *Physical Review D*, vol. 87, no. 8, Apr 2013.
- [152] Julien Lesgourgues and Sergio Pastor, “Massive neutrinos and cosmology”, *Phys. Rept.*, vol. 429, pp. 307–379, 2006.

-
- [153] Massimiliano Lattanzi and Martina Gerbino, “Status of neutrino properties and future prospects - Cosmological and astrophysical constraints”, *Front. in Phys.*, vol. 5, pp. 70, 2018.
- [154] Elena Pierpaoli, “Constraints on the cosmic neutrino background”, *Mon. Not. Roy. Astron. Soc.*, vol. 342, pp. L63, 2003.
- [155] Joseph Silk, “Cosmic black body radiation and galaxy formation”, *Astrophys. J.*, vol. 151, pp. 459–471, 1968.
- [156] K. N. Abazajian et al., “Light Sterile Neutrinos: A White Paper”, 2012.
- [157] R. K. Sachs and A. M. Wolfe, “Perturbations of a Cosmological Model and Angular Variations of the Microwave Background”, *APJ*, vol. 147, pp. 73, January 1967.
- [158] Francesco de Bernardis, Alessandro Melchiorri, Licia Verde, and Raul Jimenez, “The Cosmic Neutrino Background and the Age of the Universe”, *JCAP*, vol. 03, pp. 020, 2008.
- [159] Mario Ballardini, Matteo Braglia, Fabio Finelli, Daniela Paoletti, Alexei A. Starobinsky, and Caterina Umiltà, “Scalar-tensor theories of gravity, neutrino physics, and the H_0 tension”, 4 2020.
- [160] Jose Luis Bernal, Licia Verde, and Adam G. Riess, “The trouble with H_0 ”, *JCAP*, vol. 10, pp. 019, 2016.
- [161] E. Komatsu, K. M. Smith, J. Dunkley, C. L. Bennett, B. Gold, G. Hinshaw, N. Jarosik, D. Larson, M. R. Nolte, L. Page, and et al., “Seven-year wilkinson microwave anisotropy probe (wmap) observations: Cosmological interpretation”, *The Astrophysical Journal Supplement Series*, vol. 192, no. 2, pp. 18, Jan 2011.
- [162] J. Dunkley et al., “Five-Year Wilkinson Microwave Anisotropy Probe (WMAP) Observations: Likelihoods and Parameters from the WMAP data”, *Astrophys. J. Suppl.*, vol. 180, pp. 306–329, 2009.
- [163] Joan Simon, Licia Verde, and Raul Jimenez, “Constraints on the redshift dependence of the dark energy potential”, *Phys. Rev. D*, vol. 71, pp. 123001, 2005.
- [164] Kenneth M. Nollett and Gary Steigman, “BBN And The CMB Constrain Light, Electromagnetically Coupled WIMPs”, *Phys. Rev. D*, vol. 89, no. 8, pp. 083508, 2014.

- [165] Kevork Abazajian et al., “CMB-S4 Science Case, Reference Design, and Project Plan”, 2019.
- [166] Pablo F. de Salas and Sergio Pastor, “Relic neutrino decoupling with flavour oscillations revisited”, *JCAP*, vol. 1607, no. 07, pp. 051, 2016.
- [167] Murray Gell-Mann, Pierre Ramond, and Richard Slansky, “Complex spinors and unified theories”, 2013.
- [168] Rabindra Mohapatra and Goran Senjanović, “Neutrino mass and spontaneous parity nonconservation”, *Physical Review Letters - PHYS REV LETT*, vol. 44, pp. 912–915, 04 1980.
- [169] J. Schechter and J.W.F. Valle, “Neutrino Masses in SU(2) x U(1) Theories”, *Phys. Rev. D*, vol. 22, pp. 2227, 1980.
- [170] Peter Minkowski, “ $\mu \rightarrow e \gamma$ at a rate of one out of 109 muon decays?”, *Physics Letters B*, vol. 67, pp. 421–428, 04 1977.
- [171] J. Schechter and J.W.F. Valle, “Neutrino Decay and Spontaneous Violation of Lepton Number”, *Phys. Rev. D*, vol. 25, pp. 774, 1982.
- [172] Samoililenky, *Introduction to the physics of massive and mixed neutrinos*, vol. 817, 2010.
- [173] Marco Drewes, “The Phenomenology of Right Handed Neutrinos”, *Int. J. Mod. Phys. E*, vol. 22, pp. 1330019, 2013.
- [174] M.C. Gonzalez-Garcia and Michele Maltoni, “Phenomenology with Massive Neutrinos”, *Phys. Rept.*, vol. 460, pp. 1–129, 2008.
- [175] M. Fukugita and T. Yanagida, “Baryogenesis Without Grand Unification”, *Phys. Lett. B*, vol. 174, pp. 45–47, 1986.
- [176] Apostolos Pilaftsis and Thomas E.J. Underwood, “Resonant leptogenesis”, *Nucl. Phys. B*, vol. 692, pp. 303–345, 2004.
- [177] Evgeny K. Akhmedov, V.A. Rubakov, and A.Yu. Smirnov, “Baryogenesis via neutrino oscillations”, *Phys. Rev. Lett.*, vol. 81, pp. 1359–1362, 1998.
- [178] Takehiko Asaka and Mikhail Shaposhnikov, “The ν MSM, dark matter and baryon asymmetry of the universe”, *Phys. Lett. B*, vol. 620, pp. 17–26, 2005.
- [179] M. Drewes, B. Garbrecht, P. Hernandez, M. Kekic, J. Lopez-Pavon, J. Racker, N. Rius, J. Salvado, and D. Teresi, “ARS Leptogenesis”, *Int. J. Mod. Phys. A*, vol. 33, no. 05n06, pp. 1842002, 2018.

- [180] Marcin Chrzaszcz, Marco Drewes, Tomás E. Gonzalo, Julia Harz, Suraj Krishnamurthy, and Christoph Weniger, “A frequentist analysis of three right-handed neutrinos with GAMBIT”, *Eur. Phys. J. C*, vol. 80, no. 6, pp. 569, 2020.
- [181] Laurent Canetti, Marco Drewes, Tibor Frossard, and Mikhail Shaposhnikov, “Dark Matter, Baryogenesis and Neutrino Oscillations from Right Handed Neutrinos”, *Phys. Rev. D*, vol. 87, pp. 093006, 2013.
- [182] P. Hernandez, M. Kekic, and J. Lopez-Pavon, “ N_{eff} in low-scale seesaw models versus the lightest neutrino mass”, *Phys. Rev. D*, vol. 90, no. 6, pp. 065033, 2014.
- [183] Aaron C. Vincent, Enrique Fernandez Martinez, Pilar Hernández, Massimiliano Lattanzi, and Olga Mena, “Revisiting cosmological bounds on sterile neutrinos”, *JCAP*, vol. 04, pp. 006, 2015.
- [184] Marco Hufnagel, Kai Schmidt-Hoberg, and Sebastian Wild, “BBN constraints on MeV-scale dark sectors. Part II. Electromagnetic decays”, *JCAP*, vol. 11, pp. 032, 2018.
- [185] Oleg Ruchayskiy and Artem Ivashko, “Restrictions on the lifetime of sterile neutrinos from primordial nucleosynthesis”, *JCAP*, vol. 10, pp. 014, 2012.
- [186] Scott Dodelson and Lawrence M. Widrow, “Sterile-neutrinos as dark matter”, *Phys. Rev. Lett.*, vol. 72, pp. 17–20, 1994.
- [187] A. Boyarsky, M. Drewes, T. Lasserre, S. Mertens, and O. Ruchayskiy, “Sterile neutrino Dark Matter”, *Prog. Part. Nucl. Phys.*, vol. 104, pp. 1–45, 2019.
- [188] Jan Hamann, Steen Hannestad, Georg G. Raffelt, Irene Tamborra, and Yvonne Y.Y. Wong, “Cosmology seeking friendship with sterile neutrinos”, *Phys. Rev. Lett.*, vol. 105, pp. 181301, 2010.
- [189] Jan Hamann, Steen Hannestad, Georg G. Raffelt, and Yvonne Y.Y. Wong, “Sterile neutrinos with eV masses in cosmology: How disfavoured exactly?”, *JCAP*, vol. 09, pp. 034, 2011.
- [190] A. Aguilar, L. B. Auerbach, R. L. Burman, D. O. Caldwell, E. D. Church, A. K. Cochran, J. B. Donahue, A. Fazely, G. T. Garvey, R. M. Gunasingha, R. Imlay, W. C. Louis, R. Majkic, A. Malik, W. Metcalf, G. B. Mills, V. Sandberg, D. Smith, I. Stancu, M. Sung, R. Tayloe, G. J. Vandalen, W. Vernon, N. Wadia, D. H. White, and S. Yellin, “Evidence

- for neutrino oscillations from the observation of $\bar{\nu}_e$ appearance in a $\bar{\nu}_\mu$ beam”, *Phys. Rev. D*, vol. 64, pp. 112007, Nov 2001.
- [191] A.A. Aguilar-Arevalo et al., “Updated MiniBooNE Neutrino Oscillation Results with Increased Data and New Background Studies”, 6 2020.
- [192] Alessandro Strumia, “Interpreting the LSND anomaly: Sterile neutrinos or CPT violation or...?”, *Phys. Lett. B*, vol. 539, pp. 91–101, 2002.
- [193] Evgeny Akhmedov and Thomas Schwetz, “MiniBooNE and LSND data: Non-standard neutrino interactions in a (3+1) scheme versus (3+2) oscillations”, *JHEP*, vol. 10, pp. 115, 2010.
- [194] R. Acciarri et al., “Long-Baseline Neutrino Facility (LBNF) and Deep Underground Neutrino Experiment (DUNE): Conceptual Design Report, Volume 2: The Physics Program for DUNE at LBNF”, 12 2015.
- [195] Christopher Brust, David E. Kaplan, and Matthew T. Walters, “New Light Species and the CMB”, *JHEP*, vol. 12, pp. 058, 2013.
- [196] Ludmila Levkova, “QCD at nonzero temperature and density”, *PoS*, vol. LATTICE2011, pp. 011, 2011.
- [197] Francesco D’Eramo, Ricardo Z. Ferreira, Alessio Notari, and José Luis Bernal, “Hot Axions and the H_0 tension”, *JCAP*, vol. 11, pp. 014, 2018.
- [198] G.G. Raffelt, *Stars as laboratories for fundamental physics: The astrophysics of neutrinos, axions, and other weakly interacting particles*, 5 1996.
- [199] Georg G. Raffelt, “Particle physics from stars”, *Ann. Rev. Nucl. Part. Sci.*, vol. 49, pp. 163–216, 1999.
- [200] Georg G. Raffelt, “Axions: Motivation, limits and searches”, *J. Phys. A*, vol. 40, pp. 6607–6620, 2007.
- [201] S.I. Blinnikov, A.D. Dolgov, L.B. Okun, and M.B. Voloshin, “How strong can the coupling of leptonic photons be?”, *Nucl. Phys. B*, vol. 458, pp. 52–64, 1996.
- [202] Masahiro Ibe, Shin Kobayashi, Yuhei Nakayama, and Satoshi Shirai, “Cosmological constraint on dark photon from N_{eff} ”, *JHEP*, vol. 04, pp. 009, 2020.

- [203] Thomas Hambye, Michel H.G. Tytgat, Jérôme Vandecasteele, and Laurent Vanderheyden, “Dark matter from dark photons: a taxonomy of dark matter production”, *Phys. Rev. D*, vol. 100, no. 9, pp. 095018, 2019.
- [204] Horatiu Nastase, “Introduction to Supergravity”, 12 2011.
- [205] Emanuela Dimastrogiovanni and Lawrence M. Krauss, “ ΔN_{eff} and entropy production from early-decaying gravitinos”, *Phys. Rev. D*, vol. 98, no. 2, pp. 023006, 2018.
- [206] Gary Steigman, Basudeb Dasgupta, and John F. Beacom, “Precise Relic WIMP Abundance and its Impact on Searches for Dark Matter Annihilation”, *Phys. Rev. D*, vol. 86, pp. 023506, 2012.
- [207] Nashwan Sabti, James Alvey, Miguel Escudero, Malcolm Fairbairn, and Diego Blas, “Refined Bounds on MeV-scale Thermal Dark Sectors from BBN and the CMB”, *JCAP*, vol. 01, pp. 004, 2020.
- [208] E. Grohs, G. M. Fuller, C. T. Kishimoto, M. W. Paris, and A. Vlasenko, “Neutrino energy transport in weak decoupling and big bang nucleosynthesis”, *Phys. Rev.*, vol. D93, no. 8, pp. 083522, 2016.
- [209] Jack J. Bennett, Gilles Buldgen, Marco Drewes, and Yvonne Y. Y. Wong, “Towards a precision calculation of the effective number of neutrinos N_{eff} in the Standard Model I: The QED equation of state”, *JCAP*, vol. 2003, no. 03, pp. 003, 2020.
- [210] Claudio Coriano and Rajesh R. Parwani, “The Three loop equation of state of QED at high temperature”, *Phys. Rev. Lett.*, vol. 73, pp. 2398–2401, 1994.
- [211] Rajesh R. Parwani and Claudio Coriano, “Higher order corrections to the equation of state of QED at high temperature”, *Nucl. Phys.*, vol. B434, pp. 56–84, 1995.
- [212] Jeremiah Birrell, Cheng-Tao Yang, and Johann Rafelski, “Relic Neutrino Freeze-out: Dependence on Natural Constants”, *Nucl. Phys.*, vol. B890, pp. 481–517, 2014.
- [213] James A. D. Diacoumis and Yvonne Y. Y. Wong, “Trading kinetic energy: how late kinetic decoupling of dark matter changes N_{eff} ”, *JCAP*, vol. 1901, no. 01, pp. 001, 2019.

-
- [214] Eite Tiesinga, Peter J. Mohr, David B. Newell, and Barry N. Taylor, “The 2018 CODATA Recommended Values of the Fundamental Physical Constants”, <https://physics.nist.gov/constants>, 2018.
- [215] M. Tanabashi et al., “Review of Particle Physics”, *Phys. Rev.*, vol. D98, no. 3, pp. 030001, 2018.
- [216] P. F. de Salas, D. V. Forero, C. A. Ternes, M. Tortola, and J. W. F. Valle, “Status of neutrino oscillations 2018: 3σ hint for normal mass ordering and improved CP sensitivity”, *Phys. Lett.*, vol. B782, pp. 633–640, 2018.
- [217] Ivan Esteban, M. C. Gonzalez-Garcia, Alvaro Hernandez-Cabezudo, Michele Maltoni, and Thomas Schwetz, “Global analysis of three-flavour neutrino oscillations: synergies and tensions in the determination of θ_{23} , δ_{CP} , and the mass ordering”, *JHEP*, vol. 01, pp. 106, 2019.
- [218] C. Lunardini and A. Yu. Smirnov, “High-energy neutrino conversion and the lepton asymmetry in the universe”, *Phys. Rev.*, vol. D64, pp. 073006, 2001.
- [219] G. Sigl and G. Raffelt, “General kinetic description of relativistic mixed neutrinos”, *Nucl. Phys.*, vol. B406, pp. 423–451, 1993.
- [220] Isabel M. Oldengott, Cornelius Rampf, and Yvonne Y. Y. Wong, “Boltzmann hierarchy for interacting neutrinos I: formalism”, *JCAP*, vol. 1504, no. 04, pp. 016, 2015.